Univerzita Karlova v Praze
Přírodovědecká fakulta

Studijní program: Užitá geofyzika
Studijní obor: Aplikovaná geologie

PŘÍLOHA DOKTORSKÉ DISERTAČNÍ PRÁCE

Mgr. Petr Schnabl

Paleomagnetismus a magnetomineralogie hornin Českého masivu a tethydní oblasti

Paleomagnetism and magnetomineralogy of rocks from the Bohemian Massif and Tethyan Realm

Vedoucí disertační práce:
Ing. Petr Pruner, DrSc.

Praha, 2012

Seznam recenzovaných publikací vztahujících se k tématu

1. **Schnabl P.**, Novák J.K., Cajz V., Lang M., Balogh K., Pécskay Z., Chadima M., Šlechta S., Kohout T., Pruner P. a Ulrych J., 2010. Magnetic properties of high-Ti basaltic rocks from the Krušné hory/Erzgebirge MTS. (Bohemia/Saxony), and their relation to mineral chemistry, *Stud. Geoph. et Geodet.*, 54, 1, 77 – 94.

2. Cajz V., **Schnabl P.**, Pécskay Z., Skácelová Z., Venhodová D., Šlechta S. a Šifnerová K. Chronological implications of paleomagnetic record of the Late Cenozoic volcanic activity in Moravo-Silesian border – NE Bohemian Massif , *Geologica Carpathica* – Přijato do tisku

3. Cajz V., Rapprich V., **Schnabl P.** a Pécskay Z., 2009. Návrh litostratigrafie neovulkanitů východočeské oblasti (A proposal on lithostratigraphy of Cenozoic volcanic rocks in Eastern Bohemia). – *Zprávy o geologických výzkumech v roce 2008*, 9 – 15.

4. Pruner P., Houša V., Olóriz F., Košťák M., Krs M., Man O., **Schnabl P.**, Venhodová D., Tavera J.M. a Mazuch M., 2010, High-resolution magnetostratigraphy and biostratigraphic zonation of the Jurassic/Cretaceous boundary strata in the Puerto Escaño section (southern Spain), *Cretaceous Research*, 31, 2, 192 – 206.

5. Lukeneder A., Halásová E., Kroh A., Mayrhofer S., Pruner P., Reháková D., **Schnabl P.**, Sprovieri M. a Wagreich M., 2010. High resolution stratigraphy of the Jurassic-Cretaceous boundary interval in the Gresten Klippenbelt (Austria), *Geologica Carpathica.*, 61, 5, 365 – 381.

6. Vacek F., Hladil J. a **Schnabl P.**, 2010. Stratigraphic correlation potential of magnetic susceptibility and gamma-ray spectrometric variations in calciturbiditic facies (Silurian-Devonian boundary, Prague Synclinorium, Czech Republic) *Geologica Carpathica.*, 61, 4, 257 – 272.

7. Kletetschka G., Pruner P., **Schnabl P.**, Šifnerová K., Tasáryová Z., Manda Š., Magnetic scanning and interpretation of paleomagnetic data from Prague Synform's volcanics, *Stud. Geoph. et Geodet.* – V recenzním řízení

Schnabl P., Novák J.K., Cajz V., Lang M., Balogh K., Pécskay Z.,
Chadima M., Šlechta S., Kohout T., Pruner P. a Ulrych J.

Magnetic properties of high-Ti basaltic rocks from the Krušné hory/Erzgebirge MTS. (Bohemia/Saxony), and their relation to mineral chemistry

Stud. Geoph. et Geodet., 54, 1, 77 – 94, 2010

Cajz V., **Schnabl P.**, Pécskay Z., Skácelová Z., Venhodová D., Šlechta S. a Šifnerová K.

Chronological implications of paleomagnetic record of the Late Cenozoic volcanic ctivity in Moravo-Silesian border – NE Bohemian Massif

Geologica Carpathica – Přijato do tisku

Cajz V., Rapprich V., **Schnabl P.** a Pécskay Z.

Návrh litostratigrafie neovulkanitů východočeské oblasti (A proposal on lithostratigraphy of Cenozoic volcanic rocks in Eastern Bohemia)

Zprávy o geologických výzkumech v roce 2008, 9 – 15, 2009

Pruner P., Houša V., Olóriz F., Košťák M., Krs M., Man O., **Schnabl P.**,
Venhodová D., Tavera J.M. a Mazuch M.

High-resolution magnetostratigraphy and biostratigraphic zonation of the Jurassic/Cretaceous boundary strata in the Puerto Escaño section (southern Spain)

Cretaceous Research, 31, 2, 192 – 206, 2010

Lukeneder A., Halásová E., Kroh A., Mayrhofer S., Pruner P.,Reháková D., **Schnabl P.**, Sprovieri M. a Wagreich M.

High resolution stratigraphy of the Jurassic-Cretaceous boundary interval in the Gresten Klippenbelt (Austria)

Geol. Carpathica., 61, 5, 365 – 381, 2010

Vacek F., Hladil J. a **Schnabl P.**

Stratigraphic correlation potential of magnetic susceptibility and gamma-ray spectrometric variations in calciturbiditic facies (Silurian-Devonian boundary, Prague Synclinorium, Czech Republic)

Geologica Carpathica., 61, 4, 257 – 272, 2010

Kletetschka G., Pruner P., **Schnabl P.**, Šifnerová K., Tasáryová Z., Manda Š.

Magnetic scanning and interpretation of paleomagnetic data from Prague Synform's volcanics

Stud. Geoph. et Geodet. – V recenzním řízení

Schnabl P., Novák J.K., Cajz V., Lang M., Balogh K., Pécskay Z.,
Chadima M., Šlechta S., Kohout T., Pruner P. a Ulrych J.

Magnetic properties of high-Ti basaltic rocks from the Krušné hory/Erzgebirge MTS. (Bohemia/Saxony), and their relation to mineral chemistry

Stud. Geoph. et Geodet., 54, 1, 77 – 94, 2010

MAGNETIC PROPERTIES OF HIGH-TI BASALTIC ROCKS FROM THE KRUŠNÉ HORY/ERZGEBIRGE MTS. (BOHEMIA/SAXONY), AND THEIR RELATION TO MINERAL CHEMISTRY

PETR SCHNABL[1], JIŘÍ K. NOVÁK[1], VLADIMÍR CAJZ[1], MILOŠ LANG[1], KADOSA BALOGH[2], ZOLTAN PÉCSKAY[2], MARTIN CHADIMA[1], STANISLAV ŠLECHTA[1], TOMÁŠ KOHOUT[1,3], PETR PRUNER[1] AND JAROMÍR ULRYCH[1]

1 Institute of Geology, Acad. Sci. of the Czech Republic, v.v.i., Rozvojová 269, 165 00 Praha 6, Czech Republic (schnabl@gli.cas.cz)

2 Institute of Nuclear Research of the Hungarian Academy of Sciences, Bem tér 18/C, H-4001 Debrecen, Hungary

3 Department of Physics, University of Helsinki, P.O.Box 64, Helsinki, Finland

Received: December 22, 2008; Revised: June 1, 2009; Accepted: July 7, 2009

ABSTRACT

This study provides new thermomagnetic and petrographic data on specific basaltic rock association from the broader vicinity of the Loučná-Oberwiesenthal volcanic centre, western Bohemia/Saxony. Two types of volcanic rocks were recognized there: (i) high-Ti types (3.5–5.2 wt% TiO_2) represented by (mela)nephelinite s.s., and sporadically present (ii) medium-Ti types (2.5–3.5 wt% TiO_2) of olivine nephelinite, nepheline basanite and phonotephrite compositions. In order to examine the rock-magnetic behaviour, they were studied for their variations in the Curie temperature (T_C) and field-dependent susceptibility, spinel group minerals, chemistry and petrology.

Magnetic susceptibility of ulvöspinel-rich titanomagnetite, as a dominant magnetic carrier, depends on the amplitude of measured magnetic field, whereas pure magnetite is field-independent. Field dependence parameter k_{HD} of the studied basaltic rocks ranges from 0.8 to 18.7%, TiO_2 contents in titanomagnetite range from 12.7 to 20.1 wt.%. TiO_2 content in titanomagnetite does not correlate with whole-rock TiO_2 content (2.8 to 5.6 wt.%). The content of substituted titanium in the sublattice of magnetite is also sensitively reflected in the Curie temperature, ranging from 200 to 580 °C. The spinel group minerals are designated as titanomagnetite with the dominance of ulvöspinel, magnetite and magnesioferrite components, or titanomagnetite with the magnetite, ulvöspinel and magnesioferrite components. Only two samples are characterized by a significant presence of Cr-spinel and magnesiochromite components forming cores of titanomagnetites.

The titanomagnetite-bearing rocks in the studied area, likewise the low- to medium-Ti basaltic rocks from the České středohoří Mts., provide similar thermomagnetic curves.

Keywords: high-Ti and medium-Ti basaltic rocks, magnetic carriers, thermomagnetic experiments, Curie temperature variation, field-dependent susceptibility, Krušné hory/Erzgebirge Mts., Ohře/Eger Rift

1. INTRODUCTION

The main magnetic and titanium carrier in basaltic volcanic rocks is represented by minerals from the spinel group (mostly titanomagnetite). Titanium, as a common element in volcanics, is also incorporated in paramagnetic minerals such as Ti-bearing clinopyroxene, amphibole, ilmenite, perovskite, etc. This means that not the whole TiO_2 content is incorporated in the structure of titanomagnetite. To effectively determine the TiO_2 distribution, we used samples from a specific volcanic region with extremely high TiO_2 contents (max. 5.64 wt.%).

Magnetomineralogic methods can detect TiO_2 content in titanomagnetites using variations in the Curie temperature, field dependent susceptibility and variations in the IRM spectra. Wavelength dispersive spectroscopy brings data on mineral chemistry. We tried to establish a relationship between magnetomineralogic and chemical data. The original aim of this study is (i) to make a comparison between high-Ti (mela)nephelinites (exceptionally high-Ti olivine nephelinite) with titanomagnetite containing a higher/lower ulvöspinel component and medium- to low-Ti rock types (basanite and phonotephrite); (ii) to demonstrate the changes in magnetic susceptibility during heating/cooling experiments; (iii) to study the dependence of magnetic susceptibility on the conductive coil field and (iv) to provide magnetomineralogic data.

1.1. Geological Setting

Titanium-rich Cenozoic basaltic rocks (TiO_2 over 3.5% in whole-rock analyses) concentrate to the western Krušné hory/Erzgebirge Mts. (KH) region (*Shrbený, 1980*), outside the structure of the Ohře/Eger Rift (Fig. 1). Some authors (*Ulrych et al., 2005*; *Haase and Renno, 2008*) suppose this volcanism belongs to the rift structure at its uplifted shoulder. This unique region reaching nearly 150 km^2 (between Jáchymov, Abertamy, Kovářská and Annaberg) is centred approximately around the Loučná-Oberwiesenthal volcanic centre. Nephelinite *sensu stricto* of the centre represents a remnant of deeply eroded vent of a supposed huge Cenozoic composite volcano, situated in the crystalline rocks of the Saxothuringian Zone. Now, it is exposed in subvolcanic position as a result of long-lasting erosion from the time of its detected volcanic activity (33–30 Ma). Rocks of the centre locally bear xenoliths of alkali clinopyroxenite-ijolite, with a high proportion of Ti-Fe oxides (*Herre, 1930*; *Ulrych et al., 2005*). Similar xenolithic material has been reported from several other locations in this area (e.g. Popovský Kříž, TiB-13). In a very close vicinity to the volcanic centre, the Hammerunterwiesenthal/České Hamry maar structure is present (*Suhr, 1999*). The maar fill is intruded by phonolite (Richter Quarry, Saxony) and phonotephrite (České Hamry, TiB-06). Several additional occurrences of basaltic rocks were sampled near the bodies of Ti-rich rocks for comparison. The studied rocks range between 30 and 14 Ma in age and mostly form subvolcanic bodies. Some of them may represent vents of smaller volcanoes (esp. TiB-03, TiB-08). Only the Pöhlberg nephelinite (TiB-18) represents a relic of a lava flow. New geochronological data using K-Ar radiometry were obtained to study possible age dependence of the elevated TiO_2 contents. For details see Table 1.

In order to compare the thermomagnetic behaviour of the low- to medium-Ti basaltic rocks, we also used a set of samples from the České středohoří Mts. (CS) region (*Chadima et al., 2008*). This volcanic range represents an erosional remnant of a volcanic

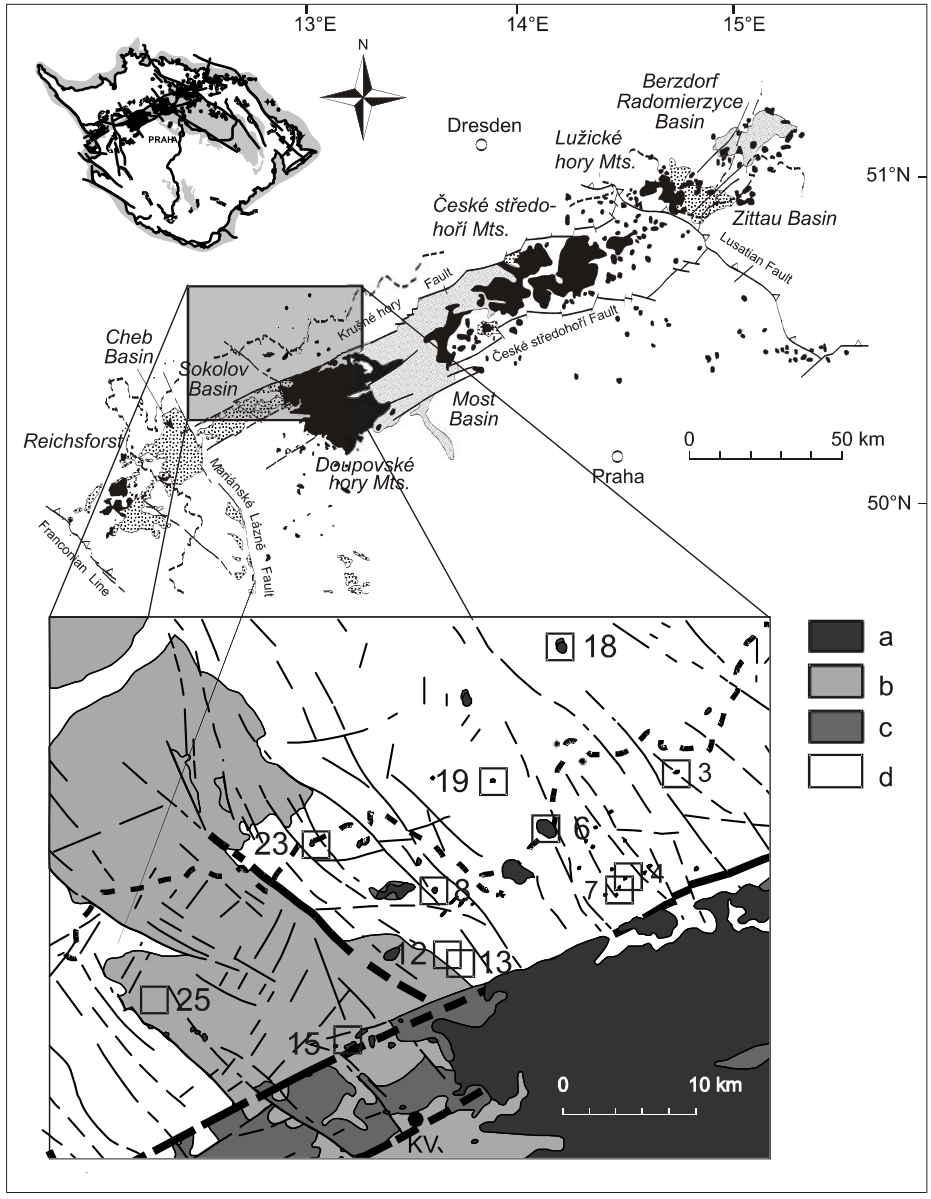

Fig. 1. Location of sampling sites and geological setting of the region. **a)** volcanic rocks; **b)** granitic pluton; **c)** Tertiary sediments (Sokolov Basin); **d)** Saxothuringian crystalline rocks.

complex with preserved superficial volcanic products, situated inside the Ohře/Eger Rift (see Fig. 1). Its volcanic activity lasted from 37 to 9 Ma, and four stratigraphic units are distinguished (*Cajz et al., 1999*; *Cajz, 2000*). Comparative samples were taken from two older units (37–25 Ma), similar in their age to the studied KH rocks. Subvolcanic bodies were chosen for their similar geological position. Several of them represent possible vents; most bodies form dykes. For adequate chemical comparison, we selected samples closest to the studied Ti-rich rocks. As nephelinite *s.s.* is not present among the CS samples, we compared the respective KH samples with olivine nephelinite or with tephrite/trachybasalt rock group.

1.2. Previous Studies

First rock magnetic characteristics of the high-Ti basaltic bodies of the KH were presented by *Kropáček and Pokorná (1975)* and *Kropáček (1976a,b; 1985)*. A high natural remanent magnetization (*NRM*) and low Curie temperature of this rock type was explained in terms of high titanomagnetite and decomposed olivine modal contents as well as high oxygen fugacity (fO_2) in basaltic melts.

The Curie temperature is influenced not only by ulvöspinel component (Ti-constituent) but also by the hercynite (Al-constituent) (*Golla-Schindler et al., 2005*) and magnesioferrite component (Mg-constituent) (*Clark, 1997*).

The effect of the ulvöspinel-magnetite system on Curie temperature was studied by *Lattard et al. (2006)* on synthetic titanomagnetites.

2. METHODS

We analysed selected bodies of high-Ti (mela)nephelinite (TiB-03, 04, 07, 08, 12, 18, 19), high-Ti olivine nephelinite (TiB-23), medium-Ti basanite (TiB-13, 15, 25), and a phonoteprite body (TiB-06) to obtain new rock magnetic and petrographic data.

Field dependence of susceptibility was measured in the field range of 10–300 A/m and frequency 2000 Hz using AGICO susceptibility meter KLF-4. Field dependence was quantitatively evaluated as:

$$k_{HD}\left[\%\right] = 100\left(k_{300} - k_{30}\right)/k_{300}\,,$$

where k_x is the susceptibility measured in the magnetic field with amplitude expressed in A/m (*sensu Vahle et al., 2007*).

The temperature dependence of magnetic susceptibility was measured using AGICO KLY-4 Kappabridge coupled with a temperature control unit CS-3 and CS-L in the temperature range from −192 to 700°C. The measurement was performed at field of 300 A/m and frequency of 875 Hz. Heating was performed using powdered samples in air atmosphere with heating rate of approximately 10°C/min.

The IRM was acquired on Magnetic Measurements Pulse Magnetiser MMPM10 in the field range from 12 to 1000 mT and measured on AGICO JR5 spinner magnetometer. The coercivity spectra were quantified by gradient acquisition plot method (*Kruiver et al., 2001*) by the IRMUNMIX v.2.2 software. Hysteresis loops were measured using a Princeton Measurements Model 3900 VSM and then plotted in Day diagram modified by *Dunlop (2002)*.

Titanium oxide concentrations of the rock samples were determined by instrumental neutron activation at the Nuclear Physics Institute AS CR v.v.i.; the precision of analytical data is about 5%. Accuracy of analytical data was tested against the reference rock standard USGS AGV-1 (*cf. Řanda et al., 2007*).

To observe the textures of magnetic mineral phases (mostly titanomagnetite), a polarized microscope and back-scatter electron images were used. Chemical data for rock-forming minerals including spinel group minerals were obtained using the CAMECA SX-100 electron microprobe working with a wavelength dispersive spectroscopy (WDS) at the Institute of Geology ASCR v.v.i., Prague. The contents of opaque minerals and olivine were determined from bulk rock chemical analyses by means of recalculation into normative mineral composition (*Burri, 1959*). The end-member composition of the spinel group minerals was calculated from the number of ions per formula unit after recalculation on 3 cations and 4 oxygens and stoichiometry. The K-Ar age determinations were carried out at ATOMKI (Debrecen, Hungary) according to the procedure described in Balogh (1985). Data were calibrated by inter-laboratory standards for dating purposes and by atmospheric Ar (*Odin et al., 1982*).

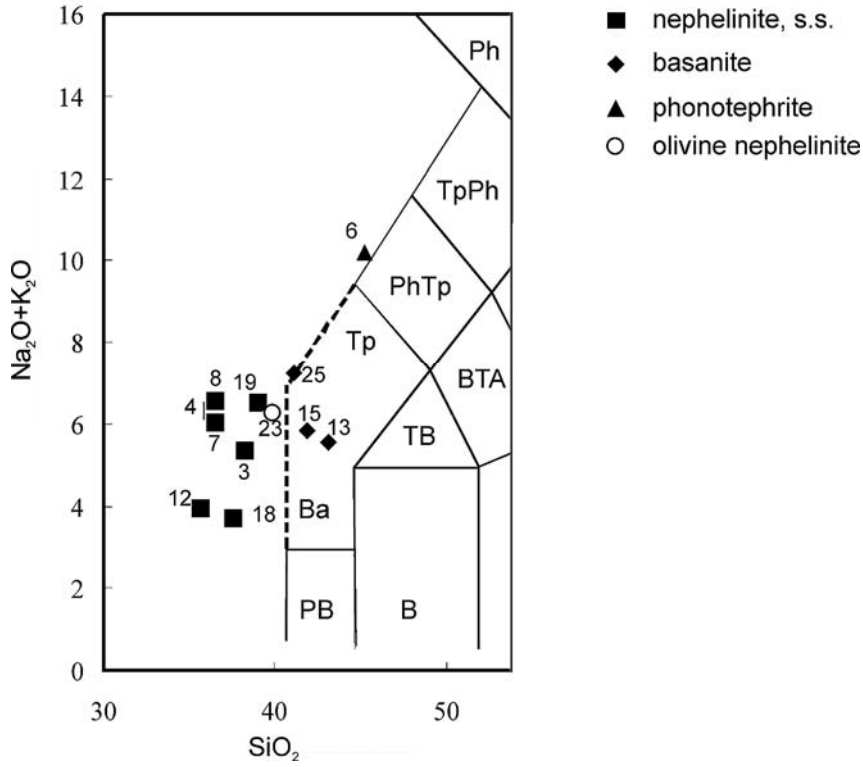

Fig. 2. The TAS classification diagram after *LeMaitre (1989)* showing the composition of the studied samples.

3. PETROGRAPHY

The studied rocks were classified according to IUGS recommendations (Fig. 2). A dominant magnetic carrier in the high-Ti basaltic rocks is titanomagnetite, with a high proportion of ulvöspinel component (18–21 wt.% TiO_2), which particularly occurs in (mela)nephelinite types and forms several grain-size populations. The TiO_2 content in whole-rock analyses does not correlate with TiO_2 content in titanomagnetite (Table 1), because additional Ti-bearing mineral phases are represented by dominant Ti-diopside and accessory kaersutite, ilmenite, titanite, and perovskite. Magnetic properties of olivine-

Table 1. Location and specification of the studied rocks; their K-Ar age, TiO2 content, Curie temperature and field-dependent susceptibility. New K-Ar data, others from ***Lustrino and Wilson (2007)* and **Pfeiffer at al. (1984)*; TiO_2 content taken from whole-rock analyses and magnetite grains using WDS; Curie temperature of original titanomagnetite (T_{C1}), Curie temperature of magnetite after exsolution of ilmenite (T_{C2}); field-dependence parameter k_{HD} after *Vahle and Kontny (2005)*.

Number	Location	Rock Type	Age [Ma]	TiO_2 (w.r.)	TiO_2 (mgn.)	T_{C1} [°C]	T_{C2} [°C]	k_{HD} [%]
Krušné hory (Erzgebirge Mts)								
TiB-03	Jelení hora	nephelinite s.s.	18.4 ± 1.0	5.12	15.66	200	550	18.4
TiB-04	Velký Špičák	nephelinite s.s.	29.3 ± 1.0	5.27	17.12	320	500	17.1
TiB-06	České Hamry	phonotephrite	22.8 ± 0.9	2.87	12.76	400	580	7.7
TiB-07	Střední Špičák	nephelinite s.s.	21.6 ± 0.9	5.64	12.93	300	500	10.4
TiB-08	Špičák-Boží Dar	nephelinite s.s.	16.9 ± 0.7	4.05	19.03	300	580	7.7
TiB-12	Popovská hora	nephelinite s.s.	25.6 ± 0.8	5.90	19.80	260	520	18.7
TiB-13	Popovský kříž	basanite	17.1 ± 1.0	1.97	20.14	320	550	13.7
TiB-15	Hutnický vrch	basanite	19.9 ± 1.1	2.90	19.42	200	580	14.0
TiB-18	Pöhlberg (D)	nephelinite s.s.	24.2 ± 0.9*	5.04	16.05	370	530	5.3
TiB-19	Neudorf (D)	nephelinite s.s.	25.3 ± 1.0	4.59	14.46	510 (290)	580	0.9
TiB-23	Rudná u Potůčků	ol. nephelinite	28.5 ± 1.4	4.37	17.92	330	550	18.2
TiB-25	Rotava-monument	basanite	14.2 ± 0.6	2.72	---	200	580	17.5
České středohoří Mts. (Böhmisches Mittelgebirge, Czech Central Mts.)								
CS-02	Dobkovice	ol. nephelinite	30.9**		---	500	---	9.0
CS-04	Dobkovice	ol. nephelinite	---	3.41	---	560	---	9.6
CS-09	Jakuby	ol. nephelinite	29.3**		---	385	---	11.6
CS-14	Štěpánov	trachybasalt	---	---	---	290	510	10.4
CS-15	Lukov	trachybasalt	---	1.24	---	130	---	27.2
CS-19	Těchlovice	trachybasalt	< CS09	---	---	550	---	–0.1
CS-21	Těchlovice	tephrite	< CS09	---	---	570	---	0.6
CS-22	Neštěmice	ol. nephelinite	26.0–26.7**	2.82	---	200	---	28.0
CS-26	Milešov	tephrite	---	---	---	155	540	20.6
CS-28	Březina	ol. nephelinite	---	---	---	130	---	27.8
CS-36	Český Bukov	trachybasalt	---	---	---	580	---	1.1

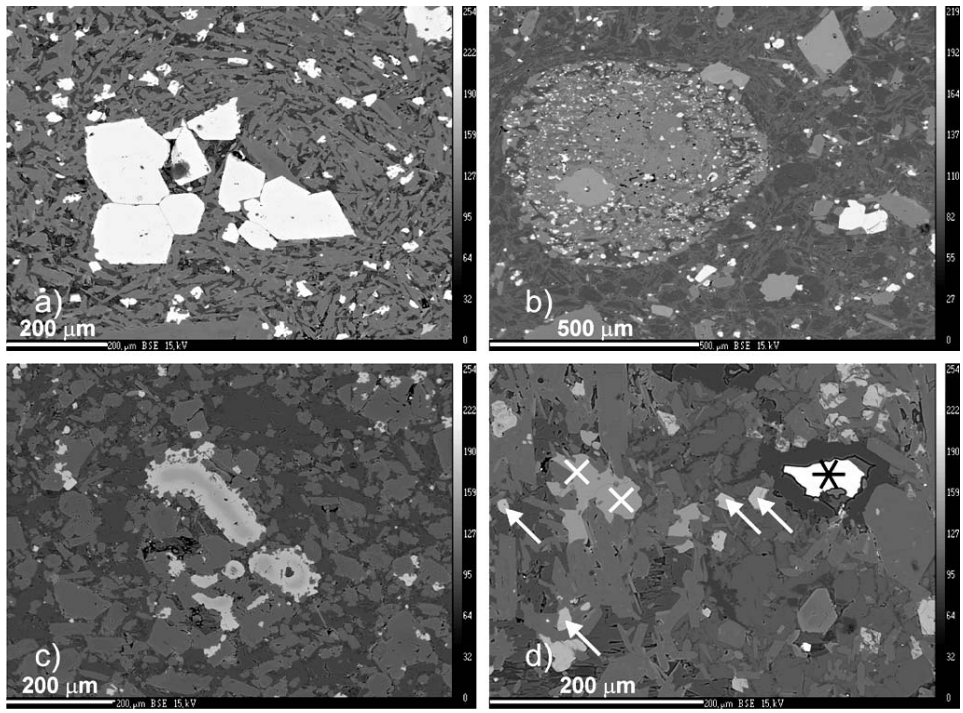

Fig. 3. BSE images of thin sections from selected locations. **a)** TiB-03 Jelení hora Hill - Enclosed pyroxenite with proper microphenocrysts of titanomagnetite, surrounded by nephelinite with small-sized crystals of titanomagnetite; **b)** TiB-06 České Hamry quarry - remnant of porphyritic nephelinite in phonotephrite with phenocrysts of kaersutite, diopside and titanomagnetite. Note two populations of titanomagnetite of different in size and composition; **c)** TiB-08 Špičák Hill at Boží Dar - zoned titanomagnetite in nephelinite. Cores of crystals are rich in the magnesiochromite component, rims are composed of ulvöspinel, magnesioferrite and magnetite; **d)** TiB-08 Špičák Hill at Boží Dar - a close-up view of nephelinite groundmass. White arrow - titanomagnetite, white cross - titanite, black "snowflake" - xenocrystic barite.

bearing rocks (high-Ti olivine nephelinite) are influenced by titanomagnetite with a high proportion of ulvöspinel component (53–58 mol.%) and by the rare presence of recrystallized dusty magnetite from decomposed olivine. Further important mineral assemblages, if present, consist of symplectic magnetite-diopside.

Other factors that are relevant for enhanced magnetization of basaltic rocks are: (i) a higher proportion of small-sized grains of the spinel group minerals (mainly titanomagnetite), (ii) large surface area to volume, and (iii) the presence of distinct spinel group mineral populations (texture). Back-scattered electron images (Fig. 3) demonstrate the most frequent minerals and structures of selected rocks.

According to microscopic observations of **(mela)nephelinite** (TiB 03, 04, 07, 08, 12, 18, 19)**,** the main silicates are zoned Ti-bearing diopside as phenocrysts (3–6 wt.% TiO_2) and a matrix constituent (0.10–0.15 wt% TiO_2), and nepheline and/or analcitized nepheline as constituents of crystalline matrix. No olivine remnants and/or pseudomorphs

after olivine were found. Titanomagnetite occurs in xenocrystic or dusty populations. The latter is sometimes associated with 30–50 μm-sized perovskite. The amount of titanomagnetite ranges from 4.5 to 8.8 vol.%.

Olivine nephelinite (TiB-23) is an igneous rock with well preserved but broken olivine and zoned diopside phenocrysts as well as with serpentinized microxenoliths. Thin reaction rims around fresh olivine and in fractures are filled with 30–50 μm-sized grains of titanian magnetite. Kaersutite prisms (0.4 mm in length) are rare. Semi-translucent holocrystalline matrix is composed of analcitized nepheline and contains up to 4.5 vol.% of dusty titanomagnetite. In the titanomagnetite composition, the ulvöspinel component significantly dominates over magnesioferrite, magnetite and hercynite.

Nepheline basanite (TiB-13, 15, 25) is a porphyritic holocrystalline rock, dominated by relatively fresh olivine in broken phenocrysts and microphenocrysts. Under a microscope, the rounded diopside phenocrysts are rimmed by clinopyroxene-magnetite intergrowths. The mineral assemblage of the matrix is composed of fresh nepheline and labradorite feldspar laths; the fine-sized titanomagnetite represents common accessory mineral (about 3.8 vol.%). The titanomagnetite composition is similar to that in olivine nephelinite.

Phonotephrite (TiB-06) is the most evolved igneous rock in the studied set, where phonolite-like groundmass is present with Na-K feldspar laths, zoned clinopyroxene prisms, minor kaersutite, and accessory titanian magnetite. Fresh phenocrysts are composed of zoned diopside and reddish brown-coloured kaersutite with opacitized rims. Analcite infills dominate on rock fractures. The magnetite and ulvöspinel in titanomagnetite dominate over the magnesioferrite, hercynite and jacobsite components.

4. MAGNETIC PROPERTIES

WDS results were recalculated to obtain the content of a possible spinel component: ulvöspinel, hercynite, jacobsite, magnesioferrite, magnesiochromite, chromite and magnetite (Table 2).

It is evident that magnetic properties of high-Ti basaltic rocks are mainly controlled by variations in titanomagnetite composition, not only in pure ulvöspinel-magnetite system. Some crystals are zoned with high magnesiochromite component in the core and increasing content of ulvöspinel, magnesioferrite and magnetite in the rim (see Fig. 3c). The studied titanomagnetites are characterized by relatively close dispersal of Fe-Ti cation constitutes (Fig. 4).

The content of secondary magnetite resulting from decomposed olivine in basanite and olivine nephelinite is very low and depends on the relatively low proportion of the fayalite component and the degree of alteration. Magnetic properties are insignificantly influenced by this.

4.1. Curie Temperature

The content of substituted titanium in the magnetite structure is also sensitively reflected in the Curie temperature (T_{C1}). The Curie temperature of pure magnetite is about 575°C and decreases with increasing content of Ti in the magnetite-ulvöspinel system; the ulvöspinel end-member is paramagnetic above −150°C and this transition temperature

Table 2. Recalculated mineral components from WDS analyses and their correlation with the Curie temperature and field-dependent susceptibility. Ulv. - ulvospinel ($TiFe_2O_4$), Herc. - hercynite ($FeOAl_2O_3$), Jacob. - jacobite ($MnOFe_2O_3$), Mgfr. - magnesioferrite ($MgOFe_2O_3$), Mgchr. - magnesiochromite ($MgOCr_2O_3$), Chr. - chromite ($FeOCr_2O_3$), Mgn. - magnetite ($FeOFe_2O_3$).

Sample	Ulv.	Herc.	Jacob.	Mgfr.	Mgchr.	Chr.	Mgn.	T_{C1} [°C]	k_{HD} [%]
TiB-03	44.94	4.95	2.95	18.14	0.09	0.03	28.90	200	18.42
TiB-04	48.00	10.89	2.45	25.40	0.06	0.02	13.17	320	17.15
TiB-06	37.21	3.82	5.25	6.31	0.01	0.00	47.38	400	7.67
TiB-07	36.00	6.02	3.88	10.57	0.02	0.01	43.51	300	10.37
TiB-08	54.80	7.02	2.70	16.74	0.13	0.04	18.57	300	7.69
TiB-12	55.78	8.46	2.12	22.77	2.07	2.07	6.71	260	18.67
TiB-13	55.73	8.32	2.25	15.98	3.47	1.16	13.09	320	13.74
TiB-15	53.03	5.96	2.45	10.82	0.97	0.65	26.13	200	13.97
TiB-18	46.23	2.34	3.72	8.70	0.08	0.03	38.91	370	5.34
TiB-19	42.04	3.29	4.63	7.57	0.02	0.01	42.44	510	0.86
TiB-23	58.64	4.07	2.81	23.10	0.18	0.18	11.02	330	18.25
Correlation Parameters									
k_{HD} [%]	0.50	**0.55**	–0.73	**0.81**	0.33	0.44	–0.73	–0.75	
T_{C1} [°C]	–0.37	–0.41	0.70	–0.44	–0.24	–0.33	0.45		–0.75

also decreases with hercynite content (*Golla-Schindler et al., 2005*), which is paramagnetic above –265°C.

Two Curie temperatures T_{C1} and T_{C2} were identified for all samples except TiB-19: T_{C1} ranges between 200 and 510°C and T_{C2} is in the range of 500 and 580°C. T_{C1} represents the Curie temperature of original titanomagnetite of the sample, and T_{C2} originated during the measurement after thermal exsolution of ilmenite.

Susceptibility after heating is slightly lower for TiB-03, 08, 12, 13, 15 and 18. Three samples TiB-04, 06, 07 are reversible with unchanged susceptibility before and after heating, and susceptibility of TiB-25 slightly increases. Samples TiB-19 and 23 show a lower Curie temperature (T_{C1}) after heating.

We observed several different patterns of magnetic susceptibility changes as a function of temperature. The first one is shown on samples TiB 03, 04, 06, 07, 08, 12, 13, 15 and 25. Its Curie temperature is between T_{C1} 200 and 320°C, and a prominent peak around 400°C indicates a secondary mineral with Curie temperature T_{C2} between 500 and 580°C. This can be explained by the exsolution of ilmenite, hercynite (*Golla-Schindler et al., 2005*) or possibly magnesioferrite lamellae during laboratory heating. Original titanomagnetite is then relatively depleted in Ti, Al or Mg, which can explain the second T_{C2} identified on the thermomagnetic curves. The second pattern can be seen on samples TiB-06, 18 and 19. A major difference from the previous pattern is in T_{C1}, which ranges between 370 and 510°C and is close to T_{C2}. This pattern is caused by the high magnetite content in the titanomagnetite. The third pattern is represented by sample TiB-23: there is

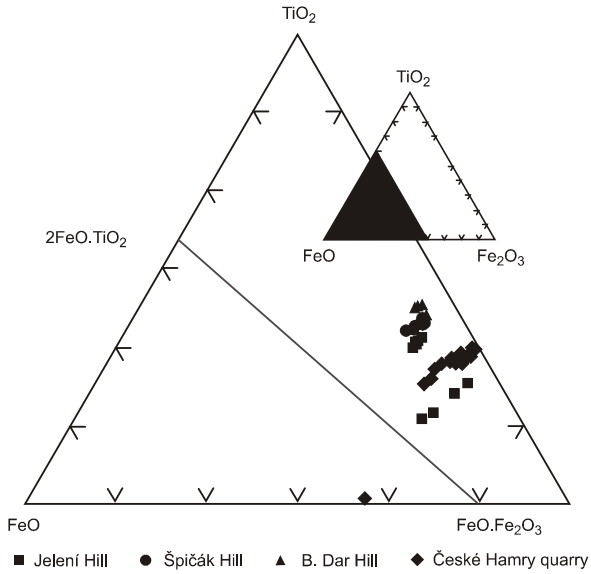

Fig. 4. Classification ternary diagram of Fe-Ti oxides after *O'Reilly and Banerjee (1966).* Projection points show a relatively close dispersal within the magnetite-ulvöspinel series.

only one peak with two Curie temperatures. This sample has a very low content of the magnetite component. Low to moderate negative correlation was proved between the Curie temperature and the ulvöspinel (–0.37), magnesioferrite (–0.44) and/or hercynite (–0.41) components, respectively (see Table 2, and following text).

In comparison, samples from the CS region show a much wider dispersion of Curie temperatures than samples from the KH. Moreover, the shape of the MS curves for the CS samples reflects titanomagnetite without any phase changes or alterations. The only exception is sample CS-14 with a peak of newly formed magnetite after ilmenite exsolution.

4.2. Field-Dependent Susceptibility

Twelve representative samples were subjected to rock magnetic experiments in order to correlate the analysed titanium, aluminium and magnesium contents in titanomagnetites (spinels) to various magnetic properties. Their magnetic susceptibility depends on the amplitude of the measuring field (Fig. 5). This dependence increases with increasing Ti content in titanomagnetite, whereas pure magnetite is field-independent. The field-dependent parameter k_{HD} is between 5.3 and 18.6%, the only exception is TiB-19, where $k_{HD} = 0.86\%$. Values of k_{HD} strongly correlate with the magnesioferrite component, the correlation parameter is 0.81. The correlation between hercynite or ulvöspinel and k_{HD} is only moderate, correlation parameters are 0.55 and 0.50, respectively. The possible reason for a moderate correlation is the relatively low dispersion in hercynite and ulvöspinel contents.

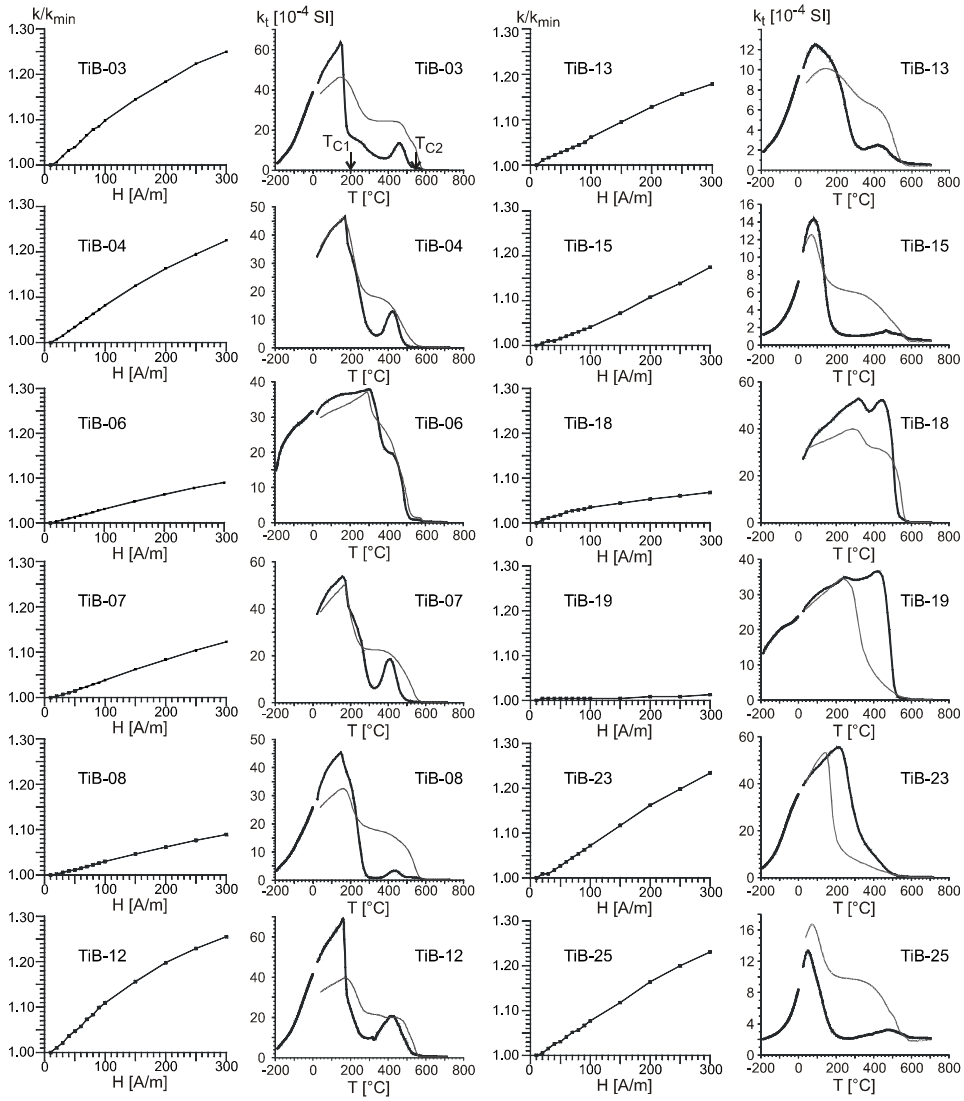

Fig. 5. Curves of temperature and field variations of magnetic susceptibility for samples from the Krušné hory Mts. The full heating curve (black) and the cooling curve (grey) were obtained as follows: (i) cooling the sample to −192°C and measuring susceptibility while heating to room temperature, (ii) heating from room temperature up to 700°C and cooling again to room temperature. The variations in magnetic susceptibility, as a function of AC field, were measured in the field intensity gradually increased from 10 to 300 A/m. Powdered samples were heated in air atmosphere.

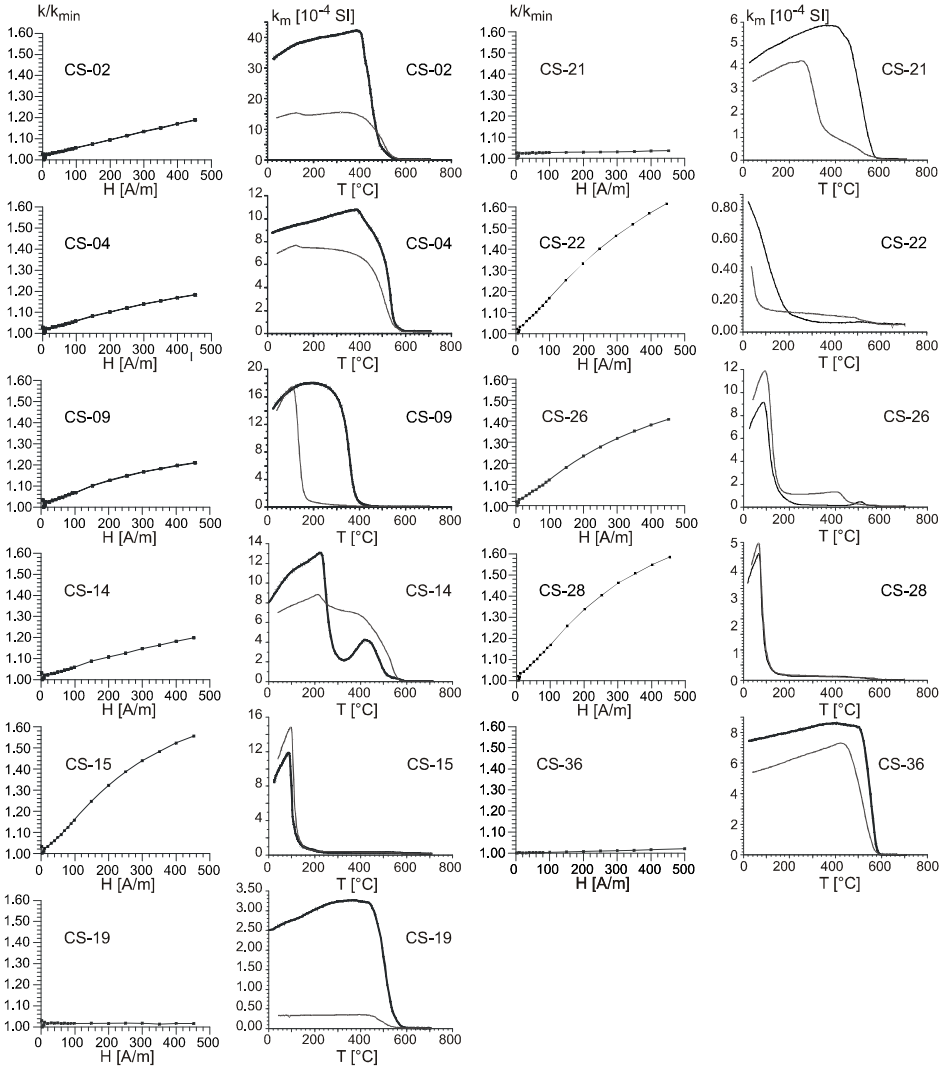

Fig. 6. Curves of temperature and field variations of magnetic susceptibility for analogous rock types in the České středohoří Mts. region. The full heating curve (black) and the cooling curve (grey) were obtained by heating from room temperature up to 700°C and cooling again to room temperature. The variations in magnetic susceptibility, as a function of AC field, were measured in the field intensity gradually increased from 2 to 700 A/m (peak values). Powdered samples were heated in air atmosphere.

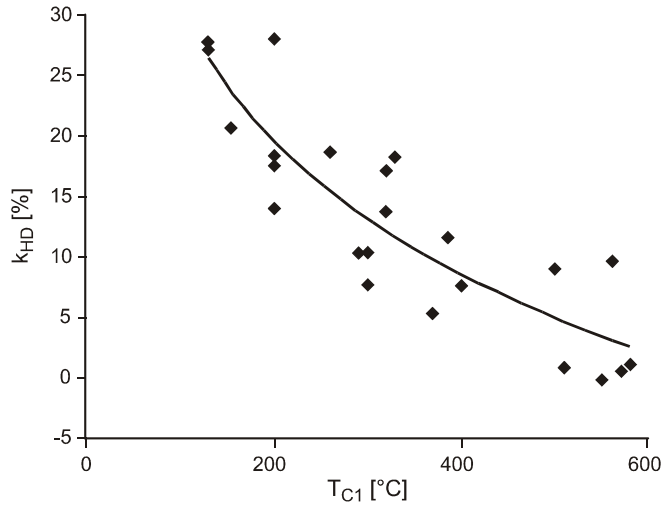

Fig. 7. Plot of T_{C1} versus k_{HD} demonstrates a logarithmic function, which is in agreement with *Vahle and Kontny (2005)*.

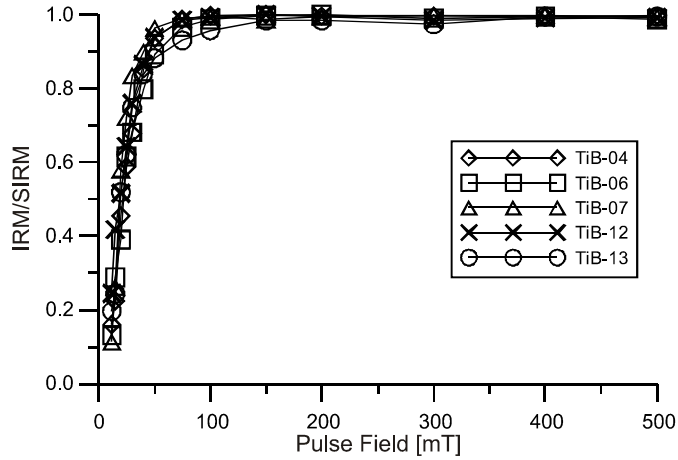

Fig. 8. Normalized IRM acquisition curves for 5 representative samples from the Krušné hory Mts. *SIRM* falls in the range 185–901 A/m. Field B1/2 when half of the SIRM is reached (*Kruiver et al., 2001*) ranges between 15 and 53 mT.

In comparison, data from similar rock types in the CS region show a much wider variety; their k_{HD} range between 0 and 28% (Fig. 6). We found a logaritmic function between T_{C1} and k_{HD} for samples from both regions (Fig. 7), which is in agreement with Vahle and Kontny (2005).

Table 3. Mean coercivity $B_{1/2}$ and dispersion *DP* acquired by IRM component analysis (*Kruiver, 2001*).

Sample	$B_{1/2}$ [mT]	log($B_{1/2}$)	*DP*
TiB-04	20.6	1.31	0.35
TiB-06a	18.3	1.26	0.32
TiB-06b	50.1	1.70	0.46
TiB-06c	50.1	1.70	0.53
TiB-07	17.0	1.23	0.26
TiB-08	15.5	1.19	0.35
TiB-13a	20.5	1.31	0.06
TiB-13b	28.2	1.45	0.51
TiB-15	53.7	1.73	0.47
TiB-19	50.1	1.70	0.47
TiB-23	50.1	1.70	0.46
TiB-25	45.7	1.66	0.53

Table 4. Magnetic properties of samples from the Krušné hory Mts. M_S - saturation magnetization, M_r - saturation remanence, H_c - coercive force, H_{cr} - remanent coercive force.

Sample	M_r [mAm^2/kg]	M_S [mAm^2/kg]	M_r/M_S	H_c [mT]	H_{cr} [mT]	H_{cr}/H_c
TiB-06	222.7	3295	0.083	5.40	19.65	3.64
TiB-13	146.4	865.4	0.169	7.69	19.53	2.54
TiB-15	204.4	783.4	0.261	10.21	19.30	1.89
TiB-18	530	3878	0.137	8.27	18.52	2.24
TiB-19	480.2	2862	0.168	11.45	29.40	2.57
TiB-23	578.7	3146	0.184	9.32	30.04	3.22
TiB-25	222.3	845	0.264	9.12	19.10	2.09

4.3. IRM Acquisition

Nine samples with different spinel compositions were chosen for the IRM acquisition study. Their coercivity spectra show small differences (Fig. 8). Component $B_{1/2}$ ranges between 15 and 53 mT (Table 3), which is considerably lower than $B_{1/2}$ (21.9–79.4 mT) obtained by *Grygar at al. (2003)* and roughly corresponds to $B_{1/2}$ (35.4–50.1 mT) obtained by *Robertson and France (1994)*. This is probably caused by high Ti, Al and Mg constituent of volcanogenic spinels compared to sedimentary magnetite or laboratory-prepared mixtures.

4.4. Hysteresis

Hysteresis parameters (Table 4) and curves (Fig. 9) for the KH samples document pseudo-single-domain (PSD) particles. The Day plot (*Day at al., 1977*) with mixing lines after *Dunlop (2002)* shows pseudo-single-domain behaviour for samples TiB-06, 13, 19 and 23, while samples Tib-18, CS-14 and CS-36 fall close to the SD–MD (single-domain to multidomain) mixing curve (Fig. 10). Samples TiB-15 and 25 are exceptional due to their slightly wasp-waisted shape, and probably contain a mixture of super paramagnetic and single-domain grains. Sample CS-19 is clearly a multidomain one.

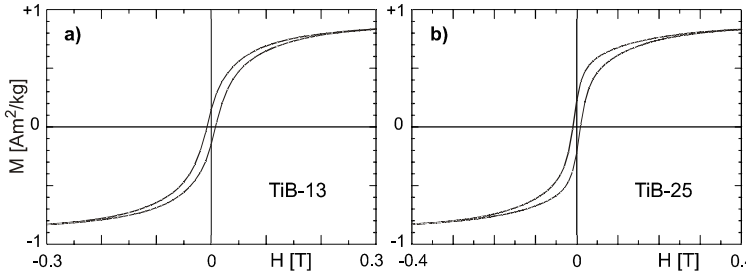

Fig. 9. Two typical hysteresis loops from the area studied. **a)** PSD particle; **b)** slightly wasp-waisted shape caused by a mixture of PSD and SP particles (cf. *Tauxe et al., 1996*).

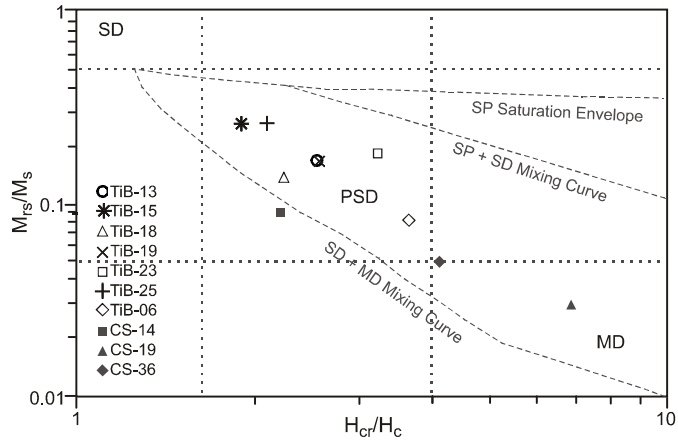

Fig. 10. Day diagram modified by *Dunlop (2002)*. Samples TiB-06, 13, 19 and 23, are PSD or a mixture of SD and MD particles; TiB-18, CS-14, 19 and 36 are close to the SD-MD mixing curve; Samples TiB-15 and 25 are in the PSD area close to the SP saturation envelope.

5. CONCLUSIONS

A moderate positive correlation was found between ulvöspinel and/or hercynite components and field-dependent susceptibility k_{HD}. A lower degree of correlation is caused by small variability of ulvöspinel component in the studied samples. A very strong positive correlation was proved between field-dependent susceptibility and the magnesioferrite component. Low to moderate negative correlation was proved between the Curie temperature and ulvöspinel, magnesioferrite and/or hercynite components, respectively.

The theoretical Curie temperature T_C^{theo} can be calculated from the mole fraction of ulvöspinel x as $T_C\,[°\mathrm{C}] = 578 - 580x - 150x^2$ (*Clark, 1997*).

In our case, the measured Curie temperature T_{C1} is higher than T_C^{theo} (Table 5). On the contrary, T_{C1} should be lower because of abundant aluminium and magnesium which should decrease the Curie temperature of the spinel group minerals. Solution of this question needs further investigation.

Standard deviation for T_C and k_{HD} from the CS region is twice as high as for those from the KH region, while the mean is slightly lower for the KH region. The shape of the MS curves for the CS samples shows titanomagnetite behaviour without any phase changes or alterations, while the KH samples indicate exsolution of ilmenite lamellae during laboratory heating.

No magnetic property is influenced by the whole-rock TiO_2 contents, the best example is CS-15 with the lowest whole-rock TiO_2 content and the lowest Curie temperature and one of the highest k_{HD}, which is quite the opposite to which should be expected.

We found neither a direct proportion nor any correlation between TiO_2 contents in the whole rock analyses and the structure of titanomagnetite. These two phenomena are totally independent. Titanium is present not only in different types of titanomagnetite but also in Ti-bearing silicates such as Ti-bearing diopside, Ti-Ba phlogopite, kaersutite, titanite, and in oxides such as ilmenite and perovskite.

In the western KH, the Cenozoic igneous activity proceeded in two volcanic episodes. According to recent results of K-Ar geochronological data, their ages range between 33–28.5 Ma and 25.6–11.9 Ma. From our samples, two sites (TiB-04 and 23) are attributed to the first sequence, while most high-Ti basaltic rocks are related to the second sequence. Moreover, there exists no time span in which the high-Ti basaltic rocks can be grouped. A more realistic idea is a spatial dependence of incidence of these rocks from a local Ti-enriched mantle source or more probably an enrichment of the ascending magma *en route*. Based on alkali pyroxenite xenolithic material in the Ti-rich basaltic magmas, we assume a contact of basaltic melt with an alkali pyroxenite body in a crustal position. This supposed body can be closely connected with the deeper subvolcanic apparatus of the Loučná-Oberwiesenthal volcanic centre.

Table 5. Theoretical T_C^{theor} using the formula presented by *Clark (1997)* compared to actual T_C.

Sample	Ulvospinel [%]	Theoretical T_C^{theor} [°C]	Measured T_{C1} [°C]
TiB-03	44.94	287	200
TiB-04	48.00	265	320
TiB-06	37.21	341	400
TiB-07	36.00	350	300
TiB-08	54.80	215	300
TiB-12	55.78	208	260
TiB-13	55.73	208	320
TiB-15	53.03	228	200
TiB-18	46.23	278	370
TiB-19	42.04	308	290
TiB-23	58.64	186	330
Average		261	299
Standard deviation		54	59

Acknowledgements: This study was supported by the Grant Agency of the Academy of Sciences CR, project IAA 300130706, and falls within the Academic Research Plan AV0Z 30130516. K-Ar dating was supported by OTKA projects No. T043344 and M41434 and performed within the Hungarian-Czech Project of cooperation of the Academy of Sciences. The authors wish to acknowledge Z. Korbelová for electron microprobe analyses, Z. Řanda for INAA of titanium, J. Drahotová, T. Elbra, D. Venhodová and J. Petráček for technical assistance. We are especially grateful to P. Suhr from the Sächsisches Landesamt für Umwelt und Geologie in Freiberg for a close cooperation.

References

Balogh K., 1985. K/Ar dating of Neogene volcanic activity in Hungary. Experimental Technique, Experience and Methods of Chronological Studies. *MS ATOMKI Reports*, **1**, Debrecen, Hungary, 277–288.

Burri C., 1959. *Petrochemische Berechnungsmethoden auf äquivalenter Grundlage (Methoden von P. Niggli)*. Birkhäuser Verlag, Basel, Switzerland, 334 pp. (in German).

Cajz V., Vokurka K., Balogh K., Lang M. and Ulrych J., 1999. The České středohoří Mts.: Volcanostratigraphy and geochemistry. *Geolines*, **9**, 21–28.

Cajz V., 2000. Proposal of lithostratigraphy for the České středohoří Mts. volcanics. *Bull. Czech Geol. Surv.*, **75**, 7–16.

Chadima M., Cajz V. and Týcová P., 2008. On the interpretation of normal and inverse magnetic fabric in dikes: Examples from the Eger Graben, NW Bohemian Massif. *Tectonophysics*, **466**, 79–88, doi: 10.1016/j.tecto.2008.09.005.

Clark D.A., 1997. Magnetic petrophysics and magnetic petrology: aids to geological interpretation of magnetic surveys. *AGSO J. Austr. Geol. Geophys.*, **17(2)**, 83–103.

Day R., Fuller M. and Schmidt V.A., 1977. Hysteresis properties of titanomagnetites: Grain size and composition dependence. *Phys. Earth. Planet. Inter.*, **13**, 260–267.

Dunlop D.J., 2002. Theory and application of the Day plot (Mrs/Ms versus Hcr/Hc) 2. Application to data for rocks, sediments, and soils. *J. Geophys. Res.*, **107(B3)**, 2057, doi: 10.1029 /2001JB000487

Dunlop D.J., Özdemir Ö. and Denis G., 2006. Rancourt magnetism of biotite crystals. *Earth Planet. Sci. Lett.*, **243**, 805–819.

Golla-Schindler U., O'Neill H.St.C. and Putnis A., 2005. Direct observation of spinodal decomposition in the magnetite-hercynite system by susceptibility measurements and transmission electron microscopy. *Am. Miner.*, **90**, 1278–1283.

Grygar T., Dědeček J., Kruiver P.P., Dekkers M.J., Bezdička P. and Schneeweiss O., 2003. Iron oxide mineralogy in late Miocene red beds from La Gloria, Spain: rock-magnetic, voltammetric and Vis spectroscopy analyses. *Catena*, **53**, 115–132.

Haase K.M. and Renno A.D., 2008. Variation of magma generation and mantle sources during continental rifting observed in Cenozoic lavas from ther Eger Rift, Central Europe. *Chem. Geol.*, **257**, 195–205.

Herre R., 1930. Petrographische und chemische Untersuchung jünger Eruptivgesteine in der Umgebung von Oberwiesenthal im Erzgebirge. *Chem. Erde*, **4**, 632–665 (in German).

Kropáček V., 1976a. Magnetic properties of volcanic rocks. *Čas. Mineral. Geol.*, **21**, 113–135 (in Czech).

Kropáček V., 1976b. Magnetic properties of young volcanic rocks of Bohemian Massif. *Publ. Inst. Geophys., Pol. Acad. Sci.*, **C-1(102)**, 65–73.

Kropáček V., 1985. *Magnetic Properties of Young Alcaline Volcanic Rocks from Central Europe*. DrSc. Thesis. Geophysical Institute AS CSSR, Prague, Czech Republic (in Czech).

Kropáček V. and Pokorná Z., 1975. Magnetische Eigenschaften basischer neovulkanischer Gesteine der Böhmischen Masse und ihre Zusammenhänge mit petrologischen Charakteristiken. *Travaux Geophys.*, **XXI** (in German).

Kruiver P.P., Dekkers M.J. and Heslop D., 2001. Quantification of magnetic coercivity components by the analysis of acquisition curves of isothermal remanent magnetisation. *Earth Planet. Sci. Lett.*, **189**, 269–276.

Lattard D., Engelmann R., Kontny A. and Sauerzapf U., 2006. Curie temperature of synthetic titanomagnetites in the Fe-Ti-O system: Effects of composition, crystal chemistry, and thermomagnetic methods. *J. Geophys. Res.*, **111**, B12S28, doi: 10.1029/2006JB004591.

Le Maitre R.W. (Ed.), 1989. *A Classification of Igneous Rocks and Glossary of Terms*. Blackwell Sci. Publ., Oxford, U.K.

Lustrino M. and Wilson M., 2007. The circum-Mediterranean anorogenic Cenozoic igneous province. *Earth Sci. Rev.*, **81**, 1–65.

Odin G.S., Worsley T.R. and 35 collaborators, 1982. Interlaboratory standards for dating purposes. In: Odin G.S. (Ed.), *Numerical Dating in Stratigraphy*. Wiley and Sons. New York, 123–149.

O'Reilly W. and Banerjee S.K., 1966. Oxidation of titanomagnetites and self-reversal. *Nature*, **211**, 5044, 26–28.

Pfeiffer L., Kaiser G. and Pilot J., 1984. K-Ar-Datierungen von jungen Vulkaniten im Süden der DDR. *Freiberger Forschungshefte*, **C389**, 93–97 (in German).

Robertson D.J. and France D.E., 1994. Discrimination of remanence-carrying minerals in mixtures, using isothermal remanent magnetisation acquisition curves. *Phys. Earth Planet. Inter.*, **82**, 223–234.

Řanda Z., Frána J., Mizera J., Kučera J., Novák J.K., Ulrych J., Belov A.G. and Maslov O.D., 2007. Instrumental neutron and photon activation analysis in the geochemical study of phonolitic and trachytic rocks. *Geostand. Geoanal. Res.*, **31**, 275–283.

Shrbený O., 1980. Chemical composition of alkaline neovolcanics of the Krušné hory Mts., Bohemia. *Věst. Ústř. úst. geol.*, **55**, 1–10 (in Czech).

Suhr P., 1999. Phreatomagmatic Structures in the Northern Environs of the Ohře Rift (Saxony). *Geolines*, **9**, 119–122.

Tauxe L., Mullender T. and Pick T., 1996. Potbellies, wasp-waists and superparamagnetism in magnetic hysteresis. *J. Geophys. Res.*, **101**, 571–583.

Ulrych J., Lloyd F.E., Balogh K., Hegner E., Langrová A., Lang M., Novák J.K. and Řanda Z., 2005. Petrogenesis of alkali pyroxenite and ijolite xenoliths from the Tertiary Loučná - Oberwiesenthal Volcanic Centre, Bohemian Massif in the light of new mineralogical, geochemical, and isotopic data. *J. Miner. Abh.*, **182/1**, 57–79.

Vahle C. and Kontny A., 2005. The use of field dependence of AC susceptibility for the interpretation of magnetic mineralogy and magnetic fabrics in the HSDP-2 basalts, Hawaii. *Earth Planet. Sci. Lett.*, **238**, 110–129.

Vahle C., Kontny A., Gunnlaugsson H.P. and Kristjansson L., 2007. The Stardalur magnetic anomaly revisited - new insight into a complex cooling and alteration history. *Phys. Earth Planet. Inter.*, **164**, 119–141.

Cajz V., **Schnabl P.**, Pécskay Z., Skácelová Z., Venhodová D., Šlechta S. a Šifnerová K.

Chronological implications of paleomagnetic record of the Late Cenozoic volcanic ctivity in Moravo-Silesian border – NE Bohemian Massif

Geologica Carpathica – Přijato do tisku

Chronological implications of paleomagnetic record of the Late Cenozoic volcanic activity in Moravo-Silesian border – NE Bohemian Massif

VLADIMÍR CAJZ[1], PETR SCHNABL[1], ZOLTAN PÉCSKAY[2], ZUZANA SKÁCELOVÁ[3], DANIELA VENHODOVÁ[1], STANISLAV ŠLECHTA[1] and KRISTÝNA ŠIFNEROVÁ[1]

[1] Institute of Geology AS CR, v.v.i., Rozvojová 269, 165 00 Praha 6, Czech Republic; cajz@gli.cas.cz; schnabl@gli.cas.cz; slechta@gli.cas.cz; sifnerova@gli.cas.cz
[2] Institute of Nuclear Research of the Hungarian Academy of Sciences, Bem tér 18/C, H-4001 Debrecen, Hungary; pecskay@namafia.atomki.hu
[3] Czech Geological Survey, Erbenova 348, 790 01 Jeseník, Czech Republic; zuzana.skacelova@geology.cz

Abstract: This paper presents the results of a paleomagnetic study carried out on Plio-Pleistocene Cenozoic basalts from the NE part of the Bohemian Massif. Paleomagnetic data were supplemented by 27 newly obtained K/Ar age determinations. Lavas and volcaniclastics of 6 volcanoes were sampled. Declination and Inclination values of paleomagnetic vector vary in the spans of 130 to 174 and -85 to -68° for reversed polarity (Pleistocene); or 345 to 350° and around 62° for normal polarity (Pliocene). Volcanological evaluation and compilation of older geophysical data from field survey served as the basis for the interpretation of these results. The Pleistocene volcanic stage consists of two volcanic phases, fairly closely spaced in time. Four volcanoes constitute the Bruntál Volcanic Field; two others are located 20 km to the E and 65 km to the NW, respectively. The volcanoes are defined as monogenetic ones, producing scoria cones and lavas. Exceptionally, the largest volcano shows a possibility of remobilization during the youngest volcanic phase, suggested by paleomagnetic properties. The oldest one (4.3–3.3 Ma), Břidličná Volcano, was simultaneously active with the Lutynia Volcano (Poland) which produced the Zálesí lava relic (normal polarity). Three other volcanoes of the volcanic field are younger and reversely polarized. The Velký Roudný Volcano was active during the Gelasian (2.6–2.1 Ma) and possibly could have been reactivated during the youngest (Calabrian, 1.8–1.1 Ma) phase which gave birth to the Venušina sopka and Uhlířský vrch volcanoes. The reliability of all available K-Ar data was evaluated using a multidisciplinary approach.

Key words: Plio-Pleistocene basalts, paleomagnetism and magnetostratigraphy, volcanology, K/Ar dating, airborne magnetometry and gravimetry, Moravia and Silesia

Introduction

Cenozoic volcanism in the NE part of the Bohemian Massif occurs prevalently in Polish Silesia. It stretches to the territory of the Czech Republic to a limited extent only. The volcanic locations of this wider area constitute the Odra Tectono-Volcanic Zone (OTVZ, *sensu* Kopecký 1987) of the WNW–ESE strike, as a part of the so-called Bohemo-Silesian Volcanic Arc. Volcanic rocks are located mostly inside the Fore-Sudetic Block which is limited by the Odra Fault in the NE (outside the studied area in

Poland) and the Sudetic Marginal Fault (SMF) in the SW, and elongated parallel to the OTVZ.

Basaltic volcanic products in northern Moravia and southernmost Silesia belong to the youngest ones in the territory of the Bohemian Massif (e.g. Ulrych et al. 2011). Their composition ranges mostly between olivine nephelinite and nepheline basanite (e.g. Barth 1977; Fediuk and Fediuková 1985, 1989; Ulrych et al. 1999; and others). These volcanics represent primitive basaltic magmas (Vokurka and Bendl 1992, 1993), much like most other similar Cenozoic volcanics in the Bohemian Massif. These rocks were studied in their paleomagnetic properties by Marek (1969, 1973, 1974) and Kolofíková (1976), in the Czech Republic and by Birkenmajer et al. (2002) in Poland.

Volcanic occurrences of this wider region concentrate on three smaller areas in the territory of the Czech Republic. The greatest concentration of basalts is in the Bruntál Volcanic Field (BVF) near Bruntál in the Nízký Jeseník Mts. These basalts are not eroded to a very high degree, and their lavas locally overlie river terraces (e.g. Horský et al. 1972). Unpublished data of Bellon from 1970s (*in* Kopecký 1987) brought first information that they formed in the Pliocene. The Plio-Pleistocene age was confirmed by Šibrava and Havlíček (1980) using the K/Ar method. The second area of basaltic occurrences lies on the Czech–Polish border near Zálesí. No radiometric datings have been published from this location but geological evidence assigns these rocks to the Lutynia area in Poland. The only other separate occurrence near Opava (third area) was dated to the Miocene (Shrbený and Vokurka 1985). The rock of the nearby situated location of Štemplovec has been totally excavated and cannot provide data anymore.

Geological setting and volcanology

Magma of the volcanic occurrences was emplaced into Upper Paleozoic rocks. Only the Lutynia area and the Zálesí area are situated in the Králický Sněžník Crystalline Complex; basalts near Bruntál are hosted/underlain by slightly metamorphosed rocks of the Horní Benešov Fm. and unmetamorphosed rocks of the Moravice Fm., both belonging to the Nízký Jeseník Mts. regional unit (Fig. 1). The Miocene Hůrka Hill near Opava and the occurrence at Štemplovec of unknown age penetrate through the Moravice Fm. sediments only.

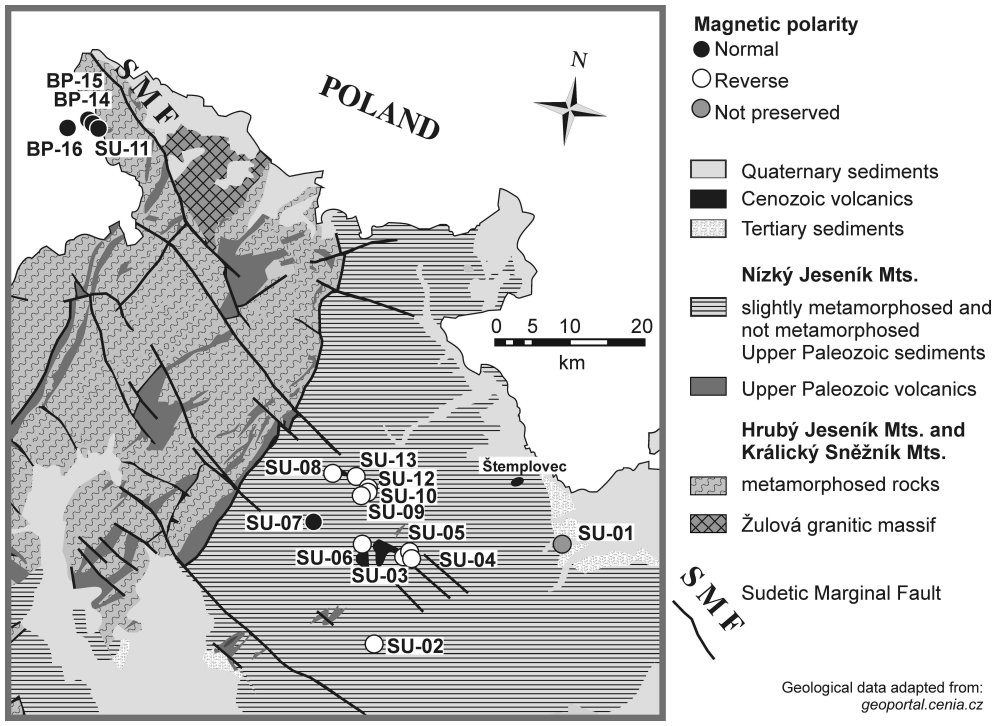

Fig. 1. A simplified geological map showing sampling sites and primary magnetic polarities of the studied rocks. Bruntál Volcanic Field (BVF) is shown by samples SU-02 to 10 and SU-12+13 in the central part of the frame. Zálesí (SU-11) and samples BP (14 to 16; taken from Birkenmajer et al. 2002) locate the Lutynia area in the NW.

The Sudetic Marginal Fault, separating the Žulová granitic massif from the crystalline complexes of the Králický Sněžník Mts. and the Hrubý Jeseník Mts. in the territory of the Czech Republic, is accompanied by several faults of similar strike in both crystalline complexes. A continuation of one of the closest faults to the SMF, or the continuation of the SMF itself, proceeds to the area of the BVF (see Fig. 1). As the SMF is presently active (Štěpančíková et al. 2010), it could be responsible for some magmatic activity during the Pleistocene or even earlier. A similar scenario of tectonic predisposition was published by Barth (1977).

Volcanic landforms have been described as stratovolcanoes or composite volcanoes. This terminological misunderstanding possibly arose from the first description of Jahn (1907) and an old-fashioned understanding of the presence of both explosive and effusive products. Volcanic activity in the BVF started as somewhat explosive one and produced scoria cones. The explosiveness was partly influenced by contact with water during magma ascent. Palagonitized tuffs were formed. This is best visible at the Venušina sopka Volcano. In this point of view, the role of the SMF-parallel faults during the volcano formation is well acceptable – surface water and ascending magma can meet on fault planes. Nevertheless, this influence was relatively small, and the activity of all the below described volcanoes of the BVF can be described as solely phreatomagmatic at the beginning. Further volcanic activity was of magmatic type, producing scoriae and plastic bombs (Fig. 2a). Then, it passed to an effusive one with smaller or larger lava production (Fig. 2b). This is a typical development of the most common type of a monogenetic volcano. We suppose mostly low-energy magmatic activity of Strombolian type, close to the Hawaiian one.

As Hůrka Hill near Opava represents an old eroded subvolcanic form and Štemplovec site does not provide any data, we focused only on four separate volcanoes and one "rootless" basaltic occurrence.

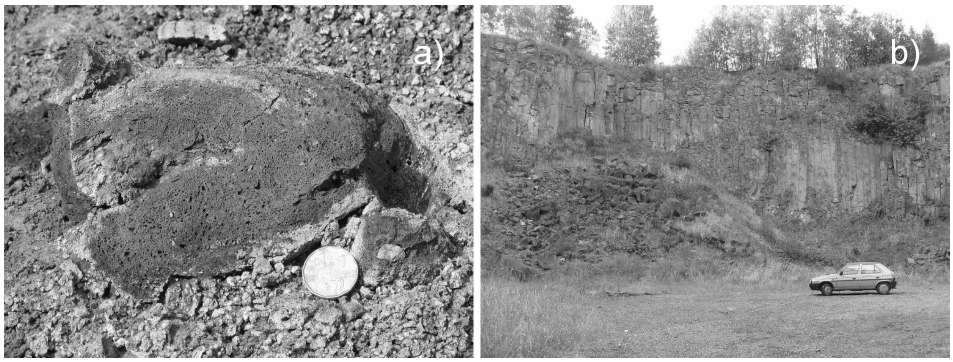

Fig. 2. Selected volcanological features visible in outcrops:
a) – A ballistic-transported plastic bomb from the Uhlířský vrch Hill Volcano (UV) cinder cone.
b) – A thick columnar-jointed lava flow of the Venušina sopka Volcano (Mezina, sampling site SU-10), the change in jointing corresponds to facies development.

Břidličná Volcano (BV)

This is the oldest preserved basaltic rock of the BVF. The volcano is eroded down to the near-surface level of magmatic vent, or just to the pre-volcanic superficial position. The inner-crater facies passing to the vent-breccia is exposed in an old quarry. Semi-plastic bombs are preserved, documenting a position very close to the vent. The majority of clastic material is represented by somewhat altered scoriae and the finest material is possibly primarily reduced in volume. The alteration visible on the outcrop can be caused by syngenetic process (phreatic influence) and by weathering, too. The massive basalt of the plug has been excavated for commercial use. The volcano very probably produced lava(s) but no outcrops are preserved now. Nevertheless, a small relic of lava was observed before exploitation (Jahn 1909). The size of the vent cut suggests a relatively large scoria cone of the Břidličná Volcano at the time of its origin.

Uhlířský vrch Hill Volcano (UV)

This volcano is situated closest to Bruntál. It represents a remnant of a scoria cone with a single thin lava flow extending to the east. Now, two walls of an old quarry expose scoriae, while the central more solid rock has been excavated. The exposed, mostly centroclinally stratified layers (the inner facies) mostly consist of scoriaceous lapilli and bombs. Centripetal layers are developed as well, farther from the feeder. The stratification is visible in grading and in colour: an alternation of more and less palagonitized pyroclastics is visible. This may be a result of a pulsation caused by interaction with water in the vent in the early stages of volcanic activity. Palagonitization decreases upwards while the frequency of semiplastic bombs increases in the same direction. Red- to brown-coloured baked clasts of country rock (accidental pyroclasts) are present. There can be found a relatively great number of large ballistic-transported bombs, which have been deposited as plastic ones. Spindle- to cow dung-shaped forms were observed, sometimes an indication of bread crust-type bomb is visible. These bombs contain primary paleomagnetic field vector – their temperature was above the Curie one. A small outcrop of slightly vesiculated and sonnenbrand-altered lava is hardly detectable in a railway cut 1 km to the E from the vent. The idea of Barth (1977) on the collapse of the cinder cone in its eastern part and production of a single small lava flow in this direction seems to be very realistic.

Venušina sopka Volcano (VS) near Mezina

This is another small volcano of the BVF but with higher effusive activity. The cinder cone in the central part of the hill is the most phreatic-influenced one among the volcanoes of the BVF. Accidental pyroclasts of Paleozioc country rocks are relatively frequent in altered scoriae. Basaltic vesiculated pyroclasts with chilled margins were observed. Spindle-shaped bombs are also present and about 1 m large bomb with a bomb-sag is exposed in an old quarry at the summit. A lava flow over 20 m thick was exploited in two abandoned quarries down on the slope, near the Černý potok Creek (see Fig. 2b). The older quarry described by Jahn (1907) really shows an unconformity dipping 40° to the E, but this does not represent the boundary between "two lava flows": no typical lower and upper facies of flows are developed. The rock is the same on both sides of this boundary; only a small difference in jointing is visible, representing a facies change inside the flow. Most probably, the unconformity originated subparallel to the dip of the lava body during cooling. A younger quarry in the same lava body exposes several facies of the same unit. Lava breccias are developed at the base, and the facies are represented by levels with different intensity of vesiculation and different intensity of sonnenbrand alteration. Columnar jointing runs across all the facies. We suppose that the thickness is not caused by a stacking of several (up to 4!) lava flows. The enormous thickness resulted from a decrease in flow velocity and its stopping by a body of hyaloclastic breccia at the lava front, now mostly eroded. This body was produced by thermal shock at the contact of the lava with an active water flow.

Velký Roudný Hill Volcano (VR)

This is the largest volcano of the BVF. Also, it displays the largest preserved effusive production. Our description of this volcano slightly differs from that of previous authors (e.g., *Barth 1977*). The two summits lying closely apart – Velký ("large") Roudný and Malý ("small") Roudný Hills – were sometimes believed to represent two separate volcanoes. We suppose that Malý Roudný Hill is not an independent volcano. Now, it represents only a part of the same volcano (its cinder cone), separated and modelled by erosion from another summit. This is supported by the presence of a single vent based on the evaluation of geophysical survey. The same idea of a large volcano is suggested from small basaltic occurrences like Volárenský vrch Hill, Křišťanovice and possibly Zlatá Lípa near Červený vrch Hill. All these may represent erosional relics of other flows from the same volcano. No signs of separate vents were found. All the exposed basalts of this position show only signs of lavas. Unfortunately, the outcrops in pyroclastics are poor for comparison. Variation in the chemistry of lava in one flow mentioned by previous authors is a usual phenomenon and cannot be used for the flow determination. Moreover, the compact facies has been altered. We suppose a location of the feeder between the future Velký Roudný and Malý Roudný Hills, building of a large cinder cone with possible (but not proved) parasitic vents and production of several lava flows (3?). The largest preserved flow fills the valley of the paleo-Moravice River (Slezská Harta, Bílčice-Leskovec). Volárna relic represents the second flow. The southern flow can be traced as far as to the proximity of Křišťanovice (4 km) now forming a small erosional relic. Pertinence of the Zlatá Lípa site to this flow is more problematic because of the large distance (ca. 12–13 km). Although it is far from the supposed vent, this connection cannot be excluded. Lava production in several flows can be deduced from the spatial distribution of the relics, not from superposition as no superimposed lavas are exposed now. The largest flow filling the paleovalley of the river shows only several facies, and the unconformity still

visible in the active quarry of Bílčice does not represent a boundary between two units. The enormous thickness of ca. 50 m can be explained by flow deceleration by hyaloclastite breccia which formed at the lava/stream interface at the front and on the surface of the flow. Sediments of fluvial terraces are known to underlie this flow (Horský et al. 1972). Kolofíková (1976) employed anisotropy of magnetic susceptibility to the study of the flow orientation. Her results correspond to the supposed directions of the flow and its facies development (*see also* Tarling and Hrouda 1993). The lens-like layer of porcelanite-rich material in the old quarry (near the lava front) mentioned in Barth and Zapletal (1978) and interpreted as a boundary between two flows may also represent a hyaloclastite breccia (not preserved now).

The volcanological results briefly described above were tested using the orientation of the paleomagnetic field vector and evaluation of magnetic and gravimetric regional fields. K/Ar dating was used as well.

The paleogeographic reconstruction of this volcano (Cajz et al. 2010) also incorporated two other sites of tuffites near the villages of Karlovec and Razová (Barth and Zapletal 1978). Our opinion on their origin is again only slightly different from previous authors. The source area for most of the scoriaceous material in tuffites can be placed in an old cone of the Břidličná Volcano, destroyed and transported by the paleo-Moravice River. The country rock surrounding this volcano (low-grade metamorphosed slates) was removed together with the scoriaceous material. Sedimentary clasts of the tuffites are low-grade metamorphosed rocks which do not correspond with the country rock of the tuffites. During effusive activity of the younger Velký Roudný Hill Volcano, a lava dam-lake was formed, the stream gradient of the river got changed, and the mixed pyroclastic-sedimentary material was deposited in the lake. Afterwards, the river used a contact of lava and the former valley side to cut the present Moravice River channel. Some of the scoriae in tuffites were possible also produced during the activity of the Velký Roudný Volcano. This can be documented by the volume of redeposited pyroclasts in the sedimentary record at Razová, which shows a very slow increase in upwards direction. We cannot exclude production of pyroclastic flows or surges into this small sedimentary basin during the possible younger VR activity. In the case of this remobilisation, the term “monogenetic” used for this volcano is questionable.

Zálesí lava flow

This erosional remnant is situated at the Czech–Polish border near Zálesí and has no vent in the territory of the Czech Republic. We suppose the production of this lava from the Lutynia area (Poland) where the vent is located, 1–2 km from the sampled location. The idea of this relation was tested using a comparison of magnetic properties of basalts on both sides of the border, comparing data of the Zálesí lava flow and previously published data from Lutynia (Birkenmajer et al. 2002).

Methods of study

Paleomagnetic and basic rock-magnetic studies

The previous studies by Krs (1968) and Marek (1969, 1973) first discovered reversed polarity in the BVF, with the exception of the Břidličná Volcano which is normally polarized. The latter author (Marek 1974) measured normal polarity at the Zálesí lava flow, which is the closest Czech location to the Polish sites, and discovered normal polarity of the basaltic occurrence from Ladek Zdrój. We have confirmed the older data obtained on an astatic magnetometer using greater number of samples and different measurement techniques (see below). Normal polarity was recently detected by Birkenmajer et al. (2002) in the Lutynia area in Poland.

Thirteen sites in the territory of the Czech Republic were newly sampled and processed. Hand-operated drilling on outcrops provided 216 laboratory samples. The natural remanent magnetization was measured using the JR5a and JR6 spinner magnetometers and 755R superconducting rock magnetometer made by AGICO and 2G Enterprises, respectively. The samples for measuring were predominantly chosen according to Koenigsberger ratio (Q-parameter) which should be lower than 10; however on the Břidličná volcano was proved that Q-parameter can primarily reach over 40. The samples were demagnetized by alternating field in LDA-3a demagnetizer and 2G600 automatic sample degaussing system in 8 to 9 successive fields between 2 and 80 mT, and thermally demagnetized in MAVACS apparatus at temperatures between 80 and 600 °C with a 40° step. On most of the samples were recorded two Curie temperatures T_{c1}=160-200° (300°) C and T_{c2}=500-580°C (Tab. 1).

code	site	area	volcano	landform	N	E	Curie temp. A(°C)	Curie temp. B(°C)	Q-ratio	pol.	declin. (°)	inclin. (°)	α 95 (°)	n/N	age *prev. studies*	age *ATOMKI*
SU-01	Kamenná hora u Otic	Opava	Otice	vent eroded	49°54.828´	17°51.541´	200		2.8	???	*206*	*-13.8*	5.4	12/12	20 ± 3 SV	
SU-02	Zlatá Lípa (Červená h.)	BVF	VR?	lava relic	49°46.455´	17°31.727´		580	0.9	R	173.9	-83.5	4.2	9/9	1.24 LW	1.79 ± 0.15
SU-03	Bílčice quarry	BVF	VR	lava-S.margin	49°53.032´	17°34.385´	200	520	1.2	R	165.3	-75.8	3.7	25/25	2.7 ± 0.5 SH	2.33 ± 0.14
SU-04	Slezská Harta 1	BVF	VR	lava-N.margin	49°53.230´	17°34.690´	200	560	1.6	R	166.1	-76	4.8	19/20	1.46 ± 0.15 SH	2.21 ± 0.16
SU-05	Slezská Harta 2	BVF	VR	lava-surface	49°52.824´	17°34.991´	160	520	2.0	R	157.4	-81.5	5.0	15/22	1.28 ± 0.4 SH	2.37 ± 0.29
SU-06	Volárna	BVF	VR	lava relic	49°53.534´	17°29.352´	200	580	1.2	R	130.8	-75.5	5.1	16/16		2.48 ± 0.31
SU-07	Břidličná	BVF	BV	vent	49°54.726´	17°23.789´	180		30.0	N	349.9	61.5	5.2	6/7		3.74 ± 0.56
SU-08	Bruntál-trať	BVF	UV	lava relic	49°58.302´	17°27.923´	200	560	1.1	R	140.5	-68.5	4.2	10/10	2.4 ± 0.5 SH	1.54 ± 0.15
SU-09	Mezina 1	BVF	VS	lava	49°57.597´	17°29.358´	200	560	4.6	R	145.1	-79.6	5.2	16/16	1.94 ± 0.22 SH	1.26 ± 0.16
SU-10	Mezina 2	BVF	VS	lava	49°57.475´	17°29.226´	200	560	0.5	R	172.1	-84.8	3.6	17/17		0.83 ± 0.12
SU-11	Zálesí u Javorníka	Lutynia	Lutynia	lava relic	50°21.300´	16°55.369´	300	500	17.5	N	345	62.8	3.6	20/20		
SU-12	Venušina sopka	BVF	VS	bomb-cinder c.	49°57.007´	17°28.733´		580	4.6	R	134	-78.4	3.9	17/17	1.11 LW	2.14 ± 0.08
SU-13	Uhlířský vrch	BVF	UV	bomb-cinder c.	49°58.366´	17°25.339´		580	8.7	R	138.7	-83.8	3.1	16/25	1.47 LW	
BP-14	Lutynia-active quarry	Lutynia	Lutynia	plug	50°21.574´	16°54.671´				N	345*	67*	3.7*			4.56 ± 0.20*
BP-15	Lutynia-old quarry	Lutynia	Lutynia	lava	50°21.827´	16°54.091´				N	348*	62*	4.4*			3.83 ± 0.17*
BP-16	Ladek Zdrój	Lutynia	?	lava	50°21.121´	16°51.849´				N	359*	61*	3.6*			5.46 ± 0.23*

explanations:

BVF = Bruntál Volcanic Field
* = paleomagnetic and radiomagnetic data from Birkenmajer et al. 2002
R - reversed polarity; N - normal polarity
n - number of samples used for statistics
N - number of measured samples
n ≤ N - reasons described in text
SH = Šibrava and Havlíček 1980
SV = Shrbený and Vokurka 1985
LW = Lustrino and Wilson 2007

Table 1: Paleomagnetic and radiometric data for the sampling sites, data of Birkenmajer et al. (2002) are added for comparison. Curie temperature A and B is adequate to T_{c1} and T_{c2}, respectively. Abbreviations of volcanoes: VR – Velký Roudný Hill, BV – Břidličná, VS – Venušina sopka Hill, UV – Uhlířský vrch Hill. For more information on age see Tables 2 and 3 and the text.

A principal component analysis by Kirschvink (1980) was performed for all measured samples and group statistics including mean direction (Fisher 1953) was computed on the distinguished primary components for all sites. The primary components were recorded in the temperature range 320°-560°C or field range 15 – 80 mT.

Representative alternating field and thermal demagnetization curves of four samples are shown in Fig. 3. Magnetic susceptibility was measured by KLY-4S. In order to identify the main magnetic carriers, temperature dependence of magnetic susceptibility was also measured in argon atmosphere from the room temperature up to 600 °C, and field-dependent magnetic susceptibility in the field range of 2–450 A/m. The Curie temperature of 180 °C and the steep field-dependent susceptibility curve (Fig. 4) obtained from the SU-7 site can be explained by the presence of titanomagnetite and other spinelid-group minerals. A similar situation was detected for the volcanics from the Krušné hory Mts. (Schnabl et al. 2010) and corresponds with the findings of Vahle and Kontny (2005).

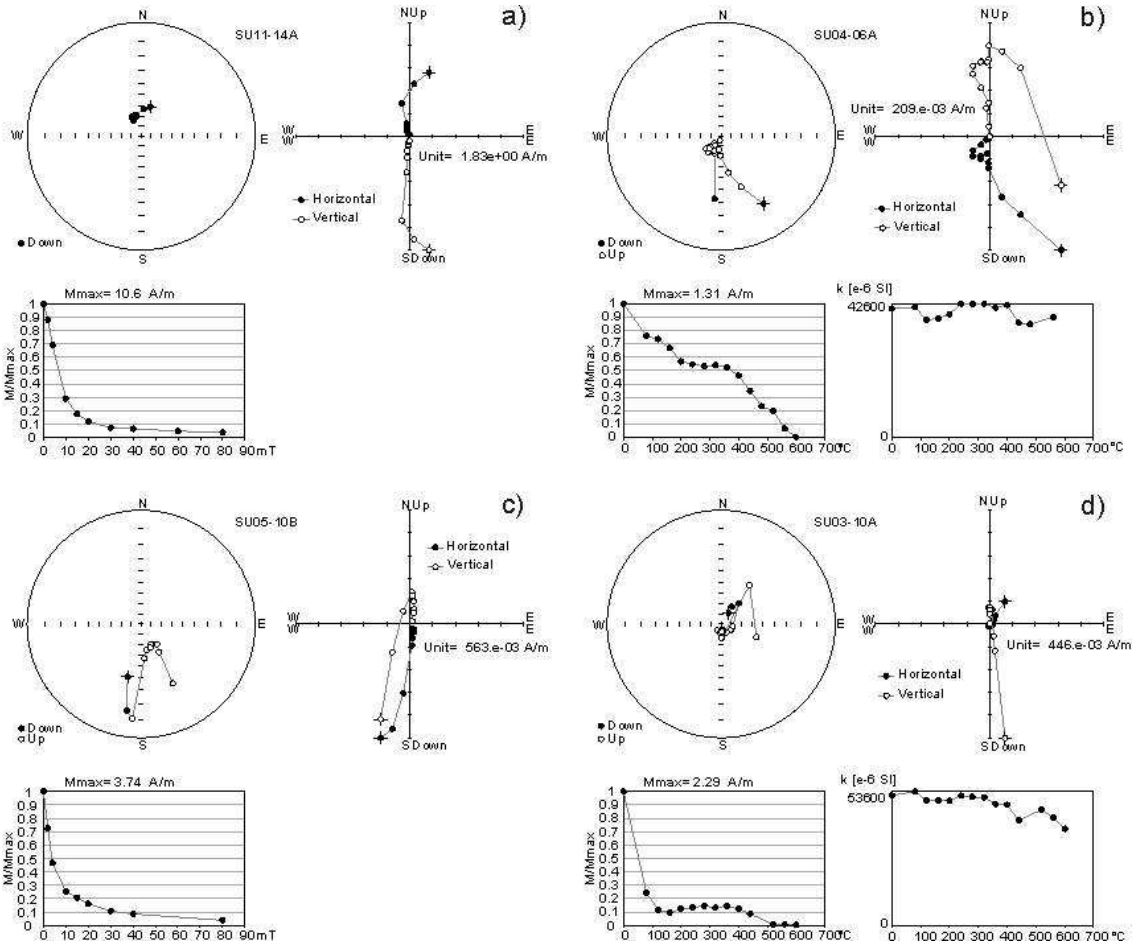

Fig. 3. Demagnetization curves and Zijderveld diagrams of four representative samples:
a) and c) – AC field demagnetization curves of samples show a low-coercivity mineral (magnetite). The reversely polarized sample has a relatively strong viscous component.
b) and d) – A thermal demagnetization curve showing the presence of magnetite with T_{C1} of 160–200 °C and T_{C2} of 560–600 °C and no change in magnetic susceptibility after individual demagnetization steps.

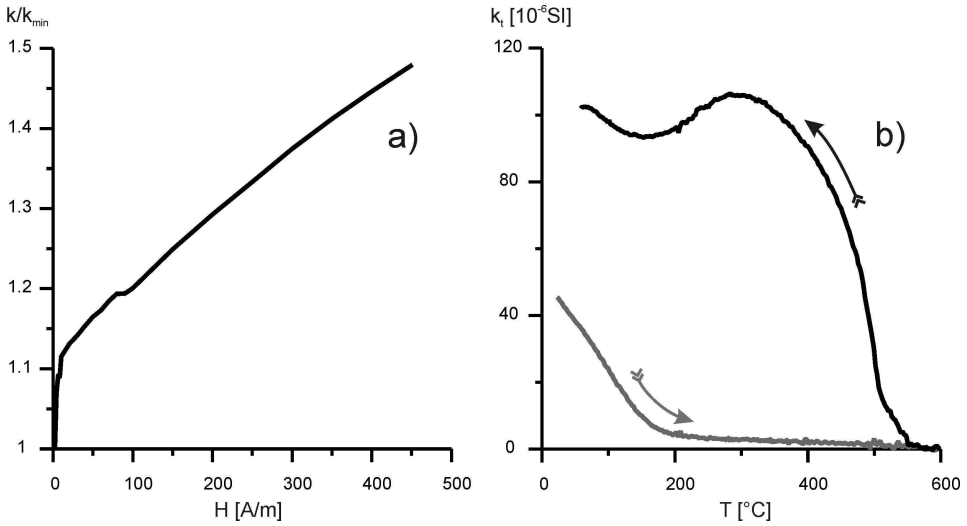

Fig. 4. Basic rock-magnetic measurements at the Břidličná Volcano (SU-07) prove the presence of minerals from the spinelid group (titanomagnetite, etc.):
a) – field-dependent magnetic susceptibility

b) – temperature-dependent magnetic susceptibility shows phase change during laboratory heating. It is caused by newly formed magnetite in the altered rock during the procedure.

Conventional K/Ar age determination

Several authors published radiometric ages of basalts from the BVF (e.g. Šibrava and Havlíček 1980; Kopecký 1987; Lustrino and Wilson 2007). Some data remained unpublished but are accessible in a report (Shrbený and Vokurka 1985). Results from ten years-old set were recently published by Pecskay et al. (2009) as an abstract during a regional conference in Olomouc. Birkenmajer et al. (2002) published data from sites in Polish Silesia close to Zálesí.

K/Ar dating of two data sets of samples was performed in the K/Ar laboratory of the Institute of Nuclear Research of the Hungarian Academy of Sciences (ATOMKI), Debrecen, Hungary. The new K/Ar data set of the BVF was obtained from the same sites as the set for paleomagnetic research. About 200 g of each rock sample were crushed and sieved to 300 μm. Adhering fine particles were removed by rinsing in distilled water. Approximately 0.8 g of sieved sample were weighed for the whole rock. The amount of radiogenic ^{40}Ar was determined by means of the isotope dilution method using ^{38}Ar as a spike. Mass discrimination of argon isotopes was corrected by measuring air Ar. Previously preheated whole rock samples were degassed by RF fusion in Mo crucibles, and usual getter materials (titanium sponge, getter pills of SAES St707 type and cold traps) were used for cleaning and transporting argon. The purified argon was directly introduced into the mass spectrometer (90º magnetic sector type of 150mm radius and operated in the static regime). For the determination of the potassium content, about 1g of the identical sample that was used for Ar measurement was ground in an agate mortar to the grain size finer than 50 μm. About 100 mg of this powdered sample was dissolved in hydrofluoric acid and nitric acid using a teflon bomb. Potassium content was determined by flame photometry with Lithium internal standard (CORNING M 480 flame photometer, digitised). The decay constants of Steiger and Jäger (1977) were used in the age calculation. All analytical errors represent one standard deviation (68% confidence level). Multiple runs of the inter-laboratory standards (Asia 1/65., LP-6, HD-B1. and GL-0) were used for checking the measurements. Details of the instruments, the applied methods and results of the calibration have been described elsewhere (e.g., *Balogh 1985*).

Gravity and airborne magnetometry used for interpretation

Geomagnetic data were acquired by a detailed airborne survey of the Nízký Jeseník Mts. to the scale 1:25,000 in late 1970s (Dědáček and Gnojek 1980). The anomalies were interpreted by Šalanský and Gnojek (2002) and Šalanský (2004). A detailed gravity survey was realized during the early 1970s (with measurement density of 3 points per km^2) and the gravity data were compiled to the Bouguer, regional and residual gravity maps (Kadlec et al. 1972).

The generally monotonous positive regional magnetic field in the study area (except for the distinct positive magnetic Šternberk–Horní Benešov Zone with iron mineralization) is modified by several local anomalies in the Bruntál area induced by Cenozoic volcanics. Reversely polarised volcanic bodies with Q-parameter above 1 cause negative anomalies. Lavas and pyroclastic rocks of the VR Volcano near Leskovec nad Moravicí represent the source of the three distinctive negative anomalies (Fig. 5).). Each negative anomaly in the original maps is accompanied by small positive anomaly on the N. It points to the tabular shape of bodies more than the steep anisometric one. But only detailed field measurements could have specify their geometry. Anomaly of about -10 nT situated to the NE along the Moravice River

reflects the largest preserved volcanic flow. The anomaly of -50 nT to the SW corresponds to Malý Roudný Hill. Central, very distinctive negative magnetic anomaly of about -60 nT coincides with a small local positive gravity anomaly of more that 15 μms^{-2} in the regional gravity survey. Such a type of coincidence is typical for a volcanic vent (e.g. Lidner et al. 2006, Cassidy et al. 2007). The close-up gravity field map places this small positive gravity anomaly close to Velký Roudný Hill. As the magnetic anomalies correspond to the tops of both hills and no solid basalts are known on their summits, the anomalies are supposed to reflect only volcaniclastics. On the other hand, their intensity is higher than that of an anomaly induced by a relatively thick lava flow. The existence of parasitic feeders of a large volcano is one of possible explanations. Volcanologic interpretation of such data is problematic because the results of geophysical survey are not unambiguous. More detailed field geophysical survey is needed for correct specification of geometry and exact location of the vent.

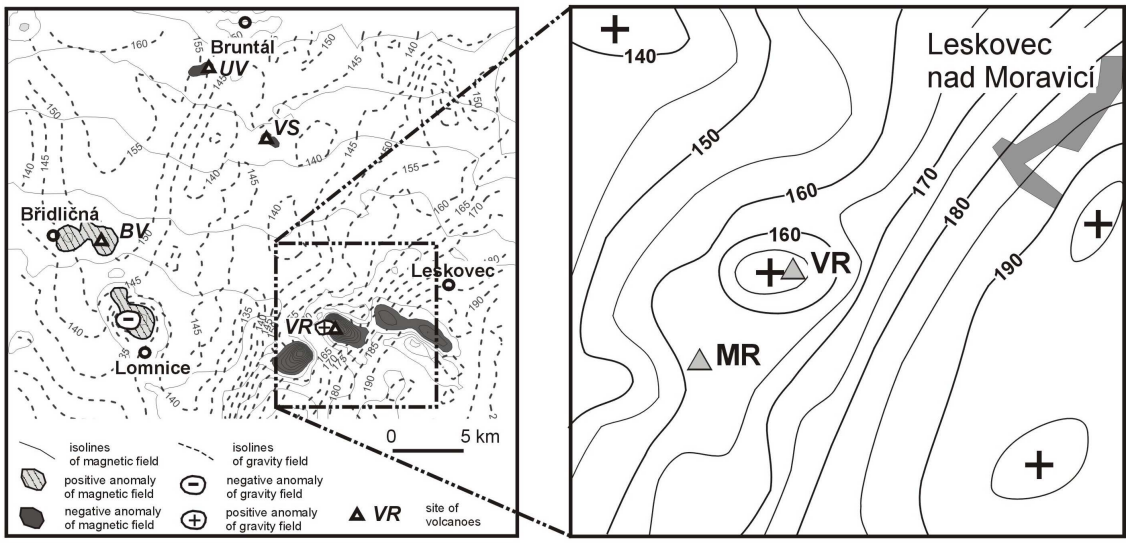

Fig. 5. Summarized regional magnetic [nT] and gravity [μms^{-2}] fields of the Bruntál Volcanic Field (BVF) and a close-up map of the gravity field at Velký and Malý Roudný Hills (VR) – (10 μms^{-2} = 1 mGal). Adapted from Šalanský and Gnojek (2002) and Kadlec et al. (1972).

The Uhlířský vrch Hill (UV) and the Venušina sopka (VS) volcanoes, closer to Bruntál, are characterized by weak negative magnetic anomalies (about -10 nT relative to background). The individual vents cannot be precisely determined from geophysical fields, they are monotonous. The Břidličná Volcano vent is indicated by an elongated local positive magnetic anomaly (normal magnetization). Similar positive magnetic anomaly about 3 km to the S, accompanied by a negative gravity anomaly (-25 μms^{-2}), indicates the supposed buried volcanic maar near Lomnice. This unique phenomenon is visible only in the gravity and magnetic data.

Results

A new volcanological evaluation of the volcano remnants was made. The older volcanological evaluation was generally confirmed. Only in the case of the largest volcano, Velký Roudný Hill and the neighbouring hill of Malý Roudný, our results are slightly different. Basalts of this area were studied in their paleomagnetic properties and several of them were processed to obtain their K/Ar ages. Paleomagnetic results were compared with existing reliable radiometric data. This, together with the analysis of magnetic and gravity fields, allowed to reconstruct volcanic activity in time and space

and supported volcanological evidence. Combination of different approaches resulted in evaluation of the whole set of K-Ar data.

Paleomagnetism

Lavas and bombs from cinder cones on both smaller volcanoes of the BVF (UV and VS) were sampled. The sampled bombs were chosen based on volcanological observation – the plastic type ones (e.g. cow-dung and spindle-shaped) were preferred. Only lavas were accessible at VR. Paleomagnetic results proved that larger bombs were transported above the Curie temperature (560 °C for VS and 400–560 °C for UV). The primary field of explosive and effusive products of Uhlířský vrch Hill is visible in Fig. 6a. The primary field of both lavas and pyroclastics of VS is documented in Fig. 6b. Differences in the paleofields between UV and VS are only 1.3°. Secular variation of all volcanoes is not centred because of the supposed short duration of volcanic activity, complying with relatively short lives of monogenetic volcanoes. From this, we can conclude about a nearly identical time of origin of the two volcanoes, moreover, when K/Ar ages are very close.

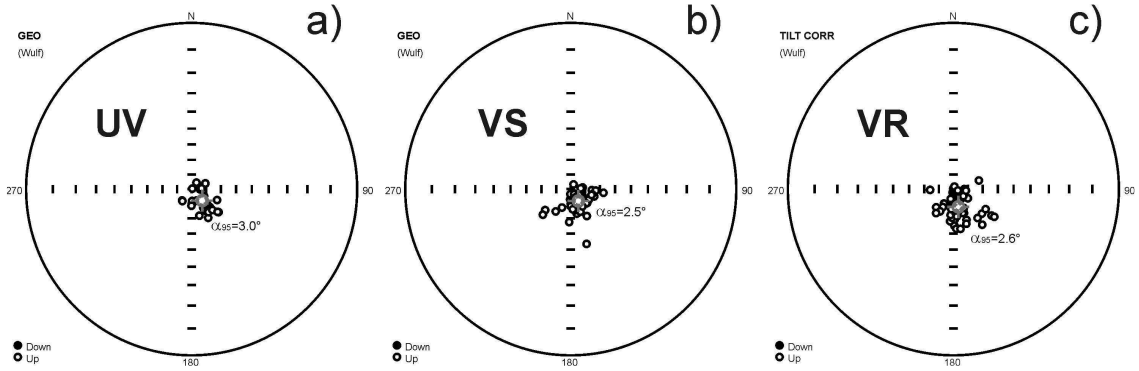

Fig. 6. Summarized paleomagnetic vector projections of the youngest volcanoes:
a) – Uhlířský vrch Hill (UV), pyroclastics and lava. Components computed between 400 and 600°C or 20 -100mT, respectively.
b) – Venušina sopka Volcano (VS), pyroclastics and lava. Components computed between 280 and 560°C or 15-80mT, respectively.
c) – Velký Roudný Hill (VR), lava. Components computed between 320 and 560°C or 15-80mT, respectively.

Paleomagnetic data from the Velký Roudný Volcano (Fig. 6c) were obtained from lava of its largest flow; pyroclastics are not available for sampling. The samples chosen for paleomagnetic evaluation come from the compact facies of the lava flow. Data from site SU-03 (Bílčice quarry) were systematically rotated 13° to the N compared to the others from the same lava flow. Horský et al. (1972) have discovered tilting of large basaltic blocks during the investigation for the dam construction. This finding is in agreement with the geological position of the sampling site and the mechanism of disintegration of the lava body. This was the reason for the apparent heterogeneity of data from one location.

One interesting effect was observed on a-a brecciated surface of the largest lava flow of VR. Figure 7 shows extraordinary distribution of samples taken from breccia clasts, which resulted in α95 value of 23.2° for the whole location. This is caused by a special type of sample – the rotation of clasts from destroyed already cooled surface incorporated into fluidal lava is responsible for this phenomenon. Grouping of these samples shows direction of axis similar to the direction of the flow and very close to the interpreted AMS data of Kolofíková (1976). This phenomenon can be derived from

style of rotation of a-a clasts at the surface in the central part of the flow. Data from only one location cannot be statistically significant; anyway, combination of AMS and direction of remanent magnetisation offers a theme for methodological study on behaviour of a-a lava flows.

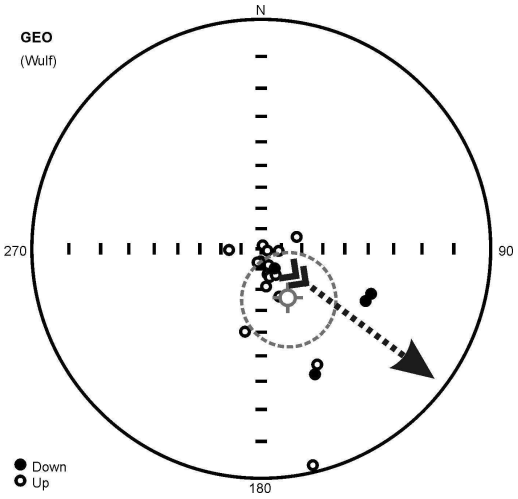

Fig. 7. Paleomagnetic vector projection of the complex data with a-a lava breccia clasts (Slezská Harta lava flow – VR) and the lava flow direction. Components computed between 280 and 600°C or 15-80mT, respectively.

Grouping of all reliable data of the VR lava flow (see Fig. 6c) enabled to compare the paleofield of the largest lava flow from VR with that of smaller volcanoes (UV and VS). The angle between the mean directions of their vectors is 4.5 and 5.0°, respectively. Unfortunately, this small difference does not provide a conclusive basis for magnetostratigraphic interpretation itself. Anyway, it agrees with new radiometric data which divide the reversely polarized volcanic bodies into two separate phases.

A wider difference of 6.4 and 8.0° is obtained if we compare the sites of isolated lava relics of Zlatá Lípa and Volárna, most possibly belonging to the VR volcano, too. From this, we conclude the possibility of production of other flows from the same volcano (VR). The Volárna relic seems to be produced close in time to the main flow, while the Zlatá Lípa relic may represent a younger flow.

Two our sampling sites are normal polarized. The Břidličná Volcano has extremely high Q-parameter (average around 30, but often exceeding 40). Usually, these high values are explained by secondary influence, e.g. the lightning. But in this case, the sampling site is situated in the depth of the old quarry, so the influence by lightning is not realistic. More probable reason can be seen in the titanomagnetite composition (see Fig. 4).

Another normal-polarized occurrence is the lava relic near Zálesí at the Czech–Polish border. Its paleomagnetic characteristics are comparable with those of the basaltic occurrences in the Polish territory (Marek 1974; Birkenmajer et al. 2002), close to the sampling site. Volcanological evaluation proves the relation of this lava relic of Zálesí to the plug of Lutynia. Figure 8 shows very close vector orientations for all normal-polarized volcanics in Lutynia vicinity, including the Břidličná Volcano. This situation can be explained by volcanic activity in a very close time span. The conclusion offers two results: the Zálesí lava flow was produced from the Lutynia Volcano as supposed from geology; and the Břidličná and Lutynia volcanoes were active nearly simultaneously.

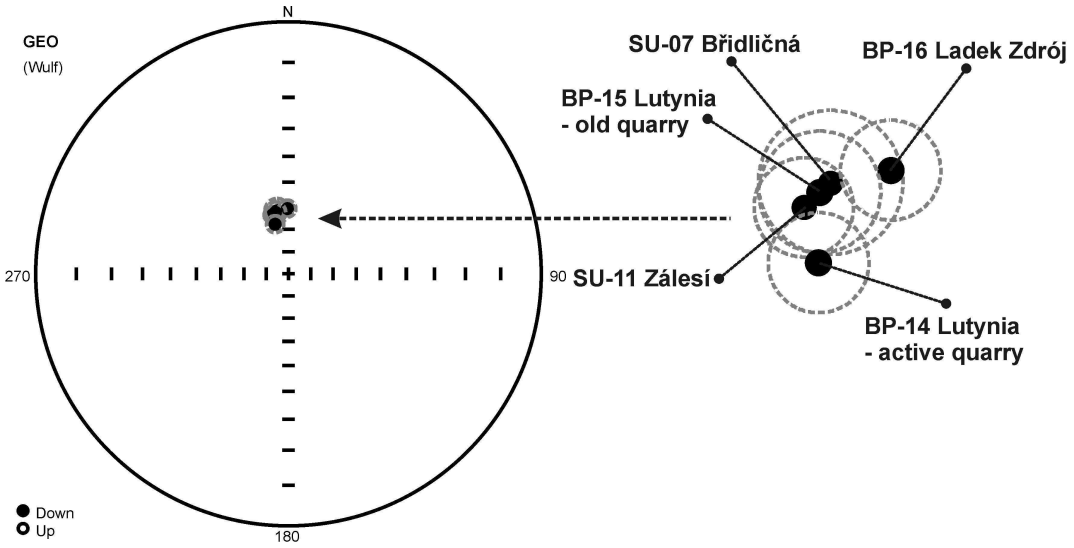

Fig. 8. Paleomagnetic vector projection of the Zálesí lava relic and the Břidličná Volcano vent, compared with products from the Lutynia area. Components computed between 200 and 500°C or 10-80mT, respectively.

The Kamenná hora Volcano near Otice is one of the oldest in the region. The site displays a deeply eroded vent whose volcanic rock was strongly altered. The main magnetic carrier is titanomagnetite (Curie temperature around 200 °C). The mean paleomagnetic directions are D = 206° and I = -14°, similar to those measured by Marek (1974). The inclination is extremely low compared to other Cenozoic rocks. Given the known age of 20 Ma (Shrbený and Vokurka, 1985), the acceptable explanation can be seen in a possible rotation of the only preserved block in an old quarry, most probably due to quarrying activities. This is the reason why we suppose that the primary polarity is impossible to reconstruct (see Fig. 1), and this location is not suitable for paleomagnetic studies.

K/Ar datings

Table 1 compares new data from the laboratory in Debrecen and older data of previous authors from other laboratories. Older data from several sites differ significantly from new ones (Tab. 2), moreover, the localization of several previous sampling sites is very poor (*see e.g.* Lustrino and Wilson 2007). The latter data were published without analytical errors, so their informative value is not fully comparable with the others.

volcano	landform	original site name	adequate to	K/Ar age (Ma)	sampling year	authors
Otice	vent (eroded)	Kamenná hora Hill	SU-01	20 ± 3	?	SV 1985
BV	vent (surface)	Břidličná	SU-07	3.69±0.56	2000	P 2009
VR 1	lava-S.margin	Velký Roudný (Bílčice)	SU-03	3.31±0.24	2000	P 2009
VR 1	lava-S.margin	Bílčice-Leskovec	SU-03	2.7 ± 0.5	?	SH 1980
VR 1	lava-S.margin	Bílčice-Leskovec	SU-03	3.4 ± 0.9	?	SH 1980
VR 1	lava-S.margin	Bílčice	SU-03	2.33±0.14	2010	this paper
VR 1	lava-N.margin	Slezská Harta 1	SU-04	2.21±0.16	2010	this paper
VR 1	lava-surface	Slezská Harta 2	SU-05	2.37±0.29	2010	this paper
VR 1	lava-front	Slezská Harta	*no sample*	1.28 ± 0.4	?	SH 1980
VR 1	lava-front	Slezská Harta	*no sample*	1.46 ± 0.15	?	SH 1980
VR 1	lava-front	Slezská Harta	*no sample*	1.6 ± 0.6	?	SH 1980
VR 1	lava-front	Slezská Harta	*no sample*	2.2 ± 0.9	?	SH 1980
VR 2	lava relic	Volárna	SU-06	2.48±0.31	2010	this paper
VR 2	lava relic	Volárenský vrch	SU-06	2.41±0.14	2000	P 2009
VR?	lava relic	Zlatá Lípa	SU-02	1.75±0.15	2000	P 2009
VR?	lava relic	Zlatá Lípa	SU-02	1.24	1992	LW 2007
VS	lava	Venušina sopka	SU-09, SU-10	0.80±0.11	2000	P 2009
VS	lava	Mezina	SU-09	1.26±0.16	2010	this paper
VS	lava	Mezina	SU-09, SU-10	1.94 ± 0.22	?	SH 1980
VS	bomb-cinder c.	Venušina sopka	SU-12	2.14±0.08	2010	this paper
VS	?	Venušina sopka	?	1.11	1992	LW 2007
UV	?	Uhlířský vrch	SU-08 ?	2,4 ± 0,5	?	SH 1980
UV	lava relic	Bruntál-trať	SU-08	1.54±0.15	2000	P 2009
UV	bomb-cinder c.	Uhlířský vrch	SU-13	1.47	1992	LW 2007
?	?	91/1 - no location	?	0.91	1992	LW 2007
?	?	91/2 - no location	?	1.22	1992	LW 2007
?	?	91/4a - no location	?	4.58	1992	LW 2007

VR1 = Velký Roudný Hill Volcano, its largest lava flow
VR2 = Velký Roudný Hill Volcano, relic of another flow
VR? = relic of possible next younger flow from the Velký Roudný Hill
VS = Venušina sopka Volcano
UV = Uhlířský vrch Hill Volcano

Table 2: All available primary K/Ar age data from the region in the territory of the Czech Republic. For abbreviations of authors see Tab. 1; and P 2009 = Pecskay et al. 2009.

Conventional K/Ar dating of 12 representative whole-rock samples was carried out in two sets (Tab. 3). The first set of 6 samples was collected and analysed 10 years ago. These preliminary data remained unpublished for a long time but were accessible. In the meantime, a new flame photometer (CORNING M 480) has been set up in Debrecen, therefore the potassium analyses made on the first set of samples were repeated. Considering that consistent results were achieved, the mean K contents were used for the recalculation of the previous K/Ar ages. At the same time, 6 additional samples were collected from the same sites for paleomagnetic studies, hoping to get confirmation of the meaningful ages obtained on the previous samples.

Based on the preliminary results, we concluded that the BVF basaltic rocks are generally younger than the alkaline basaltic rocks exposed at Lutynia and Ladek Zdrój. On the other hand, the analytical data suggested that the volcanic activity was episodic: older than 3.4 Ma, around 2.3 Ma and younger than 1.5 Ma. However, such an estimation does not consider possible geologically induced disturbances of the argon isotope system, e.g., Ar loss by alteration or excess Ar by incorporation of xenocrysts/xenoliths. Because of these uncertainties, we use all the available and reliable radiometric data in this study, determined in different laboratories (see Table 2).

The paleomagnetic data are also taken into account for the final model of the volcanic evolution.

K/Ar code	sample code	site	K (%)	$^{40}Ar_{rad}$ (ccSTP/g)	$^{40}Ar_{rad}$ (%)	K/Ar age (Ma)
5373/A	CZB-4A	Velký Roudný (Bílčice)	0.89	1.155×10^{-7}	20.2	3.35±0.23
5375/B	CZB-6B	Zlatá Lípa	1.08	7.526×10^{-8}	16.4	1.79±0.15
5370/B	CZB-1B	Břidličná	1.31	1.909×10^{-7}	9.1	3.74±0.56
5371/A	CZB-2A	Uhlířský vrch	0.66	3.973×10^{-8}	14.1	1.54±0.15
5372/A	CZB-3A	Venušina sopka	1.14	3.652×10^{-8}	9.6	0.83±0.12
5374	CZB-5	Volárenský vrch (Volárna)	1.12	1.066×10^{-7}	27.2	2.45±0.13
8012	SU-03	Bílčice	0.98	8.845×10^{-8}	23.4	2.33±0.14
8013	SU-04	Slezská Harta	0.95	8.169×10^{-8}	19.3	2.21±0.16
8014	SU-05	Slezská Harta	0.75	6.945×10^{-8}	10.9	2.37±0.29
8015	SU-06	Volárenský vrch (Volárna)	0.99	9.519×10^{-8}	11.1	2.48±0.31
8016	SU-09	Mezina	1.45	7.096×10^{-8}	11.1	1.26±0.16
8017	SU-12	Venušina sopka	1.19	9.872×10^{-8}	27.3	2.14±0.08

Table 3: Results of radiometric analyses used for this study (ATOMKI Debrecen, Hungary); sets 2000 (CZB samples) and 2010 (SU samples). Data of the set from 2000 (Pecskay et al. 2009) are recalculated with new results on potassium content.

Four new K/Ar ages of whole-rock samples (SU-03, 04, 05 and 06) are identical within the analytical error. Based on the concordant age, we consider these ages to be statistically significant for the geological setting. Therefore, one can assume that these whole rocks contain negligible rock or mineral components with insufficient Ar retentivity or with excess Ar. This assumption is confirmed by the analytical data obtained for a sample from previous set (CZB-5, sampling site identical with SU-06) – see Tab. 3. In contrast, the radiometric ages from the VS (CZB-3A and SU-12) appear to be affected by excess Ar (0.83±0.12 and 2.14±0.08 Ma), assuming that the age disturbances are mainly caused by the presence of some very fine-grained xenocrystic material, which is impossible to eliminate from the samples. Consequently, the younger age is closer to the real geological age than the older one. However, it cannot be completely excluded that sample CZB-3A was affected by a slight alteration which resulted in Ar loss. As a consequence, the analytical age determined for this sample should be considered, as a "minimum age".

Discussion

Reversed-polarized young volcanoes of the BVP must be older than 0.781 Ma (Gradstein et al., eds. 2004) – the Matuyama polarity chron. Based on polarity and group statistics results, supported by volcanological evidence, we can discuss the reliability of K/Ar datings originated during the last nearly 40 years in different laboratories. On the example of the products from Velký Roudný Hill (see Fig. 1 for location, samples SU-03 to SU-06) we can explain the result of the evaluation which is documented in Fig. 9. The data obtained in early 1980s for the largest lava flow (Slezká Harta and Bílčice-Leskovec) have relatively large analytical errors – over 30%. As a result, a part of the time period belongs to the normal polarity event. One rock body measured several times and in several sampling-places shows different ages. The possible period is therefore so wide that it looses validity. Moreover, the evaluation of volcanological phenomena, which is proved by group statistics of paleomagnetic results, now summarizes 9 ages for the same lava body (VR1 – see Tab. 2). The time span counted from all these data is 4.3–0.88 Ma, if given the same weight to each result. The high age of the two above mentioned reversed samples from VR is comparable

with normal polarized activity of BV and Lutynia only by chance; the measured polarity does not allow this possibility. Therefore, such an age is not realistic for the VR activity. So, we have chosen data which were grouped in a time period closest to the reversed polarity subchron. It is important to notice that only newly obtained data with smaller analytical errors were the result. Thus, the most possible chron of the lava flow origin is C2r2r (2.581–2.148 Ma). The Volárna lava relic with a slightly different vector orientation is very close in time, belonging to the same chron. Only the Zlatá Lípa lava relic is younger (1.24 Ma in Lustrino and Wilson 2007 or 1.79 ± 0.15 in Pécskay et al. 2009) with a possible origin during the C1r3r chron. Its vector orientation is slightly different as well.

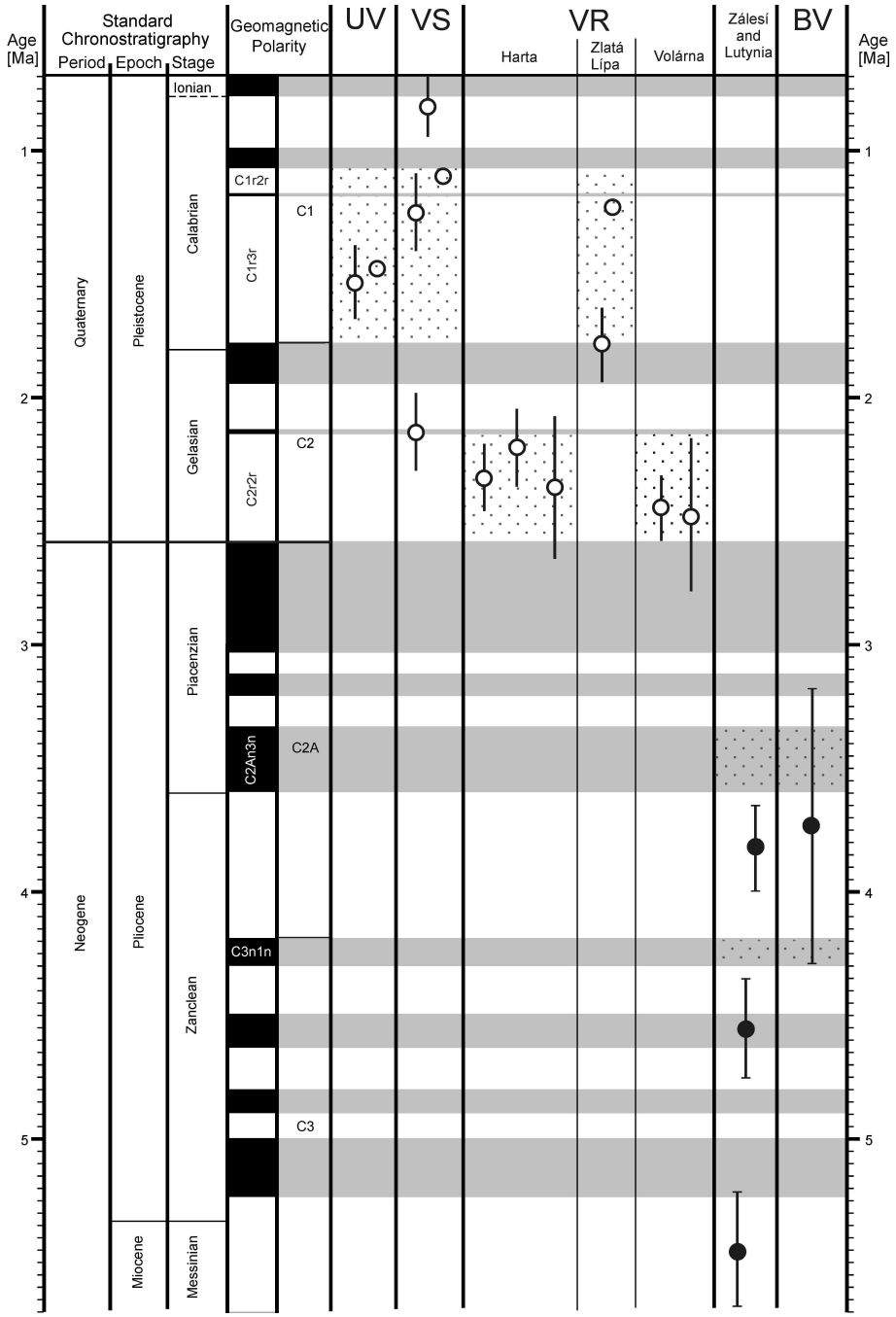

Fig. 9. The highest probability age (dotted time spans) of Pleistocene (reverse-polarized – open circles) volcanoes of the BVF compared to Pliocene (normal-polarized – black dots) volcanic activity. If

open circle only – no analytical error was given by previous authors (Lustrino and Wilson 2007). Stratigraphic chart after Gradstein et al. (2004).

Based on this, we can conclude on the production of two lava flows from the VR vent, close in time or simultaneous – to the SE (Slezská Harta) and to the W (Volárna). As has been mentioned above, another lava flow oriented to the S (Křišťanovice–Zlatá Lípa) could have been produced later, during a possible remobilization connected with UV and VS formation. This model corresponds with the new volcanological evaluation.

The orientation of the paleofield vector in the products of both smaller volcanoes is nearly identical. Therefore, we suggest that these youngest volcanoes (Uhlířský vrch Hill and Venušina sopka Volcano) were constituted most probably during C1r3r or C1r2r chrons (1.778-1.072 Ma), although one K/Ar age from VS (0.80±0.11 Ma in Pécskay et al. 2009) is younger, situated within C1r1r – see above, Chapter 5.2. The only older age (2.14±0.08 Ma), newly obtained from the bomb of the cinder cone (VS), might have been easily influenced by contamination during vesiculation or alteration during the phreatomagmatic event.

As the K/Ar age of the normal-polarized older Břidličná Volcano meets three normal subchrons (C2An2n – 3.207-3.116 Ma; C2An3n – 3.596-3.330 Ma; C3n1n – 4.300-4.187 Ma), only two older ones represent the most probable time of origin. This is substantiated by the results of group statistics, where the vectors of BV and the Lutynia Volcano are similar. From the same attitude, we can evaluate the age of the plug in Poland (Lutynia I) as slightly shifted to a higher age.

Another interesting conclusion can be seen from the point of view of tectonic development. All the studied area is influenced by tectonics of the Sudetic Marginal Fault. For the ascent of basaltic magmas, we assume the tectonic activity at the shape of relative extension, at least. It allows us to suppose close interrelationship of volcanism and tectonics (changes in paleostress field) in time. For the time of older volcanic activity (Břidličná and Lutynia), there is mentioned tectonic disquiet in the mountain ranges of Velká and Malá Fatra (Kováč et al. 2011), some 150 km SE far away. On the contrary, the time of two younger volcanic phases (Velký Roudný, Venušina sopka and Uhlířský vrch) is supposed to represent a period of tectonic quiescence at the Fatra region. Unfortunately, this study is not able to explain this disparity.

Conclusions

Newly obtained data on spatial and time distribution of volcanic activity do not confirm the idea of its shifting in time from the N to the S (sensu Birkenmajer et al. 2004) in the Czech part of Silesia. It can be only stated that three different Upper Cenozoic volcanic phases exist, with the following most probable timing:

i) Pliocene (Upper Zanclean or Lower Piacenzian) phase of normal polarity in the span of 4.3–4.2 Ma (C3n1n) or 3.6–3.3 Ma (C2An3n) constituting the Břidličná and Lutynia Volcanoes;
ii) Gelasian phase (2.6–2.1Ma, C2r2r) which formed the Velký Roudný Volcano with its large lava production; and
iii) Lower Calabrian phase (1.8–1.1 Ma, C1r1r+C1r2r) of Venušina sopka and Uhlířský vrch Hills, with possible remobilization of the Velký Roudný Volcano (southern flow of Zlatá Lípa).

These results represent a strong basis for the Upper Cenozoic volcanostratigraphy of this region. They can also contribute to the ideas on young history and development of tectonic activity, connected to the Sudetic Marginal Fault system. The Otice Volcano rock is not appropriate for paleomagnetic studies.

Acknowledgements: This research was supported by project IAA 300130612 of the GA AS CR "Combined magnetostratigraphic studies of Cenozoic volcanics, Bohemian Massif". It falls within the Research Plan of the Institute of Geology, Academy of Sciences CR, v.v.i., AV0Z30130516. We highly acknowledge the kindness of our colleague Jacek Grabowski for providing his primary data from the Lutynia area for comparison. We also thank Miroslav Radoň (Regional Museum Teplice, o.p.s.) for his great help during sample acquisition, and Jana Drahotová, Václav Sedláček and Jiří Petráček from our lab for technical assistance. We wish to express our great thanks to Klaudia Kuiper and Christine Franke for stimulating comments on paleomagnetism and to Jiří Adamovič for English revision of the manuscript.

References

Balogh K. 1985: K/Ar dating of Neogene volcanic activity in Hungary: Experimental technique, experiences and methods of chronologic studies. *ATOMKI Rep. D/1*. Institute of Nuclear Research, Debrecen, 277-288.

Barth V. 1977: Basaltic volcanoes of the central part of the Nízký Jeseník Mts (in Czech). *Čas. Mineral. Geol.*, 22, 3, 279–291.

Barth V. & Zapletal J. 1978: Geology of the Razová Pyroclastic Complex in the Nízký Jeseník Mts (in Czech). *Sbor. geol. Věd, Geol.*, 32, 97-122.

Birkenmajer K., Pécskay Z., Grabowski J., Lorenc M.W. & Zagozdzon P.P. 2002: Radiometric dating of the Tertiary volcanics in Lower Silesia, Poland. II. K/Ar and paleomagnetic data from Neogene basanites near Ladek Zdrój. *Sudetes Mts. Ann. Soc. Geol. Pol.*, 72, 119–129.

Birkenmajer K., Lorenc M.W., Pécskay Z. & Zagozdzon P.P. 2004: Age, cycles and course of migration of the Tertiary basaltic volcanism in Lower Silesia in the light of K/Ar dating. VIII (in Polish). *Ogólnopolska Sesja Naukowa Datowanie mineralów i skal*, 9–10.

Cajz V., Schnabl P., Pecskay Z. & Radoň M. 2010: Reconstruction and timing of the Plio-Pleistocene volcanism in surroundings of Bruntál, Nízký Jeseník Mts. – In: Křížek M., Nyplová P., Vočadlová K. and Borská J. (eds.). *Geomorphological proceedings 9 (11. international conference Stage of geomorphological research in 2010*, Faculty of Science, Charles University, Praha.

Cassidy J., France S.J. & Locke C.A. 2007: Gravity and magnetic investigation of maar volcanoes, Auckland volcanic field, New Zeland. *Joural of Volcanology and Geothermal Researchs, 159. 153-163.*

Dědáček K. & Gnojek I. 1980: Technical reports on airborne geophysical research in the Jeseníky area in 1978 a 1979 (in Czech). Geofyzika, Brno, 22 pp.

Fediuk F. & Fediuková E. 1985: Postmesozoic alkaline volcanics of northern Moravia (in Czech). *Acta Univ. Carol., Geol.*, 4, 355–382.

Fediuk F. & Fediuková E. 1989: Ultramafic nodules from basaltoids of northern Moravia. *Sbor. geol. Věd, Geol.*, 44, 9–49.

Fisher R.A. 1953: Dispersion on a sphere. Proceedings of the Royal Society of London, Series A, 217: 295–305.

Gradstein F., Ogg J. & Smith A., eds. 2004: *A Geologic Time Scale 2004*. Cambridge University Press.

Horský O., Muller K. & Trávníček L. 1972: Investigation of disturbance of the basalt sheet at the damsite Slezská Harta using geological and geophysical methods (in Czech with English resume). *Sbor. geol. věd, HIG*, 10, 39-57.

Jahn J.J. 1907: Über das quartäre Alter der Basalteruptionen im märisch-schlesischen Niederen Gesenke. *Sitz.-Ber. K. Akad. Wiss., math.-naturwiss*. 116, 1777-1821, Wien.

Jahn J.J. 1909: Über die Altersfrage der sudetischen Basalteruptionen. *Sitz.-Ber. K. Akad. Wiss., math.-naturwiss*. 118, 1-9, Wien.

Kadlec E., Novotný A., Bednář J., Blížkovský M. & Špaček B. 1972: Review of the gravity data processing in the Nízký Jeseník area, I. period, partial report of the „*Geophysical research of the Culm basement in the Nízký Jeseník Mts*." (in Czech). Geofyzika, Brno, 85 pp.

Kirschvink, J.L. 1980: The least-squares line and plane and the analysis of palaeomagnetic data. *Geophysical Journal International*, 62, 699–718.

Kolofíková O. 1976: Geological interpretation of measurment of magnetic properties of basalts. An example of the Chřibský les lava flow of the Velký Roudný volcano (Nízký Jeseník Mts.). *Čas. Miner. Geol.*, 21, 287-348.

Kopecký L. 1987: Young volcanism of the Bohemian Massif I – structural-geological and volcanological study (in Czech). *Geologie a hydrometalurgie uranu*, 11, 3, 30-67, Stráž pod Ralskem.

Kováč M., Hók J., Minár J., Vojtko R., Bielik M., Pipík R., Rakús M., Král J., Šujan M. & Králiková S. 2011: Neogene and Quaternary development of the Turiec Basin and landscape in its catchment: a tentative mass balance model. – Geol. Carp., 62, 4, 361-379.

Krs M. 1968: The scope rock magnetism in geology. *Sbor. geol. Věd, Geol*., 7, 43-75.

Lidner H., Gabriel G., Götze H.-J., Kaeppler R. & Suhr P. 2006: Geological and geophysical investigation of maar structures in the Upper Lusatia region (East Saxony). *Z. d. Ges. Geowiss.* 157/3, 355-372.

Lustrino M. & Wilson M. 2007: The circum-Mediterranean anorogenic Cenozoic igneous province. *Earth Science Reviews*, 81, 1–65.

Marek F. 1969: Magnetism of the basalt formation of the Lesser Jeseník Mts. *Travaux de l'Institute Géophysique de l'Académie Tschécoslovaque des Sciences*, 307, 129-164.

Marek F. 1973: Paleomagnetism of the inner Sudeten series of volcanoes of the basalt formation of the Nízký Jeseník Mts. *Sbor. geol. Věd, UG*, 11, 31–66, Praha

Marek F. 1974: Palaeomagnetism of the outer Sudeten series of volcanoes of the Nízký Jeseník basalt formation and its surroundings. *Sbor. geol. Věd, UG*, 12, str. 131–153, Praha.

Pécskay Z., Přichystal A., Tomek Č. & Zapletal J. 2009: New radiometric data of volcanics from northern Moravia and Silesia. (in Czech). *Moravskoslezské paleozoikum*, 2009, 15-16.

Schnabl P., Novák J.K., Cajz V., Lang M., Balogh K., Pécskay Z., Chadima M, Šlechta S., Kohout T., Pruner P. & Ulrych J. 2010: Magnetic properties of high-Ti basaltic rocks from the Krušné hory/Erzgebirge Mts. (Bohemia/Saxony), and their relation to mineral chemistry. *Studia Geophysica et Geodaetica*, 54, 1, 77-94.

Shrbený O. & Vokurka K. 1985: The present state of geochronological and isotope research of neovolcanics of the Bohemian Massif and their inclusions. (in Czech). Czech Geological Survey, Praha.

Steiger R.H. & Jäger E. 1977: Subcommission on geochronology: Convention on the use of decay constants in geo-and cosmochronology. *Earth Planet. Sci. Lett.*, 36, 359-362.

Šalanský K. 2004: Geophysics of the neovolcanites in Czech Republic. (in Czech). *Czech Geol. Surv. Spec. Pap.*, 17. Praha, 174 pp.

Šalanský K. & Gnojek I. 2002: Geomagnetic anomalies in Czech Republic. (in Czech). – *Czech Geol. Surv. Spec. Pap*., 14. Praha, 141 pp.

Šibrava V. & Havlíček P. 1980: Radiometric age of Plio-Pleistocene volcanic rocks in the Bohemian Massif. *Věst. Ústř. Úst. Geol*., 55, 129–150.

Štěpančíková P., Hók J., Nývlt D., Dohnal J., Sýkorová I. and Stemberk J. 2010: Active tectonics research using trenching technique on the south-eastern section of the Sudetic Marginal Fault (NE Bohemian Massif, central Europe). *Tectonophysics*, 485, 269-282.

Tarling D.H. & Hrouda F. 1993: *The magnetic anisotropy of rocks*. Chapman and Hall, London, 217 pp.

Ulrych J., Pivec E., Lang M., Balogh K. & Kropáček V. 1999: Cenozoic intraplate volcanic rock series of the Bohemian Massif. *Geolines*, 9, 123–129.

Ulrych J., Dostal J., Adamovič J., Jelínek E., Špaček P., Hegner E & Balogh K. 2011: Recurrent Cenozoic volcanic activity in the Bohemian Massif (Czech Republic). *Lithos*, 123, 133-144.

Vahle C. & Kontny A. 2005: The use of field dependence of AC susceptibility for the interpretation of magnetic mineralogy and magnetic fabrics in the HSDP-2 basalts, Hawaii. *Earth Planet. Sci. Lett.*, 238, 110-129

Vokurka K. & Bendl J. 1992: Sr Isotope Geochemistry of Cenozoic Basalts from Bohemia and Moravia. *Chem.d.Erde*, 52, 3, 179-187.

Vokurka K. & Bendl J. 1993: Nd Isotopes of Cenozoic Basalts from Northern Moravia. – *Chem.d.Erde*, 53, 4, 307-313.

Cajz V., Rapprich V., **Schnabl P.** a Pécskay Z.

Návrh litostratigrafie neovulkanitů východočeské oblasti (A proposal on lithostratigraphy of Cenozoic volcanic rocks in Eastern Bohemia)

Zprávy o geologických výzkumech v roce 2008, 9 – 15, 2009

A – REGIONÁLNÍ GEOLOGIE A STRATIGRAFIE

Návrh litostratigrafie neovulkanitů východočeské oblasti

A proposal on lithostratigraphy of Cenozoic volcanic rocks in Eastern Bohemia

VLADIMÍR CAJZ [1, 2] – VLADISLAV RAPPRICH [3] – PETR SCHNABL [1] – ZOLTÁN PÉCSKAY [4]

[1] *Geologický ústav AV ČR, v. v. i., Rozvojová 269, 165 02 Praha 6; cajz@gli.cas.cz*
[2] *Přírodovědecká fakulta, Univerzita Jana Evangelisty Purkyně, České mládeže 8, 400 96 Ústí nad Labem*
[3] *Česká geologická služba, Klárov 3, 118 21 Praha 1; vladislav.rapprich@geology.cz*
[4] *Institute of Nuclear Research, Hungarian Academy of Sciences, Bem tér 18/C, H-4001 Debrecen, Maďarsko*

(03-32 Jablonec nad Nisou, 03-34 Sobotka, 03-41 Semily, 03-43 Jičín)

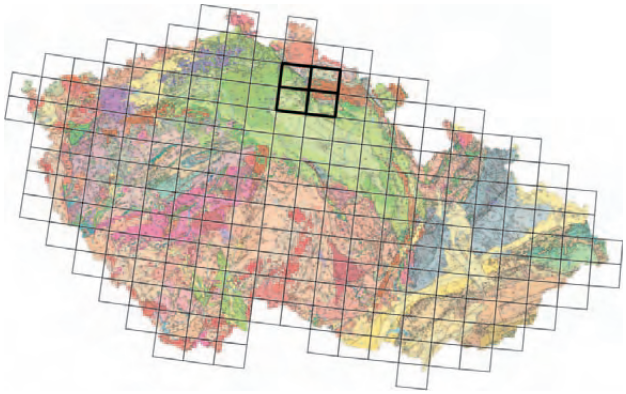

Key words: lithostratigraphy, Cenozoic basaltic volcanism, Jičín volcanic field, K-Ar dating, paleomagnetism, Bohemian Paradise Geopark

Abstract: This paper proposes lithostratigraphy of Cenozoic basaltic volcanism of the Jičín Volcanic Field (Eastern Bohemia). Two formations are distinguished: Trosky Fm. (Upper Miocene; 15.7–18.3/24.6? Ma) and Kozákov Fm. (Lower Pliocene; 4.6–5.2Ma). Both of them are represented by products of Strombolian- or phreatomagmatic-type volcanic activity with preserved relics of cinder/tuff cones and lava-filled maar craters (Trosky Fm.) and lavas with their feeder (Kozákov Fm.). Accuracy of radiometric data of the volcanic activity is evaluated using results of paleomagnetic research.

Kenozoický vulkanismus Českého masivu je převážně soustředěn do oherské struktury. Přesto existuje několik dalších oblastí, kde jsou produkty sopečné činnosti vyvinuty v takové míře, že je lze definovat jako oblasti vulkanické. Jičínské vulkanické pole, jehož dochované projevy tvoří dominanty Českého ráje, je oblastí donedávna považovanou za území výskytu hluboce erodovaných kenozoických vulkanických projevů. Poslední výzkumy však potvrdily existenci výskytů předpokládaných povrchových forem (Rapprich et al. 2007). Výsledky dosavadního výzkumu proto nyní dovolují navrhnout stratigrafické členění neovulkanitů této oblasti, založené na odlišnosti litologické, paleomagnetické, časové i petrografické. V souladu s mezinárodně uznávanými stratigrafickými principy (Salvador ed. 1994) navrhujeme kenozoický vulkanismus východních Čech členit do dvou souvrství – kozákovského (spodní pliocén) a troseckého (svrchní miocén).

Jičínské vulkanické pole (JVP) je oblast zahrnující území přibližně mezi Železným Brodem, Turnovem, Mnichovým Hradištěm, Jičínem, Lázněmi Bělohrad, Novou Pakou a Lomnicí nad Popelkou. Produkty vulkanismu jsou tvořeny horninami skupiny olivinických bazaltoidů. S výjimkou lávových reliktů v blízkém okolí vrchu Kozákov mají neovulkanity charakter izolovaných těles většinou relativně izometrických tvarů. Ty z nich, které jsou tvořeny vulkanoklastickými horninami, byly dříve souhrnně zobrazovány jako subvulkanické (*intruzivní, komínové*) brekcie. Napomáhala tomu představa značné eroze (od předpokládané doby vulkanické aktivity) i analogie s tělesy kompaktních bazaltoidů (žíly, vypreparované sopouchy). JVP je modelovou oblastí vývoje drobnějších monogenetických vulkánů strombolského (struskové kužele) a freatomagmatického (tufové kužele) erupčního typu, a to podle míry interakce magmatu s okolím v době aktivity. Za silně magmatickou lze označit např. lokalitu Prackov, nejvyšší freatické ovlivnění je pozorovatelné na žilném tělese pod hradem Frýdštejn. Jednotlivé lokality JVP nabízejí možnost studia vulkanického aparátu v různých erozních úrovních od sopečného kužele až po hluboké partie přívodní dráhy. Blíže charakterizovali některá tělesa Rapprich et al. (2007), kteří zpracovali 13 lokalit.

Lávy na samotném vrchu Kozákov a v jeho blízkém okolí jsou produkty patrně jediné spojité efuzivní aktivity z přívodní dráhy solitérního vulkánu u Prackova. Vytékaly v několika směrech, což dokládají další drobné relikty v okolí. Láva ve své distální části u Semil a Železného Brodu leží na mladoterciérních sedimentech Paleojizery, což vedlo již před zjištěním prvních radiometrických údajů k zařazení vulkanické činnosti do mladších třetihor (např. Fediuk 1972). Současná výšková rozrůzněnost bází lávových segmentů a reliktů je důsledkem kombinace postvulkanické tektoniky a tvarů paleoreliéfu. K diskusi o tektonické stavbě, míře eroze a na vyplývající souvislosti odkazujeme na studii Rappricha et al. (2007).

Litostratigrafie

Při terénním pozorování kenozoických vulkanitů zjišťujeme v oblasti dvě horninové skupiny definovatelné jako kompaktní bazaltoidy a vulkanoklastika. Z jiného pohledu pak opět dvě skupiny – typy povrchové a subvulkanické. V tomto druhém přístupu se velmi uplatňuje stáří sopečné činnosti, tedy úroveň eroze, v níž jsou dnes tělesa zachována. Ač posuzováno z odlišného úhlu pohledu, do značné míry se oba odlišné přístupy prolínají a to spolu s výsledky radiometrického datování a paleomagnetických studií umožňuje navrhnout litostratigrafické členění kenozoických vulkanických hornin oblasti:

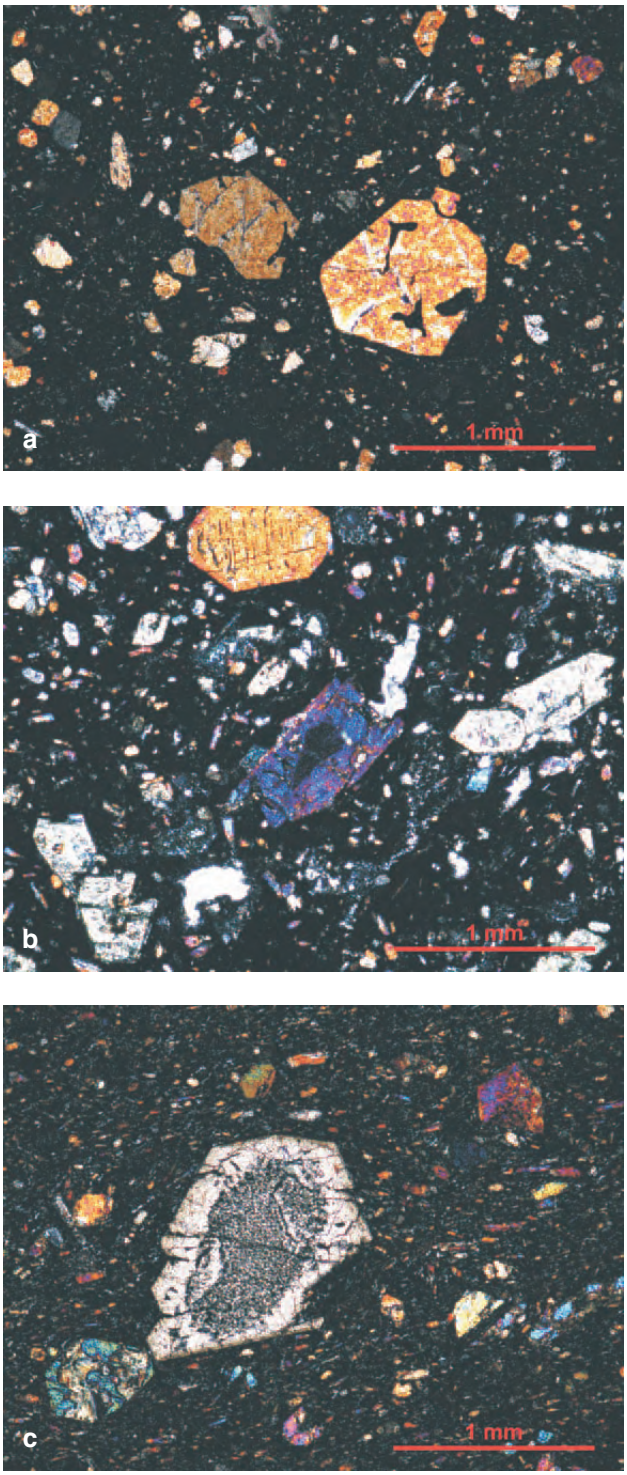

Obr. 1. Rozdíl mezi horninovým typem kozákovským (a – Prackov) a troseckým (b – Dubolka, c – Kumburk) je dán absencí/přítomností vyrostlic klinopyroxenu. Zkřížené nikoly.

Kozákovské souvrství

Kozákovské souvrství (Kozákov Formation – podle vrchu Kozákov, k. 744; 3,54–6,69 Ma, resp. 4,92 ± 0,25 Ma) je tvořeno bazanitovými lávami s hojnými svrchnoplášťovými uzavřeninami s převahou olivínu (lherzolitovými nodulemi). Tyto horniny byly a jsou předmětem zvýšeného petrologického zájmu (naposledy Ackerman et al. 2007). Přívodní dráha láv je erozním reliktem struskového kužele (*cinder cone*) u Prackova se zachovanou vnitřní kráterovou facií pyroklastik a výplní kráteru kompaktní lávou (zbytek lávového jezera). V širším okolí kozákovského hřebene lze nalézt též několik drobných erozních reliktů, které jsou pozůstatky dalších lávových proudů produkovaných týmž vulkánem. V dnešní podobě lávy pokrývají značnou část kozákovského hřebene a zasahují téměř až k současné Jizeře. Stávající převýšení reliéfu pokrytého lávami – přes 300 m – je druhotné, způsobené vertikální složkou následných tektonických pohybů. Ačkoliv jsou to vše produkty jediného vulkánu, tvoří plošně i objemově převážnou většinu kenozoických vulkanických hornin oblasti. Lávy vytékaly do depresí tehdejšího reliéfu, který se patrně generelně svažoval k S. Soudíme tak podle vzájemné pozice přívodní dráhy a maximálního objemu zachovaných láv. Nicméně jsou známy i drobné relikty láv v jižní, pokleslé kře. Proto předpokládáme spíše členitý směr toku lávy než přímý. Lávy u Semil a Železného Brodu dosáhly koryta Paleojizery (Gotthard 1931), kde nasedají na její štěrkopískové nánosy. Dalšími mladšími sedimenty jsou částečně překryty (Fediuk 1953). Rostlinné zbytky z asi 10 cm mocné vložky hnědého jílovitého prachovce ve štěrkopíscích v podloží proudu byly zařazeny Konzalovou (1973) do středního až svrchního miocénu.

Hornina je klasifikována jako olivinický bazalt až nefelinický bazanit. Tvoří ji hojné vyrostlice olivínu (až 1 cm), ale vyrostlice klinopyroxenu se prakticky nevyskytují. Toto je významné rozlišovací kritérium (obr. 1). Základní hmotu tvoří hojný drobný olivín, méně hojný klinopyroxen, Fe-Ti oxidy a sklo (méně často krystalované fáze – plagioklas a nefelin). Absence klinopyroxenu mezi vyrostlicemi může souviset s vyšší teplotou magmatu při erupci.

Výsledky prvých radiometrických rozborů metodou K-Ar z bazanitových láv, odebraných v lomech Slap a Smrčí, publikovali Bellon a Kopecký (1977) a Šibrava a Havlíček (1980). Souhrnně vykazují stáří v intervalu 3,54–6,69 Ma, což je pro vývoj malého strombolského vulkánu příliš dlouhá doba. Údaj 4,25 Ma, bez udané chyby, z lomu Chuchelna (Lustrino – Wilson 2007) do tohoto intervalu vhodně zapadá a zároveň je též velmi blízký novému údaji 4,92 ± 0,25 Ma získanému z místa výstupu láv. Z porovnání radiometrických a paleomagnetických dat (obr. 2) vyplývá, že aktivita s jistotou probíhala v jednom z období normální polarity v zóně C3 (4,2–5,2 Ma). Vý-

sledky paleomagnetických studií ze šestnácti lokalit vykazují malou sekulární variaci a extrémní magnetickou inklinaci vektoru přirozené remanentní magnetizace (obr. 3). Malá sekulární variace při extrémních hodnotách inklinace dokládá krystalizaci všech vzorkovaných hornin během velmi krátkého časového úseku (např. Butler 1992), a tedy rychlé tuhnutí lávy. Odpovídá to také představě spojité efuzivní aktivity. Na základě charakteru produktů, tedy minimální petrologické variability, typu vulkanické aktivity a zhodnocení přívodní dráhy (Rapprich et al. 2007), předpokládáme vývoj vulkánu v době rozhodně nepřesahující jeden milion let. **Proto se přikláníme spíše k době udané posledně zjištěným radiometrickým rozborem, a to pro všechny produkty tohoto souvrství.**

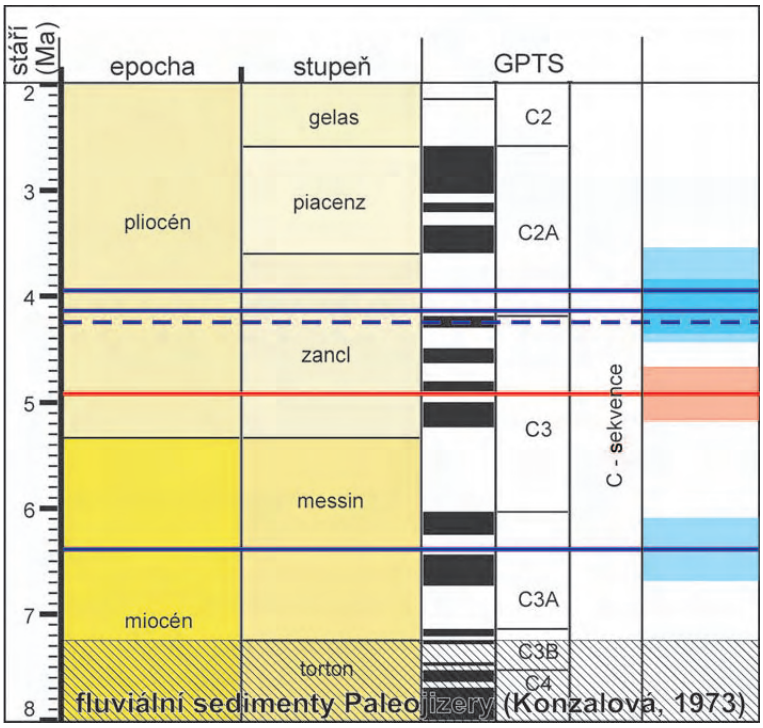

Obr. 2. Pozice radiometrických dat kozákovského souvrství ve stratigrafické škále v porovnání s geomagnetickou polaritní časovou škálou (http://www.stratigraphy.org/). Výška barevných obdélníčků představuje rozsah analytické chyby. Modře starší data z lávových proudů, červeně nově přívodní dráha Prackov, šrafou dřívější paleontologické určení podložních sedimentů.

a) Lomy Smrčí (50°37,25'N; 15°17,12'E) a ***Pelechov*** (50°38,01´ N; 15°16,20´ E) v témže proudu – holostratotyp

Činný lom (Smrčí) má odkrytou mocnost bazanitového proudu až 20 m. Pozorovatelné jsou tři facie – nejnižší sloupcovitě odlučná se svislými sloupci o průměru 30–40 cm (kolonáda), vyšší nepravidelně bločkově odlučná (entablatura) a nejvyšší pórovitá a alterovaná facie bez známek brekciace. Hranice mezi spodními faciemi je „opticky" výrazná (to dříve vedlo k interpretaci rozhraní dvou předpokládaných proudů), při bližším ohledání však jde pouze o náhlou změnu odlučnosti v jediném proudu (Fediuk 1972). V nejvyšší facii pak pozvolna přibývají drobné vezikuly a s jejich množstvím se stupňuje alterace, předpokládaná brekciovitá facie při povrchu proudu chybí. Opuštěný lom (Pelechov) odkrývá tentýž bazanitový proud ve sloupcově odlučné a dosti alterované facii. V nadloží lávy jsou uloženy povulkanické štěrky Paleojizery. Podle starší dokumentace (např. Fediuk 1953) byla při bázi proudu v nadloží předvulkanických štěrkopísků popisována vulkanoklastika, tehdy interpretovaná jako „tufy". Vzhledem k okolnosti, že výlev dostihl koryta řeky, lze je i bez možnosti ověření ve výchoze reinterpretovat jako hyaloklastické spodní brekcie (nejnižší facie proudu). Tomu odpovídá také zmiňovaný zapracovaný písčitý materiál.

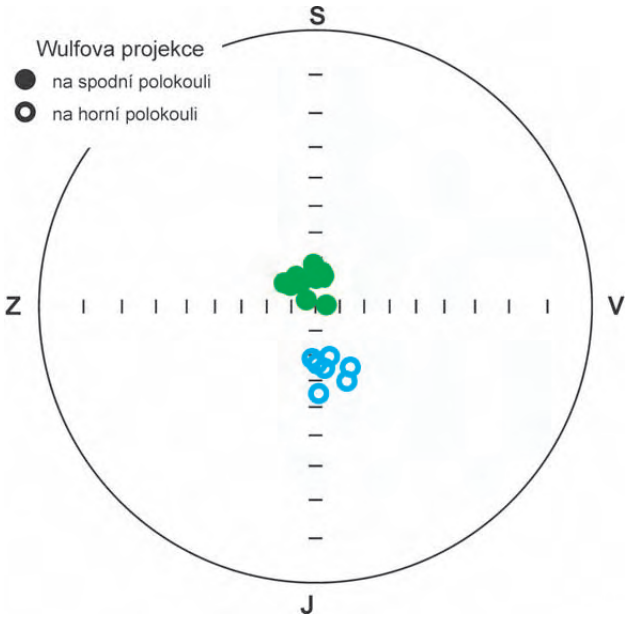

Obr. 3. Projekce paleomagnetických směrů vektorů hornin obou definovaných souvrství – malá sekulární variace dokládá krátký časový úsek tvorby hornin v obou případech. Plné zelené body značí normální polaritu kozákovského souvrství (projekce na dolní polokouli), prázdné modré body pak reverzní polaritu troseckého souvrství (projekce na horní polokouli).

b) Prackov (50°36,25'N; 15°14,71'E; 4,92 ± 0,25 Ma) – parastratotyp

Výchozy ve strmém svahu z. a zjz. od obce. Odkryty jsou nespékané a netříděné, avšak vrstvené uloženiny bazaltických strusek se stratifikací uklánějící se dovnitř vulkanického tělesa. Tento trend je pozorovatelný po značné části obvodu tělesa. Velikost struskových částic kolísá průměrně kolem 1–10 cm (lapilli až bomby), lze nalézt i vřetenové bomby o velikosti přes 30 cm. Často je jádrem takové bomby lherzolitová nodule. Erozí je zde obnažena vnitřní partie struskového kužele – vnitřní svahy kráteru, povrchového aparátu strombolského vulkánu. Původní kráter vyplňuje kompaktní bazanitová hornina s vysokým obsahem nodulí, dnes tvořící rovinu nad výchozy. Je to pozůstatek lávového jezera, odkud byly produkovány lávy tohoto souvrství.

Trosecké souvrství

Trosecké souvrství [Trosky Formation – podle vrchu Trosky, k. 488; 15,7–18,3 (24,6?) Ma] sestává z produktů a přívodních aparátů mnoha solitérních vulkánů v podobě struskových kuželů, tufových kuželů a freatomagmatických kráterů (maarů). Vzhledem k vyššímu stáří a tedy déle trvající erozi jsou produkty zachovány v podstatně menší míře než u souvrství mladšího. Rozdíly v erupčním stylu jednotlivých monogenetických vulkánů jsou dány prostředím, ve kterém k erupci došlo – především hydrologickými a hydrogeologickými podmínkami. Jednotlivé porce magmatu byly drobné a po eruptivní aktivitě docházelo k intruzím kompaktního magmatu do erupčního aparátu. Není známa produkce láv, i když z charakteru sopečné činnosti je značně pravděpodobná alespoň v případě některých z vulkánů. V současnosti jsou sopky tohoto souvrství zachovány v podobě erozních trosek, více či méně postižených odnosem. Nejlépe jsou povrchové vulkanické aparáty zachovány např. na lokalitách Trosky, Dubolka, Zebín anebo Kumburk. Na mnoha jiných zůstávají pouze subvulkanické aparáty, popř. pouhé hluboce erodované přívodní kanály.

Hornina v kompaktním stavu je klasifikována v převážné většině případů jako bazanit, resp. limburgit. Určení však může kolísat v hranicích olivinický bazalt až olivinický nefelinit. V horninách tohoto souvrství jsou patrné hojné vyrostlice olivínu (až 5 mm) a o něco méně hojné vyrostlice klinopyroxenu (do 3 mm) – obojí identifikovatelné pouhým okem nebo lupou na makrovzorku a zcela nezaměnitelné při ověřování ve výbrusu (viz obr. 1). Základní hmotu tvoří drobné vyrostlice olivínu a klinopyroxenu, Fe-Ti oxidy, bazický plagioklas a nefelin/analcim, nebo sklo.

Všechny analyzované horniny troseckého souvrství vykazují reverzní polaritu a malou sekulární variaci, inklinace vektoru přirozené remanentní magnetizace odpovídá průměrné hodnotě pro dané časové období (viz obr. 3). Stáří tohoto souvrství dokládají radiometrická K-Ar data nově získaná na čtyřech reliktech struskových/tufových kuželů, která leží v úzkém rozpětí 2,5 mil. let kolem stáří 17 Ma (Trosky 16,49 ± 0,79, Kumburk 17,31 ± 0,56, Dubolka 17,32 ± 0,86, Zebín 17,51 ± 0,74 – ATOMKI Debrecen 2006-7). Vzájemný překryv těchto radiometrických dat odpovídá zóně reverzní polarity C5Cr (16,7–17,2 Ma – obr. 4), tedy interval pouhých 0,5 mil. let. Dříve získaná, avšak nedávno publikovaná datování 20,6 a 24,6 Ma pro Čeřovku a Střelečskou hůrku (Lustrino – Wilson 2007) postrádají udání chyby, což významně snižuje možnost posouzení jejich objektivity. Přesto nás však v současné situaci omezených znalostí nutí rozšířit časový rozsah navrhovaného souvrství směrem ke stáří vyššímu, i když indicie zahrnující zhodnocení typu vulkanické činnosti, tektonicky podmíněné přívodní dráhy, paleomagnetické charakteristiky a absence diferenciace magmatu spíše nasvědčují předpokladu kratšího období vulkanické aktivity. Do budoucna, na základě poznatků z dalších lokalit, zdaleka není vyloučena možnost vyčlenění staršího období vulkanické aktivity, či přehodnocení výsledků předchozích radiometrických rozborů.

a) Trosky (50°31,000'N; 15°13,845'E; 16,49 ± 0,79 Ma) – holostratotyp

Dominanta a symbol Českého ráje je pozůstatkem struskového kužele vzniklého strombolskou aktivitou. Tvoří ji akumulace špatně vytříděných, nezřetelně vrstvených, nespečených, nezpevněných a nealterovaných bazaltových strusek o velikosti 0,5–3 cm (lapilli, bomby) s občasnými vřetenovými bombami až 70 cm velkými (obr. 5). Pyroklastika jsou proniknuta kompaktním limburgitem. Místy lze pozorovat struktury degazace (vyfouknutí jemnějšího materiálu odcházejícími plyny). Zachovány jsou s největší pravděpodobností pouze vnitřní kráterové facie pyroklastik.

b) Kumburk (50°29,608'N; 15°26,700'E; 17,31 ± 0,56 Ma) – parastratotyp

Lávové jezero vyplňující freatomagmatický kráter, z nějž velmi pravděpodobně mohly vytékat lávy. Tvar kompaktní výplně je konický – což koresponduje se spodní partií jezera – stejně jako uspořádání sloupcové odlučnosti v podobě milíře. V lemu kompaktní výplně jsou v hradních příkopech odkryty zbytky polymiktní brekcie. Vysoký obsah xenolitů, zejména sedimentů permokarbonu, odpovídá freatomagmatické erupci (maar).

c) Zebín (50°27,212'N; 15°22,360'E; 17,51 ± 0,74 Ma) – parastratotyp

Třetím typem aktivity troseckého souvrství jsou povrchové freatomagmatické exploze netvořící krátery, ale tufové kužele. Zebín je tvořen akumulací bazaltových slabě vezikulovaných nebo nevezikulovaných fragmentů s převažující velikostí klastů kolem 1 cm. Vrstvení ani gradace nebyly pozorovány, ve svrchní partii však byly zjištěny znaky degazace. Pyroklastické uloženiny jsou opět protnuty kompaktním limburgitem.

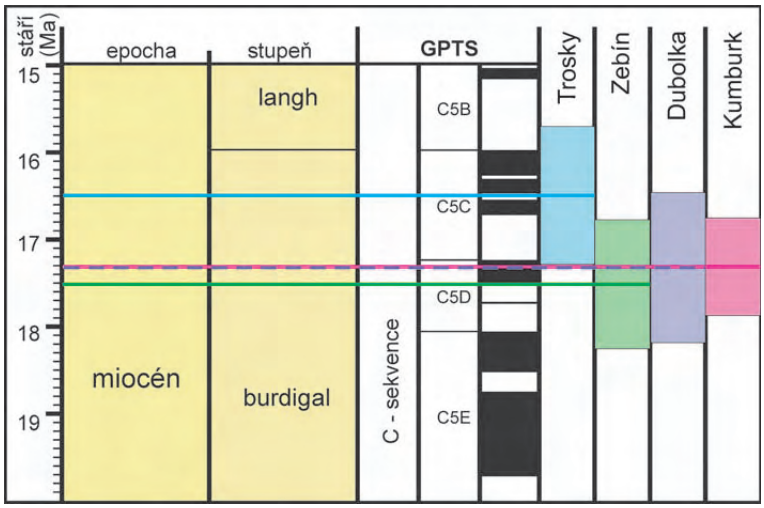

Obr. 4. Pozice radiometrických dat troseckého souvrství ve stratigrafické škále v porovnání s geomagnetickou polaritní časovou škálou (http://www.stratigraphy.org/). Výška barevných obdélníčků představuje rozsah analytické chyby na jednotlivých lokalitách.

Diskuse – vztahy definovaných litostratigrafických jednotek k okolí

Ve studované oblasti je kenozoický vulkanismus nejmladším projevem platformního vývoje, odhlédneme-li od sedimentů kvartérních. Užší stratigrafické vztahy lze definovat superpozičně pouze k sedimentům křídovým (v převážné většině výskytům troseckého souvrství) a ke staré říční terase/terasám Paleojizery (souvrství kozákovské). V prvém případě přívodní aparáty vulkánů prorážejí a jejich produkty nasedají na sedimenty křídy. V případě druhém pak s největší pravděpodobností jsou lávy synchronní s ukládáním terasy Paleojizery. To významně posunuje stáří štěrkopísků ze středního až svrchního miocénu (dřívější paleontologické určení) do spodního pliocénu. Na základě vulkanologických indicií lze důvodně předpokládat zahrazení toku výlevem (*lava-dam lake*), překrytí stávajících štěrkopísků lávou a kontinuální usazování dalších říčních sedimentů na lávě po vzedmutí hladiny toku a po alespoň částečné erozi nejvyšší lávové facie. Jelikož z okolí nejsou

Obr. 5. Bazaltové strusky pod hradem Trosky. Nezřetelně vrstvená a špatně vytříděná pyroklastika s převahou frakce lapilli; některé z bomb vykazují uložení v poloplastickém stavu – viz vřetenová bomba velikosti 70 cm vlevo nad kladivem.

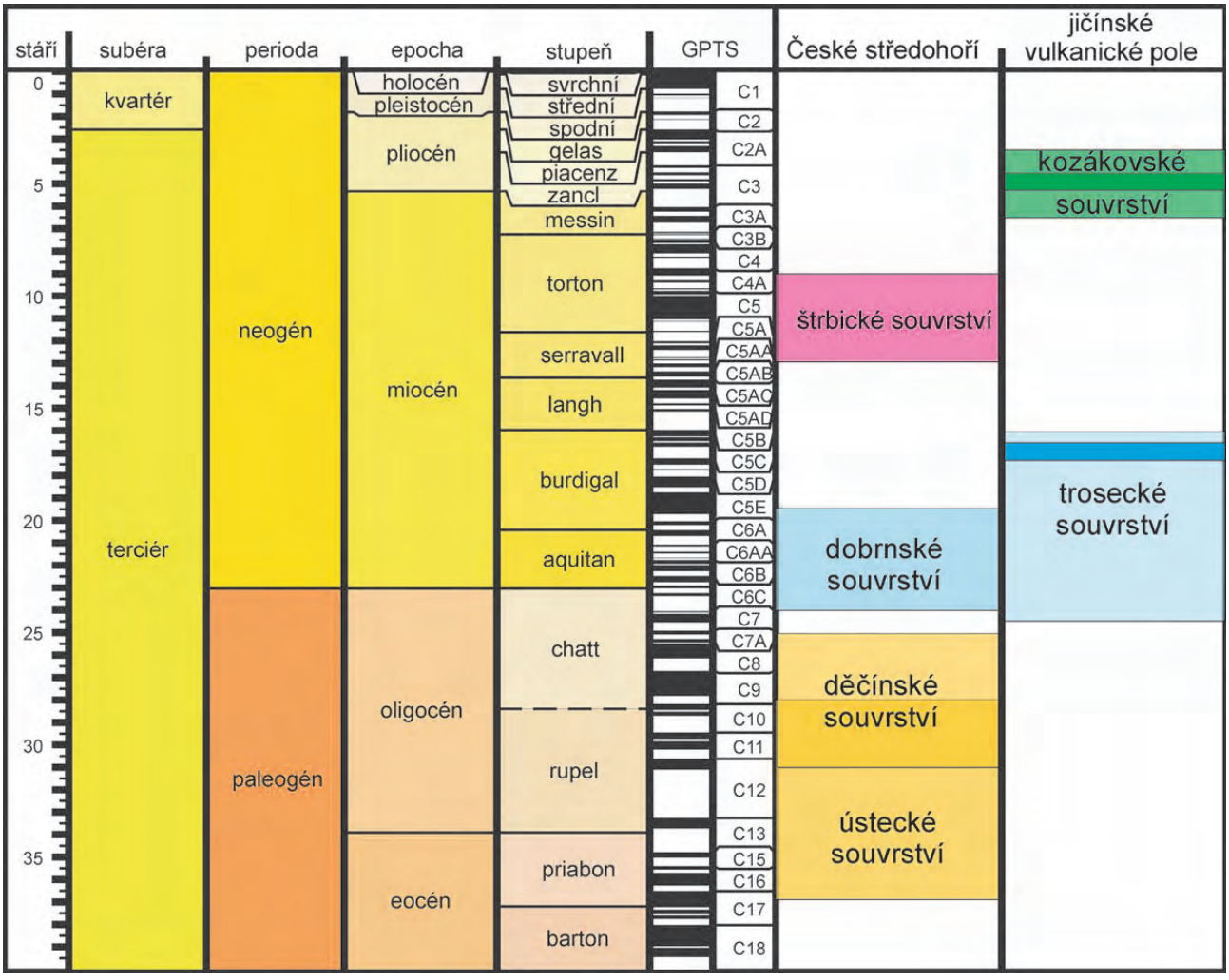

Obr. 6. Srovnání litostratigrafických jednotek vulkanosedimentárního komplexu Českého středohoří a jičínského vulkanického pole na standardní chronostratigrafické a geomagnetické polaritní časové škále (http://www.stratigraphy.org/). Intenzivní barva v pravém sloupci znázorňuje zúžení časového intervalu obou definovaných souvrství, interpretované na základě paleomagnetických studií. Překryv barev v předchozím sloupci znázorňuje doposud nevysvětlený překryv analytických dat ústeckého a děčínského souvrství, který není v souladu se superpozičními a vulkanologickými charakteristikami obou jednotek.

uváděny sedimenty obdobného stáří, které by opravňovaly k představě změny toku Paleojizery vlivem efuzí, předpokládáme návrat toku do původního koryta bezprostředně po výlevné epizodě. Vzájemné stratigrafické vztahy obou nově definovaných vulkanických jednotek byly popsány v předchozím textu a vyplývají z obrázků.

Z časového údaje mladšího kozákovského souvrství (ca 5 Ma) a charakteru výskytu jeho reliktů lze však činit závěry o stáří a charakteru jedné z fází pohybové aktivity, patrně související s vývojem lužické poruchy. V lomu Chuchelna zaznamenaná zlomová plocha (60/64°) dokumentuje čistě horizontální pohyb způsobený napěťovým vektorem ssz.-jjv. orientace. Je tudíž velmi pravděpodobné, že tektonická aktivita oblasti v blízkosti lužické poruchy mohla probíhat v některých okamžicích způsobem prostých horizontálních posunů i patrně prostých vertikálních pohybů. V každém případě je tato významná tektonická činnost – amplituda přes 300 m a prosté laterální posuny – postvulkanická, mladší než kozákovské souvrství (blíže Rapprich et al. 2007).

Obě litostratigrafické jednotky lze také porovnávat s obdobnými jednotkami vulkanosedimentárního komplexu Českého středohoří (Cajz 2000). Obě starší souvrství komplexu (ústecké a děčínské), která do současnosti tvoří valnou většinu vulkanické produkce komplexu, jsou starší než souvrství trosecké. Souvrství děčínské pak je navíc geochemicky a vulkanologicky zásadně odlišné. Dobrnské souvrství komplexu se však se souvrstvím troseckým dá porovnat časově (19–24 Ma a 16–24? Ma), typem vulkanické aktivity (solitérní strombolský vulkanismus) i petrografickými charakteristikami produktů (skupina olivinických bazaltoidů). Jak jsme však již upozornili, velký časový rozptyl osmi milionů let pro trosecké souvrství, zvláště směrem ke starším hodnotám, je způsoben pouze začleněním dvou lokalit s dříve publikovanými údaji, ačkoliv ostatní indicie nejsou v souladu s tak dlouho trvajícím obdobím vulkanické aktivity. Proto je vysoce pravděpodobné (za předpokladu správnosti údajů), že právě tyto dvě lokality jsou v oblasti východních Čech ekvivalentem souvrství dobrnského. Potom by na základě údajů z nového výzkumu souvrství trosecké (s případně redukovaným rozsahem 15,7–18,3, resp. 16,7–17,2 Ma) bylo mladší než souvrství dobrnské vulkanosedimentárního komplexu Českého středohoří. Nejmladší souvrství komplexu (štrbické) pak svým časovým rozsahem (9–13 Ma) zapadá mezi obě navrhovaná souvrství východočeské oblasti. Je jim blízké typem vulkanické aktivity i geochemií produktů. Vokurka a Kober (1993) udávají poměry $^{87}Sr/^{86}Sr$ bazanitu z láv kozákovského souvrství v hodnotách 0,7031–0,7035, které jsou blízké dobrnskému souvrství. Je však třeba upozornit na nepoměr počtu údajů ze srovnávaných souvrství.

Na základě porovnání obou oblastí by pak litostratigrafická posloupnost kenozoického vulkanismu od nejstaršího po nejmladší souvrství byla následující (obr. 6): ***ústecké – děčínské – dobrnské – trosecké – štrbické – kozákovské.***

Výsledky výzkumu nabízejí možnost popularizačních aktivit pro další rozvoj geoturistiky v Geoparku Český ráj. V této oblasti je geoturistika významnou součástí trvale udržitelného ekonomického rozvoje.

Poděkování. Tento návrh vznikl za podpory Grantové agentury AV ČR (projekt IAA 300130612) a MŽP ČR (projekt VaV SP/2e6/97/08). Výzkum je v souladu s výzkumnými záměry Geologického ústavu AV ČR, v. v. i., (AV0Z30130516) a České geologické služby (MZP0002579801). Autoři děkují za spolupráci RNDr. T. Řídkošilovi a Muzeu Českého ráje v Turnově.

Literatura

ACKERMAN, L. – MAHLEN, N. – JELÍNEK, E. – MEDARIS, G. – ULRYCH, J. – STRNAD, L. – MIHALJEVIČ, M. (2007): Geochemistry and Evolution of Subcontinental Lithospheric Mantle in Central Europe: Evidence from Peridotite Xenoliths of the Kozákov Volcano, Czech Republic. – J. Petrol., 48, 12, 2235–2260.

BELLON, H. – KOPECKÝ, L. (1977): Spectres d'ages radiométriques du volcanisme du rift du Massif Bohémien. – 5eme Réunion Ann. Sci. Terre, Rennes, Soc. Géol. Fr. éd., 57.

BUTLER, R. F. (1992): Paleomagnetism: Magnetic Domains to Geologic Terranes. – Blackwell Sci. Publ.

CAJZ, V. (2000): Proposal of lithostratigraphy for the České středohoří Mts. volcanics. – Bull. Czech Geol. Surv., 75, 1, 7–16.

FEDIUK, F. (1953): Geologicko-petrografické poměry v údolí Jizery mezi Spálovem a Bítouchovem (Železnobrodsko). – Sbor. Ústř. Úst. geol., Odd. geol., 20, 505–561.

FEDIUK, F. (1972): Staropaleozoické, mladopaleozoické a neoidní vulkanity na Železnobrodsku. Exkurzní průvodce. – Úst. geol. věd Karl. Univ. 16 s.

GOTTHARD, J. (1931): Kozákov. – Zvláštní otisk z vlastivědného sborníku Od Ještěda k Troskám.

KONZALOVÁ, M. (1973): Neogenní rostlinné mikrofosilie z říčních sedimentů v podloží neovulkanitů na Železnobrodsku. – Věst. Ústř. Úst. geol., 48, 17–23.

LUSTRINO, M. – WILSON, M. (2007): The circum-Mediterranean anorogenic Cenozoic igneous province. – Earth Sci. Rev., 81, 1–65.

RAPPRICH, V. – CAJZ, V. – KOŠŤÁK, M. – PÉCSKAY, Z. – ŘÍDKOŠIL, T. – RAŠKA, P. – RADOŇ, M. (2007): Reconstruction of eroded monogenic Strombolian cones of Miocene age: A case study on character of volcanic activity of the Jičín volcanic field (NE Bohemia) and estimation of subsequent erosional rates. – J. Geosci., 52, 3–4, 169–180.

SALVADOR, A., Ed. (1994): International stratigraphic guide (second edition). – IUGS / Geol. Soc. Amer., Boulder, Colorado, 214 s.

ŠIBRAVA, V. – HAVLÍČEK, P. (1980): Radiometric age of Plio-Pleistocene volcanic rocks of the Bohemian Massif. – Věst. Ústř. Úst. geol., 55, 129–139.

VOKURKA, K. – KOBER, B. (1993): Heterogeneity of the Earth's mantle below the Bohemian Massif. In: KUKAL, Z., Ed.: Proceedings of the 1st International Conference on the Bohemian Massif, Prague, Czechoslovakia, Sept. 26 – Oct. 3, 1988. – Czech. Geol. Surv., 327–330.

Pruner P., Houša V., Olóriz F., Košťák M., Krs M., Man O., **Schnabl P.**,
Venhodová D., Tavera J.M. a Mazuch M.

High-resolution magnetostratigraphy and biostratigraphic zonation of the Jurassic/Cretaceous boundary strata in the Puerto Escaño section (southern Spain)

Cretaceous Research, 31, 2, 192 – 206, 2010

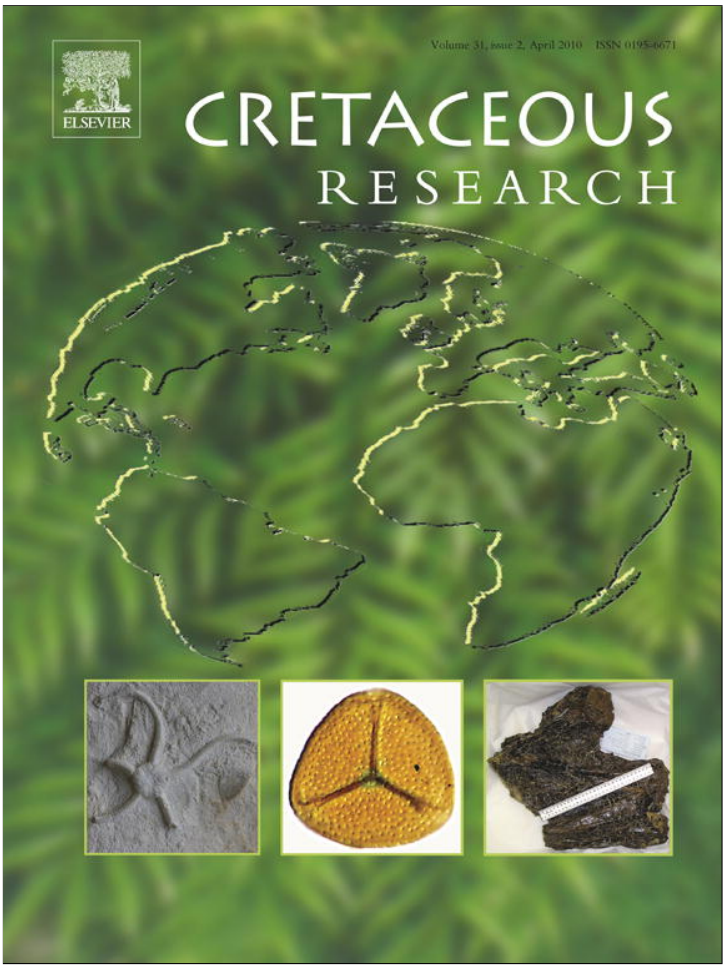

Cretaceous Research 31 (2010) 192–206

Contents lists available at ScienceDirect

Cretaceous Research

journal homepage: www.elsevier.com/locate/CretRes

High-resolution magnetostratigraphy and biostratigraphic zonation of the Jurassic/Cretaceous boundary strata in the Puerto Escaño section (southern Spain)

P. Pruner [a], V. Houša [a], F. Oloriz [b], M. Košťák [c,*], M. Krs [a], O. Man [a], P. Schnabl [a], D. Venhodová [a], J.M. Tavera [b], M. Mazuch [c]

[a] Institute of Geology, Academy of Sciences of the Czech Republic, v.v.i., Rozvojová 269, 165 00, Praha 6 – Lysolaje, Czech Republic
[b] Department of Stratigraphy and Paleontology, Faculty of Sciences, University of Granada, Av. Fuentenueva s/n Granada, Spain
[c] Institute of Geology and Palaeontology, Faculty of Science, Charles University in Prague, Albertov 6, Prague 2, Czech Republic

ARTICLE INFO

Article history:
Received 17 June 2009
Accepted in revised form 28 October 2009
Available online 10 November 2009

Keywords:
Ammonites
Magnetostratigraphy
Jurassic/Cretaceous boundary
Tintinnoids
Southern Spain
Subbetic Zone

ABSTRACT

This study summarizes the final results of magnetostratigraphic and biostratigraphic investigations of the Tithonian/Berriasian (J/K) boundary limestones at the locality of Puerto Escaño, Spain. The aim is to prepare the background for correlation of an upper Tithonian and lower Berriasian biostratigraphic zonation with global magnetoevents (manifested in detailed magnetostratigraphic profiles) between the Tethyan and the Boreal realms.

Magnetostratigraphic studies were applied to an 8.1-m-thick part of the section embracing upper Tithonian and lower Berriasian strata. The average sampling interval was 30 mm. The analysis of the IRM acquisition curves proved the presence of magnetite and hematite, the former mineral being the main carrier of the remanent magnetization. Progressive thermal demagnetization mostly revealed three NRM components, and magnetostratigraphy was based on the directions of the most stable of them, with unblocking temperature varying mostly from 300 to 540 °C. Due to almost parallel beds, the fold test applied to this component did not give convincing results. In contrast, the reversal test received the best classification 'A'. The detected polarity zones could has been unequivocally identified against the M-sequence of polarity intervals drawn from the Geomagnetic Polarity Time Scale 2004. This fact, together with the results of the reversal test, confirmed the ChRM to be the primary component. The sampled part of the section included a part of magnetozone M20r, full magnetozones M20n to M18r and a part of magnetozone M18n. Especially the detection of two reverse respectively by M20n.1r and M19n.1r with thicknesses only 40 and 90 mm, respectively, required much effort when sampling the section. The calculated sedimentation rate varied from 1 to 5 mm/ky.

The positions of the individual events of tintinnoid biostratigraphy (mainly calpionellids) relative to the global magnetic polarity timescale are precisely defined. The base of the Calpionella Standard Zone, which is considered to be a potential J/K boundary indicator in ammonite-free sections from the Tethyan realm, or in sections where calpionellid stratigraphy applies, lies within magnetozone M19n at the level of 35% of its local thickness. None of the boundaries in the calpionellid zonation coincides precisely with any of those in the palaeomagnetic zonation, but the first appearance datum (FAD) of *Calpionella grandalpina* Nagy, indicating the base of the Intermedia Subzone, lies in close proximity to the base of magnetozone M19r. The last appearance datum (LAD) for *Praetintinnopsella andrusovi* Borza in Bed 14A corresponds approximately to the base of the Kysuca Subzone.

1. Introduction

This study is included in a long-term project aiming at the correlation of biozones along the Jurassic/Cretaceous (J/K) boundary in the Tethyan and Boreal realms by means of magnetic polarity stratigraphy, which, unlike the biostratigraphic criteria, can be used for the correlation of chronostratigraphic units among diverse faunal realms, since the reversals of the polarity of the main geomagnetic dipole field are geologically rapid events recorded

* Corresponding author.
E-mail addresses: pruner@gli.cas.cz (P. Pruner), floriz@ugr.es (F. Olóriz), kostys@centrum.cz, kostak@natur.cuni.cz (M. Košťák), man@gli.cas.cz (O. Man), schnabl@gli.cas.cz (P. Schnabl), venhodova@gli.cas.cz (D. Venhodová), jtavera@goliat.ugr.es (J.M. Tavera), mmazuch@centrum.cz (M. Mazuch).

0195-6671/$ – see front matter © 2009 Elsevier Ltd. All rights reserved.
doi:10.1016/j.cretres.2009.10.004

simultaneously in all rocks in the world. Our attention is, therefore, confined to the sections where the geomagnetic polarity horizons can be precisely detected, allowing testing of the isochroneity of the biostratigraphic criteria that are currently in use.

In the last thirty years, magnetostratigraphy has been applied to many sections embracing the J/K boundary strata in the Tethyan realm (e.g., Ogg and Lowrie, 1986). These studies are, however, typically focussed on the construction of isochronous horizons in a series of stratigraphic sections rather than on detailed determination of boundaries in biostratigraphic terms and their correlation with magnetozones. The J/K boundary has been placed at various levels within the range of magnetozones M19 to M17 by different authors.

A synoptic magnetostratigraphic profile for Upper Mesozoic rocks from Tunisia was published by Nairn et al. (1981). Lowrie and Channell (1983) placed the boundary into the lowermost part of magnetozone M17 in pelagic limestones of the Maiolica Formation in the Bosso Valley, Italy. Magnetozones detected in this 110-m-thick section were correlated with the M-sequence of marine magnetic anomalies M19 to M14, or probably M13. The magnetostratigraphic investigation of the Maiolica and Calcari ad Aptici limestones from the Arcevia, Bosso, Contessa, and Gorgo a Cerbata land sections (Italy) was published by Speranza et al. (2005) including a detailed record of polarity chrons M21 to M14 and M9 to M0. Magnetozones M19–M15 were detected in pelagic limestones at the localities of Carcabuey and Sierra Gorda in southern Spain by Ogg et al. (1984). A short reverse polarity subzone was indicated in the normal part of magnetozone M20. Magnetozones M19–M14 were detected in the Umbrian Maiolica Formation in white pelagic limestones at Fonte del Giordano (Cirilli et al., 1984).

After the correlation of magnetostratigraphic data with calpionellid zones, Márton (1986) proposed placing the J/K boundary close to the base of M17; also Lowrie and Channell (1983), Channell and Grandesso (1987), Channell et al. (1987), and Ogg et al. (1991) contributed to the solution of this problem. Houša et al. (1999) detected magnetozones M20r–M17r in the Brodno section near Zilina and, on the basis of calpionellid zonation, placed the J/K boundary at approximately the middle of M19n, between M19r and reverse subzone M19n.1r (the Brodno Subzone), a solution which has been accepted by Grabowski and Pszczółkowski (2006), too. The fine structure of polarity zones was completed by the detection of subzone M20n.1r, too (the Kysuca Subzone). Namely the presence of these subzones makes the pattern of, say, eight polarity zones around the J/K boundary so distinctive that it can be unambiguously identified against the whole M-sequence of polarity intervals by a mathematical procedure (Man, 2008). To generalize the obtained results, particularly with respect to equal definition of calpionellid zones and their position relative to the detected magnetozones, the project was completed by other localities in the Tethyan realm, namely: (1) the Bosso Valley, central Italy, Umbria, where the magnetostratigraphy and biostratigraphy were well documented (Houša et al., 2004); (2) Rio Argos, Caravaca, Province of Murcia, SE Spain (Hoedemaeker et al., 1998) where limestones throughout the section were, however, found to be syn-tectonically and post-tectonically remagnetized.

This paper presents conclusive results concerning sub-section GA-7 located at Puerto Escaño, Spain (Fig. 1). This section complied with our requirements in three fundamental criteria: (1) lithological succession showing relatively "continuous" sedimentation not interrupted by marked diastems or hiatuses (i.e., sedimentary discontinuities with biostratigraphic relevance); (2) occurrence of rich fossil assemblages (calpionellids, ammonites) allowing a detailed biostratigraphic division; and (3) rocks evidencing magnetic properties that are favourable for reliable determination of palaeomagnetic polarity. The calpionellid assemblages are very well preserved and highly diversified. The record of their evolution is practically complete. Boundaries between individual zones and subzones of calpionellid stratigraphy could, therefore, be very precisely determined.

In the Tethyan realm, J/K boundary strata are ususally identified in limestones lacking ammonites (and other macrofossils) and therefore interpreted as relatively deep-water deposits. These sections also provide a relatively continuous lithological succession (i.e., hiatuses being below biostratigraphic resolution) which is assumed to represent a sedimentary record with minor incidence of hiatuses, thus, a very suitable condition for obtaining the magnetostratigraphic framework. Stratigraphy of these sections is therefore based on microfossils, among which calpionellid assemblages in particular provide very good possibilities for detailed biostratigraphic subdivision. However, the Puerto Escaño sub-section reflects not so deep environment with a relatively rich ammonite assemblage, belemnites, brachiopods, echinoids and less abundant bivalves.

A generally accepted provisional J/K boundary based on calpionellids is the base of the Calpionella Standard Zone (Remane et al., 1986). It was considered to be practically identical to the base of the ammonite Jacobi Zone. However, the interpretation of the J/K boundary coinciding with the lower boundary of calpionellid Zone A and the boundary between the Durangites and Jacobi ammonite zones has been proved wrong in Tethyan areas such as the Subbetic Zone and the Majorca Island (Olóriz and Tavera, 1989, 1990; Tavera et al., 1994; Olóriz et al., 1995). In accordance with data given by the authors mentioned, Tavera et al. (1994) showed that the base of the Jacobi Zone at Puerto Escaño is somewhat older than the base of the Calpionella Zone, which was detected ca. 1 m higher there. Inasmuch ammonites are absent from Brodno and other sites in deeper basinal facies of the Tethys, the J/K boundary in the Tethyan basinal sediments is defined as the base of the Calpionella Standard Zone. The position of this boundary in sections can usually be determined precisely (within the range of a few centimetres), mostly lying within a particular bed. In contrast, a precise J/K boundary determination on the basis of ammonites is possible in most probably shallower mid-outer shelf and epioceanic deposits (i.e, swells seawards from epicontinental shelves, underlain by continental crust) within the Tethyan realm. Ammonite taxa stratigraphically significant for the J/K boundary identification unfortunately occur "restricted" to these settings, whereas calpionellid assemblages are widely distributed in mid-outer shelf, epioceanic swells and deeper basinal troughs. Thus, looking for enhancig the correlation potential as the most, the provisional J/K boundary at the base of the Calpionella Standard Zone is favoured as the reference in this research.

2. Geological setting

The upper part of section GA-7, UTM 30SUG449859, investigated at Puerto Escaño, province of Córdoba, approximate coordinates 37°27' N, 4°17' W, belongs to the External Subbetic, Betic Cordillera, exposed in southeastern Spain (Fig. 1). Palaeogeographically, the External Subbetic corresponded to a distal, epioceanic environment during the Late Jurassic and the earliest Cretaceous (e.g., Olóriz et al., 2004). The upper Jurassic to lowermost Cretaceous deposits in section GA-7 consist of Ammonitico Rosso and related facies, ranging from well-bedded limestones to clayey limestone horizons of nodular aspect reflecting deposition on distal, epioceanic swell. Although the depositional conditions on raised blocks (swells) commonly resulted in omission/erosion below biostratigraphic resolution (e.g., frequent firmgrounds as identified by Caracuel et al., 2000 in the studied sub-section GA-7), precise biostratigraphy at the biozone level is available for both ammonites and tintinnoids (Olóriz, 1978; Tavera, 1985; Tavera et al., 1994; Caracuel, 1996, Olóriz et al., 2004 and references therein) and, hence, biochronostratigraphic

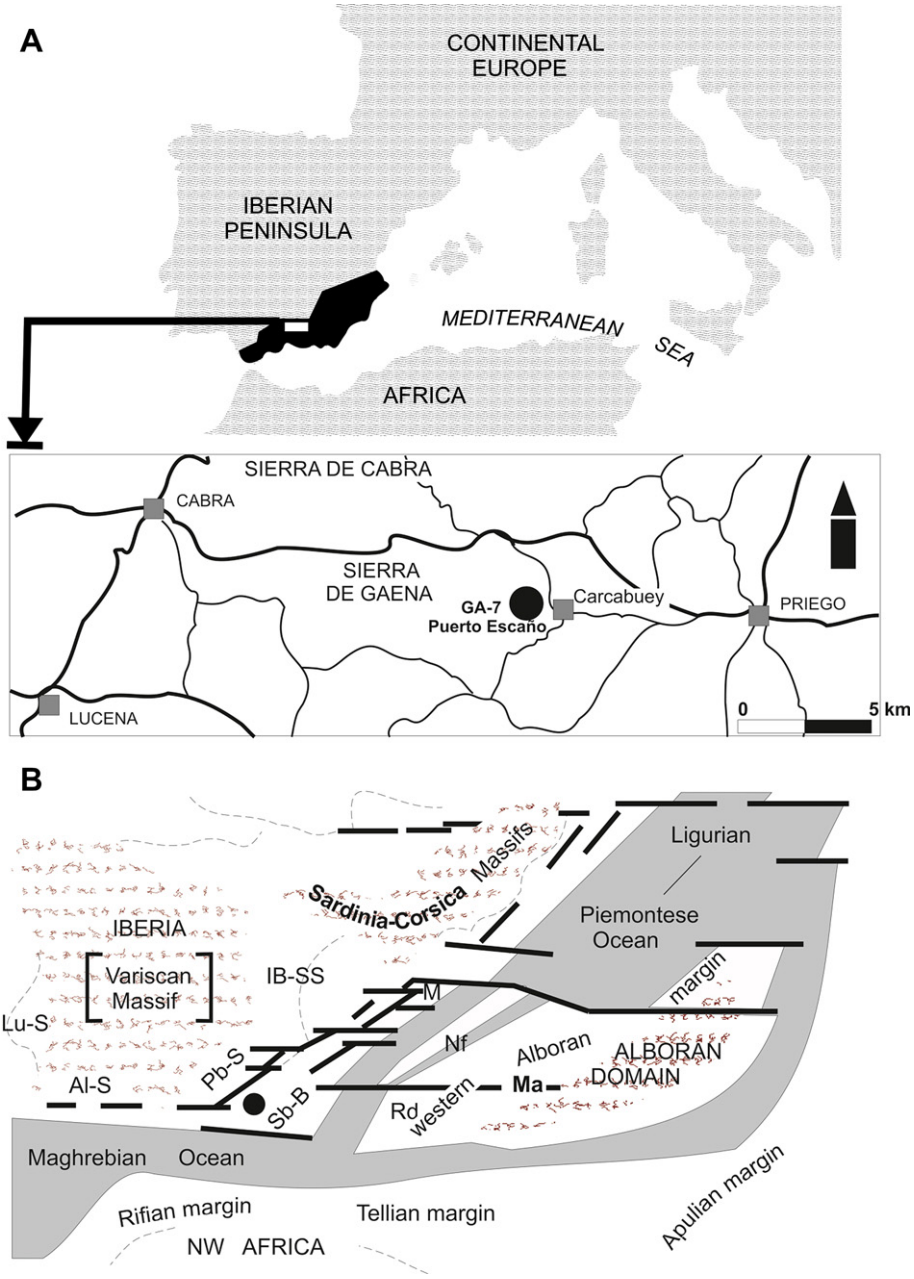

Fig. 1. A, Geographical location of the area with the studied section (top); inserted map showing the position of section GA-7 at Puerto Escaño (geographical coordinates: 37.44° N; 4.28° W) and roads in the surroundings (bottom): black area for the Betic Cordillera. B, Palaeogeographic sketch for Tithonian - Berriasian as interpreted in Olóriz et al. (2004): Algarve Shelf [AL-S]; Iberian Shelf-System [IB-SS]; Lusitanian Shelf [Lu-S]; Majorca and related areas [M], except Minorca; Malaguide Complex [Ma]; Nevado-Filabride Complex [Nf]; Prebetic Shelf [Pb-S]; Rondaides Complex [Rd]; Subbetic Basin [Sb-B]. Section GA-7 at Puerto Escaño [black point]; Epicontiental (AL-S, IB-SS, Lu-S, PB-S) and epioceanic (Sb-B & M) environments [white]; Oceanic environments [shaded].

correlation with the standard zonation for the Western Tethys (e.g., Geyssant, 1997).

The studied sub-section is dominated by wackestones showing microfacies with variable contents of radiolarians, calcisphaeres, dinoflagellates, planktonic crinoids, unidentifiable foraminifers (planktonic and benthic), organic and hyaline loricated tintinnoids ("chitinoidellids" and calpionellids, respectively), ostracodes, cephalopods (ammonitella, and fragments of juvenile and adult ammonite shells), and broken molluscs, echinoderms (plates and spines), sponge spicules and pelagic bivalves, among others. Dominant, macroscopic fossil remains are ammonoids, and less abundant components are belemnites, brachiopods and echinoids. Burrowing was common and mainly realized through *Thalassinoides*- *Chondrites*- and *Planolites*-makers (e.g., Caracuel, 1996; Caracuel et al., 2000).

3. Rock magnetism and magnetostratigraphy

Our approach is confronted below with the quality criteria proposed by Opdyke and Channel (1996). Their list is too long to be reproduced here, but its separate points will be mentioned in the following text. The first of these criteria, requiring the stratigraphic age of the section to be known to the level of the stage, has been satisfied by the nature of the project. The ninth and the tenth

criteria, however, requiring radiometric dating and multiple sections, respectively, have not been satisfied; radiometric dating could not be carried out due to the absence of magmatic rocks.

3.1. Sampling

An 8.1-m-thick part of the section embracing upper Tithonian and lower Berriasian sediments was accurately measured and systematically logged (the second criterion). The beds were labelled with numbers. Orientated hand samples for magnetic measurements were not collected once and for all; instead, we started with relatively few samples, took the necessary measurements, and constrained the levels of the expected geomagnetic polarity horizons. With the increasing number of samples, these levels and the boundaries between biostratigraphic zones were progressively detected with higher precision. The sampling density was, however, limited by the 20 mm size of the cubes used for magnetic measurements. The above described economic sampling strategy finally yielded 278 samples. The average sampling interval was 30 mm. Taking into account the average deposition rate estimated in sub-section 3.5, this value corresponds to 8.6 ky in the time scale, classifying our magnetostratigraphic data as high-resolution data.

The uniform bedding-plane orientation of the beds with strike of $44.1 \pm 19.4^{\circ}$ and dip angle of $29.2 \pm 6.3^{\circ}$ was unfavourable for the successive fold-test applied to the directions of the natural remanent magnetization (NRM).

3.2. Laboratory equipment

NRM measurements were carried out using either the spinner magnetometers JR-5A and JR-6A (AGICO Brno) or Liquid helium-free Superconducting Rock Magnetometer type 755 4 K SRM (2G ENTERPRISES). In order to resolve the components of NRM, the latter equipment used the alternating field demagnetization up to the peak field of 160 mT, while the former was mostly combined with the thermal demagnetization in the field-free space produced by the MAVACS equipment, and seldom with the Mu metal shielded alternating field demagnetizer LDA-3A (AGICO Brno). The ambient magnetic field in the cooling chamber of the MAVACS demagnetizer did not exceed 1 nT owing to a built-in rotating coil magnetometer controlling the currents in its Helmholtz coil system (Příhoda et al., 1989). Processing of the output data, including, e.g., the multicomponent analysis of the demagnetization path, was carried out by Remasoft 3.0 software (Chadima and Hrouda, 2006). Magnetic susceptibility was measured by the KLY-4 Kappabridge (AGICO Brno) (Jelínek, 1966, 1973).

3.3. Identification of magnetic minerals and significance of the NRM components

According to the sixth criterion of Opdyke and Channel (1996), particular attention should be given to magnetic mineralogy, which may constrain the timing of remanence acquisition. The coercivity spectrum of magnetic minerals studied by means of acquisition curves of the isothermal remanent magnetization (IRM) provides one possible key to it. Having been obtained for ten pilot samples in magnetic field progressively increasing up to 2 T, these curves demonstrated the presence of magnetite and hematite (see examples in Fig. 2). These components, widely differing in their coercivities, were quantified by the method of Kruiver et al. (2001), which is based on the assumption that the IRM acquisition curve of a particular mineral can be approximated by a log-normal distribution function described by two parameters, of which parameter $B_{1/2}$ represents the field at which the mineral phase would acquire half of its saturation IRM. The application of the Irmunmix V2.2 software proved that magnetite, with parameter $B_{1/2}$ between 8 mT and 12.5 mT, contributed by 70 to 93 % to the bulk IRM curve, while hematite, with parameter $B_{1/2}$ between 63 mT and 630 mT,

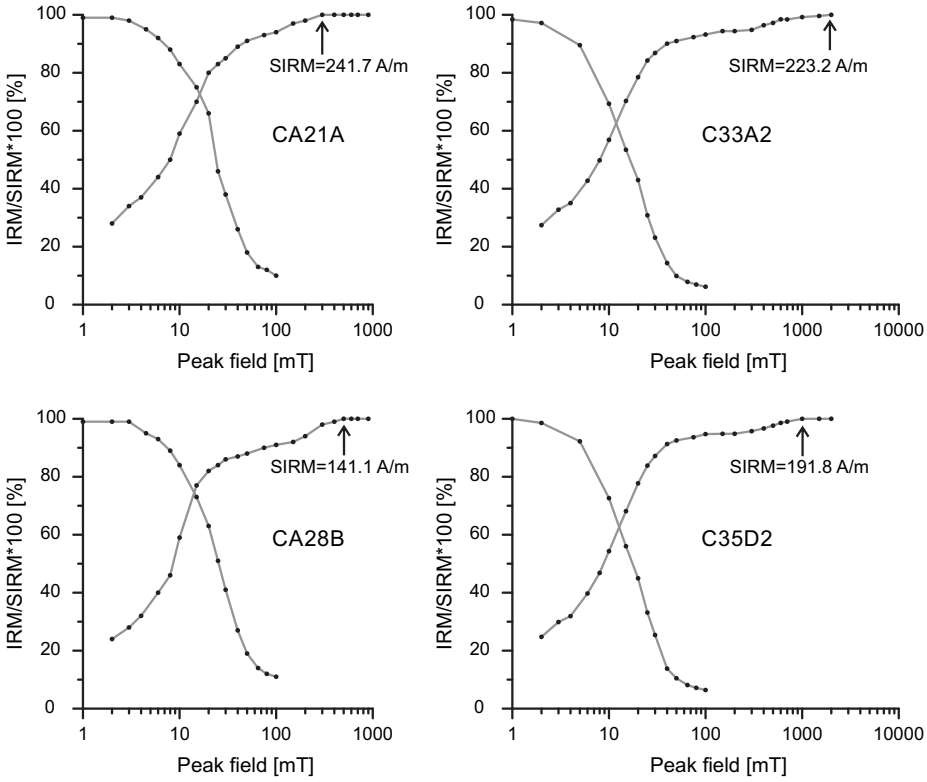

Fig. 2. Examples of IRM acquisition and AF demagnetization curves for limestone samples CA21A (2.14 m), CA28B (4.41 m), C33A2 (5.17 m), CA35D2 (5.55 m).

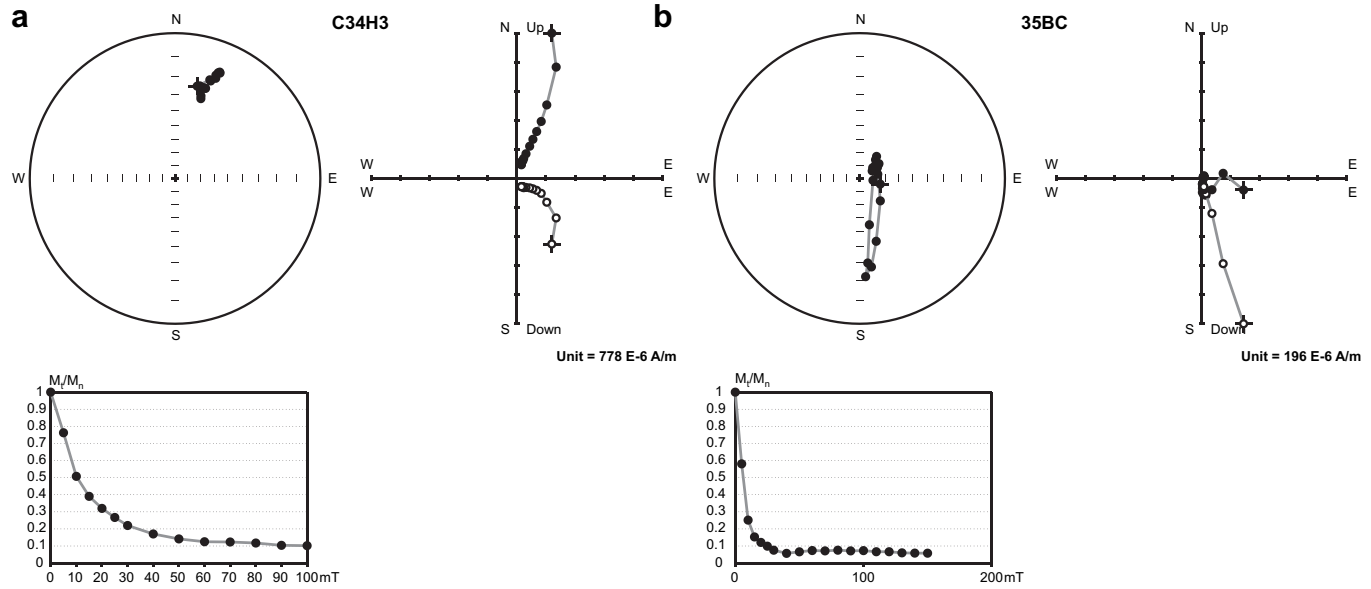

Fig. 3. Results of the progressive AF demagnetization of two limestone samples (a – C34H3 (5.40 m); b – C35BC (7.73 m). The NRM directions are tilt-corrected. Top left, stereographic projection of these directions after each demagnetization step. Solid and open circles represent projections on the lower and upper hemispheres, respectively. Top right, the Zijderveld diagram, showing projections of the demagnetization paths. Projections onto horizontal (*XY*) and vertical (*XZ*) planes are marked by solid and open circles, respectively. Bottom left, normalized remanent magnetization depending on the AF intensity.

contributed by 7 to 30 %. Since the saturation magnetization of magnetite is almost thousand times higher than that of hematite, it can be concluded that, although magnetite is the main NRM carrier in the studied rocks, the rocks contain higher amounts of hematite, likely the authigenic secondary mineral formed during diagenesis.

The third criterion requires complete thermal/AF demagnetization of all specimens and analysis of the components of the NRM carried out using orthogonal projections. An experiment carried out with several pilot samples proved that the progressive stepwise demagnetization in 11 or 12 thermal fields gave better results than the AF demagnetization (Fig. 3). The former procedure was, therefore, applied to the majority of samples. Each heating step was followed by the measurements of both the vector of NRM and the magnetic susceptibility. If the symbols M_n and M_t denote the NRM in the natural state and that heated to temperature t and cooled in magnetic vacuum to the room temperature, respectively, the ratio M_t/M_n plotted against temperature t shows the unblocking temperatures of the NRM carriers. Similarly, the bulk magnetic susceptibility measured after the above heating step plotted against the temperature t can detect possible phase changes of minerals during the thermal processing. The examples are given in Figs. 4 and 5, showing also the demagnetization paths expressed both by

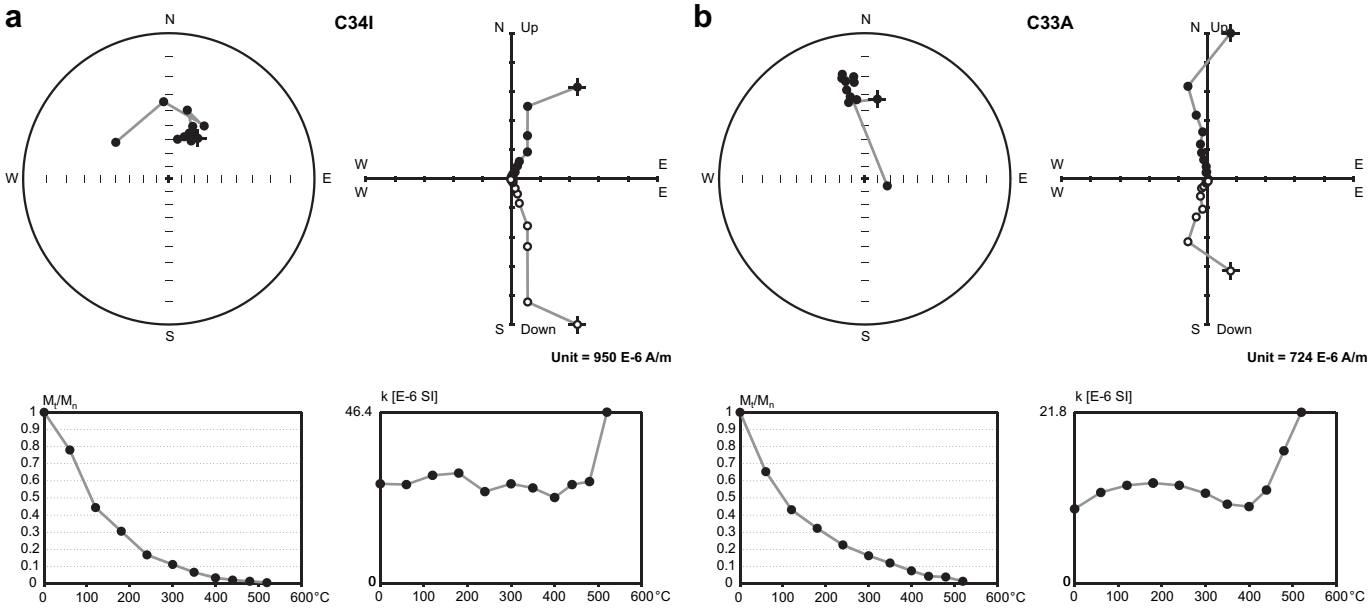

Fig. 4. Results of the progressive thermal demagnetization of two limestone samples (a – C34I (5.42 m); b – C33A (5.17 m) with normal polarity of component C. The NRM directions are tilt-corrected. Top left, stereographic projections of these directions after each heating step. Top right, the demagnetization path expressed by the Zijderveld diagram. Bottom left, the normalized remanent magnetization M_t/M_n. Bottom right, the bulk magnetic susceptibility depending on the temperature achieved during the previous heating step.

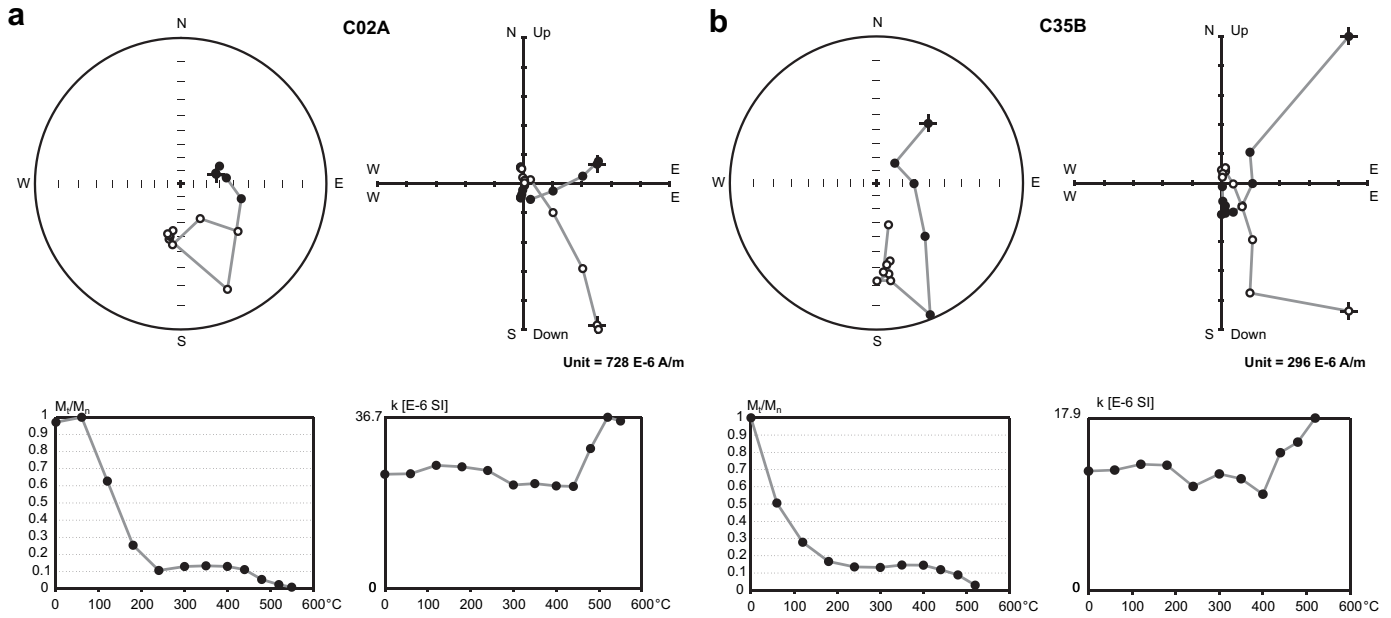

Fig. 5. Results of the progressive thermal demagnetization of two limestone samples (a – C02A (-0.14 m); b – C35B (5.53 m) with reverse polarity of component C. See the caption of Fig. 4.

Zijderveld diagrams consisting of two orthogonal projections of NRM vectors after each heating step, and by stereographic projections of their directions.

The fourth criterion requires the directions of particular NRM components to be determined from the least squares line fitting of the demagnetization path (Kirschvink, 1980). This multicomponent analysis of thermal demagnetization paths revealed that the NRM of the vast majority of samples is composed of three components. The A-component was erased in the temperature range of 20 to 60 °C (sometimes 120 °C), the B-component in the temperature range of 60 to 240 °C, and the C-component in the temperature range 300 to 520 °C (580 °C). The B-component is not always visible in the AF demagnetization path. The most stable C-component is the characteristic component of NRM (ChRM). Since it cannot exceed the Curie temperature, the above unblocking temperature confirms magnetite and, maybe, hematite, as the carriers of this component.

The A-component is undoubtedly of viscous origin. The B-component is the dominant one and its direction reflects always the normal polarity of the geomagnetic field. Applied to the directions of this component, the fold test after McElhinny (1964) has proved that there is no significant difference at the 95% significance level in the precision parameter between distributions of bedding-tilt-corrected directions and those expressed in geographic coordinates (Table 1). The mean direction in geographic coordinates is close to the direction of the present-day geocentric axial dipole field ($D = 358°$, $I = 51.5°$), suggesting that this component has been acquired in the near past, probably during the Neogene. It is worth mentioning that similar post-tectonic components have been detected at other localities in the Tethyan realm (Parés and Roca, 1996, Villalaín et al., 1996, Hoedemaeker et al., 1998, Houša et al., 2004). In contrast to the B-component, the bedding-tilt-corrected directions of the ChRM (Fig. 6) reflect both the normal and the reverse polarities of the geomagnetic field. The directions of the latter group having been reversed (see the following sub-section), the fold test applied to the set of all directions did not prove a significant difference in the precision parameter between two possible coordinate systems, which can be attributed to the almost uniform bedding mentioned in sub-section 3.1. The virtual pole position corresponding to ChRM (Table 2) is not very different from the positions given by other authors for nearby localities and Late Jurassic to Early Cretaceous Periods, for example locality Carcabuey, 146 to 155 Ma, VGP 62.3° N, 113.49° E (Ogg et al., 1984) and locality Cehegin, 136 to 146 Ma, VGP 63.8° N, 100.5° E (Ogg et al., 1988). This fact makes the primary origin of the ChRM very likely, but the definite evidence will be given in sub-section 3.5.

3.4. The NRM and the bulk magnetic susceptibility

Susceptibilities and NRM values are plotted against the sample level (also termed stratigraphic distance, cf. Opdyke and Channel, 1996) in Fig. 7. An obvious decrease in these values from older to younger rocks in the vicinity of J/K boundary (cf. Table 3) was observed also in Brodno and Bosso Valley sections (Houša et al., 1999; 2004) as well as in sections from the Tatra Mts (Central Carpathians, see Grabowski and Pszczółkowski, 2006). A local decrease in these values observed around the level of 4.3 m may be attributed to the partial recrystalization of Bed 28.

Table 1
Results of the fold test applied to the particular NRM components.

Age	Component of NRM	Number of samples	Bedding-tilt corrected directions				Directions expressed in geographic coordinates				κ_2/κ_1	Result
			Mean		α_{95} [°]	κ_2	Mean		α_{95} [°]	κ_1		
			D [°]	I [°]			D [°]	I [°]				
L. Tithonian – E. Berriasian	B	278	57.3	58.6	1.41	35.4	15.5	50.4	1.41	35.4	1.00	Insignificant
L. Tithonian – E. Berriasian	C	272	29.6	45.9	1.54	30.4	9.6	30.2	1.59	28.7	1.06	Insignificant

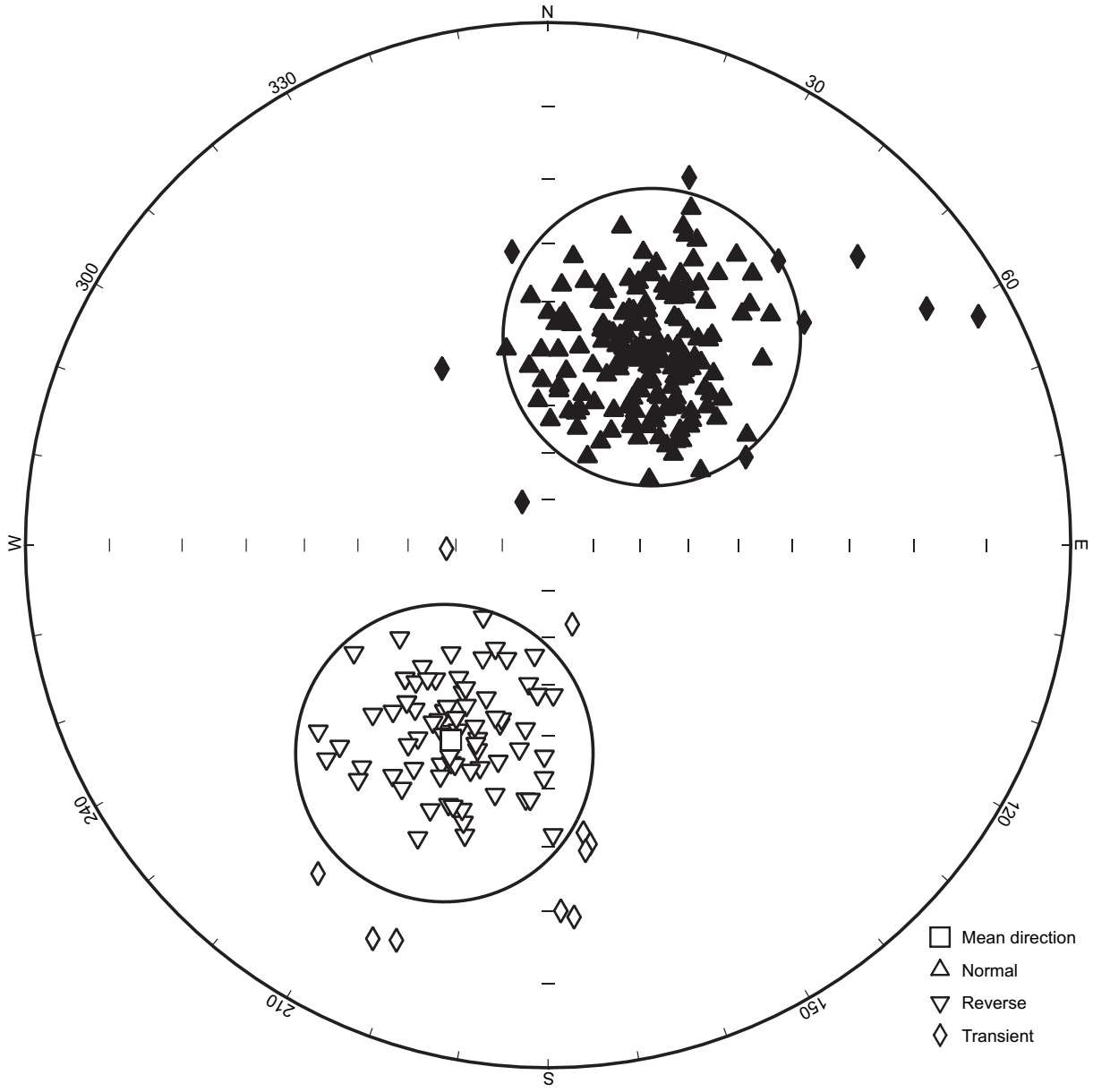

Fig. 6. Stereographic projections of the bedding-tilt-corrected directions of the ChRM and the classification of these directions. The directions of normal, reverse, and intermediate polarities are plotted by different symbols.

3.5. Magnetostratigraphy

Magnetostratigraphy is based on the bedding-tilt-corrected directions of ChRM (herein termed simply 'directions', for short), depending on the sample level (Fig. 7). The resolution of geomagnetic polarity zones and their identification against the geomagnetic polarity time scale (GPTS, Gradstein et al., 2004) were carried out by the MPS program available at http://gli.cas.cz/man (see also Man, 2008).

Table 2
VGP position corresponding to ChRM.

Age	Location		Palaeomagnetic pole position		Ovals of confidence	
	Lat. [°]	Long. [°]	ϕ_p [°]	λ_p [°]	δ_m [°]	δ_p [°]
L. Tithonian - E. Berriasian	37.45N	4.28W	63.13N	99.26 E	1.3	2.0

In order to be classified, the directions, regarded as axial vectors at the beginning, were characterized by a principal axis, i.e., by the eigenvector of the orientation matrix linked with its greatest eigenvalue (cf. Fisher et al., 1987); this approach was recommended by Opdyke and Channel (1996). The principal axis has, however, two possible orientations. The orientation $D = 26°$, $I = 45°$ has been regarded as a positive one, since the corresponding VGP (65°N, 105°E) was situated on the northern hemisphere, and each direction was characterized by the cosine of its deflection from the orientation of the principal axis, which is herein termed the discriminant function. The set of directions has been partitioned into two basic groups according to the sign of this function. The hypotheses that in both groups the mean directions are identical with the respective orientations of the principal axis and the deflections from these mean directions are equally distributed could not be rejected at the 5% significance level. This result may be taken for the evidence that the ChRM is really the primary component (the eighth criterion – reversals are antipodal). Moreover the hypothesis that the above

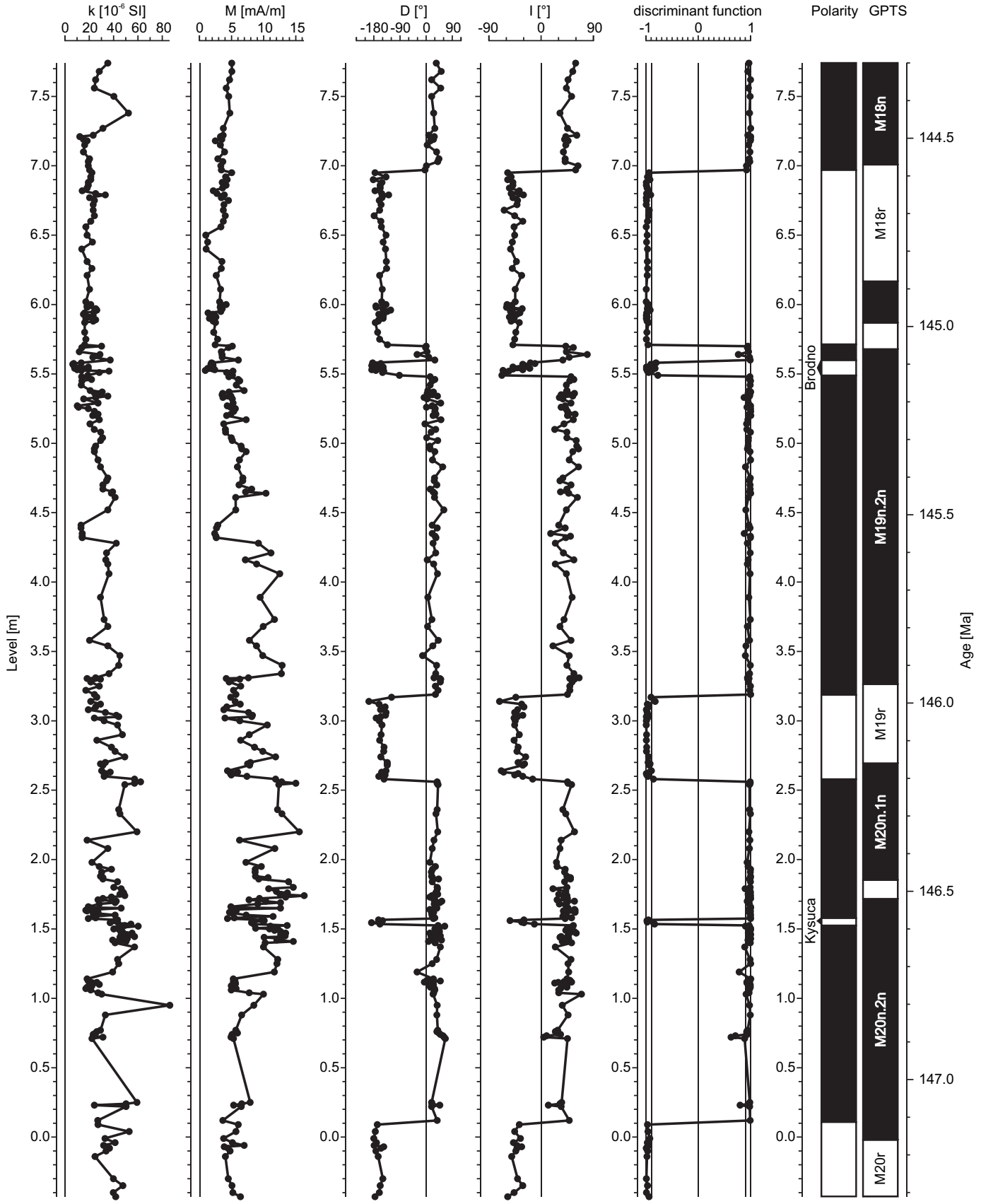

Fig. 7. Important palaeomagnetic data plotted along the section. From the left: the measured values of both bulk magnetic susceptibility and NRM (denoted by symbols *k* and *M*, respectively), the direction of the ChRM, found by the line fitting of the demagnetization path and expressed by declination *D* and inclination *I*, and the discriminant function of this direction, all plotted against the sample level (or stratigraphic distance). Polarity zones inferred from the discriminant function and expressed by the black (normal) and white (reverse) bar diagram are compared with the corresponding part of the GPTS 2004, against which they have been identified (on the right).

Table 3
Natural remanent magnetization and bulk magnetic susceptibility.

Age	Number of samples	NRM [10-6A/m]		Bulk magnetic susceptibility [10-6 SI]	
		Mean value	Standard deviation	Mean value	Standard deviation
Late Tithonian	157	8281	3190	35.3	12.0
Early Berriasian	121	3937	1640	22.0	8.0

distribution is Fisherian (Fisher, 1953) with precision parameter $\kappa = 29$ could be rejected. The normal or reverse polarities were, therefore, assigned to the directions within the cones of 95% confidence (whose deflections from the mean direction did not exceed 26.4°), while the directions beyond these limits were considered intermediate (see Fig. 6). This way, 166, 86, and 20 directions were classified as normal, reverse, and intermediate, respectively.

In order to enable the conventional classification of our data, the reversal test after McFadden and McElhinny (1990) was applied to both groups of directions. The results shown in Table 4 are in good agreement with the previous ones. With $\gamma_c = 1.9°$, the reversal test must be classified as 'A' (as for the definition of angle γ_c, see McFadden and McElhinny, 1990).

The above classification of directions is visible in Fig. 7, too, the range (-1,1) of the discriminant function being partitioned by two vertical lines into three intervals, corresponding (from the left) to reverse, intermediate, and normal polarities, respectively. Having omitted the intermediate directions, opposite polarities of the successive samples indicated the borders between successive geomagnetic polarity zones, i.e., the polarity reversal horizons (GPRH). Since we considered the above approach to be superior to the widely recommended one based on the VGP latitudes, these latitudes were not included into Fig. 7.

The detected levels of the GPRH are shown in Table 5, as required by the fifth criterion of Opdyke and Channel (1996). As the stratigraphic position of the section was inferred from palaeontology, the detected polarity zones could be easily identified against the Geomagnetic Polarity Time Scale (GPTS) 2004 redrawn at a proper scale (Fig. 7). This way, GPRH levels were given numerical ages according to the Geologic Time Scale 2004 (Gradstein et al., 2004). The striking similarity between the sequence of polarity zones and that of polarity intervals leaves no doubts about the completeness of the former sequence and the correctness of the identification. This similarity, together with the convincing result of the reversal test, represents the definite evidence that the characteristic component is really the primary one.

In fact, the constraints inferred from palaeontology were not necessary for the unequivocal identification of polarity zones against the M-sequence of polarity intervals. In order to prove it, a special transform reducing the impact of the variable sedimentation rate (Man, 2008, Eq. (1)) was applied to the thicknesses of the polarity zones. The M-sequence of polarity intervals was transformed in a similar way (Man, 2008, Eq. (2)) and the resemblance between both sequences shifted relative to each other was assessed by their cross-correlation function. The lag maximizing this function linked the uppermost detected GPRH with the reversal M18r/M18n (Fig. 8). The reliability of this identification was about 99 %

Table 4
The reversal test.

Polarity	Number of samples	Mean direction		κ	α_{95} [°]
		D [°]	I [°]		
Normal	166	26.8	44.9	33.8	1.9
Reverse	86	205.5	−46.1	35.7	2.5

Table 5
The GPRH levels and their identification against the GPTS.

GPRH level [m]	Reversal	Age in Ma (GPTS 2004)
0.105 ± 0.015	M20r/ M20n.2 n	147.16
1.530 ± 0.005	M20n.2 n/M20n.1r	146.52
1.570 ± 0.005	M20n.1r/ M20n.1n	146.47
2.580 ± 0.020	M20n.1n/M19r	146.16
3.180 ± 0.010	M19r/M19n.2n	145.95
5.495 ± 0.015	M19n.2 n/M19n.1r	145.06
5.585 ± 0.015	M19n.1r/M19n.1 n	144.99
5.705 ± 0.005	M19n.1 n/M18r	144.88
6.960 ± 0.010	M18r/M18n	144.57

owing to characteristic features of the sequence of the polarity intervals around the J/K boundary, mentioned in Sect. 1, namely to the existence of short polarity intervals M20n.1r and M19n.1r.

The studied portion of the section included a part of magnetozone M20r, full magnetozones M20n to M18r and a part of magnetozone M18n (Fig. 7). A special attention, expressed by sampling density, was focused on the detection of two narrow reverse subzones M20n.1r and M19n.1r, named Kysuca Subzone and Brodno Subzone, respectively (Houša et al., 1999). Being situated in the upper parts of zones M20n and M19n, they are only 40 and 90 mm thick, respectively (Figs. 9 and 10). Previously detected in the Brodno and Bosso Valley sections (Houša et al., 1999; 2004), and in the Tatra Mts. (Grabowski and Pszczółkowski, 2006), these subzones were correlated with the distribution of calpionellid taxa. Like with the Brodno and Bosso Valley sections, the thickness of the detected polarity zone M20n.1r was much smaller than the thickness of 14 cm deduced from the average sedimentation rate and the length of the polarity interval given by the GPTS 2004. A possible explanation is that the latter has been overestimated.

Using a substantial part of Table 5, the time-dependent section thickness was expressed by a smoothing spline, whose derivative showed the smoothed sedimentation rate ranging from 1 to 5 mm/ky (Fig. 11). Regarding this sedimentation rate as a stationary Gaussian random process, its parameters were estimated by the maximum likelihood method as follows: mean 2.87 mm/ky, standard deviation 1.17 mm/ky. These values are in general agreement with those expected for pelagic sediments (cf. Butler, 1991, p. 191). When combined with the smoothed sedimentation rate, Table 5 confirms that the duration of some polarity reversals does not exceed 3.5 ky.

4. Biostratigraphy

4.1. Biozonation based on tintinnoids

From the basal part of the sub-section (i.e., Beds 5–13, Fig. 12) the registered assemblage of tintinnoids consists of species belonging to the Deflandronellidea family Chitinoidellidae [*Longicollaria dobeni* (Borza) (Beds 5–11) and *Chitinoidella boneti* Doben (Beds 7–13)] and clearly proves the presence of the *Chitinoidella* Zone, as previously identified in the area as well as in more or less distant Tethyan sections (e.g., Olóriz and Tavera, 1981, 1989; Benzaggagh and Atrops, 1995; Olóriz et al., 1995; Caracuel 1996; Reháková 2000a,b; 2002; Zeiss, 2001; Houša et al. 1999, 2004). *Longicollaria dobeni* has been recorded from the base of the subsection (from Bed 5): from the topmost part of the M20r and basal part of the M20n magnetic zones. Tintinnoid diversity is very low in the interval between Bed 5 and Bed 11, and only *Chitinoidella* species occur in this part of sub-section. The combined record of the single occurrence (LAD) of *Borziella slovenica* (Borza) in Bed 5 and the FAD of *Chitinoidella boneti* in Bed 7 support the interpretation of the *Longicollaria dobeni*/*Chitinoidella boneti* Subzones boundary at the top of Bed 6.

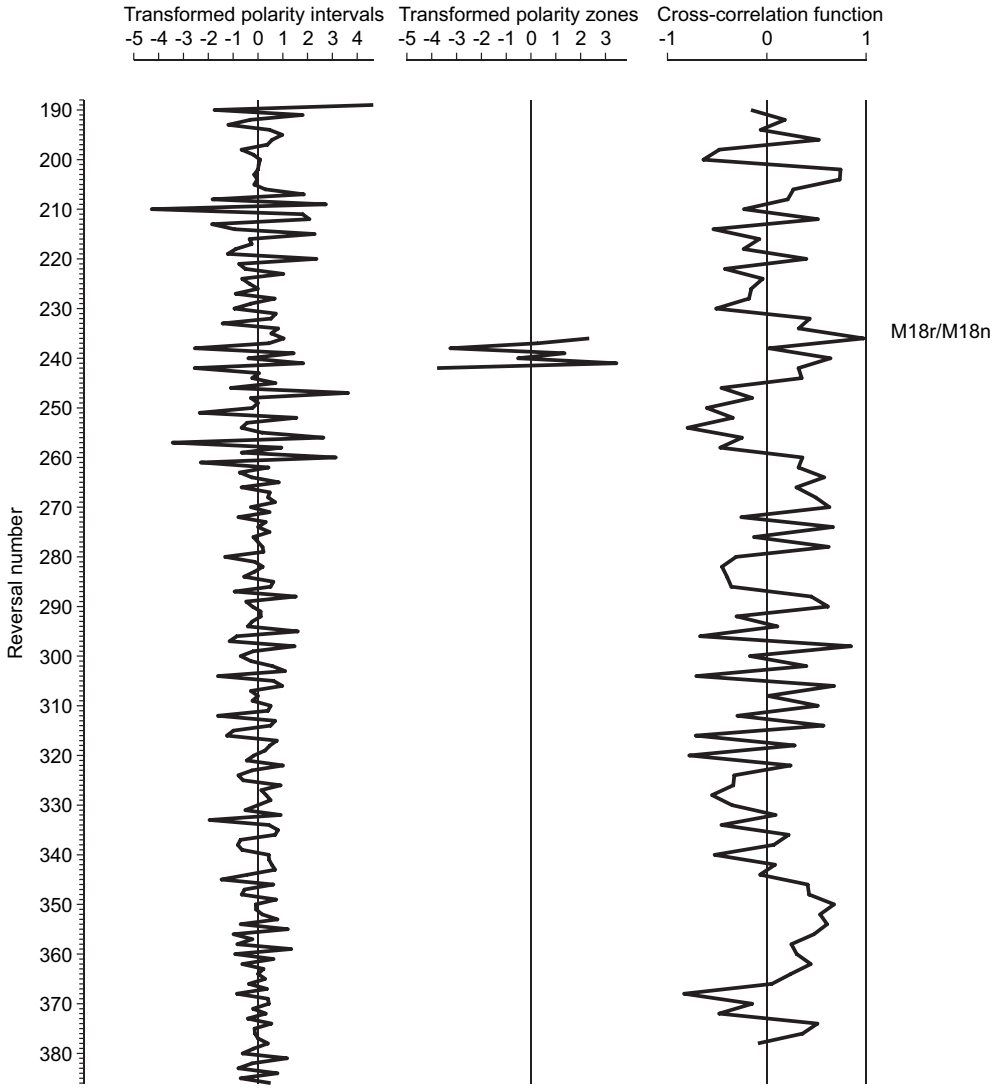

Fig. 8. Identification of the detected polarity zones against the M-sequence of polarity intervals. The thicknesses of polarity zones were replaced by the differences of their logarithms, and the lengths of polarity intervals were transformed in a similar way. The resemblance of these two sequences, having been shifted against each other, is expressed by the cross-correlation function, whose maximum identifies the former sequence against the latter.

Middle to upper parts of Bed 11 show a higher diversity of tintinnoids, including the FAD of Semichitinoidellidea (Semichitinoidellidae). The first appearance datum (FAD) of the Semichitinoidellidae *Praetintinnopsella andrusovi* Borza in Bed 11 defines the base of the *Praetintinnopsella* Zone, located in the middle part of the M20n magnetic zone, and the last appearance (LAD) was recorded just below the reverse Kysuca Subzone (M20n.1r) – i.e., the upper part of Bed 15 at Puerto Escaño. The FAD of *P. andrusovi* at Puerto Escaño is in accordance with that in the Brodno section in Slovakia (Houša et al., 1999; Reháková 2000b). In the Bosso Valley section in Italy, however, *P. andrusovi* appears later – in the upper but not the uppermost part of the M20n magnetic

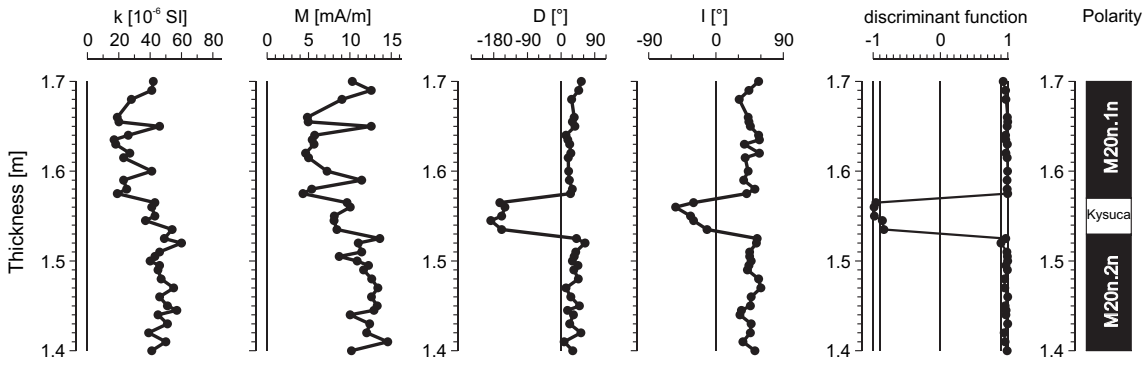

Fig. 9. A part of Fig. 7 that includes the Kysuca Subzone (M20 n.1r) redrawn at a more detailed scale. See the caption of Fig. 7.

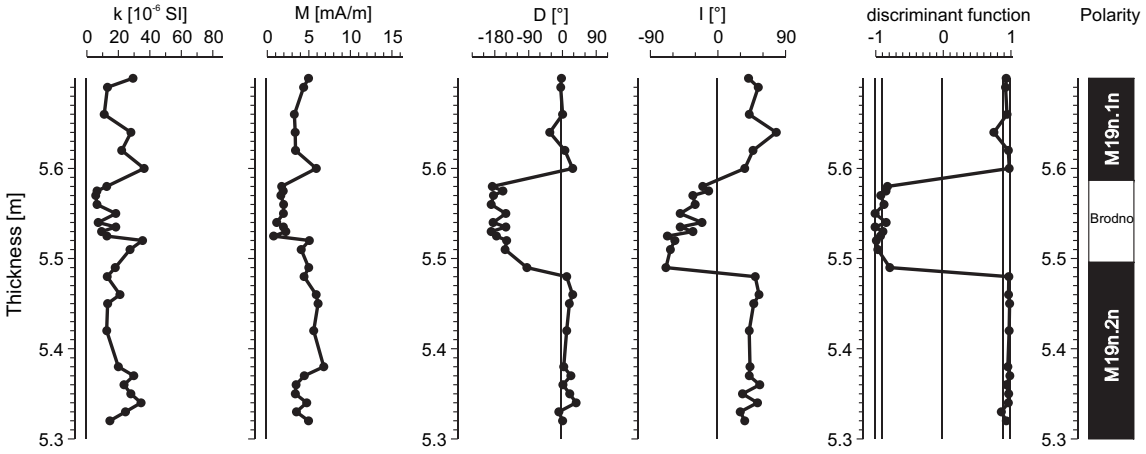

Fig. 10. A part of Fig. 7 that includes the Brodno Subzone (M19 n.1r) redrawn at a more detailed scale. See the caption of Fig. 7.

zone (i.e., about 4 m above the Kysuca Subzone M20n.1r, Houša et al., 2004 – see below). In the studied sub-section GA-7, the base of the *Praetintinnopsella* Zone coincides with the FAD of Calpionellidae – i.e., *Calpionella* species (*Calpionella* sp A and B; Houša et al., 2004), which are morphologically closely related to the large Berriasian form of *Calpionella alpina* Lorenz. However, their stratigraphic range at Puerto Escaño is limited to the interval between Beds 11 and 16, and 11 and 20, respectively. In west-Tethyan areas, the FAD of scarce calpionellids together with a variable record of the youngest *Chitinoidella* have been previously interpreted as the lowermost part of the *Crassicollaria* Zone (e.g., Olóriz et al., 1995), even below the FAD of *Tintinnopsella remanei* Borza (e.g., Benzaggagh and Atrops, 1995), and referred to the standard *Remanei* Subzone or to a slightly older horizon where the index species is scarce.

The first *Tintinnopsella* (*Tintinnopsella remanei* and *T. carpathica* (Murgeanu et Filipescu)) appears in Bed 14. The *Praetintinnopsella*/*Crassicollaria* zonal boundary is placed at the FAD of *T. carpathica* (Remane et al., 1986) – i.e. 15 cm below the base of the reverse Kysuca Subzone (M20n.1r). This occurrence corresponds to the situation in the Brodno section (Houša et al., 1999). In the Bosso Valley, the major part of the M20n including the M20n.1r Kysuca Subzone does not contain any relevant calpionellid record (see Houša et al., 2004, fig. 9) and the stratigraphic position is indicated by the presence of cysts of calcareous dinoflagellates. The range zone of *Tintinnopsella remanei* at Puerto Escaño was recorded from Bed 14 (base of the *Crassicollaria* Zone) to the lower part of the Bed 22 (lower part of the *Crassicollaria* Zone). The base of the *Remanei* Subzone was established at the FAD of *Tintinnopsella remanei* and *T. carpathica*.

The reported records from the nearby Tethyan areas indicate an alternative record of *Tintinnopsella remanei* below the FAD of *Crassicollaria intermedia* (Morocco, Benzaggagh and Atrops, 1995) or their co-occurrence (Majorca Island, Olóriz et al., 1995). It seems

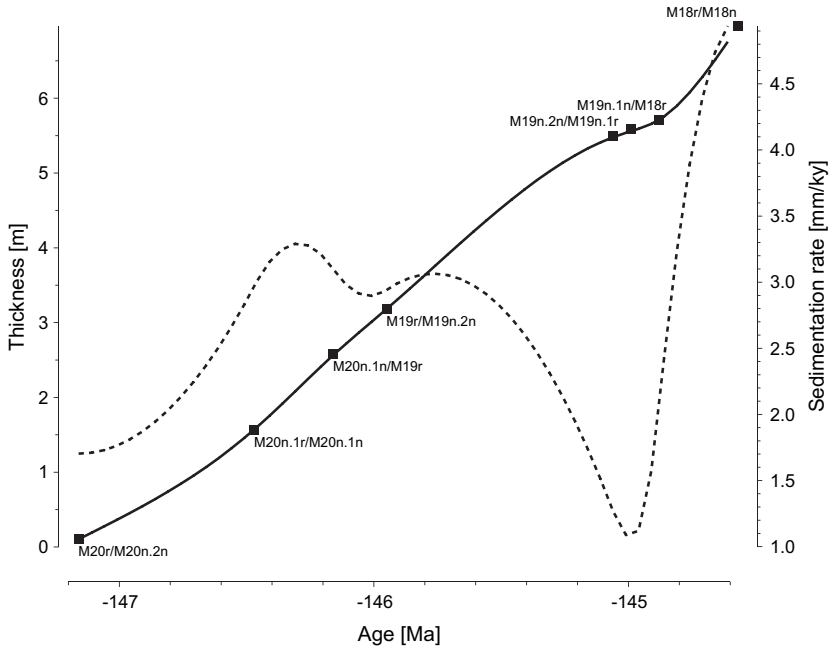

Fig. 11. The thickness of the section plotted against the age according to Table 5 (squares) and interpolated by a smoothing spline (full line). The reversal of M20 n.1r/M20 n.1 n was omitted because the length of polarity interval M20 n.1r given by the GPTS 2004 was likely overestimated. The derivative of the spline function (dashed line) represents the smoothed sedimentation rate.

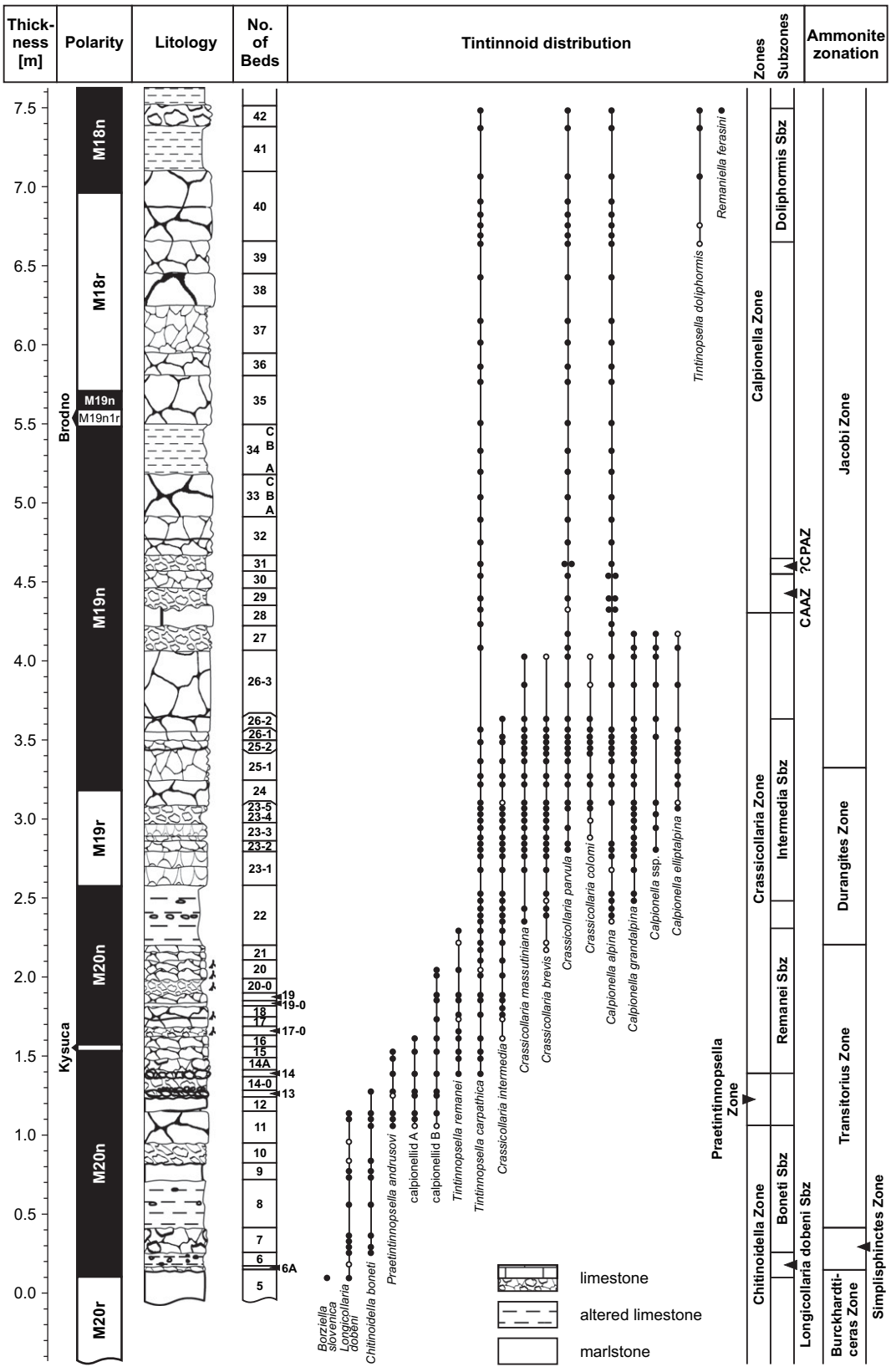

Fig. 12. Lithostratigraphy and biostratigraphy (calpionellid and ammonite data) plotted together with the detected polarity zones. Note: Bed numbers in intervals 5-21 and 30-42 are newly re-numbered in more detail. CAAZ - Calpionella alpina "acme zone" (=epibole), ?CPAZ - Crassicollaria parvula "acme zone" (= potential epibole). Black dots – abundant specimens, null dots – rare occurrences.

that the range of *Tintinnopsella remanei* Subzone in the studied Puerto Escaño sub-section reveals an intermediate case, the relevance of which will deserve attention in the future.

Crassicollaria intermedia (Durang Delga) first appears in Bed 16 (LAD in Bed 26-2) in the middle part of the M20n, about 5 cm above the M20n.1r Kysuca Subzone and indicates the base of the *Crassicollaria* Zone. Its FAD is therefore identical with that registered at Bosso Valley and Brodno (Houša et al. 1999; 2004). The LAD of *Crassicollaria intermedia* was registered in Bed 26-2 and, therefore, the identification of the Subzone (*Intermedia* Subzone) is conclusively supported for Puerto Escaño as well (see also Olóriz in Tavera et al., 1994, p. 474; Caracuel, 1996). The base of the *Crassicollaria intermedia* Subzone is defined by the FAD of *Calpionella grandalpina* in the upper part of Bed 22. The same interpretation was adopted by Olóriz et al. (1995) using the FAD of medium- to large-sized *C. alpina* in the relatively close Majorca Island.

The increase in calpionellid diversity was registered from Bed 22 (uppermost part of the M20n), and culminated between Bed 23-5 (upper part of the M19r) and the lower part of Bed 26-2. This assemblage consists of *Crassicollaria*, *Calpionella* and minor *Tintinnopsella* (see Fig. 12). A decrease in calpionellid diversity was found between Beds 26-3 and 27 (middle part of the M19 n). Beds 22 to 26-3 are characterized by the typical Tithonian *Crassicollaria* assemblage (e.g., *Crassicollaria massutiniana* (Colom), *C. brevis* and *C. intermedia*), as recognized by Tavera et al., (1994, p. 474; Fig. 2a-b) for the same sub-section GA-7.

The J/K boundary *sensu* Remane et al. (1986), Olóriz and Tavera (1989, 1990), Olóriz in Tavera et al. (1994), Olóriz et al. (1995) and Houša et al. (1999, 2004) was defined by the mass occurrence of smaller globular (spherical) *Calpionella alpina*. Cecca et al. (1989) used the same *C. alpina* explosion level as the base of Zone B to identify the Tithonian/Berriasian boundary, but they proposed its correlation with ammonite horizons older than established in the GA-7 sub-section investigated at Puerto Escaño (to compare with Tavera et al., 1994). In the Puerto Escaño sub-section, the base of the *Calpionella* Zone falls within Bed 28 (the second option for establishing the J/K boundary noted in Tavera et al., 1994, p. 474). The boundary between the *Crassicollaria* and *Calpionella* Zones at Puerto Escaño therefore lies inside the Bed 28, approximately in the middle of the M19n magnetic zone. Abundant occurrence of *C. alpina* (relative frequency of *C. alpina* reaches more than 80-90%, being *Tintinnopsella carpathica* and *Crassicollaria parvula* the remaining record of calpionellid) is recorded at the base of the *Calpionella* zone. On the assumption of its relative isochrony, the mass occurrence of *C. alpina* at the base of the *Calpionella* Zone should be considered as indicating the epibole for this species. It can be correlated with other Tethyan sections: Brodno and Bosso Valley (Houša et al. 1999, 2004) and the relatively close Majorca Island (e.g., Olóriz et al., 1995), although the recorded abundance may vary in the nearby Tethyan areas (Caracuel, 1996). Another important bioevent, the abundant occurrence of *Crassicollaria parvula* Remane (above the *C. alpina* acme, Bed 31) has been also recorded in the Brodno and Bosso Valley sections. However, in these sections, the *C. parvula* acme lies in somewhat younger sediments, most probably revealing local acmes (potential), but see Olóriz et al. (1995) for allusion to depositional dynamics in analogous situations.

Calpionellid taxonomic diversity recorded at the Bed 27 (Fig. 12) decreased rapidly at the base of Bed 28. Through the J/K boundary interval, calpionellids show a less diversified and monotonous assemblage of *Tintinnopsella carpathica*, *Crassicollaria parvula* and *Calpionella alpina*. No calpionellid bioevents were observed either in the M19n.1r Brodno Subzone or at the boundary of the M19n/M18r zones. *Tintinnopsella doliphormis* (Colom) was first registered in the uppermost part of Bed 39 (upper part of the M18r zone). This species is supposed to be a phyletic ancestor of *Remaniella ferasini* (Catalano), which appears in the youngest part of the measured sub-section – i.e. in Bed 42 (lower part of the M18n). Stratigraphic occurrences of these species are also in accordance with other Tethyan sections in relatively nearby areas, rather indicating the upper part of the *Doliformis* interval (e.g., Olóriz et al., 1995) within the lower *Remaniella* Subzone.

4.2. Ammonite zonation

The ammonite assemblages collected from bottom to top in the studied GA-7 sub-section at Puerto Escaño allow to identify the following biozones (Fig. 12). Only ammonites relevant to biostratigraphy are cited:

Burckhardticeras Zone (Beds up to 5): *Burckhardticeras peroni* (Roman), *B.* sp., *Kutekiceras pseudocolubrinus* (Kilian), *Lemencia* sp. cf. *pseudociliata* Oloriz, *L.* sp. cf. *pergrata* (Schneid), *L.* sp. cf. *patula* (Schneid), *Aulacosphinctes sulcatus* Tavera, *Simoceras* (*Simoceras*) *volanense* (Oppel), *S.* (*S.*) sp. gr. *volanense* (Oppel), *Cordubiceras maius* Tavera, *Haploceras* (*Hyppolissoceras*) sp. cf. *rhinotonum* (*Zittel*), *H.* (*H.*) sp. cf. *cristifer* (Zittel).

Simplisphinctes Zone (Beds 6 to 7 = 20 cm): *Oloriziceras magnum* Tavera, *O. salariensis* Tavera, *O.* sp. cf. *checai* Tavera, *Simplisphinctes* sp. cf. *rivasi* Tavera, *S.* sp., *Micracanthoceras (Micracanthoceras)* sp. gr. *radians-flexuosum* Tavera, *Micracanthoceras (Corongoceras)* sp. juv., *Cordubiceras* sp.

Transitorius Zone (Beds 8 to 21): *Paraulacosphinctes transitorius* (Oppel), *P. senex* (Oppel), *P. senoides* Tavera, *P. algariensis* Tavera, *P. zakharovi* Tavera, *P. complanatus* Tavera, *P.* sp. cf. *exigus* Tavera, *P.* sp. cf. *compressus* Tavera, *P.* sp. cf. *validus* Tavera, *P.* sp. cf. *elegans* Tavera, *P.* sp., *Moravisphinctes moravicus* (Oppel), *M. fischeri* (Kilian), *M.* sp. cf. *tenuis* Tavera, *Andalusphinctes* sp. cf. *fontannesi* Tavera, *A.* sp., *Aulacosphinctes sulcatus* Tavera, *A.* sp., *Tithopeltoceras haranensis* Olóriz and Tavera, *Micracanthoceras (Micracanthoceras) microcanthum* Oppel, *M. (M.)* sp., "*Corongoceras*" sp. cf. *hexagonus* Tavera.

Durangites Zone (Beds 22 to 25-1): *Paraulacosphinctes senoides* Tavera, *P. senex* (Oppel), *Protacanthodiscus andreaei* (Kilian), *P. nodosus* Tavera, *P. heterocosmus* (Canavari), *P.* sp. cf. *coronatus* Tavera, *P. darwini* Tavera, *P.* sp. cf. *coronatus* Tavera, *P.* sp. 1 gr. *andreaei* (Kilian in Tavera, 1985), *Durangites vulgaris* Burckhardt, *D. acanthicus* (Burckhardt), *D. heilprini* (Aguilera), *D. gigantis* Tavera, *D. astillerensis* Imlay, *D.* sp. cf. *apertus* Tavera, *D. singularis* Tavera, *D. sutneroides* Tavera, *D.* sp. cf. *heilprini* (Aguilera), *D.* sp. cf. *acanthicus* Burckhardt, *Neoperisphinctes falloti* (Kilian) and *N. nexus* Tavera, *Berriasella (Berriasella) tithonica* Tavera, *Proniceras* sp. gr. *simile* Spath, *Aspidoceras* sp. gr, *taverai* Checa.

Jacobi Zone (Beds 25-1 to 42): Protacanthodiscus heterocosmus (Canavari), *P. berriasensis* (Tavera), *Durangites sutneroides* Tavera, *D.* sp. cf. *apertus* Tavera, "*Corongoceras*" sp. cf. *köllikeri* (Oppel), *Berriasella (Berriasella) chomeracensis* (Toucas), *B. (B.) moreti* Mazenot, *B. (B.) sabatasi* Le Hegarat, *B. (B.) jacobi* Mazenot, *B. (B.) subcallisto* (Toucas), *B. (B.) aurousei* (Le Hegarat), *B. (B.)* sp. cf. *oxycostata* (Jacob) *B. (B.)* sp. cf. *elmii* (Le Hegarat), *B. (B.)* sp. cf. *oppeli* (Kilian), *B. (B.)* sp. cf. *mazenoti* Breistroffer, *B. (B.)* sp. cf. *berthei* (Toucas), *Elenaella cularensis* (Mazenot), *Malbosiceras chaperi* (Pictet), *M. tarini* (Kilian), *Fauriella floquinensis* Le Hegarat, *Jabronella companyi* Tavera, *J. subbetica* Tavera, *Tirnovella* sp. cf. *allobrogensis* (Mazenot), *Dalmasiceras sayniforme* Tavera, *D. subloevis* Mazenot, *D. progenitor* (Oppel), *D.* sp. cf. *praecox* (Jacob), *D.* sp. cf. *toucasi* Mazenot, "*Corongoceras*" sp. gr. *köllikeri* (Oppel), *Proniceras* sp. aff. *scorpionum* Imlay, *Negreliceras* sp. cf. *negreli* (Matheron).

5. Conclusions

Section GA-7, located at Puerto Escaño, Spain, is formed by limestones of epioceanic origin rich in fossils like calpionellids and

ammonites. Magnetostratigraphic studies were applied to an 8.1-m-thick part of the section embracing upper Tithonian and lower Berriasian strata, the average sampling interval was 30 mm.

The analysis of the IRM acquisition curves proved magnetite to be the main carrier of the NRM and hematite to be the most abundant magnetic mineral. As a rule, the progressive thermal demagnetization revealed three NRM components. Magnetostratigraphy was based on the directions of the most stable component, whose unblocking temperature varied from 300 to 520 °C or, possibly, to 580 °C. Due to only slightly varying strike and dip of the beds, the fold test applied to this component did not give convincing results. In contrast, the reversal test received the best classification 'A'.

The detected polarity zones could be unequivocally identified against the M-sequence of polarity intervals drawn from the GPTS 2004. This fact, together with the results of the reversal test, confirmed the ChRM to be the primary component. The sampled part of the section included a part of magnetozone M20r, full magnetozones M20n to M18r and a part of magnetozone M18n (Fig. 7). A special attention was paid to two reverse subzones M20n.1r and M19n.1r, named Kysuca Subzone and Brodno Subzone, with thicknesses only 40 and 90 mm, respectively. Their presence enabled easy identification of the detected polarity zones. The smoothed sedimentation rate has been deduced to vary from 1 to 5 mm/ky.

This study satisfied at least seven of the ten quality criteria considered by Opdyke and Channel (1996); the high density of sampling of the section and high data quality confirmed by the classification of the reversal test are its extraordinary features. The J/K boundary defined by mass occurrence of *Calpionella alpina* lies approximately in the middle part of the M19n magnetozone. The boundary between *Durangites* and *Jacobi* Zones is located below the top of the *Intermedia* Subzone, inside the *Crassicollaria* Zone - i.e. above the base of the M19n.

Acknowledgements

This research honors the memory of Václav Houša, an outstanding Czech geologist and paleontologist and our friend who had encouraged this collaboration for several years but could finish neither his valuable contribution nor related projects for the near future.

We are grateful to Dr. Jacek Grabowski and Prof. Andrzej Pszczółkowski for their scientific reviews and constructive comments. We thank Dr. J. Adamovič for his review and improving our English. We also gratefully acknowledge the Grant Agency of the Czech Republic for financial support (Grant No.GACR 205-07-1365), MSM 0021620855 and Research Plan of the IG AS CR No. CEZ AV0Z30130516, and facilities from the EMMI Group (RNM-178, J.A.) and Project CGL2005-01316 MICINN, Spain.

References

Benzaggagh, M., Atrops, F., 1995. Les zones à Chitinoidella et à Crassicollaria (Tithonien) dans la partie interne du Préfrif(Maroc). Données nouvelles et corrélation avec les zones d'ammonites. Compte Rendue de l'Académie des Sciences Paris 320, Série Iia, 227–320.

Butler, R.F., 1991. Paleomagnetism: magnetic domains to geologic terranes. Boston Blackwell Scientific Publications, Cambridge, Massachusetts, 319 pp.

Caracuel, J., 1996. Asociaciones de megainvertebrados, Evolución ecosedimentaria e Interpretaciones ecoestratigráficas en umbrales epioceánicos del Tethys occidental (Jurásico superior). PhD Thesis, Universidad de Granada, 475pp.

Caracuel, J., Monaco, P., Olóriz, F., 2000. Taphonomic tools to evaluate sedimentation rates and stratigraphic completeness in Rosso Ammonitico Facies (epioceanic Tethyan Jurassic). Rivista Italiana di Paleontologia e Stratigrafia 106 (3), 353–368.

Cecca, F., Enay, R., Le Hegarat, G., 1989. L'Ardescien (Tithonique Superieur) de la région stratotypique: Series de référence et faunes (ammonites, calpionelles) de la Bordure Ardechoise. Documents des Laboratoires de Géologie Lyon, Sciences de la Terre. Université Claude-Bernard, Lyon 1 107. 1–115.

Chadima, M., Hrouda, F., 2006. Remasoft 3.0-A user-friendly paleomagnetic data browser and analyzer. Travaux Géophysiques XXXVIII, 20–21.

Channell, J.E.T., Bralower, T.J., Grandesso, P., 1987. Biostratigraphic correlation of Mesozoic polarity chrons CM1 to CM23 at Capriolo and Xausa (Southern Alps, Italy). Earth and Planetary Science Letters 85, 203–221.

Channell, J.E.T., Grandesso, P., 1987. A revised correlation of Mesozoic polarity chrons and calpionellid zones. Earth and Planetary Science Letters 85, 222–240.

Cirilli, S., Marton, P., Vigli, L., 1984. Implications of a combined biostratigraphic and palaeomagnetic study of the Umbrian Maiolica Formation. Earth and Planetary Science Letters 69, 203–214.

Fisher, R., 1953. Dispersion on a sphere. Proceedings of the Royal Society A 217, 295–305.

Fisher, N.I., Lewis, T., Embleton, B.J.J., 1987. Statistical analysis of spherical data. Cambridge University Press, Cambridge, 329 pp.

Geyssant, J., 1997. Tithonien. In: Cariou, E., Hantzpergue, P. (Eds.), Biostratigraphy du Jurassique ouest-européen et méditerranéen: Zonations parallèles et distribution des invertébrés et microfossiles. Bulletin Centre Recherches Elf Exploration Production, 17. Mémoire, pp. 97–102.

Grabowski, J., Pszczółkowski, A., 2006. Magneto- and biostratigraphy of the Tithonian-Berriasian pelagic sediments in the Tatra Mountains (central Western Carpathians, Poland): sedimentary and rock magnetic changes at the Jurassic/Cretaceous boundary. Cretaceouc Research 27, 398–417.

Gradstein, F.M., Ogg, J.G., Smith, A.G. (Eds.), 2004. A gelogic Time Scale 2004. Cambridge University Press, Cambridge, U.K., p. 589.

Hoedemaeker, P.J., Krs, M., Man, O., Parés, J.M., Pruner, P., Venhodová, D., 1998. The Neogene remagnetization and petromagnetic study of the Early Cretaceous limestone beds from the Río Argos, (Caravaca, Province Murcia, SE Spain). Geologica Carpathica 49, 15–32.

Houša, V., Krs, M., Krsová, M., Man, O., Pruner, P., Venhodová, D., 1999. High-resolution magnetostratigraphy and micropaleontology across the J/K boundary strata at Brodno near Žilina, western Slovakia: summary results. Cretaceous Research 20, 699–717.

Houša, V., Krs, M., Man, O., Pruner, P., Venhodová, D., Cecca, F., Nardi, G., Piscitello, M., 2004. Combined magnetostratigraphic, paleomagnetic and calpionellid investigations across Jurassic/Cretaceous boundary strata in the Bosso Valley, Umbria, central Italy. Cretaceous Research 25, 771–785.

Jelínek, V., 1966. A high sensitivity spinner magnetometer. Studia Geophysica at Geodaetica 10, 58–78.

Jelínek, V., 1973. Precision A.C. bridge set for measuring magnetic susceptibility and its anisotropy. Studia Geophysica at Geodaetica 17, 36–48.

Kirschvink, J.L., 1980. The least-squares line and plane and the analysis of palaeomagnetic data. Geophysical Journal of the Royal Astronomical Society 62, 699–718.

Kruiver, P.P., Dekkers, M.J., Heslop, D., 2001. Quantification of magnetic coercivity components by the analysis of acquisition curves of isothermal remanent magnetisation. Earth and Planetary Science Letters 189, 269–276.

Lowrie, W., Channell, J.E.T., 1983. Magnetostratigraphy of the Jurassic–Cretaceous boundary in the Maiolica Limestone (Umbria, Italy). Geology 12, 44–47.

Man, O., 2008. On the identification of magnetistratigraphic polarity zones. Studia Geophysica at Geodaetica 52, 173–186.

Márton, E., 1986. The problems of correlation between magnetozones and calpionellid zones in Late Jurassic–Early Cretaceous sections. Acta Geologica Hungarica 29, 125–131.

McElhinny, M.W., 1964. Statistical significance of the fold test in palaeomagnetism. Geophysical Journal of the Royal Astronomical Society. 8, 338–340.

McFadden, P.L., McElhinny, M.W., 1990. Classification of the reversal test in palaeomagnetism. Geophysical Journal International 103, 725–729.

Nairn, A.E.M., Schmitt, T.J., Smithwick, M.E., 1981. A palaeomagnetic study of the upper Mesozoic succesion in northern Tunisia. Geophysical Journal of the Royal Astronomical Society 65, 1–18.

Ogg, J.G., Hasenyager, R.W., Wimbledon, W.A., Channell, J.E.T., Bralower, T.J., 1991. Magnetostratigraphy of the Jurassic-Cretaceous boundary interval e Tethyan and English faunal realms. Cretaceous Research 12, 455–482.

Ogg, J.G., Lowrie, W., 1986. Magnetostratigraphy of the Jurassic/ Cretaceous boundary. Geology 14, 547–550.

Ogg, J., Steiner, M.B., Company, M., Tavera, J.M., 1988. Magnetostratigraphy across the Barriasian-Valanginian stage boundary (Early Cretaceous), at Cehegin (Murcia Province, southern Spain). Earth Planet Science Letters 87, 204–215.

Ogg, J.G., Steiner, M.B., Olóriz, F., Tavera, J.M., 1984. Jurassic magnetostratigraphy, 1. Kimmeridgian–Tithonian of Sierra Gorda and Carcabuey, southern Spain. Earth Planet Science Letters 71, 147–162.

Olóriz, F., 1978. Kimmeridgiense-Tithónico inferior en el sector central de las Cordilleras Béticas (Zona Subbética). Paleontología. Bioestratigrafia. Tesis Doctorales Universidad de Granada no 84, v. I-II: 758 pp.

Olóriz, F., Reolid, M., Rodríguez-Tovar, F.J., 2004. Microboring and taphonomy in Middle Oxfordian to lowermost Kimmeridgian (Upper Jurassic) from the Prebetic Zone (southern Iberia). Palaeogeography, Palaeoclimatology, Palaeoecology 212, 181–197.

Olóriz, F., Tavera, J.M., 1981. El Jurásico superior en el sector central de la Zona Subbética. Programa Internacional de Correlación Geológica. Real Academia de Ciencias Físicas y Naturales, Madrid. 207–239.

Olóriz, F., Tavera, J.M., 1989. The significance of Mediterranean ammonites with regard to the traditional Jurassic-Cretaceous boundary. Cretaceous Research 10, 221–237.
Olóriz, F., Tavera, J.M., 1990. The Jurassic-Cretaceous boundary in Southern Spain. Some eco-stratigraphical considerations. Transactions Institute of Geology and Geophysics, 699. Siberian Branch of the Academy of Sciences, CCCP (USSR), Hayka (Nauka), Mockba (Moscow). 64–77.
Olóriz, F., Caracuel, J.E., Marques, B., Rodríguez-Tovar, F.J., 1995. Asociaciones de Tintinnoides en facies ammonitico rosso de la Sierra Norte (Mallorca). Revista Española de Paleontología, 77–93. No Extra Homenaje al Dr. Guillermo Colom.
Opdyke, N.D., Channel, J.E.T., 1996. Magnetic stratigraphy. Academic Press, New York, 346 pp.
Parés, J.M., Roca, E., 1996. The significance of tectonic-related Tertiary remagnetization along the margins of the Valencia trough. Journal of Geodynamics 22, 207–227.
Příhoda, K., Krs, M., Pešina, B., Bláha, J., 1989. MAVACS – a new system creating a nonmagnetic environment for palaeomagnetic studies. In: Banda, E. (Ed.), Paleomagnetismo – palaeomagnetism. CSIC, Madrid, pp. 223–250. 1988–1989, Cuadernos de Geologia Iberica.
Reháková, D., 2000a. Evolution and distribution of the Late Jurassic and Early Cretaceous calcareous dinoflagellates recorded in the Western Carpathian pelagic carbonate facies. Mineralia Slovaca 32, 79–88.
Reháková, D., 2000b. Calcareous dinoflagellate and calpionellid bioevents versus sea-level fluctuations recorded in the West Carpathian (Late Jurassic/Early Cretaceous) pelagic environments. Geologica Carpathica 51, 229–243.
Reháková, D., 2002. Chitinoidella Trejo, 1975 in Middle Tithonian carbonate pelagic sequences of the West Carpathian Tethyan area. Geoogica Carpathica 53 (6) 396–379.
Remane, J., Bakalova-Ivanova, D., Borza, K., Knauer, J., Nagy, I., Pop, G., Tardi-Filácz, E., 1986. Agreement on the subdivision of the standard calpionellid zones defined at the IInd Planktonic Conference, Rome 1970. Acta Geologica Hungarica 29, 5–14.
Speranza, F., Satoli, S., Mattioli, E., Calamita, F., 2005. Magnetic stratigraphy of Kimmeridgian–Aptian sections from Umbria-Marche (Italy): New details on the M polarity sequence. Journal of Geophysical Research 110 (B1209), 1–26.
Tavera, J.M., 1985. Los ammonites del Tithonico superior – Berriasense de la Zona Subbética (Cordilleras Béticas). PhD. Thesis, University of Granada, 381pp.
Tavera, J.M., Aguado, R., Company, M., Olóriz, F., 1994. Integrated biostratigraphy of the Durangites and Jacobi Zones (J/K boundary) at the Puerto Escaño section in southern Spain (Province of Cordoba). Geobios, Mémoire Special no 17, 469–476.
Villalaín, J.J., Osete, M.L., Vegas, R., García-Dueñas, V., Heller, F., 1996. The Neogene remagnetization in the western Betics: a brief comment on the reliability of palaeomagnetic directions. In: Morris, A., Tarling, D.H. (Eds.), Palaeomagnetism and Tectonics of the Mediterranean Region, 105. Spec. Publ.. (Geol. Soc. London), pp. 33–41.
Zeiss, A., 2001. Die Ammoniten fauna der Tithonklippen von Ernstbrunn, Niederösterreich. Neue Denk-Schriften des Naturhistorischen Museums in Wien 6, 8–114.

Lukeneder A., Halásová E., Kroh A., Mayrhofer S., Pruner P.,Reháková D., **Schnabl P.**, Sprovieri M. a Wagreich M.

High resolution stratigraphy of the Jurassic-Cretaceous boundary interval in the Gresten Klippenbelt (Austria)

Geol. Carpathica., 61, 5, 365 – 381, 2010

GEOLOGICA CARPATHICA, OCTOBER 2010, 61, 5, 365–381 doi: 10.2478/v10096-010-0022-3

High resolution stratigraphy of the Jurassic-Cretaceous boundary interval in the Gresten Klippenbelt (Austria)

ALEXANDER LUKENEDER[1,*], EVA HALÁSOVÁ[2], ANDREAS KROH[1], SUSANNE MAYRHOFER[1], PETR PRUNER[3], DANIELA REHÁKOVÁ[2], PETR SCHNABL[3], MARIO SPROVIERI[4] and MICHAEL WAGREICH[5]

[1]Geological and Paleontological Department, Natural History Museum, Burgring 7, 1010 Vienna, Austria; *alexander.lukeneder@nhm-wien.ac.at
[2]Department of Geology and Paleontology, Faculty of Natural Sciences, Comenius University, Mlynská dolina G-1, 842 15 Bratislava, Slovak Republic; halasova@fns.uniba.sk; rehakova@fns.uniba.sk
[3]Institute of Geology, Academy of Sciences of the Czech Republic, v.v.i., Rozvojová 269, 165 00 Praha 6, Lysolaje, Czech Republic
[4]Institute for Marine and Coastal Environment (IAMC-CNR), Calata Porta di Massa (Interno Porto di Napoli), 80133 Napoli, Italy
[5]Department for Geodynamics and Sedimentology, Center for Earth Sciences, University of Vienna, Althanstrasse 14, 1090 Vienna, Austria

(Manuscript received February 8, 2010; accepted in revised form June 10, 2010)

Abstract: The key objective of investigation of hemipelagic sediments from the Gresten Klippenbelt (Blassenstein Formation, Ultrahelvetic paleogeographic realm) was to shed light on environmental changes around the Jurassic-Cretaceous (J/K) boundary on the northern margin of the Penninic Ocean. This boundary is well exposed in a newly discovered site at Nutzhof. Around the critical interval including the boundary, this new outcrop bears a rich microplanktonic assemblage characterized by typical J/K (Tithonian/Berriasian) boundary faunas. The Nutzhof section is located in the Gresten Klippenbelt (Lower Austria) tectonically wedged into the deep-water sediments of the Rhenodanubian Flysch Zone. In Late Jurassic–Early Cretaceous time the Penninic Ocean was a side tract of the proto-North Atlantic Oceanic System, intercalated between the European and the Austroalpine plates. Its opening started during the Early Jurassic, induced by sea floor spreading, followed by Jurassic–Early Cretaceous deepening of the depositional area of the Gresten Klippenbelt. These tectonically induced paleogeographic changes are mirrored in the lithology and microfauna that record a deepening of the depositional environment from Tithonian to Berriasian sediments of the Blassenstein Formation at Nutzhof. The main lithological change is observed in the Upper Tithonian *Crassicollaria* Zone, in Chron M20N, whereas the J/K boundary can be precisely fixed at the *Crassicollaria–Calpionella* boundary, within Chron M19n.2n. The lithological turnover of the deposition from more siliciclastic pelagic marl-limestone cycles into deep-water pelagic limestones is correlated with the deepening of the southern edge of the European continent at this time. Within the Gresten Klippenbelt Unit, this transition is reflected by the lithostratigraphic boundary between siliciclastic-bearing marl-limestone sedimentation in the uppermost Jurassic and lowermost Cretaceous limestone formation, both within the Blassenstein Formation. The cephalopod fauna (ammonites, belemnites, aptychi) and crinoids from the Blassenstein Formation, correlated with calcareous microfossil and nannofossil data combined with isotope and paleomagnetic data, indicate the Tithonian to middle Berriasian (*Hybonoticeras hybonotum* Zone up to the *Subthurmannia occitanica* Zone; M17r–M21r). The succession of the Nutzhof section thus represents deposition of a duration of approximately 7 Myr (ca. 150–143 Ma). The deposition of the limestone, marly limestone and marls in this interval occurred during tectonically unstable conditions reflected by common allodapic material. Along with the integrated biostratigraphic, geochemical and isotopic analysis, the susceptibility and gamma-ray measurements were powerful stratigraphic tools and important for the interpretation of the paleogeographic setting. Two reverse magneto-subzones, Kysuca and Brodno, were detected within magnetozones M20n and M19n, respectively.

Key words: Jurassic/Cretaceous boundary, Penninic Ocean, paleoecology, paleogeography, environmental changes.

Introduction

Jurassic and Lower Cretaceous pelagic sediments are known to form a major elements of the northernmost tectonic units of the Gresten Klippenbelt (Czjžek 1852; Kühn 1962; Küpper 1962; Gottschling 1965; Decker & Rögl 1988; Decker 1990; Piller et al. 2004). Preliminary results on a Jurassic-Cretaceous boundary section of the Gresten Klippenbelt were presented including description of new faunas and localities (Lukeneder 2009; Kroh & Lukeneder 2009; Pruner et al. 2009; Reháková et al. 2009).

The Gresten Klippenbelt at Nutzhof comprises Upper Jurassic (Tithonian) to Lower Cretaceous sediments belonging to the Blassenstein Formation. The lower part of the succession consists of marls, marly limestone and marl-limestone alternations, whereas the upper part of the Blassenstein Formation (Tithonian to Valanginian) is composed of very pure limestones. The biostratigraphy of the Lower Cretaceous sediments in the study area is mainly based on microfossils (Reháková et al. 2009). The first description of the lithology and stratigraphy of this area was provided by Czjžek (1852), followed by Küpper (1962). Biostratigraphic data on the Blassenstein Formation (Stollberger Schichten of Küpper 1962) near Nutzhof are remarkably scarce (Czjžek 1852; Küpper 1962).

The tectonically highly active northern zone of the Penninic Ocean (the southern margin of the European continent) is crucial for understanding the formation of the Penninic

Ocean, its subsequent subduction and the following Alpine history.

Formation of the Penninic Ocean, here defined to include the Ligurian Basin (sensu Dercourt et al. 1993, 2000; Masse et al. 2000; Mandic & Lukeneder 2008) and synonymous with the Alpine Tethys (Stampfli & Borel 2002 and Stampfli et al. 2002) was initiated in the Late Triassic by rifting and disjunction of the Austroalpine microcontinent from the southern European Plate margin (Stampfli & Mosar 1999; Scotese 2001). It formed an eastern prolongation of the North Atlantic Rift-System, which affected the final break-up of the Permo-Triassic supercontinent Pangaea (e.g. Faupl 2003). The formation of the oceanic crust and the sea-floor spreading lasted from the Middle Jurassic to the Early Cretaceous, terminating with the introduction of its southward-directed subduction beneath the northern Austroalpine plate margin (Faupl & Wagreich 2000; Mandic & Lukeneder 2008). This tectonic phase is reflected by the lithological change within the Nutzhof section. An increasing deepening, reflected in the sedimentary succession (e.g. allodapic limestones and microturbidites), in the section at Nutzhof, marks the opening of the Penninic Ocean. The pelagic carbonate sedimentation, which started in the Late Jurassic, changes from siliciclastic-dominated limestone deposition to pure limestone-dominated. The Penninic Ocean persisted from the Late Jurassic until close to the end of the Cretaceous.

The paleomagnetic and rock-magnetic study is a continuation of detailed paleontological and magnetostratigraphic studies of the Jurassic/Cretaceous (J/K) boundary in the Tethyan Realm (Houša et al. 1999). The section at Brodno near Žilina, W Slovakia, was the first section investigated with high-resolution magnetostratigraphy and micropaleontology in the Carpathians (Houša et al. 1999). Magnetostratigraphic studies were carried out in the Bosso Valley of Umbria, Italy (Houša et al. 2004) and the Tatra Mountains, Poland (Grabowski & Pszczółkowski 2006). The magnetostratigraphic investigations published by Pruner et al. (2009) preliminarily determine the boundaries of magnetozones M17n to M22r (six reverse and six normal zones). The aim of these studies was to globally and objectively establish a correlation between biozones around the J/K boundary in the Tethyan Realm using global paleomagnetic events and precisely determine the boundaries of magnetozones M19 and M20 including narrow reverse subzones. These studies provided a precise record of polarity changes in the Earth's magnetic field and determined their stratigraphic positions precisely within a biochronostratigraphic zonation.

The Nutzhof locality represents the only known section that includes the J/K boundary interval in the Gresten Klippenbelt. The section contains rich assemblages of radiolarians, calpionellids, saccocomids, nannofossils and in some intervals ammonites. The J/K boundary sediments of the Nutzhof section provide an excellent succession for quantitative and integrated methods due to their fossiliferous and undisturbed bedding for a period of almost 7 million years.

Location and geological setting of Nutzhof

Locality description

The Nutzhof locality is situated in the Gresten Klippenbelt of Lower Austria (48°04′49″ N, 15°47′36″ E), about 20 km south of Böheimkirchen and 5 km north of Hainfeld (Fig. 1), 600 m above sea level (m a.s.l.) (ÖK 1:50,000, sheet 56 St. Pölten). The outcrop is located in an abandoned quarry in the south-eastern-most part of the northeast-southwest striking Gresten Klippenbelt, between Kasberg (785 m a.s.l.) to the east and the vicinity of the Nutzhof (550 m a.s.l.) to the west. The quarry is located on the northern side of the Kasberg ridge and the measured section is exposed on the eastern side of the quarry.

Geological setting

The Gresten Klippenbelt at Nutzhof is surrounded by deep-water successions of the Rhenodanubian Flysch Zone. The Gresten Klippenbelt represents an independent and scarcely known geological unit. It is tectonically incorporated in the Flysch Zone as a long, thin, east-west striking marly and calcareous unit (Fig. 1). Sediments from the Gresten Klippenbelt are considered to belong to the southern part of the Helvetic paleogeographic realm. The Gresten Klippenbelt sediments were deposited on the southern shelf and

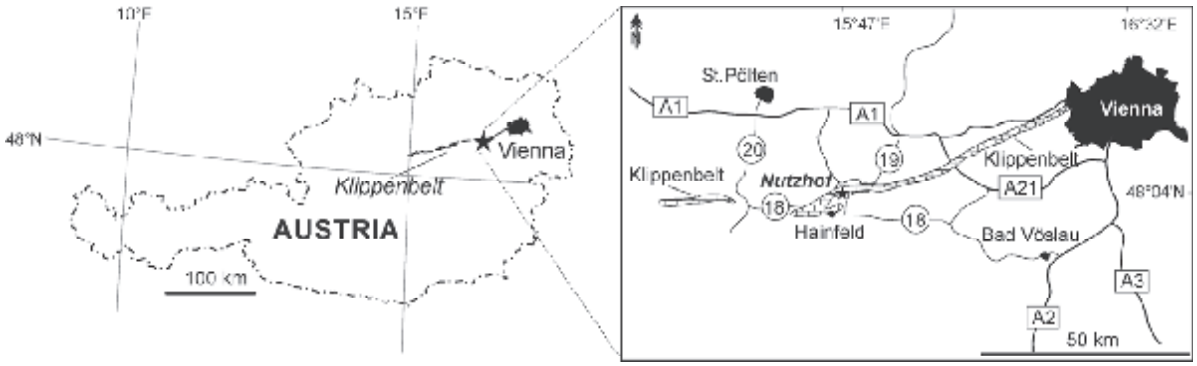

Fig. 1. Locality map of Austria with indicated position of the Nutzhof locality in Lower Austria (left). Detailed map of the area around Nutzhof with outcrop position within the Jurassic–Cretaceous Klippenbelt (right).

slope of the European continent, on the slope of the Bohemian Massif at the north-western margin of the Penninic Ocean. The Nutzhof site consists of two different facies within the Blassenstein Formation (Lukeneder 2009). The lower part (Tithonian; 18.0–10.0 m) with dark marl-limestone alternations and its characteristically intercalated limestone beds, and the upper part (Tithonian–Berriasian; 10.0–0.0 m) with light grey, almost pure limestone. Limestone beds display uniform overturned bedding-plane orientation. The mean strike is 151°±30° and the mean dip angle 44°±22°. The succession is characterized by a marked lithological and faunal change at Nu 10.0 which does not coincide with the Jurassic/Cretaceous boundary at bed Nu 7.0 (Nu for Nutzhof samples). Sediments occur as wacke-, pack- or mudstones.

The Nutzhof section

The Jurassic-Cretaceous boundary in the Gresten Klippenbelt

The most recent reports concerning the J/K boundary interval from the Gresten Klippenbelt present preliminary results (Lukeneder 2009; Kroh & Lukeneder 2009; Pruner & al. 2009; Reháková et al. 2009) (Fig. 2). Therein first results have been presented on macro-, micro- and nannofossils. Tectonic units including the J/K boundary of the Gresten Klippenbelt were reported by Cžjžek (1852), Kühn (1962), Küpper (1962), Gottschling (1965), Decker & Rögl (1988), Decker (1990) and Piller et al. (2004).

Materials and methods

The Jurassic-Cretaceous boundary section at Nutzhof was studied with an integrated approach. Beds were sampled for biostratigraphical, paleomagnetic, geochemical ($CaCO_3$, TOC, S) and istotopic ($\delta^{18}O$, $\delta^{13}C$, $\delta^{87}Sr$) data. Focus is directed to an interval of about 18.0 m (Nu 0.0–Nu 18.0) that was studied in detail (Figs. 2, 3, 4). Macro-, micro- and nannofossil contents were quantitatively investigated (Fig. 4). Samples were collected at intervals of 0.1 and 0.2 meters for stable isotopes, total organic carbon (TOC), sulphur (S), calcium carbonate ($CaCO_3$), susceptibility and gamma log. The microfossil content was analysed for calpionellids, radiolarians, saccocomids (thin sections) and insoluble residues. High resolution studies were combined with grey-scale quantification, gamma-ray and susceptibility analyses. Sample numbers, for example Nu 10.0, correspond to the sample interval at 10.0 m within the log (for all numbers and figures, Nu = Nutzhof). All samples are stored at the Natural History Museum of Vienna, in the collection of the Department of Geology and Paleontology.

Gamma-ray analysis

The gamma log measures the radioactivity of the rock, which represents a direct function of its clay-mineral content. Increasing radioactivity reflects the increasing clay content. Gamma response (counts per second — cps) was measured using a hand-held standard gamma-ray scintillometer.

Macrofossils

Macrofossil material includes 46 ammonite specimens, 238 lamellaptychi and 82 rhyncholites were examined. Four brachiopods and three inoceramids as well as a single belemnite specimen were collected. Ammonites are preserved as steinkerns or are represented by calcitic aptychi. Shell-preservation is restricted to organisms with primary skeletal calcite of belemnite-rostra and brachiopods in addition to rare inoceramid fragments (calcitic prisms). The ammonite assemblage contains six different genera: *Subplanites*, *Haploceras*, *Phylloceras*, *Ptychophylloceras*, *Lytoceras* and *Leptotetragonites* dominated by the perisphinctid genus *Subplanites* (Lukeneder 2009).

Calpionellids and calcareous nannofossils

Quantitative micro- and nannofacies analysis includes study of calpionellids and calcareous dinoflagellates in 93 thin sections. The thin sections are deposited in the Natural History Museum in Vienna; NHMW 2007z0271/0000. Changes in the distribution of calpionellids and calcareous nannofossils were studied in detail in order to correlate them with the changes in nannoplankton associations (Figs. 2, 3 and 4).

Calcareous nannofossils were analysed semiquantitatively in 19 smear slides, prepared from all lithologies by standard techniques, using a light polarizing microscope at 1250× magnification. At least 200 specimens were counted in each slide to record relative abundances and the stratigraphic range of taxa (Figs. 2, 3). Nannofossil preservation can be characterized as moderately to intensely etched by dissolution. The calcareous nannofossil zones were adopted from the zonal scheme proposed by Bralower et al. (1989).

Magnetic components

Paleomagnetic analyses presented in this studies come from 244 samples, but the preliminary results include only 111 samples (see Pruner et al. 2009). All the samples were subjected to progressive thermal demagnetization (TD) or alternating field (AF) demagnetization in 11–12 temperatures or fields. The individual components were precisely established using multicomponent analysis of remanence (Kirschvink 1980). Isothermal remanent magnetization (IRM) to saturation was measured to identify magnetically active minerals. Magnetomineralogical analyses and unblocking temperature determination show that magnetite and goethite are the main carriers of remanent magnetization.

Microfossils

Apart from thin sectioning also employed for a study of calpionellids, an effort was made to obtain three-dimensional specimens of the crinoids and other microfossils commonly observed in the thin sections (namely foraminifers, ostracods, rhyncholites, small aptychi, ophiuroid remains,

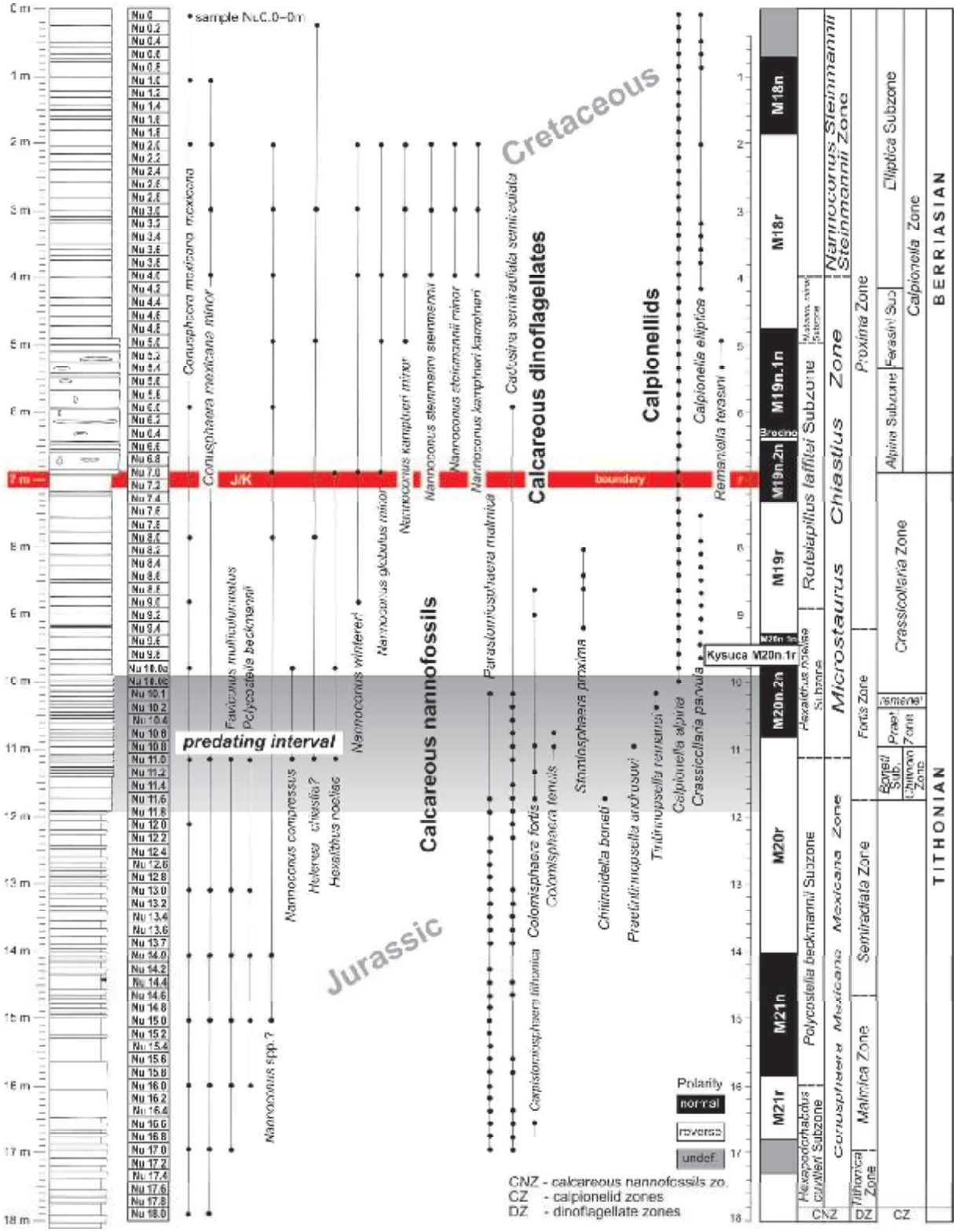

Fig. 2. Nutzhof log with occurrence and range of calcareous nannofossils, calcareous dinoflagellates and calpionellids and indicated paleomagnetic zonation: normal magnetozones are denoted black, reverse zones in white, and unknown parts in grey.

etc.). Bulk samples were collected in closely spaced intervals in the lower, marly part of the succession (10.0–18.0 m). Strong lithification hampered dense bulk sampling in the upper part of the section (0 to 10.0 m). These beds were analysed by thin sections only. Traditional washing methods were not applicable due to strong lithification of the sediment. Partial disaggregation was achieved by repetitive, combined treatment with hydrogen-superoxide and the tenside Rewoquat (see Lierl 1992). After cleaning, the microfossils were hand picked under a microscope. For the present study we used the sediment fractions larger than 250 μm only.

TC and TOC content

Calcium carbonate contents ($CaCO_3$; wt. % bulk rock, TC) were determined using the carbonate bomb technique. Total carbon content was determined using a LECO WR-12 analyser. Total organic carbon (TOC) contents were calculated as the difference between total carbon and carbonate carbon, assuming that all carbonate is pure calcite. All the chemical analyses were carried out in the laboratories of the Department of Forest Ecology at the University of Vienna.

Stable isotopes

A total of 37 bulk sample stable isotope analyses were measured by automated continuous flow carbonate preparation GasBenchII device (Spötl & Vennemann 2003) and ThermoElectron Delta Plus XP mass spectrometer at the IAMC-CNR (Naples) isotope geochemistry laboratory. Acidification of samples was performed at 50 °C. For each six samples, an internal standard (Carrara Marble with $\delta^{18}O = -2.43$ vs. V-PDB and $\delta^{13}C = 2.43$ vs. V-PDB) was run, and for each 30 samples, the NBS19 international standard was measured. Standard deviations of carbon and oxygen isotope measures were estimated 0.1 and 0.08 ‰, respectively, on the basis of ~10 repeated samples.

All the isotope data are reported in per mil (‰) relative to the V-PDB standard.

$^{87}Sr/^{86}Sr$ isotope data were analysed from 19 bulk-rock samples of limestones at the Geochronological Laboratory of the Department of Lithospheric Research, Centre for Earth Sciences, University of Vienna using strontium separation by standard methods of ion-exchange chromatography and isotope ratio measurements on a TIMS (Triton mass spectrometer). The measured NBS 987 standard value during measurements was 0.710256+/–0.000004 (7 measurements) and samples were not adjusted to the NBS 987 standard value of 0.710248.

Data and results

Biostratigraphy and magnetostratigraphy

The stratigraphic investigation of the calcareous microfossils (calpionellids, calcareous dinoflagellates) and nannofossils demonstrate that the Nutzhof section represent the Lower Tithonian–middle Berriasian. The calcareous dinoflagellate cyst zonation of Reháková (2000a) was followed. The presence of the Lower Tithonian *Tithonica*, *Malmica* and *Semiradiata* cyst Zones is demonstrated. The standard calpionellid zones and subzones proposed by Reháková (1995) and Reháková & Michalík (1997) were adopted for the biostratigraphic subdivision of the section into the *Chitinoidella* Zone (*Boneti* Subzone), the *Praetintinnopsella* Zone and the *Crassicollaria* Zone (*Remanei* Subzone). These belong to the middle to Upper Tithonian. The standard *Calpionella* Zone (*Alpina*, *Ferasini* and *Elliptica* Subzones) were observed in the overlying Lower Cretaceous (Fig. 2).

The nannofossil zones include the *Conusphaera mexicana mexicana* Zone, *Microstaurus chiastus* and *Nannoconus steinmannii steinmannii* Zones. This stratigraphic interval corresponds to the Lower Tithonian *Hybonoticeras hybonotum* ammonite Zone to the middle Berriasian *Subthurmannia occitanica* ammonite Zone, demonstrated in the Nutzhof section on chronostratigraphic diagnostic cephalopods (*Subplanites fasciculatiformis*, *Ptychophylloceras ptychoicum*, *Leptotetragonites honnoratianus*, *Haploceras elimatum*, *Hibolithes* (gr.) *semisulcatus* and some lamellaptychi.

The magnetostratigraphic log across the Nutzhof section includes the M21r to the M17r magnetozones subdivided into the Kysuca (M20r) and Brodno (M19r) subzones (Figs. 2, 6). The average sedimentation rate in the Nutzhof section is ca. 3.7 m/Myr (Fig. 7), but with high dispersion (from 2–11 m/Myr). The scatter of the sedimentation rate is similar to Hlboča profile in Slovakia (Grabowski et al. 2010). The main difference between these two sections is in the thickness of M19 and M20 mangentozones. Nutzhof has higher sedimentation rate at M19 while Hlboča appears with higher rates in M20.

Macrofossil content

The macrofossil content is characterized by ammonoids, aptychi, belemnites, brachiopods, bivalves and echinoderms. The ammonite fauna comprises six different genera represented by *Lytoceras sutile* Oppel, *Lytoceras* sp., *Leptotetragonites honnoratianus* (d'Orbigny), *Phylloceras* sp., *Ptychophylloceras ptychoicum* (Quenstedt), *Haploceras* (*Haploceras*) *elimatum* (Oppel), *Subplanites fasciculatiformis* Lukeneder. The ammonite fauna is dominated by the perisphinctid-type. Ammonitina is the most common component (60 %; *Subplanites* and *Haploceras*), followed by the Phylloceratina (25 %; *Ptychophylloceras* and *Phylloceras*), and the Lytoceratina (15 %; represented by *Lytoceras* and *Leptotetragonites*). The belemnite *Hibolithes* (gr.) *semisulcatus* (Münster) and aptychi (*Lamellaptychus*) occur. Only Mediterranean cephalopod elements are present at Nutzhof. Brachiopods are represented by *Triangope*, bivalves by inoceramid shells and echinoderms by crinoids (*Phyllocrinus belbekensis* Arendt, *Balanocrinus* sp., *Crassicoma*? sp. and *Saccocoma tenella* (Goldfuss).

The crinoid fauna recovered from the bulk samples of Nutzhof is typical for Upper Jurassic strata of Central and Eastern Europe. The low diversity of stalked crinoids, common in many contemporaneous deposits (Hess et al. 1999), may be interpreted as a result of the distal position of the sec-

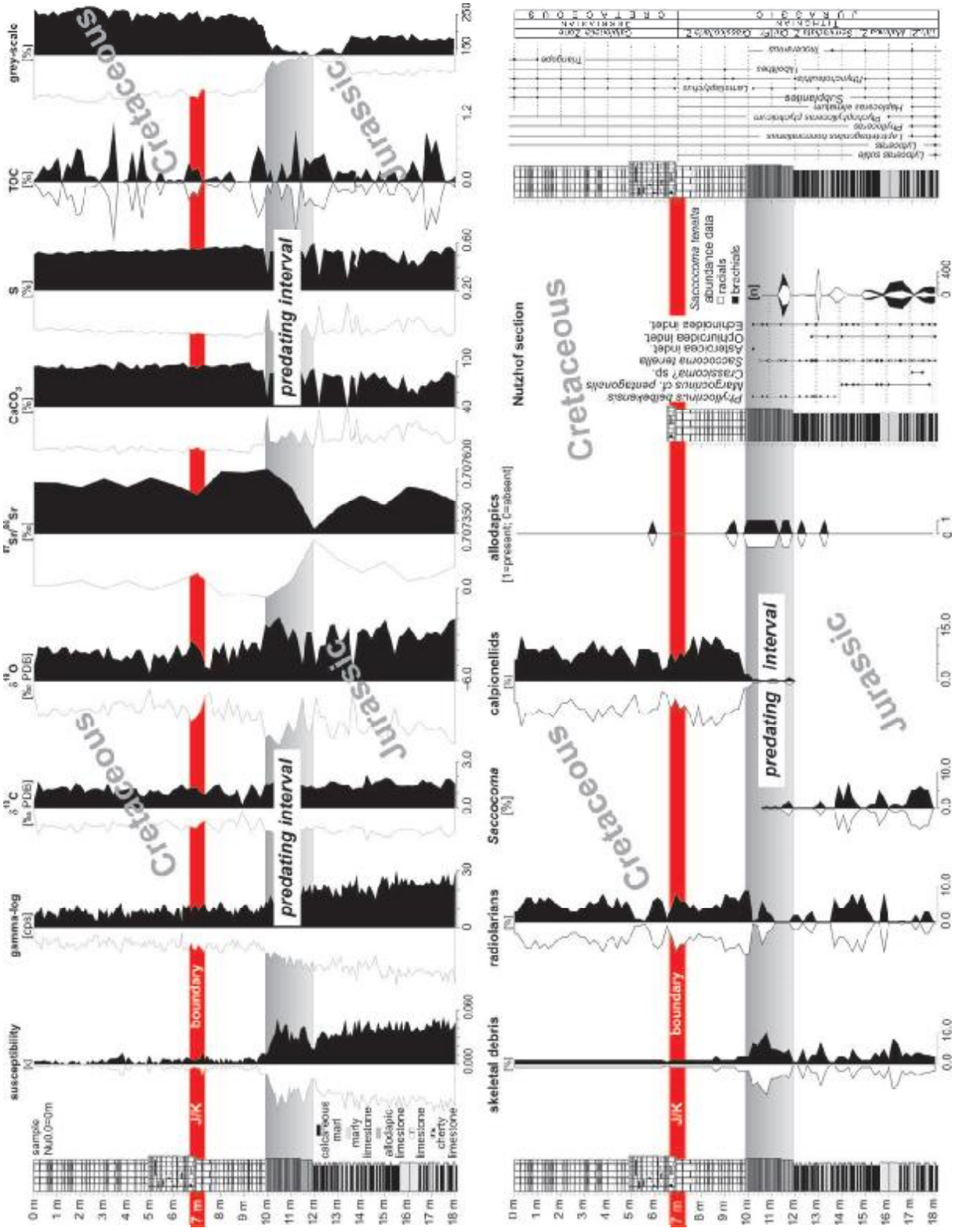

Fig. 3. Compiled geochemical, isotope and fossil data on the J/K boundary at Nutzhof. Note the change at the predating interval at meter 7 below the J/K boundary.

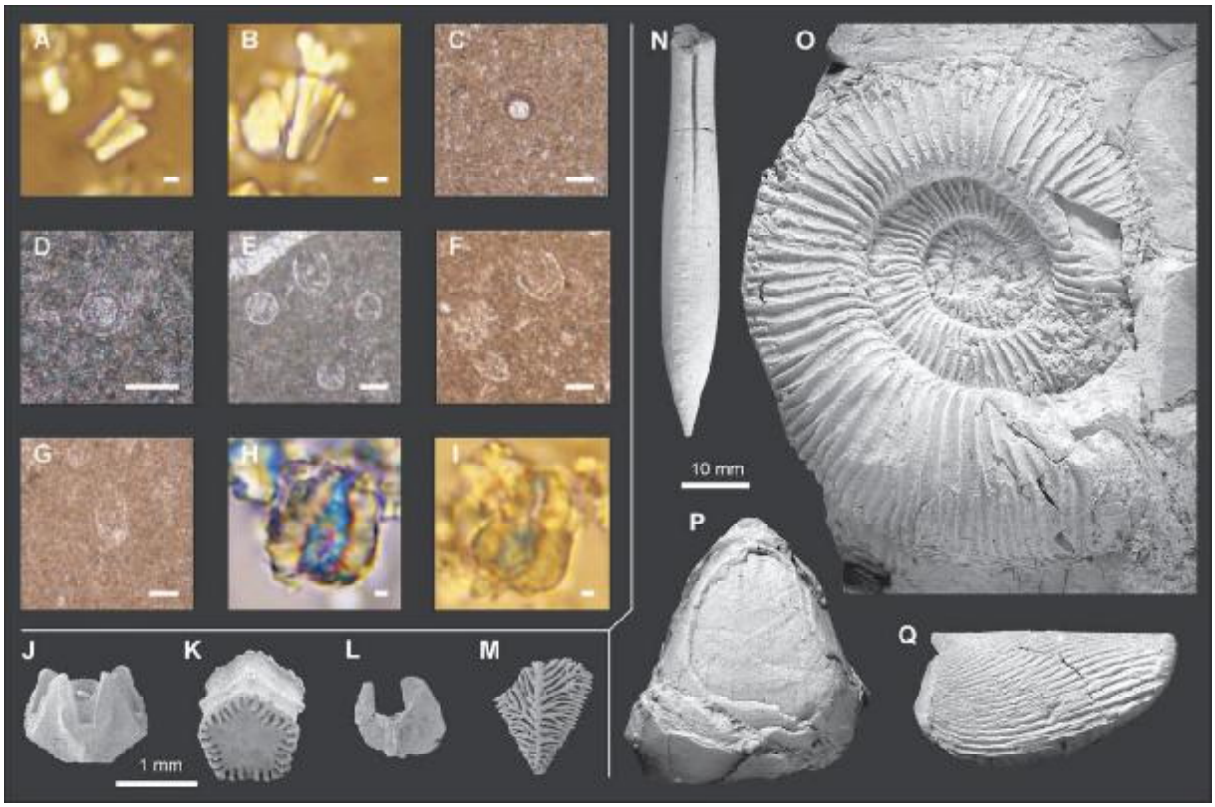

Fig. 4. A — *Conusphaera mexicana minor* Bown & Cooper; Nu 18.0, NHMW2008z0271/0028. **B —** *Conusphaera mexicana mexicana* Bralower et al.; Nu 17.0, NHMW2008z0271/0003. **C —** *Cadosina semiradiata semiradiata* Wanner; 17.0, NHMW2008z0271/0003. **D —** *Parastomiosphaera malmica* (Borza); Nu 13.0, NHMW2008z0271/0002. **E —** *Calpionella alpina* Lorenz and *Calpionella grandalpina* Nagy; Nu 9.8, NHMW2008z0271/0011. **F —** *Crassicollaria parvula* Remane and *Calpionella grandalpina*; Nu 9.6, NHMW2008z0271/0012. **G —** *Calpionella elliptica* Cadisch; Nu 3.2, NHMW2008z0271/0014. **H —** *Nannoconus steinmannii steinmannii* Kamptner; Nu 4.0, NHMW2008z0271/0034. **I —** *Nannoconus kamptneri kamptneri* Brönnimann; Nu 2.0, NHMW2008z0271/0035. **J —** *Phyllocrinus belbekensis* Arendt; Nu 12.3; NHMW 2008z0226/001. **K —** *Balanocrinus* sp.; Nu 14.6, NHMW2008z0228/0003. **L —** *Saccocoma tenella* (Goldfuss); Nu 11.5, NHMW2008z0236/0015. **M —** *Saccocoma tenella* (Goldfuss); Nu 13.0, NHMW2008z0236/0012. **N —** *Hibolithes* (gr.) *semisulcatus* (Münster); Nu 14.3, NHMW2008z0264/0025. **O —** *Subplanites fasciculatiformis* Lukeneder; Nu 17.0, NHMW2008z0264/0012. **P —** *Triangope* sp.; Nu 1.0, NHMW2008z0264/0028. **Q —** *Lamellaptychus* sp.; Nu 18.0, NHMW2008z0264/0024. Graphic scale bars equal 1 μm for A, B and H, I; 50 μm for C–G; 1 mm for J–K, and 10 mm for N–Q.

tion, which represents a deep-water facies. The incomplete size ranges of isocrinid and phyllocrinid ossicles, the lack of fragile elements and the presence of allodapic material (Lukeneder 2009) suggest that the majority of the crinoid material is allochthonously deposited. Saccocomid fragments, in contrast, are not sorted and include abundant fragile elements suggesting that these crinoids are autochthonous.

Of the crinoid material only the saccocomids can be used for biostratigraphy. *Saccocoma tenella* is restricted to the Upper Kimmeridgian–Upper Tithonian. From a biogeographic point of view the faunal composition indicates connections with contemporaneous units of the northern Tethys shelf in Eastern Europe.

Microfacies and calcareous microplankton assemblages

The limestones in the section include wackestones, packstones and mudstones. Fine-grained micrite with pelagic microfossils (calpionellids, calcareous dinoflagellates, radiolarians) and calcareous nannofossils characterize an open-marine environments. Rare skeletal debris from fragmented and disintegrated shells of invertebrates (benthic foraminifers, echinoderms, molluscs) are derived from shallower environments. The studied microfacies are typical for basinal settings.

Calpionellids

Calpionellids in the studied samples are generally well-preserved. Hyaline forms dominate, whereas chitinoidellids are rare. The chitinoidellid taxonomy of Pop (1997) and Reháková (2002) is followed here. The group is represented by *Borziella slovenica* (Borza), *Dobeniella tithonica* (Borza) and *Chitinoidella boneti* Doben, species typical for the *Boneti* Subzone of the *Chitinoidella* Zone (Figs. 2, 4). The appearance of first hyaline calpionellid loricas of *Praetintinnopsella andrusovi* Borza and *Tintinnopsella remanei* Borza

precede the crassicollarian radiation. *Crassicollaria parvula* Remane and *Calpionella alpina* Lorenz dominate relative to *Crassicollaria massutiniana* (Colom), *Calpionella grandalpina* Nagy and *Tintinnopsella carpathica* (Murgeanu & Filipescu) in the *Remanei* Subzone of the *Crassicollaria* Zone. Higher in the section, crassicollarians abruptly decrease in abundance, being replaced by an interval with radiation of small spherical forms of *Calpionella alpina* Lorenz. The diversification of a monospecific calpionellid association started in the overlying *Ferasini* and *Elliptica* Subzones of the standard *Calpionella* Zone where *Calpionella alpina* Lorenz is accompanied by *Tintinnopsella carpathica* (Murgeanu & Filipescu), *Remaniella ferasini* Pop, *R. duranddelgai* Pop, *R. catalanoi* Pop, *Calpionella elliptica* (Cadisch), *Tintinnopsella longa* (Colom), and *Lorenziella hungarica* Knauer.

Calcareous dinoflagellates

Calcareous dinoflagellates predominate in the Lower and Upper Tithonian being represented by *Cadosina parvula* Nagy, *Carpistomiosphaera borzai* (Nagy), *Schizosphaerella minutissima* (Colom), *Parastomiosphaera malmica* (Borza), *Cadosina semiradiata semiradiata* Wanner, *Cadosina semiradiata fusca* (Wanner), *Carpistomiosphaera tithonica* Nowak, *Colomisphaera fortis* Řehánek, *Colomisphaera tenuis* (Nagy), *Colomisphaera carpathica* (Borza), and *Stomiosphaerina proxima* Řehánek. For the first time the appearance of *Colomisphaera fortis* Řehánek precedes the appearance of *Colomisphaera tenuis* (Nagy), hampering the determination of the *Tenuis* and *Fortis* dinoflagellate Zones sensu Řehánek (1992) (Figs. 2, 4).

Calcareous nannofossils

The semiquantitative study (Figs. 2, 3) reveals that only the taxa *Conusphaera* spp., *Polycostella* spp., *Nannoconus* spp., *Cyclagelosphaera margerelii* Noël, *Watznaueria barnesae* (Black) Perch-Nielsen, and *W. manivitae* Bukry occur in significant abundances. Nannofossils indicative of eutrophic environments such as *Zeugrhabdotus erectus* (Deflandre) Reinhardt, *Diazomatholithus lehmannii* Noël, and *Discorhabdus ignotus* (Górka) Perch-Nielsen occur sporadically.

The calcareous nannofossil assemblage from the basal part of the Nutzhof section (samples 17, 18, *Tithonica* dinoflagellate Zone) contains the dissolution-resistant nannofossil species *Conusphaera mexicana mexicana* Bralower et al., *Conusphaera mexicana minor* Bown & Cooper, *Cyclagelosphaera margerelii*, *Cyclagelosphaera deflandrei* (Manivit) Roth, *Watznaueria barnesae*, *Watznaueria britannica* (Stradner) Reinhardt, and *Watznaueria manivitae*. The FO (first occurrence datum) of *Faviconus multicolumnatus* Bralower was recorded. The absence of the nannolith *Polycostella beckmannii* Thierstein allowed us to distinguish the *Conusphaera mexicana mexicana* NJ20 Zone; *Hexapodorhabdus cuvillieri* Subzone NJ20-A (Roth et al. 1983; emended Bralower et al. 1989) of the Lower Tithonian.

The calcareous nannofossil assemblages from the samples Nu 16.0 to Nu 12.0 show dominance of *Watznaueria* and *Conusphaera*. The FOs of *Zeugrhabdotus embergeri* (Noël) Perch-Nielsen, *Zeugrhabdotus erectus*, and *Diazomatholithus lehmannii* were observed. The FO of the nannolith *Polycostella beckmannii* is the most significant marker indicating the base of the *Polycostella beckmannii* Subzone NJ20-B of the *Conusphaera mexicana mexicana* Zone, NJ20 (Roth et al. 1983; emended Bralower et al. 1989). The age of this Subzone is middle Tithonian. The range of the *Polycostella beckmannii* Subzone NJ20-B fits with dinoflagellate *Malmica* and *Semiradiata* Zones and the lower part of the *Chitinoidella* Zone.

The calcareous nannofossils investigated in sample Nu 11 reflect a rather distinct change. The FO of *Helenea chiastia* Worsley, *Hexalithus noeliae* Loeblich & Tappan and the nannolith species *Nannoconus compressus* Bralower et al. are evidence for the base of the *Microstaurus chiastius* Zone NJK Bralower et al., 1989 and its *Hexalithus noeliae* Subzone NJK-A, which is thought to represent the Late Tithonian interval. The Subzone coincides with the upper part of the *Chitinoidella* Zone.

The calcareous nannofossil assemblages from samples Nu 9.0 to Nu 6.0 contain dissolution-resistant nannofossil genera *Conusphaera*, *Cyclagelosphaera*, *Watznaueria*, *Diazomatholithus* and *Assipetra*. The FAD of *Nannoconus wintereri* Bralower & Thierstein (1989) was observed (sample 9.0). Many remains of dissolution-susceptible coccoliths are present. In the upper part of the studied interval, the abundance of *Conusphaera* drops. This interval was correlated with the *Microstaurus chiastius* Zone NJK, Subzone *Rotelapillus laffitei* NJK-C, determining the J/K boundary interval. It shows good correlation with the upper part of the Upper Tithonian *Crassicollaria* Zone and the *Calpionella* Zone (*Alpina* Subzone), which represent the J/K boundary interval.

The interval bearing the calpionellid species of the Lower Berriasian *Calpionella* Zone (*Ferasini* Subzone) (sample Nu 5.0) shows a distinctive change in the calcareous nannofossil assemblage — the onset of nannoconids (*Nannoconus globulus minor* Bralower, *Nannoconus steinmannii minor* Deres & Achéritéquy, *Nannoconus kamptneri minor* Bralower, *Nannoconus cornuta* Deres & Achéritéquy). This nannofossil event indicates the base of the *Nannoconus steinmannii minor* Subzone NJK-D (*Microstaurus chiastius* Zone NJK) Bralower et al., which belongs to the lowermost Berriasian.

The calcareous nannofossils studied from the sample interval Nu 4.0–Nu 0.0 (correlating with the calpionellid *Calpionella* Zone, *Elliptica* Subzone) record the diversification of nannoconids. The FAD of *Nannoconus steinmannii steinmannii* Kamptner is recorded at level Nu 2.0. It could reflect the explosion in nannoconid abundance (sensu Bralower et al. 1989: p. 188). *Nannoconus globulus minor, Nannoconus kamptneri minor*, *Nannoconus wintereri*, *Nannoconus globulus globulus* Deres & Achéritéquy, *Nannoconus steinmannii minor* Deres & Achéritéquy, *Nannoconus steinmannii steinmannii*, and *Nannoconus kamptneri kamptneri* Brönnimann, *Nannoconus* spp. indicative of the *Nannoconus steinmannii steinmannii* Zone NK-1, Bralower et al. (1989), which is middle Berriasian in age.

On the basis of calcareous nannofossil distribution, the interval between the FO of *Nannoconus wintereri* co-occurring with small nannoconids in bed Nu 9.0 and the FO of *Nanno-*

conus steinmannii minor in bed Nu 5.0 (FAD after Hardenbol et al. 1998 — 143.92 Ma) is interpreted as the Tithonian-Berriasian boundary interval (Figs. 2, 3).

Stable isotope data

Oxygen and carbon (O, C)

The bulk carbon-isotope values (Fig. 3) lie between +0.49 and +2.10 ‰ corresponding to biogenic calcite precipitated under open marine conditions during the Jurassic–Cretaceous (e.g. Weissert et al. 1985). All $\delta^{18}O$ values are between –1.94 to –5.49 ‰ and appear depleted relative to diagenetically unaltered marine calcite (e.g. van de Schootbrugge et al. 2000, and reference therein). This reflects elevated temperature during burial diagenesis and/or effects of meteoric diagenesis (Weissert 1989). The carbon isotope signal is considered of primary importance as a calibration tool between ammonites and magnetostratigraphy (Hennig et al. 1999), but it should be noted that the absence of covariance between $\delta^{18}O$ and $\delta^{13}C$ suggests a limited influence of secondary diagenesis on the isotope record (Fig. 3).

A positive trend in the $\delta^{13}C$, from the base of the section at Nu 18.0 up to Nu 14.0, is followed by a decreasing excursion shifting the isotope values to their lowest values (0.69 ‰) at about Nu 10.0. After that point the $\delta^{13}C$ values stabilize at near constant averages of ~1.20 ‰.

Strontium (Sr)

$^{87}Sr/^{86}Sr$ isotope data from the section show a range from 0.707370 +/–0.000004 to 0.707598 +/–0.000004. A gentle trend from lower values in the lower, Jurassic part of the section (Nu 18.0–Nu 12.0: mean 0.707472) to higher values in the upper part including the J/K boundary and the Cretaceous interval (Nu 11.0–Nu 0.0: mean 0.707553) can be recognized (Fig. 3). A special interval is represented in the strong increase from Nu 13.0 (lowest isotope value) to Nu 11.0 (highest isotope value) and probably indicate a local diagenetic phenomenon. The slight increase of mean strontium isotope ratios in the section is compatible with the general increase of strontium isotope ratios from the latest Jurassic into the earliest Cretaceous as reported by the strontium isotope seawater curve of McArthur et al. (2001) and McArthur & Howarth (2004). The values measured in the present study are generally higher by a factor of ca. 0.0002 compared to the values reported by McArthur & Howarth (2004), who measured Upper Tithonian values around 0.707150 and Berriasian values between 0.707200–0.70725 (see also McArthur et al. 2007) with the Berriasian/Valanginian boundary slightly above 0.707300. Thus, the lowest measured value in the Nutzhof section thus does not fall within the J/K boundary range of values recorded by McArthur & Howarth (2004). This confirms a strong diagenetic overprint upon strontium isotope values. However, the increase in mean values is within the reported magnitude of increase expected for the J/K boundary interval, thus being compatible with the stratigraphy inferred by other methods, but precluding detailed dating.

Geochemistry

The $CaCO_3$ (calcium carbonate contents, equivalents calculated from total inorganic carbon; carbonate bomb) differ markedly in the lower and upper part of the log. The lower part shows variations from 89.03 % (Nu 12.0) in limestone beds to 40.72 % (Nu 13.4) in marl beds, whereas the upper part displays more constant values ranging from 86.16 % (Nu 9.6) up to the highest measured value of 97.4 % (Nu 3.6).

As recorded by the biostratigraphic results, the strong lithological and faunal changes at Nu 12.00 and Nu 10.0 are 3 to 5 meters below the Jurassic/Cretaceous boundary (Bed Nu 7.0) indicating changes in depositional environment 0.5 to 1 million years before the end of the Jurassic. The interval from Nu 12.0–10.0 ($CaCO_3$ 89.03–68.97 %; S 0.59–0.45 %; TOC up to 0.97 %) differs markedly and heralds the environmental change observed (Fig. 3).

Both the $CaCO_3$ and the S content clearly show a trend towards higher values and stable conditions from bed Nu 10.00 to Nu 18.00. Unstable conditions are mirrored in alternating values in the lower part of the log by variations from 89.03 % $CaCO_3$ and 0.59 % S (Nu 12.0) in limestone beds to 40.72 % and 0.30 % (Nu 13.4) in marl beds.

The range is smaller and more constant in the interval Nu 10.0–18.0 with $CaCO_3$ values from 86.16 % at Nu 9.6 up to the maximum value of 97.4 % at Nu 3.6. The total sulphur content is positively correlated to the $CaCO_3$ values. The maximum value is at bed Nu 9.0 with 0.58 % S and its minimum with 0.5 % S in bed Nu 0.0. As confirmed by Hirano (1993) the sulphur content is a reliable index for oxic-anoxic conditions of the bottom water and sediment at the time of preservation.

The weight % TOC values show no positive correlation with S or $CaCO_3$. TOC values oscillate throughout the log. They vary from 0.001 % to 0.91 % (Nu 11.2) in the lower part and from 1.07 % (Nu 3.4) to 0.001 % in the upper part.

The above described geochemistry is also reflected in the results of grey-scale data marking siliciclastic input. The section can be subdivided into three parts: a lower part (Nu 18.0–12.0) with 170–111 (mean 140.5), a middle part (Nu 12.0–10.0) with 138–90 (mean 114) and an upper part (Nu 10.0–0.0) with 254–195 (mean 224.5). In combination with other analyses, the grey-scale factor is a good indicator for siliciclastic input (clay, not sandstone) in pelagic to hemipelagic sediments. This indicates the dominance of siliciclastic components and allodapic microturbidites within the dark mid-part. These results corroborate those obtained from susceptibility and gamma log (increasing values show higher contents in clay minerals), thin sectioning and microfacies analysis.

Susceptibility

Susceptibility measurements at Nutzhof represent a direct function of the clastic or turbiditic content and associated mineral spectra (Fig. 3). Higher susceptibility data reflect higher detritic input of terrigenous material. The paleomagnetic data given in the magnetostratigraphic profile indicate a significant jump of remanent magnetization and magnetic

susceptibility, at Nu 10.0. This change marks the change from marls and marly limestone to pure limestone. Magnetosusceptibility measurements allow a subdivision of the Nutzhof section into three parts or intervals. A general decreasing trend throughout the log reflects a decreasing content of siliciclastic material indicating a decrease in clastic input to the depositional area at Nutzhof during the Late Jurassic–Early Cretaceous. Mean values of volume magnetic susceptibility (k) are shown in Table 1. The k ranges from –8.6 to 15.6×10^{-6} SI for upper interval between 0–10 m of the section and from 30 to 85.1×10^{-6} SI for the lower part (10.12–18.4 m). The lower part from Nu 18.0–12.0 shows values from 0.052–0.028 (mean 0.039). Above Nu 12.0 values range from 0.050–0.026 (mean 0.033). The most marked change appears at Nu 10.0 from values of 0.050 to 0.010. The upper interval from Nu 10.0 to 0.0 is characterized by very low values from 0.012–0.000 (mean 0.004). The J/K boundary strata itself are not characterized by significant changes in values.

Gamma log

The radioactivity variation of the studied section is measured by gamma-ray measures and represents a direct function of the variation of the clay-mineral content. Hence, higher radioactivity reflects higher clay contents. Measurements of gamma response (cps) are a powerful tool for interpreting the stratigraphy in the outcrop.

Generally measured cps values range between 4 and 30. The gamma response allows a clear subdivision of the section into three parts each corresponding to the three identified main lithological units within the Blassenstein Formation. The gamma response gradually decreases from Nu 18.0 to Nu 0.0, reaching the highest values at Nu 16.5 and lowest values at Nu 7.7 and Nu 3.3. Within this gradually decreasing trend, the biggest excursion is recorded close to bed Nu 10.0. Values range in the lower interval (Nu 18.0–12.0) from 15–30 cps (mean 22.53 cps), in the middle interval (Nu 12.0–10.0) from 13–23 cps (mean 19.95 cps), and in the upper interval (Nu 10.0–0.0) from 4–14 cps (mean 9.07 cps) (Fig. 3).

The gamma response becomes gradually weaker in the upper, undisturbed part of the section. The uppermost part of the section, however, shows an upwards decreasing gamma response. The curve pattern therefore shows a vertically congruent curve to the susceptibility values.

The decreasing gamma log values together with the characteristic pattern in decreasing susceptibility suggest a more stable depositional environment from about Nu 10.0 and upwards, predating the J/K boundary by 3 meters or 0.5 million years.

Paleomagnetism

The paleomagnetic study of the section identifies the boundaries of magnetozones from M17r to M21r and the reverse subzones Kysuca and Brodno (M20n.1r and M19n.1r, respectively). The record of polarity changes in the Earth's magnetic field can determine the precise age. The identification of the detected polarity zones against the M-sequence of polarity intervals given by the GPTS (Gradstein et al. 2004) is the most important topic. The preliminary determination of boundaries of magnetozones M17n to M22r was the result from 30 samples of C-component direction (Pruner et al. 2009). The number of polarity zones, namely six normal and six reverse, is the same number as in preliminary results. The mean values of the modulus of NRM (Jn) and of volume magnetic susceptibility (k) for 244 samples of Upper Tithonian and Lower Berriasian limestones are shown in Table 1. The k ranges from –8.6 to 15.6×10^{-6} SI for the upper interval between 0–10 m of the section and from 30 to 85.1×10^{-6} SI for the lower part (10.12–18.4 m). The results of AF and TD demagnetization procedures are displayed in Pruner et al. (2009: figs. 3, 4). The A-component is of viscous origin and is demagnetizable in the temperature range of 20–100 °C (or AF 0–5 mT). The origin of the B-components, low temperature (LTC) or low field (LFC) were undoubtedly imprinted, most probably in the Neogene, after Alpine folding. Both magnetic polarities are present in C-component (high temperature — HTC or high field — HFC) directions, but the directions are highly scattered (Table 2, Fig. 5). The statistical

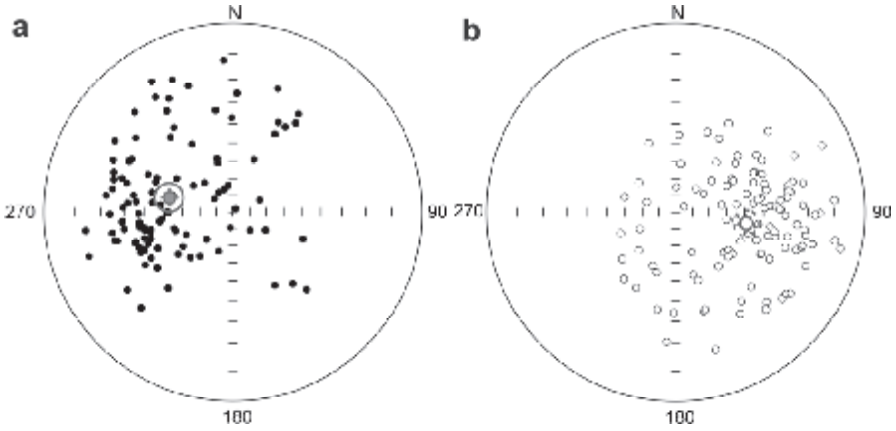

Fig. 5. J/K limestones and marls, directions of N polarity (left) and R polarity (right) of C-components of RM corrected for dip of strata. Stereographic projection, full (open) small circles represent projection onto the lower (upper) hemisphere. The mean direction calculated according to Fisher (1953) is marked by a small crossed circle, the confidence circle at the 95% probability level is circumscribed about the mean direction.

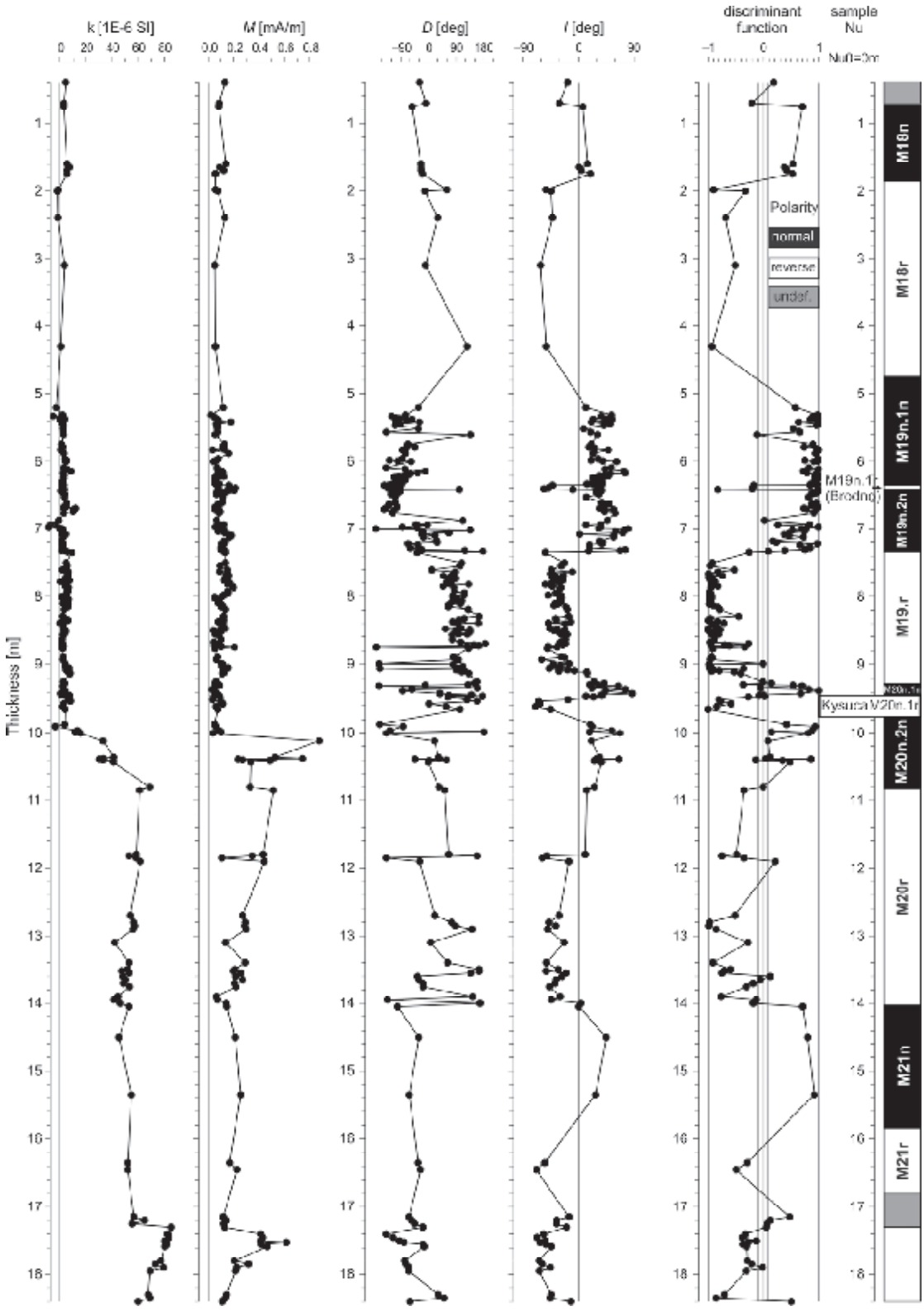

Fig. 6. Magnetostratigraphic profile across the Nutzhof J/K boundary strata, paleomagnetic and lithostratigraphic data. *M* — NRM in the natural state; *k* — value of volume magnetic susceptibility in the natural state; D — declination; I — inclination. Normal (reverse) magnetozones are denoted black (white), unknown (grey).

Table 1: Basic magnetic parameters and statistical properties of the physical quantities in the basic groups of samples from the Nutzhof.

Age	Polarity	Number of samples	Modulus of NRM J_n [10^{-6} A/m]		Volume magnetic susceptibility k [10^{-6} SI]	
			Mean value	Standard deviation	Mean value	Standard deviation
Early Berriasian	N+R	82	88	39	2.3	3.1
Late Tithonian	N+R	155	165	132	21.4	26.5

Table 2: Mean directions of B (LFC or LTD) and C-components (HFC or HTD) corrected and not corrected for structural tilt.

Age of rocks	Component of remanence	Polarity	Structural tilt correction				No structural tilt correction (in-situ directions)				n
			Mean directions		α_{95} [°]	k	Mean directions		α_{95} [°]	k	
			Decl. [°]	Incl. [°]			Decl. [°]	Incl. [°]			
L. Tith.+ E.Berr.	B	R	351.7	–55.4	3.1	12.1	10.4	77.5	3.1	11.9	168
L. Tith.+ E.Berr.	C	N	278.0	53.3	7.1	3.2	199.3	–27.3	8.0	2.6	119
L. Tith.+ E.Berr.	C	R	104.1	–46.1	6.4	4.8	19.3	13.2	6.4	4.8	101
L. Tith.+ E.Berr.	C	N*)	286.1	44.5	4.7	4.0	198.1	–15.0	5.2	3.7	220

parameters for component C (total number 220) are influenced by samples close to the boundary of shorter polarity zones. The mean values of C-component directions are anomalous, having been affected by counter clockwise paleotectonic rotation. The paleomagnetic data given in the magnetostratigraphic profile (Fig. 6) indicate a significant change of remanent magnetization and magnetic susceptibility, at level Nu 10 due to the significant change in lithology from marl (Nu 18.0–10.0) to limestone (Nu 10.0–0.0).

Figure 5 presents the results of the magnetostratigraphic profile with indicated moduli values of natural remanent magnetization (*Jn*), volume magnetic susceptibility values of samples in the natural state (*k*), paleomagnetic declination Dp and inclination Ip (of C-components of remanence inferred by multi-component analysis). The values of the angular deflection of the direction of C-components of remanence from the mean direction, with only normal polarity being taken into consideration (reverse directions were transformed into normal directions for the calculation of the mean direction), are given in the next column. The resulting normal and reverse magnetozones are indicated in the last column.

Discussion

The high-resolution quantitative analysis of selected organic groups (calpionellids, radiolarians, saccocomids) indicates major variations in their abundance and composition (Figs. 2, 3, 4). The Upper Jurassic (Tithonian) depositional setting at Nutzhof was influenced by the periodic input of biodetritus from surrounding shallow marine paleoenvironments, whereas deposition was more constant during the Berriasian and characterized by pelagic sediments predominantly composed of planktonic microorganisms (radiolarians, calcareous dinoflagellates, calpionellids, and nannofossils).

Calcareous dinoflagellates predominate in the Lower and Upper Tithonian. Their stratigraphic and paleoecological potential has been discussed by Reháková (2000a,b). In the Nutzhof section, the Lower Tithonian record of calcareous dinoflagellates shows a distinct change in abundance and composition. Forms with radial orientation of calcite crystallites in their cyst walls dominate in the *Tithonica* and *Malmica* Zones, whereas cadosinid species with oblique arrangement of the calcite crystallites dominate the *Semiradiata* Zone. According to Michalík et al. (2009), coinciding acme peaks of *Cadosina semiradiata semiradiata* Wanner and *Conusphaera* spp. probably indicate warmer surface waters.

Chitinoidellids are very rare in the Nutzhof section. The appearance of the first hyaline calpionellid loricas precedes the crassicollarian radiation. A monospecific calpionellid association consisting predominantly of *Calpionella alpina* Lorenz characterizes the section. A similar calpionellid evolution and biostratigraphy of the Jurassic-Cretaceous boundary interval was recorded by Remane (1986), Pop (1994), Reháková (1995), Olóriz et al. (1995), Grün & Blau (1997), and Andreini et al. (2007). Reháková (in Michalík et al. 2009) demonstrated that the J/K boundary interval can be characterized by several calpionellid events: the onset, diversification, and extinction of chitinoidellids (middle Tithonian); the onset, diversification, and extinction of crassicollarians (Upper Tithonian); and the onset of the monospecific *Calpionella alpina* association at the J/K boundary. Due to synsedimentary erosion probably originating during several extensional pulses, which denivelated the sea bottom, clast-bearing calpionellid biomicrites were documented along the Upper Jurassic and Lower Cretaceous (Lower Berriasian) formations in several areas studied (Michalík et al. 1990, 1995; Grabowski et al. 2010).

The calcareous nannofossil ranges in the Nutzhof section provides a tool for biostratigraphic subdivision of the J/K boundary interval. The coccoliths of the family Watznaueriaceae and three nannolithic genera *Conusphaera*, *Polycostella*, and *Nannoconus* dominate the assemblages. This is in accordance with nannofossil studies in other locations at low latitudes sections across the J/K boundary (Thierstein 1971, 1973, 1975; Erba 1989; Gardin & Manivit 1993; Özkan 1993;

Tavera et al. 1994; Bornemann et al. 2003; Pszczółkowski & Myczyński 2004; Tremolada et al. 2006; Halásová in Michalík et al. 2009).

The lowermost occurrences of nannofossils are partly obscured due to poor preservation, but we tentatively identified the boundaries of zones and subzones based on certain stratigraphic markers (*Polycostella beckmannii*, *Helenea chiastia*, *Hexalithus noeliae*, *Nannoconus wintereri*, *Nannoconus globulus minor*, *Nannoconus steinmannii minor*, *Nannoconus kamptneri minor*, *Nannoconus steinmannii steinmannii*, *Nannoconus kamptneri kamptneri*, *Nannoconus globulus globulus*).

Tremolada et al. (2006) detected that *Conusphaera* dominates the nannolith assemblage in the upper middle Tithonian ("*Conusphaera* world"). This is corroborated by data obtained in this study. The acme peak of the genus *Polycostella* in samples Nu 13.0 and 14.0 coincides with the middle Tithonian *Semiradiata* Subzone (Reháková 2000b). Comparison with the Brodno section (Michalík et al. 2007 and Michalík et al. 2009) indicate that the dominance of the nannolith *Polycostella beckmannii* occurs somewhat lower in the *Chitinoidella* Zone in the Nutzhof section. The first appearance of *Helenea chiastia* is also demonstrated to be diachronous, being close to the base of the calpionellid *Crassicollaria* Zone in the Brodno section, but recorded in the uppermost part of the *Chitinoidella* Zone in the Nutzhof section.

The most distinct nannofossil event is the onset of nannoconids which was observed in the interval comprising the calpionellid *Calpionella* Zone, *Ferasini* Subzone (lowermost Berriasian). This indicates a change in the paleooceanographic regime. From the biostratigraphic point of view, the upper J/K boundary datum based on nannofossils (Bornemann et al. 2003).

The change of saccocomid marl and limestone by overlying calpionellid limestone in the Upper Tithonian also characterizes J/K-boundary successions reported from numerous other localities in Austria (e.g. Kristan-Tollmann 1962; Flügel 1967; Holzer 1968; Holzer & Poltnik 1980; Reháková et al. 1996), Germany (Lackschewitz et al. 1989), Poland (Pszczółkowski & Myczyński 2004) and Slovakia (Vašíček et al. 1992). Many of these localities, however, differ lithologically from the section studied at Nutzhof. In most cases the saccocomid-bearing beds are pure, reddish limestone.

Saccocomid limestones have often been interpreted as Kimmeridgian (e.g. Flügel 1967: p. 35; Sauer et al. 1992: p. 183; Wessely 2008: p. 210, fig. 5) and have been used as the marker bed for that stage (Bernouli 1972). Reliable stratigraphic data is, however, commonly lacking. Based on well-dated sections, the majority of the recorded saccocomid-occurrences are of Tithonian age (Nicosia & Parisi 1979; Keupp & Matyszkiewicz 1997). This is corroborated/supported by the data from the present study.

Summary and conclusions

The studied section at Nutzhof represent a J/K-boundary succession deposited in a distal slope-setting in the Gresten Klippenbelt, a part of the Helvetic paleogeographic realm. The Upper Jurassic to Lower Cretaceous pelagic sediments represent a major sedimentation cycle.

The significant depositional change from a mixed siliciclastic/carbonate to a pure carbonate depositional system is marked by a change from a lower marly cyclic part to an upper calcareous part. Accordingly, the lower (Tithonian) marly part is characterized by dark, laminated pelagic marls and marly limestones with intercalated turbiditic limestone beds (e.g. allodapic limestones). The upper part (limestone) represents a phase of autochthonous pelagic sedimentation characterized by bright, chert- and aptychi-bearing nannoconid limestone. The macro-invertebrate fauna of the Berriasian limestone succession is sparse, comprising rare ammonoids, aptychi, belemnites and brachiopods. The macro-invertebrate fauna of the Tithonian marl-limestone succession is rich in saccocomids accompanied by rare bivalves (inoceramids) and partly by abundant ammonites. The microfauna, in contrast, is abundant, with dominating calpionellids and radiolarians in the limestone succession and saccocomid blooms within the marl-limestone succession.

The macrofauna, as already stated, is represented especially by ammonoids, belemnoids, aptychi and bivalves. The whole section yielded 46 ammonite individuals/specimens. Sampling of the sparse ammonites was difficult due to hardite sediments. The ammonite biostratigraphy is integrated with micro- and nannofossil biostratigraphic data from the marl-limestone succession and indicates Early Tithonian to middle Berriasian ages (*Hybonoticeras hybonotum* Zone up to the *Subthurmannia occitanica* Zone). Descendants of *Subplanites* have not previously been reported within the Gresten Klippenbelt. All ammonoids are typical of the Mediterranean Province.

The limitation of ammonite biostratigraphy obtained by the new ammonite findings from Nutzhof has demonstrated the importance of integrating macrofauna biostratigraphy with the micro- and nannofossil biostratigraphy. The described fauna increases our understanding of ammonite faunas from the area of the Gresten Klippenbelt and the neighbouring Waschberg Zone during deposition of the Jurassic/Cretaceous boundary interval. Both areas were at the time located on the passive northern margin of the Penninic Ocean.

Magnetostratigraphic, geochemical and isotopes studies contribute to the understanding of the environmental history during the Jurassic-Cretaceous boundary interval in a little known area. Sediment deposition took place during conditions of relatively stable water masses with relatively low sedimentation rates in an unstable sedimentological environment. This is reflected by a change in lithology from Nu 11.0 to Nu 13.0 (11 to 13 m). A series of event layers with redeposited faunal elements (e.g. phyllocrinids) indicate a transport of sediment from shallower areas in the North. The depositional area was influenced by the opening of the Penninic Ocean during the Late Jurassic to Early Cretaceous. A phase of an earlier Penninic opening, is reflected as a significant change in lithology and composition of faunal assemblage in the uppermost Tithonian (at Nu 10.0 m).

There is no evidence for redeposition of ammonites, which are considered autochthonous and parautochthonous pelagic elements from the open sea. Four crinoid taxa are recorded in

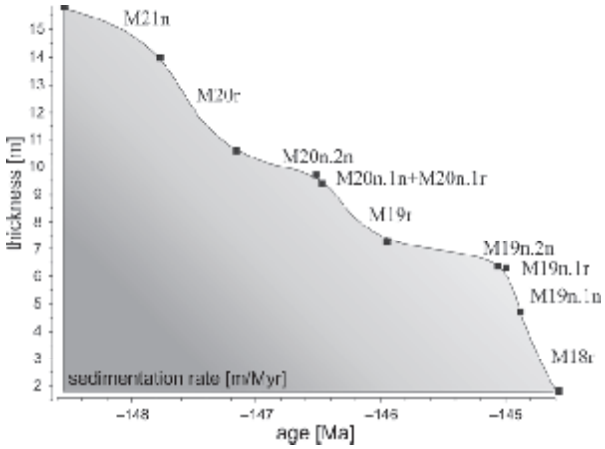

Fig. 7. Estimated average sedimentation rate diagram around the J/K boundary at Nutzhof based on magnetostratigraphic and biostratigraphic data.

the Tithonian Blassenstein Formation and comprise *Balanocrinus* sp., *Saccocoma tenella* (Goldfuss), *Crassicoma*? sp., and *Phyllocrinus belbekensis* Arendt. Only *S. tenella* is abundant. The other taxa, in particular the benthic isocrinids and phyllocrinids are rare. Preservation and ossicle size range of the latter groups indicate their allochthonous origin. The saccocomid remains are restricted to the Tithonian, the saccocomid-rich facies being overlain by calpionellid limestones.

The biostratigraphic study based on the distribution of calpionellids allowed an identification of the *Boneti* Subzone of the *Chitinoidella* Zone. The J/K boundary is recorded between the *Crassicollaria* and *Calpionella* Zone and is defined by the morphological change of *Calpionella alpina* tests. The base of the *Crassicollaria* Zone approximately coincides with the onset of *Tintinnopsella remanei* Borza and the base of the standard *Calpionella* Zone, with the monospecific calpionellid association being dominated by *Calpionella alpina* Lorenz. Two further Subzones (*Ferasini* and *Elliptica*) of the standard *Calpionella* Zone were recognized in radiolarian-calpionellid and calpionellid-radiolarian wackestones in the overlying uppermost part of the section.

The appearance of several important nannofossil genera allow the identification of the Lower, middle and Upper Tithonian, and a relatively accurate identification of the Tithonian-Berriasian boundary, and the definition of the Lower Berriasian nannofossil zones. Coccoliths of the family Watznaueriaceae and nannoliths of the genera *Conusphaera*, *Nannoconus* and *Polycostella* dominate the assemblages. The interval between the FAD of *Nannoconus wintereri* co-occurring with small nannoconids in sample Nu 9 (the uppermost Tithonian) and the FAD of *Nannoconus kamptneri minor* in sample Nu 5 (lowermost Berriasian) is interpreted as the Tithonian-Berriasian boundary interval. The nannoconid dominance in the lowermost Berriasian, known as the "*Nannoconus* world" sensu Tremolada et al. (2006) is now recorded in the Nutzhof section.

Paleomagnetic data across the J/K boundary strata allow the construction of a detailed magnetostratigraphic zonation. The interval between Nu 5 to 10.5 m provides a high-resolution profile with an almost continuous record of magnetic and paleomagnetic parameters, that records the critical intervals with boundaries of the magnetozones M19n–M20n. According to magnetozone M19n and Brodno Subzone, the J/K boundary is identified within the interval between Nu 6.5–7 m. Significant changes do not occur at the J/K boundary itself. The step of remanent magnetization and magnetic susceptibility, at level Nu 10.0, occurs in magnetozone M20n below the Kysuca Subzone. A similar jump of NRM and susceptibility lies in the M20n just above the Kysuca Subzone in the Bosso section. The average sedimentation rate in the Nutzhof section is ca. 3.7 m/Myr (Fig. 7), but with high dispersion (from 2–11 m/Myr) differing from the average sedimentation rates of 2.27 m/Myr recorded in Brodno and 2.88 m/Myr in Puerto Escaño. Relatively low rates (1 m/Myr) are recorded in the Bosso Valley, but higher rates (3–11 m/Myr) are reported by Grabowski & Pszczółkowski (2006) from the Tatra Mountains. No significant change can be noted at or within the J/K boundary interval. The integration of fossil and magnetostratigraphic data demonstrates a duration of approximately 7 million years (approximately 150–143 Ma) for the deposition of the Nutzhof section (Figs. 6 and 7).

The carbon isotope record documents a significant change in the C-cycle dynamic suggesting a sluggish 3-D dynamic of the marine system possibly associated with a decrease in primary productivity. Abrupt oscillations mainly recorded between the levels 10 and 6 m suggest a significantly unstable global carbon system during the Jurassic but a change towards balanced conditions in the Cretaceous interval.

Acknowledgments: We are indebted to Hans Egger (Geological Survey of Austria) who made us aware of the studied locality. The study was supported by the Austrian Science Fund (FWF; Project P20018-N10) and by the Grant Agency of the Czech Republic (Grant No. GACR 205-07-1365) and Research Plan of the IG AS CR No. CEZ AV0Z30130516. This is also a contribution to the 506 IGCP UNESCO Project, APVV-0280-07, APVV-0248-07, APVV- 0465-06, APVT 51-011305 and LPP 0120-09. MW thanks IGCP 555 and the Austrian Academy of Sciences for financial support. Thanks go to members of the Kilian Group (Lower Cretaceous Ammonite Working Group; president Stephane Reboulet, Lyon) for fruitful discussions on the ammonoid fauna. Technical support for photography was provided by Alice Schumacher (Vienna). Franz Topka (Vienna) assisted with the preparation of ammonoid specimens and Anton Englert (Vienna) prepared the thin sections. Paleomagnetic analyses were performed by Daniela Venhodová, Jana Drahotová, and Jiří Petráček. The software for the evaluation of paleomagnetic measurements was prepared by Otakar Man (Institute of Geology ASCR v.v.i.). We thank Luc Bulot (Marseille) and Jacek Grabowski (Warsaw) for their comments which helped to improve the quality of the manuscript.

References

Andreini G., Caracuel J.E. & Parisi G. 2007: Calpionellid biostratigraphy of the Upper Tithonian–Upper Valanginian inter-

val in Western Sicily (Italy). *Swiss J. Geosci*. 100, 179–198.
Bernouli D. 1972: North Atlantic and Mediterranean Mesozoic facies: A comparison. *Init. Repts. DSDP* 11, 631–643.
Bornemann A., Aschwer U. & Mutterlose J. 2003: The impact of calcareous nannofossils on the pelagic carbonate accumulation across the Jurassic-Cretaceous boundary interval. *Palaeogeogr. Palaeoclimatol. Palaeoecol*. 199, 187–228.
Bralower T.J., Monechi S. & Thierstein H.R. 1989: Calcareous nannofossil zonation of the Jurassic-Cretaceous boundary interval and correlation with the geomagnetic polarity timescale. *Mar. Micropaleont*. 14, 153–235.
Cžjžek J. 1852: Aptychenschiefer in Niederösterreich. *Jb. K.-Kön. Geol. Reichsanst.* 3, 3, 1–7.
Decker K. 1990: Plate tectonics and pelagic facies: Late Jurassic to Early Cretaceous deep-sea sediments of the Ybbsitz ophiolite unit (Estern Alps, Austria). *Sed. Geol*. 67, 85–99.
Decker K. & Rögl F. 1990: Early Cretaceous agglutinated foraminifera from limestone-marly rhythmites of the Gresten Klippen Belt (Eastern Alps Austria). *Abh. Geol. B.–A*. 41, 41–59.
Dercourt J., Ricou L.E. & Vrielynck B. (Eds.) 1993: Atlas Tethys palaeoenvironment maps, 14 maps, 1 pl. *Gauthier-Villars*, Paris, 1–307.
Dercourt J., Gaetani M., Vrielynck B., Barrier E., Biju Duval B., Brunet M.F., Cadet J.P., Crasquin S. & Sandulescu M. (Eds.) 2000: Atlas Peri-Tethys, Palaeogeographical maps, 24 maps and explanatory notes: I-XX. *CCGM/CGMW*, Paris, 1–269.
Erba E. 1989: Calcareous nannofossil zonation of the Jurassic-Cretaceous boundary interval and correlation with the geomagnetic polarity timescale. *Mar. Micropaleont*. 14, 153–235.
Faupl P. 2003: Historische Geologie: eine Einführung. *Facultas*, Wien, 1–271.
Faupl P. & Wagreich M. 2000: Late Jurassic to Eocene Palaeogeography and Geodynamic Evolution of the Eastern Alps. *Mitt. Österr. Geol. Gesell*. 92, 79–94.
Fisher R.A. 1953: Dispersion on a sphere. *Proc. R. Soc. London A*. 217, 295–305.
Flügel H.W. 1967: Die Lithogenese der Steinmühl-Kalke des Arracher Steinbruches (Jura, Österreich). *Sedimentology* 9, 23–53.
Gardin S. & Manivit H. 1993: Upper Tithonian and Berriasian calcareous nannofossils from the Vocontian Trough (SE France): Biostratigraphy and sequence stratigraphy. *Bull. Centres Rech. Explor.-Prod. Elf-Aquitaine* 17, 1, 277–289.
Gottschling P. 1965: Zur Geologie der Hauptklippenzone und der Laaber Teildecke im Bereich von Glashütte bis Bernreith (Niederösterreich). *Mitt. Geol. Gesell. Wien* 58, 23–86.
Grabowski J. & Pszczółkowski A. 2006: Magneto- and biostratigraphy of the Tithonian-Berriasian pelagic sediments in the Tatra Mountains (central Western Carpathians, Poland): sedimentary and rock magnetic changes at the Jurassic/Cretaceous boundary. *Cret. Research* 27, 398–417.
Grabowski J., Michalík J., Pszczółkowski A. & Lintnerová O. 2010: Magneto-, and isotope stratigraphy around the Jurassic/Cretaceous boundary in the Vysoká Unit (Malé Karpaty Mts, Slovakia): correlations and tectonic implications. *Geol. Carpathica* 61, 4, 309–326.
Gradstein F.M., Ogg J.G. & Smith A.G. (Eds.) 2004: A geologic time scale 2004. *Cambridge University Press*, Cambridge, U.K., 1–589.
Grün B. & Blau J. 1997: New aspects of calpionellid biochronology: proposal for a revised calpionellid zonal and subzonal division. *Rev. Paléobiol.* 16, 197–214.
Hardenbol J., Thierry J., Farley M.B., Jacquin T., de Graciansky P.C. & Vail P.R. 1998: Mesozoic and Cenozoic sequence stratigraphy of European basins. *SEPM, Spec. Publ.*, Tulsa 60, 1998.
Hennig S., Weissert H. & Bulot L. 1999: C-isotope stratigraphy, a calibration tool between ammonite- and magnetostratigraphy: the Valanginian-Hauterivian transition. *Geol. Carpathica* 50, 91–96.
Hess H., Ausich W.I., Brett C.E. & Simms M.J. 1999: Fossil crinoids. *Cambridge University Press*, Cambridge, MA, xv+275.
Hirano H. 1993: Phyletic evolution of desmoceratine ammonoids through the Cenomanian-Turonian oceanic anoxic event. In: House M.R. (Ed.): The Ammonoidea: environment, ecology, and evolutionary change. *Clarendon Press*, Oxford, UK, 267–283.
Holzer H.-L. 1968: Stratigraphie und Lithologie der Jura-Kreide-Folge im nördlichsten Pechgraben-Steinbruch. *Mitt. Naturwiss. Vereins Steiermark* 98, 47–57.
Holzer H.-L. & Poltnig W. 1980: Erster Nachweis einer Radialplatten-Fossillagerstätte der Schwebcrinoide *Saccocoma* im oberostalpinen Malm (Ostkarawanken, Kärnten). *Carinthia II* 170, 201–216.
Houša V., Krs M., Krsová M., Man O., Pruner P. & Venhodová D. 1999: High-resolution magnetostratigraphy and micropaleontology across the J/K boundary strata at Brodno near Žilina, western Slovakia: summary results. *Cret. Research* 20, 699–717.
Houša V., Krs M., Man O., Pruner P., Venhodová D., Cecca F., Nardi G. & Piscitello M. 2004: Combined magnetostratigraphic, paleomagnetic and calpionellid investigations across Jurassic/Cretaceous boundary strata in the Bosso Valley, Umbria, central Italy. *Cret. Research* 25, 771–785.
Keupp H. & Matyszkiewicz J. 1997: Zur Faziesrelevanz von *Saccocoma*-Resten (Schwebcrinoiden) in Oberjura-Kalken des nördlichen Tethys-Schelfs. *Geol. Blätter für Nordost-Bayern und angrenzende Gebiete* 47, 53–70.
Kirschvink J.L. 1980: The least-squares line and plane and the analysis of palaeomagnetic data. *Geophys. J. Roy. Astr. Soc*. 62, 699–718.
Kristan-Tollmann E. 1962: Stratigraphisch wertvolle Mikrofossilien aus dem Oberjura und Neokom der Nördlichen Kalkalpen. *Erdoel-Z*. 78, 637–549.
Kroh A. & Lukeneder A. 2009: Crinoids from the Late Jurassic–Early Cretaceous of the Nutzhof section (Lower Austria, Pieniny Klippenbelt). *Ann. Naturhist. Mus. Wien, Serie A* 110, 383–399.
Kühn O. 1962: Autriche. *Lexique Stratigr. Int.*, Europe 8, 1–646.
Küpper H. 1962: Beobachtungen in der Hauptklippenzone bei Stollberg, N.Ö. *Verh. Geol. B.–A*. 2, 263–268.
Lackschewitz K., Grützmacher U., Suhr J. & Kiel R.H. 1989: Synsedimentäre Kippschollentektonik: Becken- und Schwellenfazies oberjurassischer Karbonate der Chiemgauer Alpen. *Geol. Paläont. Mitt. Innsbruck* 16, 163–165.
Lierl H.J. 1992: Tenside — ihre Verwendung für die Präperation geologisch-paläontologischer Objekte. *Der Präperator* 38, 12–17.
Lukeneder A. 2009: New biostratigraphic ammonite data from the Jurassic/Cretaceous boundary at Nutzhof (Gresten Klippenbelt, Lower Austria). *Ann. Naturhist. Mus. Wien, Serie A* 110, 313–330.
Mandic O. & Lukeneder A. 2008: Dating the Penninic Ocean subduction: new data from planktonic foraminifera. *Cret. Research* 29, 901–912.
Masse J.P. et al. (12 co-authors) 2000: Early Aptian. In: Dercourt J., Gaetani M. et al. (Eds.). Atlas Peri-Tethys, Palaeogeographical Maps 13, (CCGM/CGMW) Paris.
McArthur J.M. & Howarth R.J. 2004: Strontium isotope stratigraphy. In: Gradstein F.M., Agterberg F.P. & Smith A.G. (Eds.): A geologic time scale 2004. *Cambridge University Press*, 96–105.
McArthur J.M., Howarth R.J. & Bailey T.R. 2001: Strontium isotope stratigraphy: LOWESS Version 3: best fit to the marine Sr-isotope curve for 0–509 Ma and accompanying look-up table for deriving numerical age. *J. Geol*. 109, 155–170.
McArthur J.M., Janssen N.M.M., Reboulet S., Leng M.J., Thirlwall

M.F. & van de Schootbrugge B. 2007: Early Cretaceous ice-cap volume, palaeo-temperatures (Mg, ^{18}O), and isotope stratigraphy (^{13}C, $^{87}Sr/^{86}Sr$) from Tethyan belemnites. *Palaeogeogr. Palaeoclimatol. Palaeoecol.* 248, 391–430.

Michalík J., Reháková D. & Halásová E. 1990: Stratigraphy of the Jurassic/Cretaceous boundary beds in the Hlboč Valley (Vysoká Unit of the Krížna Nappe, Malé Karpaty Mts). *Knihovnička ZPN* 9a, 183–204 (in Slovak, with English summary).

Michalík J., Reháková D. & Vašíček Z. 1995: Early Cretaceous sedimentary changes in west Carpathian area. *Geol. Carpathica* 46, 285–296.

Michalík J., Reháková D., Halásová E. & Lintnerová O. 2007: Integrated stratigraphy of the Jurassic/Cretaceous boundary at the Brodno section (the Kysuca Unit, Pieniny Klippen Belt, Western Carpathians). *Abstract book, International geological correlation programme 506 — Jurassic marine: non-marine correlation*, *Univ. Bristol*, 1–3.

Michalík J., Reháková D., Halásová E. & Lintnerová O. 2009: A possible West Carpathian regional stratotype of the Jurassic/Cretaceous boundary (the Brodno section near Žilina). *Geol. Carpathica* 60, 3, 213–232.

Nicosia U. & Parisi G. 1979: *Saccocoma tenella* (Goldfuss) — Distribuzione stratigrafica e geografica. *Boll. Soc. Paleont. Ital.* 18, 320–326.

Olóriz F., Caracuel J.E., Marques B. & Rodríguez-Tovar F.J. 1995: Asociaciones de Tintinnoides en facies Ammonitico Rosso de la Sierra Norte (Mallorca). *Rev. Esp. Paleont., No. Homenaje al Dr. G. Colom*, 77–93.

Özkan S. 1993: Calcareous nannofossils from the Late Jurassic–Early Cretaceous of Northwest Anatolia, Turkey. *Geol. J.* 28/3–4, 295–307.

Piller W. et al. 2004: Die Stratigraphische Tabelle von Österreich 2004 (sedimentäre Schichtfolgen). *Österr. Akad. Wissenschaft. Österr. Stratigr. Kommission*, Wien.

Pop G. 1994: Calpionellid evolutive events and their use in biostratigraphy. *Rom. J. Stratigraphy* 76, 7–24.

Pop G. 1997: Révision systématique des chitinoidelles tithoniennes des carpathes méridionales (Roumanie). *Compt. Rendus Acad. des Sci., Sér. IIa*, Paris 342, 931–938.

Pruner P., Schnabl P. & Lukeneder A. 2009: Preliminary results of magnetostratigraphic investigations across the Jurassic/Cretaceous boundary strata in the Nutzhof, Austria. *Ann. Naturhist. Mus. Wien*, *Ser. A* 110, 331–344.

Pszczółkowski A. & Myczyński R. 2004: Ammonite-supported microfossil and nannoconid stratigraphy of the Tithonian-Hauterivian limestones in selected sections of the Branisko Succession, Pieniny Klippen Belt (Poland). *Stud. Geol. Pol.* 123, 133–197.

Reháková D. 1995: New data on calpionellid distribution in the Upper Jurassic/Lower Cretaceous formations (Western Carpathians). *Miner. Slovaca* 27, 308–318 (in Slovak).

Reháková D. 1998: Calpionellid genus *Remaniella* Catalano 1956 in Lower Cretaceous pelagic deposits of Western Carpathians. *Miner. Slovaca* 30, 443–452.

Reháková D. 2000a: Calcareous dinoflagellate and calpinellid bioevents versus sea-level fluctuations recorded in the West-Carpathian (Late Jurassic/Early Cretaceous) pelagic environments. *Geol. Carpathica* 51, 4, 229–243.

Reháková D. 2000b: Evolution and distribution of the Late Jurassic and Early Cretaceous calcareous dinoflagellates recorded in the Western Carpathian pelagic carbonate facies. *Miner. Slovaca* 32, 79–88.

Reháková D. 2002: *Chitinoidella* Trejo, 1975 in Middle Tithonian carbonate pelagic sequences of the West Carpathian Tethyan area. *Geol. Carpathica* 55, 6, 369–379.

Reháková D. & Michalík J. 1997: Evolution and distribution of calpionellids — the most characteristic constituents of Lower Cretaceous Tethyan microplankton. *Cret. Research* 18, 493–504.

Reháková D., Michalík J. & Ožvoldová L. 1996: New microbiostratigraphical data from several Lower Cretaceous pelagic sequences of the Northern Calcareous Alps, Austria (Preliminary results). *Geol. Paläont. Mitt. Innsbruck* 4, 57–81.

Reháková D., Halásová E. & Lukeneder A. 2008: The Jurassic/Cretaceous boundary in the Austrian Klippen belt (Nutzhof, Lower Austria): Implications on micro- and nannofacies analysis. *Ber. Geol. B.–A.* 74, 95–97.

Reháková D., Halásová E. & Lukeneder A. 2009: The Jurassic-Cretaceous boundary in the Austrian Klippen Belt (Nutzhof, Lower Austria): Implications on Micro- and Nannofacies analysis. *Ann. Naturhist. Mus. Wien*, *Ser. A* 110, 345–381.

Remane J. 1986: Calpionellids and the Jurassic-Cretaceous boundary. *Acta Geol. Hung.* 29, 15–26.

Roth P.H., Medd A.W. & Watkins D.K. 1983: Jurassic calcareous nannofossil zonation, an overview with new evidence from Deep Sea Drilling Project Site 534A. In: Sheridan R.E., Gradstein F.M. et al. *Init. Repts. DSDP* 76, 573–579.

Řehánek J. 1992: Valuable species of cadosinids and stomiosphaerids for determination of the Jurassic-Cretaceous boundary (vertical distribution, biozonation). *Scripta* 22, 117–122.

Sauer R., Seifert P. & Wessely G. 1992: Guidebook to excursions in the Vienna Basin and the adjacent Alpine-Carpathian Thrustbelt in Austria. Part II. *Mitt. Österr. Geol. Gesell.* 85, 97–239.

Scotese C.R. 2001: Atlas of earth history. *Paleomap project*, Arlington, Texas, 1–52.

Spötl C. & Vennemann T. 2003: Continuous-flow isotope ratio mass spectrometric analysis of carbonate minerals. *Rapid Communications in Mass Spectrometry* 17, 1004–1006.

Stampfli G.M. & Borel G.D. 2002: A plate tectonic model for the Paleozoic and Mesozoic constrained by dynamic plate boundaries and restored synthetic oceanic isochrons. *Earth Planet. Sci. Lett.* 196, 17–33.

Stampfli G. & Mosar J. 1999: The making and becoming of Apulia. *Mem. Sci. Géol. Padova. Spec. Vol.*, *3rd Workshop on Alpine Geology* 51/1, 141–154.

Stampfli G.M., Borel G.D., Marchant R. & Mosar J. 2002: Western Alps geological constraints on western Tethyan reconstructions. In: Rosenbaum G. & Lister G.S. (Eds.): Reconstruction of the evolution of the Alpine-Himalayan Orogen. *J. Virtual Explorer* 8, 77–106.

Tavera J.M., Aguado R., Company M. & Olóriz F. 1994: Integrated biostratigraphy of the Durangites and Jacobi Zones (J/K boundary) at the Puerto Escaño section in Southern Spain (province of Cordoba). *Geobios* 17, 469–476.

Thierstein H. 1971: Tentantive Lower Cretaceous calcareous Nanoplankton Zonation. *Eclogae Geol. Helv.* 64, 3, 437–652.

Thierstein H. 1973: Lower Cretaceous calcareous nannoplankton biostratigraphy. *Abh. Geol. B.–A.* 29, 3–52.

Thierstein H. 1975: Calcareous nannoplankton biostratigraphy at the Jurassic-Cretaceous boundary. Colloque sur la Limite Jurassique-Crétacé. *Bur. Rech. Geol. Minieres, Mem.*, 84–94.

Tremolada F., Bornemann A., Bralower T., Koeberl C. & van de Schootbrugge B. 2006: Paleoceanographic changes across the Jurassic/Cretaceous Boundary: the calcareous phytoplankton response. *Earth Planet. Sci. Lett.* 241, 361–371.

van de Schootbrugge B., Föllmi K.B., Bulot L.G. & Burns S.J. 2000: Paleoceanographic changes during the Early Cretaceous (Valanginian–Hauterivian): Evidence from oxygen and carbon stable isotope. *Earth Planet. Sci. Lett.* 181, 15–31.

Vašíček Z., Reháková D., Michalík J., Peterčáková M. & Halásová E. 1992: Ammonites, aptychi, nanno- and microplankton from the Lower Cretaceous Pieniny Formation in the "Kysuca Gate" near Žilina (Western Carpathian Klippen Belt, Kysuca Unit).

Západ. Karpaty Paleont. 16, 43–57.

Weissert H. 1989: C-isotope stratigraphy, a monitor of paleoenvironmental changes: A case study from the Early Cretaceous. *Surv. Geophys.* 10, 1–16.

Weissert H., McKenzie J.A. & Channell J.E.T. 1985: Natural variations in the carbon cycle during the Early Cretaceous. In: The carbon cycle and atmospheric CO_2: Natural variations Archean to the present. *Geophysic. Monograph.* 32, 531–545.

Wessely G. 2008: Kalkalpine Schichtfolgen und Strukturen im Wienerwald. *J. Alp. Geol.* 49, 201–214.

Appendix

Crossplot of the $\delta^{18}O$ vs. $\delta^{13}C$ values at Nutzhof (both vs. V-PDB).

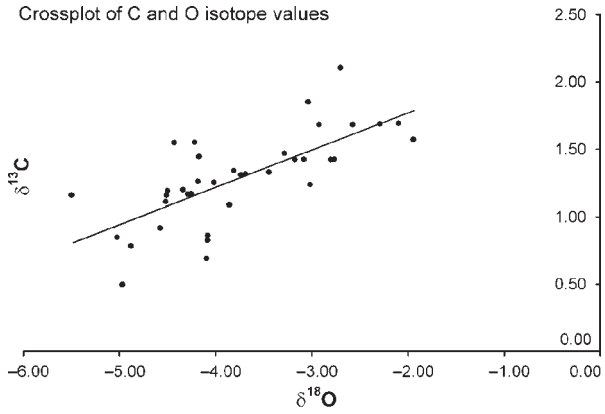

Vacek F., Hladil J. a **Schnabl P.**

Stratigraphic correlation potential of magnetic susceptibility and gamma-ray spectrometric variations in calciturbiditic facies (Silurian-Devonian boundary, Prague Synclinorium, Czech Republic)

Geologica Carpathica., 61, 4, 257 – 272, 2010

GEOLOGICA CARPATHICA, OCTOBER 2010, 61, 5, 365–381 doi: 10.2478/v10096-010-0022-3

High resolution stratigraphy of the Jurassic-Cretaceous boundary interval in the Gresten Klippenbelt (Austria)

ALEXANDER LUKENEDER[1,*], EVA HALÁSOVÁ[2], ANDREAS KROH[1], SUSANNE MAYRHOFER[1], PETR PRUNER[3], DANIELA REHÁKOVÁ[2], PETR SCHNABL[3], MARIO SPROVIERI[4] and MICHAEL WAGREICH[5]

[1]Geological and Paleontological Department, Natural History Museum, Burgring 7, 1010 Vienna, Austria; *alexander.lukeneder@nhm-wien.ac.at
[2]Department of Geology and Paleontology, Faculty of Natural Sciences, Comenius University, Mlynská dolina G-1, 842 15 Bratislava, Slovak Republic; halasova@fns.uniba.sk; rehakova@fns.uniba.sk
[3]Institute of Geology, Academy of Sciences of the Czech Republic, v.v.i., Rozvojová 269, 165 00 Praha 6, Lysolaje, Czech Republic
[4]Institute for Marine and Coastal Environment (IAMC-CNR), Calata Porta di Massa (Interno Porto di Napoli), 80133 Napoli, Italy
[5]Department for Geodynamics and Sedimentology, Center for Earth Sciences, University of Vienna, Althanstrasse 14, 1090 Vienna, Austria

(Manuscript received February 8, 2010; accepted in revised form June 10, 2010)

Abstract: The key objective of investigation of hemipelagic sediments from the Gresten Klippenbelt (Blassenstein Formation, Ultrahelvetic paleogeographic realm) was to shed light on environmental changes around the Jurassic-Cretaceous (J/K) boundary on the northern margin of the Penninic Ocean. This boundary is well exposed in a newly discovered site at Nutzhof. Around the critical interval including the boundary, this new outcrop bears a rich microplanktonic assemblage characterized by typical J/K (Tithonian/Berriasian) boundary faunas. The Nutzhof section is located in the Gresten Klippenbelt (Lower Austria) tectonically wedged into the deep-water sediments of the Rhenodanubian Flysch Zone. In Late Jurassic–Early Cretaceous time the Penninic Ocean was a side tract of the proto-North Atlantic Oceanic System, intercalated between the European and the Austroalpine plates. Its opening started during the Early Jurassic, induced by sea floor spreading, followed by Jurassic–Early Cretaceous deepening of the depositional area of the Gresten Klippenbelt. These tectonically induced paleogeographic changes are mirrored in the lithology and microfauna that record a deepening of the depositional environment from Tithonian to Berriasian sediments of the Blassenstein Formation at Nutzhof. The main lithological change is observed in the Upper Tithonian *Crassicollaria* Zone, in Chron M20N, whereas the J/K boundary can be precisely fixed at the *Crassicollaria–Calpionella* boundary, within Chron M19n.2n. The lithological turnover of the deposition from more siliciclastic pelagic marl-limestone cycles into deep-water pelagic limestones is correlated with the deepening of the southern edge of the European continent at this time. Within the Gresten Klippenbelt Unit, this transition is reflected by the lithostratigraphic boundary between siliciclastic-bearing marl-limestone sedimentation in the uppermost Jurassic and lowermost Cretaceous limestone formation, both within the Blassenstein Formation. The cephalopod fauna (ammonites, belemnites, aptychi) and crinoids from the Blassenstein Formation, correlated with calcareous microfossil and nannofossil data combined with isotope and paleomagnetic data, indicate the Tithonian to middle Berriasian (*Hybonoticeras hybonotum* Zone up to the *Subthurmannia occitanica* Zone; M17r–M21r). The succession of the Nutzhof section thus represents deposition of a duration of approximately 7 Myr (ca. 150–143 Ma). The deposition of the limestone, marly limestone and marls in this interval occurred during tectonically unstable conditions reflected by common allodapic material. Along with the integrated biostratigraphic, geochemical and isotopic analysis, the susceptibility and gamma-ray measurements were powerful stratigraphic tools and important for the interpretation of the paleogeographic setting. Two reverse magneto-subzones, Kysuca and Brodno, were detected within magnetozones M20n and M19n, respectively.

Key words: Jurassic/Cretaceous boundary, Penninic Ocean, paleoecology, paleogeography, environmental changes.

Introduction

Jurassic and Lower Cretaceous pelagic sediments are known to form a major elements of the northernmost tectonic units of the Gresten Klippenbelt (Czjžek 1852; Kühn 1962; Küpper 1962; Gottschling 1965; Decker & Rögl 1988; Decker 1990; Piller et al. 2004). Preliminary results on a Jurassic-Cretaceous boundary section of the Gresten Klippenbelt were presented including description of new faunas and localities (Lukeneder 2009; Kroh & Lukeneder 2009; Pruner et al. 2009; Reháková et al. 2009).

The Gresten Klippenbelt at Nutzhof comprises Upper Jurassic (Tithonian) to Lower Cretaceous sediments belonging to the Blassenstein Formation. The lower part of the succession consists of marls, marly limestone and marl-limestone alternations, whereas the upper part of the Blassenstein Formation (Tithonian to Valanginian) is composed of very pure limestones. The biostratigraphy of the Lower Cretaceous sediments in the study area is mainly based on microfossils (Reháková et al. 2009). The first description of the lithology and stratigraphy of this area was provided by Czjžek (1852), followed by Küpper (1962). Biostratigraphic data on the Blassenstein Formation (Stollberger Schichten of Küpper 1962) near Nutzhof are remarkably scarce (Czjžek 1852; Küpper 1962).

The tectonically highly active northern zone of the Penninic Ocean (the southern margin of the European continent) is crucial for understanding the formation of the Penninic

Ocean, its subsequent subduction and the following Alpine history.

Formation of the Penninic Ocean, here defined to include the Ligurian Basin (sensu Dercourt et al. 1993, 2000; Masse et al. 2000; Mandic & Lukeneder 2008) and synonymous with the Alpine Tethys (Stampfli & Borel 2002 and Stampfli et al. 2002) was initiated in the Late Triassic by rifting and disjunction of the Austroalpine microcontinent from the southern European Plate margin (Stampfli & Mosar 1999; Scotese 2001). It formed an eastern prolongation of the North Atlantic Rift-System, which affected the final break-up of the Permo-Triassic supercontinent Pangaea (e.g. Faupl 2003). The formation of the oceanic crust and the sea-floor spreading lasted from the Middle Jurassic to the Early Cretaceous, terminating with the introduction of its southward-directed subduction beneath the northern Austroalpine plate margin (Faupl & Wagreich 2000; Mandic & Lukeneder 2008). This tectonic phase is reflected by the lithological change within the Nutzhof section. An increasing deepening, reflected in the sedimentary succession (e.g. allodapic limestones and microturbidites), in the section at Nutzhof, marks the opening of the Penninic Ocean. The pelagic carbonate sedimentation, which started in the Late Jurassic, changes from siliciclastic-dominated limestone deposition to pure limestone-dominated. The Penninic Ocean persisted from the Late Jurassic until close to the end of the Cretaceous.

The paleomagnetic and rock-magnetic study is a continuation of detailed paleontological and magnetostratigraphic studies of the Jurassic/Cretaceous (J/K) boundary in the Tethyan Realm (Houša et al. 1999). The section at Brodno near Žilina, W Slovakia, was the first section investigated with high-resolution magnetostratigraphy and micropaleontology in the Carpathians (Houša et al. 1999). Magnetostratigraphic studies were carried out in the Bosso Valley of Umbria, Italy (Houša et al. 2004) and the Tatra Mountains, Poland (Grabowski & Pszczółkowski 2006). The magnetostratigraphic investigations published by Pruner et al. (2009) preliminarily determine the boundaries of magnetozones M17n to M22r (six reverse and six normal zones). The aim of these studies was to globally and objectively establish a correlation between biozones around the J/K boundary in the Tethyan Realm using global paleomagnetic events and precisely determine the boundaries of magnetozones M19 and M20 including narrow reverse subzones. These studies provided a precise record of polarity changes in the Earth's magnetic field and determined their stratigraphic positions precisely within a biochronostratigraphic zonation.

The Nutzhof locality represents the only known section that includes the J/K boundary interval in the Gresten Klippenbelt. The section contains rich assemblages of radiolarians, calpionellids, saccocomids, nannofossils and in some intervals ammonites. The J/K boundary sediments of the Nutzhof section provide an excellent succession for quantitative and integrated methods due to their fossiliferous and undisturbed bedding for a period of almost 7 million years.

Location and geological setting of Nutzhof

Locality description

The Nutzhof locality is situated in the Gresten Klippenbelt of Lower Austria (48°04′49″ N, 15°47′36″ E), about 20 km south of Böheimkirchen and 5 km north of Hainfeld (Fig. 1), 600 m above sea level (m a.s.l.) (ÖK 1:50,000, sheet 56 St. Pölten). The outcrop is located in an abandoned quarry in the south-eastern-most part of the northeast-southwest striking Gresten Klippenbelt, between Kasberg (785 m a.s.l.) to the east and the vicinity of the Nutzhof (550 m a.s.l.) to the west. The quarry is located on the northern side of the Kasberg ridge and the measured section is exposed on the eastern side of the quarry.

Geological setting

The Gresten Klippenbelt at Nutzhof is surrounded by deep-water successions of the Rhenodanubian Flysch Zone. The Gresten Klippenbelt represents an independent and scarcely known geological unit. It is tectonically incorporated in the Flysch Zone as a long, thin, east-west striking marly and calcareous unit (Fig. 1). Sediments from the Gresten Klippenbelt are considered to belong to the southern part of the Helvetic paleogeographic realm. The Gresten Klippenbelt sediments were deposited on the southern shelf and

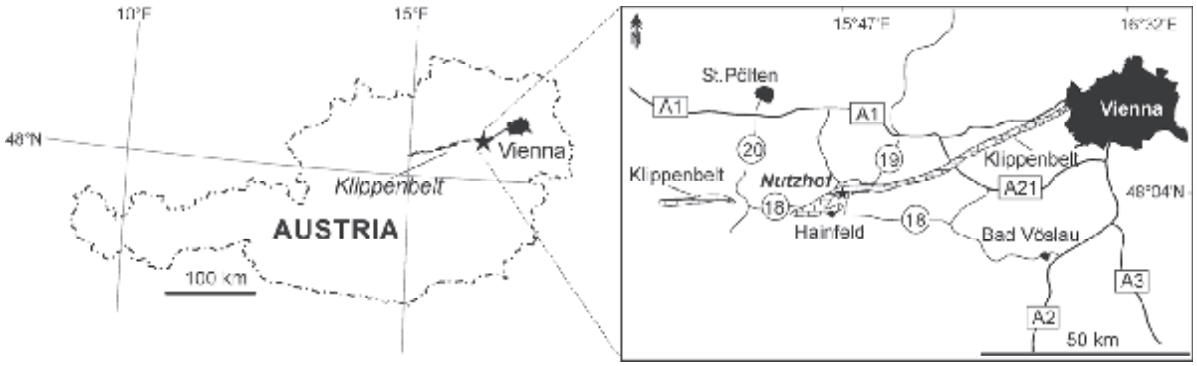

Fig. 1. Locality map of Austria with indicated position of the Nutzhof locality in Lower Austria (left). Detailed map of the area around Nutzhof with outcrop position within the Jurassic–Cretaceous Klippenbelt (right).

slope of the European continent, on the slope of the Bohemian Massif at the north-western margin of the Penninic Ocean. The Nutzhof site consists of two different facies within the Blassenstein Formation (Lukeneder 2009). The lower part (Tithonian; 18.0–10.0 m) with dark marl-limestone alternations and its characteristically intercalated limestone beds, and the upper part (Tithonian–Berriasian; 10.0–0.0 m) with light grey, almost pure limestone. Limestone beds display uniform overturned bedding-plane orientation. The mean strike is 151°±30° and the mean dip angle 44°±22°. The succession is characterized by a marked lithological and faunal change at Nu 10.0 which does not coincide with the Jurassic/Cretaceous boundary at bed Nu 7.0 (Nu for Nutzhof samples). Sediments occur as wacke-, pack- or mudstones.

The Nutzhof section

The Jurassic-Cretaceous boundary in the Gresten Klippenbelt

The most recent reports concerning the J/K boundary interval from the Gresten Klippenbelt present preliminary results (Lukeneder 2009; Kroh & Lukeneder 2009; Pruner & al. 2009; Reháková et al. 2009) (Fig. 2). Therein first results have been presented on macro-, micro- and nannofossils. Tectonic units including the J/K boundary of the Gresten Klippenbelt were reported by Cžjžek (1852), Kühn (1962), Küpper (1962), Gottschling (1965), Decker & Rögl (1988), Decker (1990) and Piller et al. (2004).

Materials and methods

The Jurassic-Cretaceous boundary section at Nutzhof was studied with an integrated approach. Beds were sampled for biostratigraphical, paleomagnetic, geochemical ($CaCO_3$, TOC, S) and istotopic ($\delta^{18}O$, $\delta^{13}C$, $\delta^{87}Sr$) data. Focus is directed to an interval of about 18.0 m (Nu 0.0–Nu 18.0) that was studied in detail (Figs. 2, 3, 4). Macro-, micro- and nannofossil contents were quantitatively investigated (Fig. 4). Samples were collected at intervals of 0.1 and 0.2 meters for stable isotopes, total organic carbon (TOC), sulphur (S), calcium carbonate ($CaCO_3$), susceptibility and gamma log. The microfossil content was analysed for calpionellids, radiolarians, saccocomids (thin sections) and insoluble residues. High resolution studies were combined with grey-scale quantification, gamma-ray and susceptibility analyses. Sample numbers, for example Nu 10.0, correspond to the sample interval at 10.0 m within the log (for all numbers and figures, Nu = Nutzhof). All samples are stored at the Natural History Museum of Vienna, in the collection of the Department of Geology and Paleontology.

Gamma-ray analysis

The gamma log measures the radioactivity of the rock, which represents a direct function of its clay-mineral content. Increasing radioactivity reflects the increasing clay content. Gamma response (counts per second — cps) was measured using a hand-held standard gamma-ray scintillometer.

Macrofossils

Macrofossil material includes 46 ammonite specimens, 238 lamellaptychi and 82 rhyncholites were examined. Four brachiopods and three inoceramids as well as a single belemnite specimen were collected. Ammonites are preserved as steinkerns or are represented by calcitic aptychi. Shell-preservation is restricted to organisms with primary skeletal calcite of belemnite-rostra and brachiopods in addition to rare inoceramid fragments (calcitic prisms). The ammonite assemblage contains six different genera: *Subplanites*, *Haploceras*, *Phylloceras*, *Ptychophylloceras*, *Lytoceras* and *Leptotetragonites* dominated by the perisphinctid genus *Subplanites* (Lukeneder 2009).

Calpionellids and calcareous nannofossils

Quantitative micro- and nannofacies analysis includes study of calpionellids and calcareous dinoflagellates in 93 thin sections. The thin sections are deposited in the Natural History Museum in Vienna; NHMW 2007z0271/0000. Changes in the distribution of calpionellids and calcareous nannofossils were studied in detail in order to correlate them with the changes in nannoplankton associations (Figs. 2, 3 and 4).

Calcareous nannofossils were analysed semiquantitatively in 19 smear slides, prepared from all lithologies by standard techniques, using a light polarizing microscope at 1250× magnification. At least 200 specimens were counted in each slide to record relative abundances and the stratigraphic range of taxa (Figs. 2, 3). Nannofossil preservation can be characterized as moderately to intensely etched by dissolution. The calcareous nannofossil zones were adopted from the zonal scheme proposed by Bralower et al. (1989).

Magnetic components

Paleomagnetic analyses presented in this studies come from 244 samples, but the preliminary results include only 111 samples (see Pruner et al. 2009). All the samples were subjected to progressive thermal demagnetization (TD) or alternating field (AF) demagnetization in 11–12 temperatures or fields. The individual components were precisely established using multicomponent analysis of remanence (Kirschvink 1980). Isothermal remanent magnetization (IRM) to saturation was measured to identify magnetically active minerals. Magnetomineralogical analyses and unblocking temperature determination show that magnetite and goethite are the main carriers of remanent magnetization.

Microfossils

Apart from thin sectioning also employed for a study of calpionellids, an effort was made to obtain three-dimensional specimens of the crinoids and other microfossils commonly observed in the thin sections (namely foraminifers, ostracods, rhyncholites, small aptychi, ophiuroid remains,

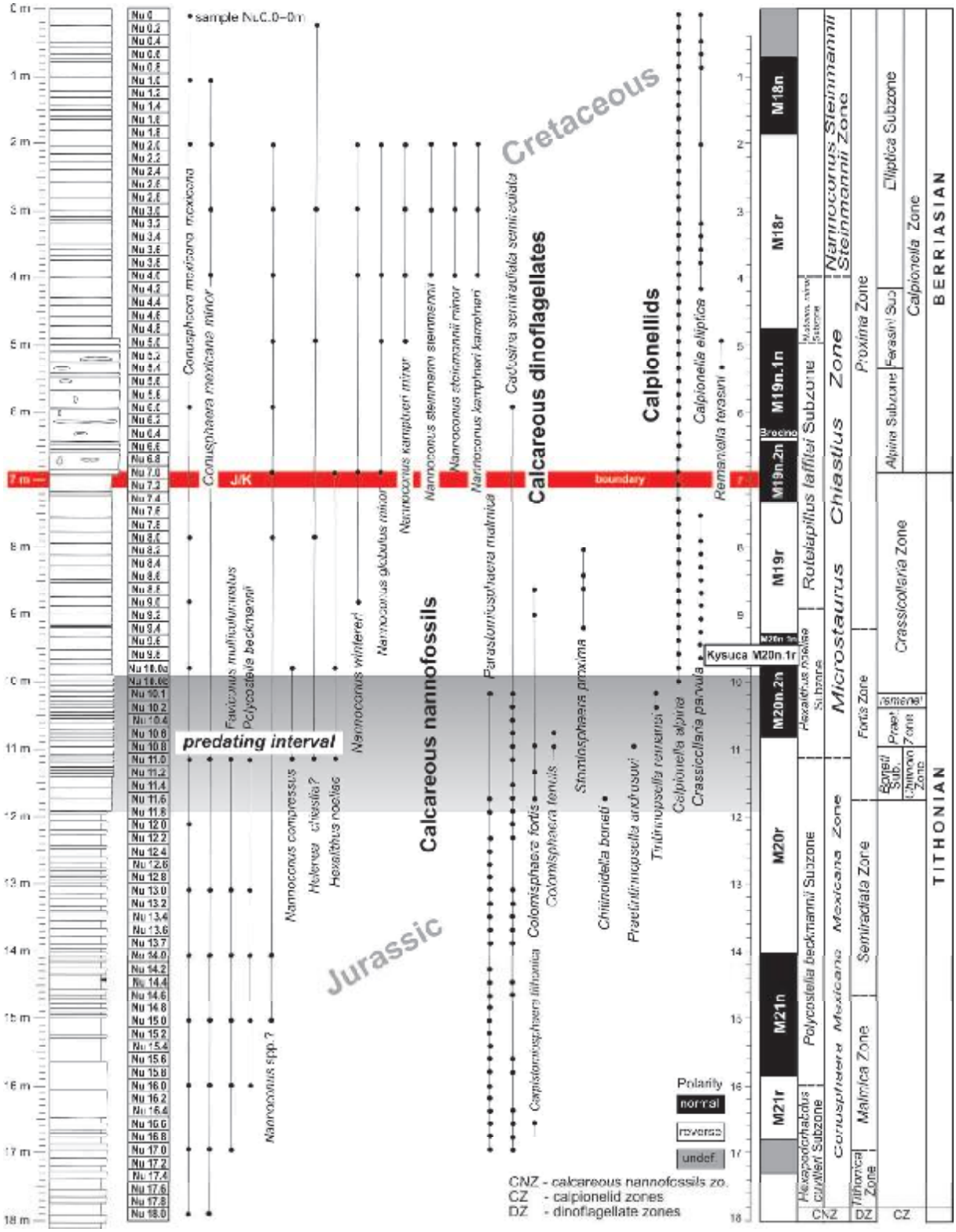

Fig. 2. Nutzhof log with occurrence and range of calcareous nannofossils, calcareous dinoflagellates and calpionellids and indicated paleomagnetic zonation: normal magnetozones are denoted black, reverse zones in white, and unknown parts in grey.

etc.). Bulk samples were collected in closely spaced intervals in the lower, marly part of the succession (10.0–18.0 m). Strong lithification hampered dense bulk sampling in the upper part of the section (0 to 10.0 m). These beds were analysed by thin sections only. Traditional washing methods were not applicable due to strong lithification of the sediment. Partial disaggregation was achieved by repetitive, combined treatment with hydrogen-superoxide and the tenside Rewoquat (see Lierl 1992). After cleaning, the microfossils were hand picked under a microscope. For the present study we used the sediment fractions larger than 250 μm only.

TC and TOC content

Calcium carbonate contents ($CaCO_3$; wt. % bulk rock, TC) were determined using the carbonate bomb technique. Total carbon content was determined using a LECO WR-12 analyser. Total organic carbon (TOC) contents were calculated as the difference between total carbon and carbonate carbon, assuming that all carbonate is pure calcite. All the chemical analyses were carried out in the laboratories of the Department of Forest Ecology at the University of Vienna.

Stable isotopes

A total of 37 bulk sample stable isotope analyses were measured by automated continuous flow carbonate preparation GasBenchII device (Spötl & Vennemann 2003) and ThermoElectron Delta Plus XP mass spectrometer at the IAMC-CNR (Naples) isotope geochemistry laboratory. Acidification of samples was performed at 50 °C. For each six samples, an internal standard (Carrara Marble with $\delta^{18}O = -2.43$ vs. V-PDB and $\delta^{13}C = 2.43$ vs. V-PDB) was run, and for each 30 samples, the NBS19 international standard was measured. Standard deviations of carbon and oxygen isotope measures were estimated 0.1 and 0.08 ‰, respectively, on the basis of ~10 repeated samples.

All the isotope data are reported in per mil (‰) relative to the V-PDB standard.

$^{87}Sr/^{86}Sr$ isotope data were analysed from 19 bulk-rock samples of limestones at the Geochronological Laboratory of the Department of Lithospheric Research, Centre for Earth Sciences, University of Vienna using strontium separation by standard methods of ion-exchange chromatography and isotope ratio measurements on a TIMS (Triton mass spectrometer). The measured NBS 987 standard value during measurements was 0.710256+/–0.000004 (7 measurements) and samples were not adjusted to the NBS 987 standard value of 0.710248.

Data and results

Biostratigraphy and magnetostratigraphy

The stratigraphic investigation of the calcareous microfossils (calpionellids, calcareous dinoflagellates) and nannofossils demonstrate that the Nutzhof section represent the Lower Tithonian–middle Berriasian. The calcareous dinoflagellate cyst zonation of Reháková (2000a) was followed. The presence of the Lower Tithonian *Tithonica*, *Malmica* and *Semiradiata* cyst Zones is demonstrated. The standard calpionellid zones and subzones proposed by Reháková (1995) and Reháková & Michalík (1997) were adopted for the biostratigraphic subdivision of the section into the *Chitinoidella* Zone (*Boneti* Subzone), the *Praetintinnopsella* Zone and the *Crassicollaria* Zone (*Remanei* Subzone). These belong to the middle to Upper Tithonian. The standard *Calpionella* Zone (*Alpina*, *Ferasini* and *Elliptica* Subzones) were observed in the overlying Lower Cretaceous (Fig. 2).

The nannofossil zones include the *Conusphaera mexicana mexicana* Zone, *Microstaurus chiastus* and *Nannoconus steinmannii steinmannii* Zones. This stratigraphic interval corresponds to the Lower Tithonian *Hybonoticeras hybonotum* ammonite Zone to the middle Berriasian *Subthurmannia occitanica* ammonite Zone, demonstrated in the Nutzhof section on chronostratigraphic diagnostic cephalopods (*Subplanites fasciculatiformis*, *Ptychophylloceras ptychoicum*, *Leptotetragonites honnoratianus*, *Haploceras elimatum*, *Hibolithes* (gr.) *semisulcatus* and some lamellaptychi.

The magnetostratigraphic log across the Nutzhof section includes the M21r to the M17r magnetozones subdivided into the Kysuca (M20r) and Brodno (M19r) subzones (Figs. 2, 6). The average sedimentation rate in the Nutzhof section is ca. 3.7 m/Myr (Fig. 7), but with high dispersion (from 2–11 m/Myr). The scatter of the sedimentation rate is similar to Hlboča profile in Slovakia (Grabowski et al. 2010). The main difference between these two sections is in the thickness of M19 and M20 mangentozones. Nutzhof has higher sedimentation rate at M19 while Hlboča appears with higher rates in M20.

Macrofossil content

The macrofossil content is characterized by ammonoids, aptychi, belemnites, brachiopods, bivalves and echinoderms. The ammonite fauna comprises six different genera represented by *Lytoceras sutile* Oppel, *Lytoceras* sp., *Leptotetragonites honnoratianus* (d'Orbigny), *Phylloceras* sp., *Ptychophylloceras ptychoicum* (Quenstedt), *Haploceras* (*Haploceras*) *elimatum* (Oppel), *Subplanites fasciculatiformis* Lukeneder. The ammonite fauna is dominated by the perisphinctid-type. Ammonitina is the most common component (60 %; *Subplanites* and *Haploceras*), followed by the Phylloceratina (25 %; *Ptychophylloceras* and *Phylloceras*), and the Lytoceratina (15 %; represented by *Lytoceras* and *Leptotetragonites*). The belemnite *Hibolithes* (gr.) *semisulcatus* (Münster) and aptychi (*Lamellaptychus*) occur. Only Mediterranean cephalopod elements are present at Nutzhof. Brachiopods are represented by *Triangope*, bivalves by inoceramid shells and echinoderms by crinoids (*Phyllocrinus belbekensis* Arendt, *Balanocrinus* sp., *Crassicoma*? sp. and *Saccocoma tenella* (Goldfuss).

The crinoid fauna recovered from the bulk samples of Nutzhof is typical for Upper Jurassic strata of Central and Eastern Europe. The low diversity of stalked crinoids, common in many contemporaneous deposits (Hess et al. 1999), may be interpreted as a result of the distal position of the sec-

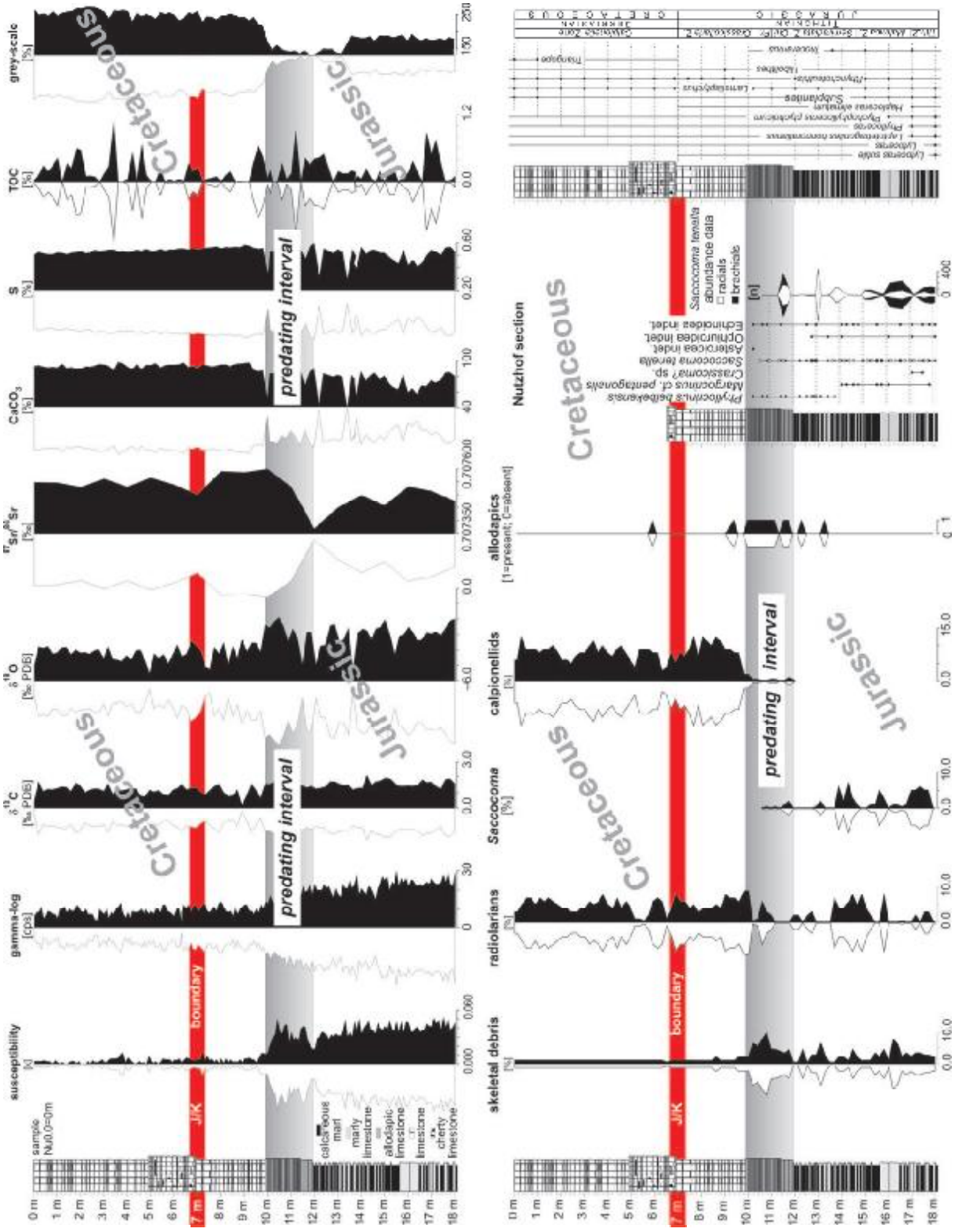

Fig. 3. Compiled geochemical, isotope and fossil data on the J/K boundary at Nutzhof. Note the change at the predating interval at meter 7 below the J/K boundary.

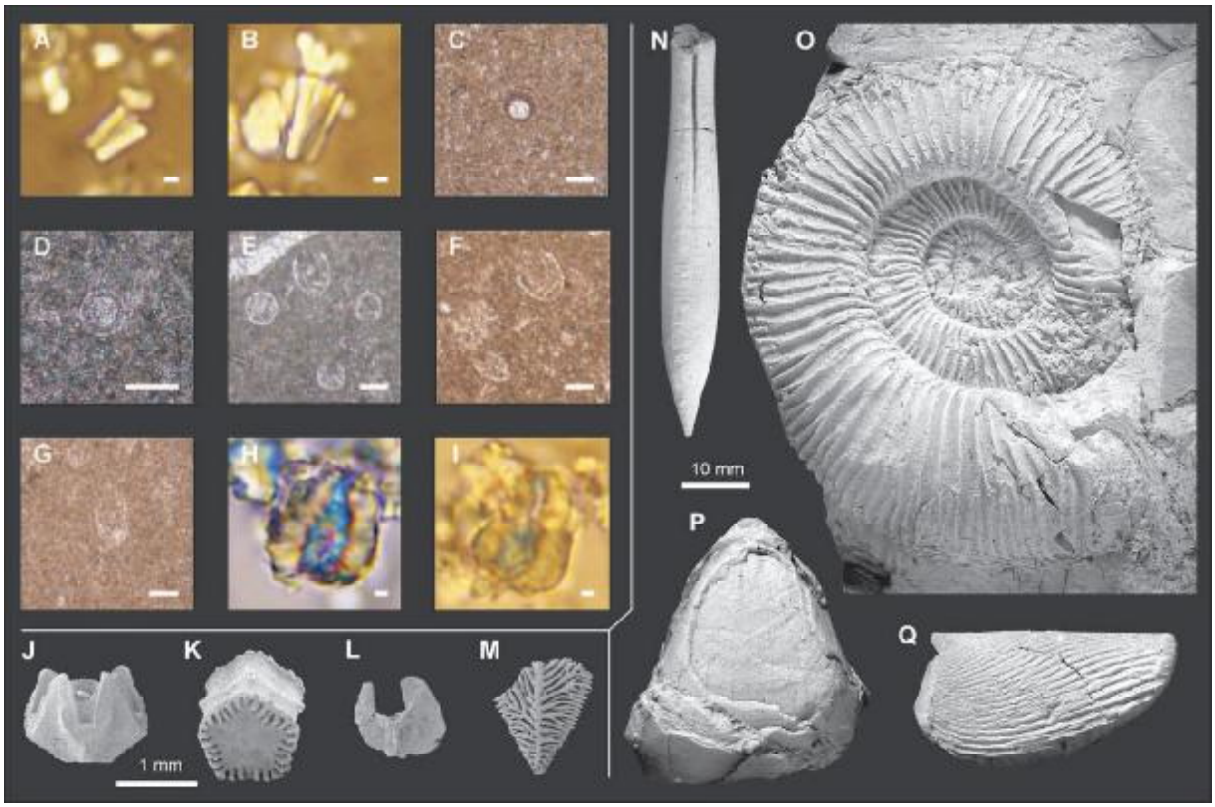

Fig. 4. A — *Conusphaera mexicana minor* Bown & Cooper; Nu 18.0, NHMW2008z0271/0028. **B —** *Conusphaera mexicana mexicana* Bralower et al.; Nu 17.0, NHMW2008z0271/0003. **C —** *Cadosina semiradiata semiradiata* Wanner; 17.0, NHMW2008z0271/0003. **D —** *Parastomiosphaera malmica* (Borza); Nu 13.0, NHMW2008z0271/0002. **E —** *Calpionella alpina* Lorenz and *Calpionella grandalpina* Nagy; Nu 9.8, NHMW2008z0271/0011. **F —** *Crassicollaria parvula* Remane and *Calpionella grandalpina*; Nu 9.6, NHMW2008z0271/0012. **G —** *Calpionella elliptica* Cadisch; Nu 3.2, NHMW2008z0271/0014. **H —** *Nannoconus steinmannii steinmannii* Kamptner; Nu 4.0, NHMW2008z0271/0034. **I —** *Nannoconus kamptneri kamptneri* Brönnimann; Nu 2.0, NHMW2008z0271/0035. **J —** *Phyllocrinus belbekensis* Arendt; Nu 12.3; NHMW 2008z0226/001. **K —** *Balanocrinus* sp.; Nu 14.6, NHMW2008z0228/0003. **L —** *Saccocoma tenella* (Goldfuss); Nu 11.5, NHMW2008z0236/0015. **M —** *Saccocoma tenella* (Goldfuss); Nu 13.0, NHMW2008z0236/0012. **N —** *Hibolithes* (gr.) *semisulcatus* (Münster); Nu 14.3, NHMW2008z0264/0025. **O —** *Subplanites fasciculatiformis* Lukeneder; Nu 17.0, NHMW2008z0264/0012. **P —** *Triangope* sp.; Nu 1.0, NHMW2008z0264/0028. **Q —** *Lamellaptychus* sp.; Nu 18.0, NHMW2008z0264/0024. Graphic scale bars equal 1 μm for A, B and H, I; 50 μm for C–G; 1 mm for J–K, and 10 mm for N–Q.

tion, which represents a deep-water facies. The incomplete size ranges of isocrinid and phyllocrinid ossicles, the lack of fragile elements and the presence of allodapic material (Lukeneder 2009) suggest that the majority of the crinoid material is allochthonously deposited. Saccocomid fragments, in contrast, are not sorted and include abundant fragile elements suggesting that these crinoids are autochthonous.

Of the crinoid material only the saccocomids can be used for biostratigraphy. *Saccocoma tenella* is restricted to the Upper Kimmeridgian–Upper Tithonian. From a biogeographic point of view the faunal composition indicates connections with contemporaneous units of the northern Tethys shelf in Eastern Europe.

Microfacies and calcareous microplankton assemblages

The limestones in the section include wackestones, packstones and mudstones. Fine-grained micrite with pelagic microfossils (calpionellids, calcareous dinoflagellates, radiolarians) and calcareous nannofossils characterize an open-marine environments. Rare skeletal debris from fragmented and disintegrated shells of invertebrates (benthic foraminifers, echinoderms, molluscs) are derived from shallower environments. The studied microfacies are typical for basinal settings.

Calpionellids

Calpionellids in the studied samples are generally well-preserved. Hyaline forms dominate, whereas chitinoidellids are rare. The chitinoidellid taxonomy of Pop (1997) and Reháková (2002) is followed here. The group is represented by *Borziella slovenica* (Borza), *Dobeniella tithonica* (Borza) and *Chitinoidella boneti* Doben, species typical for the *Boneti* Subzone of the *Chitinoidella* Zone (Figs. 2, 4). The appearance of first hyaline calpionellid loricas of *Praetintinnopsella andrusovi* Borza and *Tintinnopsella remanei* Borza

precede the crassicollarian radiation. *Crassicollaria parvula* Remane and *Calpionella alpina* Lorenz dominate relative to *Crassicollaria massutiniana* (Colom), *Calpionella grandalpina* Nagy and *Tintinnopsella carpathica* (Murgeanu & Filipescu) in the *Remanei* Subzone of the *Crassicollaria* Zone. Higher in the section, crassicollarians abruptly decrease in abundance, being replaced by an interval with radiation of small spherical forms of *Calpionella alpina* Lorenz. The diversification of a monospecific calpionellid association started in the overlying *Ferasini* and *Elliptica* Subzones of the standard *Calpionella* Zone where *Calpionella alpina* Lorenz is accompanied by *Tintinnopsella carpathica* (Murgeanu & Filipescu), *Remaniella ferasini* Pop, *R. duranddelgai* Pop, *R. catalanoi* Pop, *Calpionella elliptica* (Cadisch), *Tintinnopsella longa* (Colom), and *Lorenziella hungarica* Knauer.

Calcareous dinoflagellates

Calcareous dinoflagellates predominate in the Lower and Upper Tithonian being represented by *Cadosina parvula* Nagy, *Carpistomiosphaera borzai* (Nagy), *Schizosphaerella minutissima* (Colom), *Parastomiosphaera malmica* (Borza), *Cadosina semiradiata semiradiata* Wanner, *Cadosina semiradiata fusca* (Wanner), *Carpistomiosphaera tithonica* Nowak, *Colomisphaera fortis* Řehánek, *Colomisphaera tenuis* (Nagy), *Colomisphaera carpathica* (Borza), and *Stomiosphaerina proxima* Řehánek. For the first time the appearance of *Colomisphaera fortis* Řehánek precedes the appearance of *Colomisphaera tenuis* (Nagy), hampering the determination of the *Tenuis* and *Fortis* dinoflagellate Zones sensu Řehánek (1992) (Figs. 2, 4).

Calcareous nannofossils

The semiquantitative study (Figs. 2, 3) reveals that only the taxa *Conusphaera* spp., *Polycostella* spp., *Nannoconus* spp., *Cyclagelosphaera margerelii* Noël, *Watznaueria barnesae* (Black) Perch-Nielsen, and *W. manivitae* Bukry occur in significant abundances. Nannofossils indicative of eutrophic environments such as *Zeugrhabdotus erectus* (Deflandre) Reinhardt, *Diazomatholithus lehmannii* Noël, and *Discorhabdus ignotus* (Górka) Perch-Nielsen occur sporadically.

The calcareous nannofossil assemblage from the basal part of the Nutzhof section (samples 17, 18, *Tithonica* dinoflagellate Zone) contains the dissolution-resistant nannofossil species *Conusphaera mexicana mexicana* Bralower et al., *Conusphaera mexicana minor* Bown & Cooper, *Cyclagelosphaera margerelii*, *Cyclagelosphaera deflandrei* (Manivit) Roth, *Watznaueria barnesae*, *Watznaueria britannica* (Stradner) Reinhardt, and *Watznaueria manivitae*. The FO (first occurrence datum) of *Faviconus multicolumnatus* Bralower was recorded. The absence of the nannolith *Polycostella beckmannii* Thierstein allowed us to distinguish the *Conusphaera mexicana mexicana* NJ20 Zone; *Hexapodorhabdus cuvillieri* Subzone NJ20-A (Roth et al. 1983; emended Bralower et al. 1989) of the Lower Tithonian.

The calcareous nannofossil assemblages from the samples Nu 16.0 to Nu 12.0 show dominance of *Watznaueria* and *Conusphaera*. The FOs of *Zeugrhabdotus embergeri* (Noël) Perch-Nielsen, *Zeugrhabdotus erectus*, and *Diazomatholithus lehmannii* were observed. The FO of the nannolith *Polycostella beckmannii* is the most significant marker indicating the base of the *Polycostella beckmannii* Subzone NJ20-B of the *Conusphaera mexicana mexicana* Zone, NJ20 (Roth et al. 1983; emended Bralower et al. 1989). The age of this Subzone is middle Tithonian. The range of the *Polycostella beckmannii* Subzone NJ20-B fits with dinoflagellate *Malmica* and *Semiradiata* Zones and the lower part of the *Chitinoidella* Zone.

The calcareous nannofossils investigated in sample Nu 11 reflect a rather distinct change. The FO of *Helenea chiastia* Worsley, *Hexalithus noeliae* Loeblich & Tappan and the nannolith species *Nannoconus compressus* Bralower et al. are evidence for the base of the *Microstaurus chiastius* Zone NJK Bralower et al., 1989 and its *Hexalithus noeliae* Subzone NJK-A, which is thought to represent the Late Tithonian interval. The Subzone coincides with the upper part of the *Chitinoidella* Zone.

The calcareous nannofossil assemblages from samples Nu 9.0 to Nu 6.0 contain dissolution-resistant nannofossil genera *Conusphaera*, *Cyclagelosphaera*, *Watznaueria*, *Diazomatholithus* and *Assipetra*. The FAD of *Nannoconus wintereri* Bralower & Thierstein (1989) was observed (sample 9.0). Many remains of dissolution-susceptible coccoliths are present. In the upper part of the studied interval, the abundance of *Conusphaera* drops. This interval was correlated with the *Microstaurus chiastius* Zone NJK, Subzone *Rotelapillus laffitei* NJK-C, determining the J/K boundary interval. It shows good correlation with the upper part of the Upper Tithonian *Crassicollaria* Zone and the *Calpionella* Zone (*Alpina* Subzone), which represent the J/K boundary interval.

The interval bearing the calpionellid species of the Lower Berriasian *Calpionella* Zone (*Ferasini* Subzone) (sample Nu 5.0) shows a distinctive change in the calcareous nannofossil assemblage — the onset of nannoconids (*Nannoconus globulus minor* Bralower, *Nannoconus steinmannii minor* Deres & Achéritéquy, *Nannoconus kamptneri minor* Bralower, *Nannoconus cornuta* Deres & Achéritéquy). This nannofossil event indicates the base of the *Nannoconus steinmannii minor* Subzone NJK-D (*Microstaurus chiastius* Zone NJK) Bralower et al., which belongs to the lowermost Berriasian.

The calcareous nannofossils studied from the sample interval Nu 4.0–Nu 0.0 (correlating with the calpionellid *Calpionella* Zone, *Elliptica* Subzone) record the diversification of nannoconids. The FAD of *Nannoconus steinmannii steinmannii* Kamptner is recorded at level Nu 2.0. It could reflect the explosion in nannoconid abundance (sensu Bralower et al. 1989: p. 188). *Nannoconus globulus minor, Nannoconus kamptneri minor*, *Nannoconus wintereri*, *Nannoconus globulus globulus* Deres & Achéritéquy, *Nannoconus steinmannii minor* Deres & Achéritéquy, *Nannoconus steinmannii steinmannii*, and *Nannoconus kamptneri kamptneri* Brönnimann, *Nannoconus* spp. indicative of the *Nannoconus steinmannii steinmannii* Zone NK-1, Bralower et al. (1989), which is middle Berriasian in age.

On the basis of calcareous nannofossil distribution, the interval between the FO of *Nannoconus wintereri* co-occurring with small nannoconids in bed Nu 9.0 and the FO of *Nanno-*

conus steinmannii minor in bed Nu 5.0 (FAD after Hardenbol et al. 1998 — 143.92 Ma) is interpreted as the Tithonian-Berriasian boundary interval (Figs. 2, 3).

Stable isotope data

Oxygen and carbon (O, C)

The bulk carbon-isotope values (Fig. 3) lie between +0.49 and +2.10 ‰ corresponding to biogenic calcite precipitated under open marine conditions during the Jurassic–Cretaceous (e.g. Weissert et al. 1985). All $\delta^{18}O$ values are between –1.94 to –5.49 ‰ and appear depleted relative to diagenetically unaltered marine calcite (e.g. van de Schootbrugge et al. 2000, and reference therein). This reflects elevated temperature during burial diagenesis and/or effects of meteoric diagenesis (Weissert 1989). The carbon isotope signal is considered of primary importance as a calibration tool between ammonites and magnetostratigraphy (Hennig et al. 1999), but it should be noted that the absence of covariance between $\delta^{18}O$ and $\delta^{13}C$ suggests a limited influence of secondary diagenesis on the isotope record (Fig. 3).

A positive trend in the $\delta^{13}C$, from the base of the section at Nu 18.0 up to Nu 14.0, is followed by a decreasing excursion shifting the isotope values to their lowest values (0.69 ‰) at about Nu 10.0. After that point the $\delta^{13}C$ values stabilize at near constant averages of ~1.20 ‰.

Strontium (Sr)

$^{87}Sr/^{86}Sr$ isotope data from the section show a range from 0.707370 +/–0.000004 to 0.707598 +/–0.000004. A gentle trend from lower values in the lower, Jurassic part of the section (Nu 18.0–Nu 12.0: mean 0.707472) to higher values in the upper part including the J/K boundary and the Cretaceous interval (Nu 11.0–Nu 0.0: mean 0.707553) can be recognized (Fig. 3). A special interval is represented in the strong increase from Nu 13.0 (lowest isotope value) to Nu 11.0 (highest isotope value) and probably indicate a local diagenetic phenomenon. The slight increase of mean strontium isotope ratios in the section is compatible with the general increase of strontium isotope ratios from the latest Jurassic into the earliest Cretaceous as reported by the strontium isotope seawater curve of McArthur et al. (2001) and McArthur & Howarth (2004). The values measured in the present study are generally higher by a factor of ca. 0.0002 compared to the values reported by McArthur & Howarth (2004), who measured Upper Tithonian values around 0.707150 and Berriasian values between 0.707200–0.70725 (see also McArthur et al. 2007) with the Berriasian/Valanginian boundary slightly above 0.707300. Thus, the lowest measured value in the Nutzhof section thus does not fall within the J/K boundary range of values recorded by McArthur & Howarth (2004). This confirms a strong diagenetic overprint upon strontium isotope values. However, the increase in mean values is within the reported magnitude of increase expected for the J/K boundary interval, thus being compatible with the stratigraphy inferred by other methods, but precluding detailed dating.

Geochemistry

The $CaCO_3$ (calcium carbonate contents, equivalents calculated from total inorganic carbon; carbonate bomb) differ markedly in the lower and upper part of the log. The lower part shows variations from 89.03 % (Nu 12.0) in limestone beds to 40.72 % (Nu 13.4) in marl beds, whereas the upper part displays more constant values ranging from 86.16 % (Nu 9.6) up to the highest measured value of 97.4 % (Nu 3.6).

As recorded by the biostratigraphic results, the strong lithological and faunal changes at Nu 12.00 and Nu 10.0 are 3 to 5 meters below the Jurassic/Cretaceous boundary (Bed Nu 7.0) indicating changes in depositional environment 0.5 to 1 million years before the end of the Jurassic. The interval from Nu 12.0–10.0 ($CaCO_3$ 89.03–68.97 %; S 0.59–0.45 %; TOC up to 0.97 %) differs markedly and heralds the environmental change observed (Fig. 3).

Both the $CaCO_3$ and the S content clearly show a trend towards higher values and stable conditions from bed Nu 10.00 to Nu 18.00. Unstable conditions are mirrored in alternating values in the lower part of the log by variations from 89.03 % $CaCO_3$ and 0.59 % S (Nu 12.0) in limestone beds to 40.72 % and 0.30 % (Nu 13.4) in marl beds.

The range is smaller and more constant in the interval Nu 10.0–18.0 with $CaCO_3$ values from 86.16 % at Nu 9.6 up to the maximum value of 97.4 % at Nu 3.6. The total sulphur content is positively correlated to the $CaCO_3$ values. The maximum value is at bed Nu 9.0 with 0.58 % S and its minimum with 0.5 % S in bed Nu 0.0. As confirmed by Hirano (1993) the sulphur content is a reliable index for oxic-anoxic conditions of the bottom water and sediment at the time of preservation.

The weight % TOC values show no positive correlation with S or $CaCO_3$. TOC values oscillate throughout the log. They vary from 0.001 % to 0.91 % (Nu 11.2) in the lower part and from 1.07 % (Nu 3.4) to 0.001 % in the upper part.

The above described geochemistry is also reflected in the results of grey-scale data marking siliciclastic input. The section can be subdivided into three parts: a lower part (Nu 18.0–12.0) with 170–111 (mean 140.5), a middle part (Nu 12.0–10.0) with 138–90 (mean 114) and an upper part (Nu 10.0–0.0) with 254–195 (mean 224.5). In combination with other analyses, the grey-scale factor is a good indicator for siliciclastic input (clay, not sandstone) in pelagic to hemipelagic sediments. This indicates the dominance of siliciclastic components and allodapic microturbidites within the dark mid-part. These results corroborate those obtained from susceptibility and gamma log (increasing values show higher contents in clay minerals), thin sectioning and microfacies analysis.

Susceptibility

Susceptibility measurements at Nutzhof represent a direct function of the clastic or turbiditic content and associated mineral spectra (Fig. 3). Higher susceptibility data reflect higher detritic input of terrigenous material. The paleomagnetic data given in the magnetostratigraphic profile indicate a significant jump of remanent magnetization and magnetic

susceptibility, at Nu 10.0. This change marks the change from marls and marly limestone to pure limestone. Magnetosusceptibility measurements allow a subdivision of the Nutzhof section into three parts or intervals. A general decreasing trend throughout the log reflects a decreasing content of siliciclastic material indicating a decrease in clastic input to the depositional area at Nutzhof during the Late Jurassic–Early Cretaceous. Mean values of volume magnetic susceptibility (k) are shown in Table 1. The k ranges from –8.6 to 15.6×10^{-6} SI for upper interval between 0–10 m of the section and from 30 to 85.1×10^{-6} SI for the lower part (10.12–18.4 m). The lower part from Nu 18.0–12.0 shows values from 0.052–0.028 (mean 0.039). Above Nu 12.0 values range from 0.050–0.026 (mean 0.033). The most marked change appears at Nu 10.0 from values of 0.050 to 0.010. The upper interval from Nu 10.0 to 0.0 is characterized by very low values from 0.012–0.000 (mean 0.004). The J/K boundary strata itself are not characterized by significant changes in values.

Gamma log

The radioactivity variation of the studied section is measured by gamma-ray measures and represents a direct function of the variation of the clay-mineral content. Hence, higher radioactivity reflects higher clay contents. Measurements of gamma response (cps) are a powerful tool for interpreting the stratigraphy in the outcrop.

Generally measured cps values range between 4 and 30. The gamma response allows a clear subdivision of the section into three parts each corresponding to the three identified main lithological units within the Blassenstein Formation. The gamma response gradually decreases from Nu 18.0 to Nu 0.0, reaching the highest values at Nu 16.5 and lowest values at Nu 7.7 and Nu 3.3. Within this gradually decreasing trend, the biggest excursion is recorded close to bed Nu 10.0. Values range in the lower interval (Nu 18.0–12.0) from 15–30 cps (mean 22.53 cps), in the middle interval (Nu 12.0–10.0) from 13–23 cps (mean 19.95 cps), and in the upper interval (Nu 10.0–0.0) from 4–14 cps (mean 9.07 cps) (Fig. 3).

The gamma response becomes gradually weaker in the upper, undisturbed part of the section. The uppermost part of the section, however, shows an upwards decreasing gamma response. The curve pattern therefore shows a vertically congruent curve to the susceptibility values.

The decreasing gamma log values together with the characteristic pattern in decreasing susceptibility suggest a more stable depositional environment from about Nu 10.0 and upwards, predating the J/K boundary by 3 meters or 0.5 million years.

Paleomagnetism

The paleomagnetic study of the section identifies the boundaries of magnetozones from M17r to M21r and the reverse subzones Kysuca and Brodno (M20n.1r and M19n.1r, respectively). The record of polarity changes in the Earth's magnetic field can determine the precise age. The identification of the detected polarity zones against the M-sequence of polarity intervals given by the GPTS (Gradstein et al. 2004) is the most important topic. The preliminary determination of boundaries of magnetozones M17n to M22r was the result from 30 samples of C-component direction (Pruner et al. 2009). The number of polarity zones, namely six normal and six reverse, is the same number as in preliminary results. The mean values of the modulus of NRM (Jn) and of volume magnetic susceptibility (k) for 244 samples of Upper Tithonian and Lower Berriasian limestones are shown in Table 1. The k ranges from –8.6 to 15.6×10^{-6} SI for the upper interval between 0–10 m of the section and from 30 to 85.1×10^{-6} SI for the lower part (10.12–18.4 m). The results of AF and TD demagnetization procedures are displayed in Pruner et al. (2009: figs. 3, 4). The A-component is of viscous origin and is demagnetizable in the temperature range of 20–100 °C (or AF 0–5 mT). The origin of the B-components, low temperature (LTC) or low field (LFC) were undoubtedly imprinted, most probably in the Neogene, after Alpine folding. Both magnetic polarities are present in C-component (high temperature — HTC or high field — HFC) directions, but the directions are highly scattered (Table 2, Fig. 5). The statistical

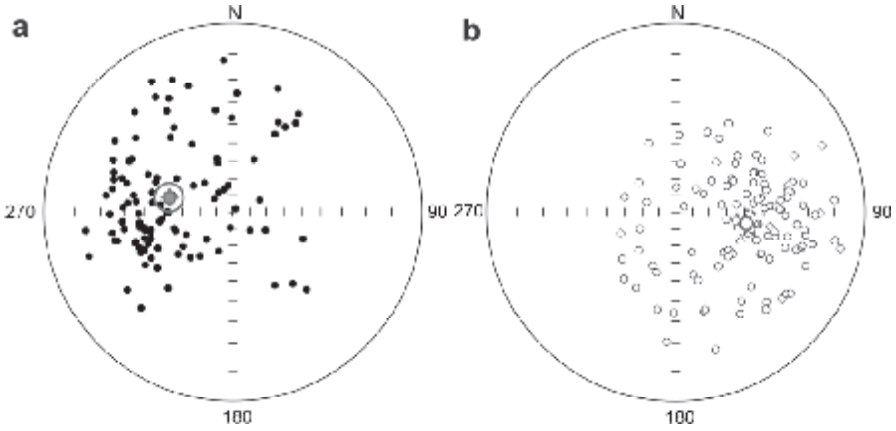

Fig. 5. J/K limestones and marls, directions of N polarity (left) and R polarity (right) of C-components of RM corrected for dip of strata. Stereographic projection, full (open) small circles represent projection onto the lower (upper) hemisphere. The mean direction calculated according to Fisher (1953) is marked by a small crossed circle, the confidence circle at the 95% probability level is circumscribed about the mean direction.

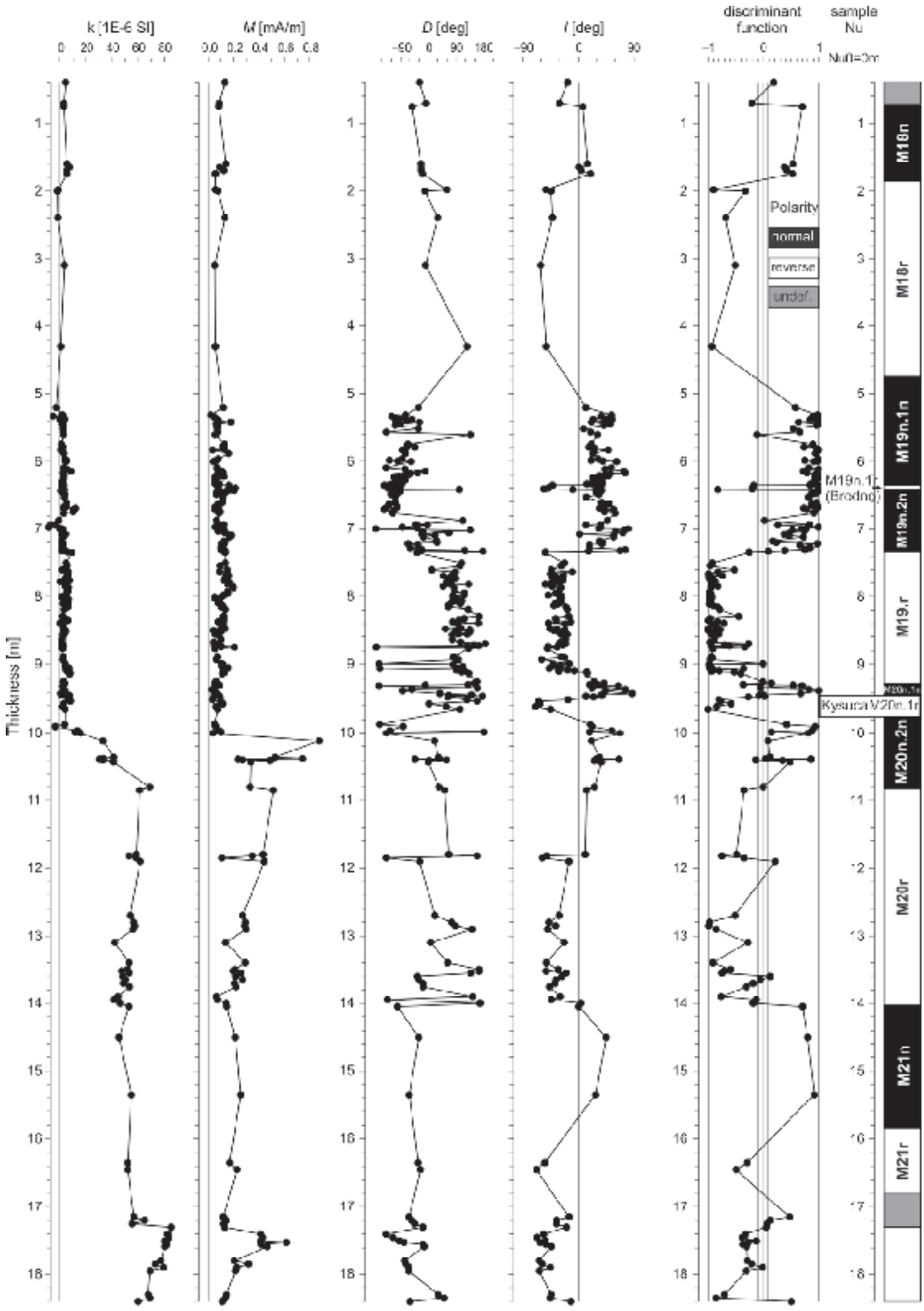

Fig. 6. Magnetostratigraphic profile across the Nutzhof J/K boundary strata, paleomagnetic and lithostratigraphic data. *M* — NRM in the natural state; *k* — value of volume magnetic susceptibility in the natural state; D — declination; I — inclination. Normal (reverse) magnetozones are denoted black (white), unknown (grey).

Table 1: Basic magnetic parameters and statistical properties of the physical quantities in the basic groups of samples from the Nutzhof.

Age	Polarity	Number of samples	Modulus of NRM J_n [10^{-6} A/m]		Volume magnetic susceptibility k [10^{-6} SI]	
			Mean value	Standard deviation	Mean value	Standard deviation
Early Berriasian	N+R	82	88	39	2.3	3.1
Late Tithonian	N+R	155	165	132	21.4	26.5

Table 2: Mean directions of B (LFC or LTD) and C-components (HFC or HTD) corrected and not corrected for structural tilt.

Age of rocks	Component of remanence	Polarity	Structural tilt correction				No structural tilt correction (in-situ directions)				n
			Mean directions		α_{95} [°]	k	Mean directions		α_{95} [°]	k	
			Decl. [°]	Incl. [°]			Decl. [°]	Incl. [°]			
L. Tith.+ E.Berr.	B	R	351.7	–55.4	3.1	12.1	10.4	77.5	3.1	11.9	168
L. Tith.+ E.Berr.	C	N	278.0	53.3	7.1	3.2	199.3	–27.3	8.0	2.6	119
L. Tith.+ E.Berr.	C	R	104.1	–46.1	6.4	4.8	19.3	13.2	6.4	4.8	101
L. Tith.+ E.Berr.	C	N*)	286.1	44.5	4.7	4.0	198.1	–15.0	5.2	3.7	220

parameters for component C (total number 220) are influenced by samples close to the boundary of shorter polarity zones. The mean values of C-component directions are anomalous, having been affected by counter clockwise paleotectonic rotation. The paleomagnetic data given in the magnetostratigraphic profile (Fig. 6) indicate a significant change of remanent magnetization and magnetic susceptibility, at level Nu 10 due to the significant change in lithology from marl (Nu 18.0–10.0) to limestone (Nu 10.0–0.0).

Figure 5 presents the results of the magnetostratigraphic profile with indicated moduli values of natural remanent magnetization (*Jn*), volume magnetic susceptibility values of samples in the natural state (*k*), paleomagnetic declination Dp and inclination Ip (of C-components of remanence inferred by multi-component analysis). The values of the angular deflection of the direction of C-components of remanence from the mean direction, with only normal polarity being taken into consideration (reverse directions were transformed into normal directions for the calculation of the mean direction), are given in the next column. The resulting normal and reverse magnetozones are indicated in the last column.

Discussion

The high-resolution quantitative analysis of selected organic groups (calpionellids, radiolarians, saccocomids) indicates major variations in their abundance and composition (Figs. 2, 3, 4). The Upper Jurassic (Tithonian) depositional setting at Nutzhof was influenced by the periodic input of biodetritus from surrounding shallow marine paleoenvironments, whereas deposition was more constant during the Berriasian and characterized by pelagic sediments predominantly composed of planktonic microorganisms (radiolarians, calcareous dinoflagellates, calpionellids, and nannofossils).

Calcareous dinoflagellates predominate in the Lower and Upper Tithonian. Their stratigraphic and paleoecological potential has been discussed by Reháková (2000a,b). In the Nutzhof section, the Lower Tithonian record of calcareous dinoflagellates shows a distinct change in abundance and composition. Forms with radial orientation of calcite crystallites in their cyst walls dominate in the *Tithonica* and *Malmica* Zones, whereas cadosinid species with oblique arrangement of the calcite crystallites dominate the *Semiradiata* Zone. According to Michalík et al. (2009), coinciding acme peaks of *Cadosina semiradiata semiradiata* Wanner and *Conusphaera* spp. probably indicate warmer surface waters.

Chitinoidellids are very rare in the Nutzhof section. The appearance of the first hyaline calpionellid loricas precedes the crassicollarian radiation. A monospecific calpionellid association consisting predominantly of *Calpionella alpina* Lorenz characterizes the section. A similar calpionellid evolution and biostratigraphy of the Jurassic-Cretaceous boundary interval was recorded by Remane (1986), Pop (1994), Reháková (1995), Olóriz et al. (1995), Grün & Blau (1997), and Andreini et al. (2007). Reháková (in Michalík et al. 2009) demonstrated that the J/K boundary interval can be characterized by several calpionellid events: the onset, diversification, and extinction of chitinoidellids (middle Tithonian); the onset, diversification, and extinction of crassicollarians (Upper Tithonian); and the onset of the monospecific *Calpionella alpina* association at the J/K boundary. Due to synsedimentary erosion probably originating during several extensional pulses, which denivelated the sea bottom, clast-bearing calpionellid biomicrites were documented along the Upper Jurassic and Lower Cretaceous (Lower Berriasian) formations in several areas studied (Michalík et al. 1990, 1995; Grabowski et al. 2010).

The calcareous nannofossil ranges in the Nutzhof section provides a tool for biostratigraphic subdivision of the J/K boundary interval. The coccoliths of the family Watznaueriaceae and three nannolithic genera *Conusphaera*, *Polycostella*, and *Nannoconus* dominate the assemblages. This is in accordance with nannofossil studies in other locations at low latitudes sections across the J/K boundary (Thierstein 1971, 1973, 1975; Erba 1989; Gardin & Manivit 1993; Özkan 1993;

Tavera et al. 1994; Bornemann et al. 2003; Pszczółkowski & Myczyński 2004; Tremolada et al. 2006; Halásová in Michalík et al. 2009).

The lowermost occurrences of nannofossils are partly obscured due to poor preservation, but we tentatively identified the boundaries of zones and subzones based on certain stratigraphic markers (*Polycostella beckmannii*, *Helenea chiastia*, *Hexalithus noeliae*, *Nannoconus wintereri*, *Nannoconus globulus minor*, *Nannoconus steinmannii minor*, *Nannoconus kamptneri minor*, *Nannoconus steinmannii steinmannii*, *Nannoconus kamptneri kamptneri*, *Nannoconus globulus globulus*).

Tremolada et al. (2006) detected that *Conusphaera* dominates the nannolith assemblage in the upper middle Tithonian ("*Conusphaera* world"). This is corroborated by data obtained in this study. The acme peak of the genus *Polycostella* in samples Nu 13.0 and 14.0 coincides with the middle Tithonian *Semiradiata* Subzone (Reháková 2000b). Comparison with the Brodno section (Michalík et al. 2007 and Michalík et al. 2009) indicate that the dominance of the nannolith *Polycostella beckmannii* occurs somewhat lower in the *Chitinoidella* Zone in the Nutzhof section. The first appearance of *Helenea chiastia* is also demonstrated to be diachronous, being close to the base of the calpionellid *Crassicollaria* Zone in the Brodno section, but recorded in the uppermost part of the *Chitinoidella* Zone in the Nutzhof section.

The most distinct nannofossil event is the onset of nannoconids which was observed in the interval comprising the calpionellid *Calpionella* Zone, *Ferasini* Subzone (lowermost Berriasian). This indicates a change in the paleooceanographic regime. From the biostratigraphic point of view, the upper J/K boundary datum based on nannofossils (Bornemann et al. 2003).

The change of saccocomid marl and limestone by overlying calpionellid limestone in the Upper Tithonian also characterizes J/K-boundary successions reported from numerous other localities in Austria (e.g. Kristan-Tollmann 1962; Flügel 1967; Holzer 1968; Holzer & Poltnik 1980; Reháková et al. 1996), Germany (Lackschewitz et al. 1989), Poland (Pszczółkowski & Myczyński 2004) and Slovakia (Vašíček et al. 1992). Many of these localities, however, differ lithologically from the section studied at Nutzhof. In most cases the saccocomid-bearing beds are pure, reddish limestone.

Saccocomid limestones have often been interpreted as Kimmeridgian (e.g. Flügel 1967: p. 35; Sauer et al. 1992: p. 183; Wessely 2008: p. 210, fig. 5) and have been used as the marker bed for that stage (Bernouli 1972). Reliable stratigraphic data is, however, commonly lacking. Based on well-dated sections, the majority of the recorded saccocomid-occurrences are of Tithonian age (Nicosia & Parisi 1979; Keupp & Matyszkiewicz 1997). This is corroborated/supported by the data from the present study.

Summary and conclusions

The studied section at Nutzhof represent a J/K-boundary succession deposited in a distal slope-setting in the Gresten Klippenbelt, a part of the Helvetic paleogeographic realm. The Upper Jurassic to Lower Cretaceous pelagic sediments represent a major sedimentation cycle.

The significant depositional change from a mixed siliciclastic/carbonate to a pure carbonate depositional system is marked by a change from a lower marly cyclic part to an upper calcareous part. Accordingly, the lower (Tithonian) marly part is characterized by dark, laminated pelagic marls and marly limestones with intercalated turbiditic limestone beds (e.g. allodapic limestones). The upper part (limestone) represents a phase of autochthonous pelagic sedimentation characterized by bright, chert- and aptychi-bearing nannoconid limestone. The macro-invertebrate fauna of the Berriasian limestone succession is sparse, comprising rare ammonoids, aptychi, belemnites and brachiopods. The macro-invertebrate fauna of the Tithonian marl-limestone succession is rich in saccocomids accompanied by rare bivalves (inoceramids) and partly by abundant ammonites. The microfauna, in contrast, is abundant, with dominating calpionellids and radiolarians in the limestone succession and saccocomid blooms within the marl-limestone succession.

The macrofauna, as already stated, is represented especially by ammonoids, belemnoids, aptychi and bivalves. The whole section yielded 46 ammonite individuals/specimens. Sampling of the sparse ammonites was difficult due to hardite sediments. The ammonite biostratigraphy is integrated with micro- and nannofossil biostratigraphic data from the marl-limestone succession and indicates Early Tithonian to middle Berriasian ages (*Hybonoticeras hybonotum* Zone up to the *Subthurmannia occitanica* Zone). Descendants of *Subplanites* have not previously been reported within the Gresten Klippenbelt. All ammonoids are typical of the Mediterranean Province.

The limitation of ammonite biostratigraphy obtained by the new ammonite findings from Nutzhof has demonstrated the importance of integrating macrofauna biostratigraphy with the micro- and nannofossil biostratigraphy. The described fauna increases our understanding of ammonite faunas from the area of the Gresten Klippenbelt and the neighbouring Waschberg Zone during deposition of the Jurassic/Cretaceous boundary interval. Both areas were at the time located on the passive northern margin of the Penninic Ocean.

Magnetostratigraphic, geochemical and isotopes studies contribute to the understanding of the environmental history during the Jurassic-Cretaceous boundary interval in a little known area. Sediment deposition took place during conditions of relatively stable water masses with relatively low sedimentation rates in an unstable sedimentological environment. This is reflected by a change in lithology from Nu 11.0 to Nu 13.0 (11 to 13 m). A series of event layers with redeposited faunal elements (e.g. phyllocrinids) indicate a transport of sediment from shallower areas in the North. The depositional area was influenced by the opening of the Penninic Ocean during the Late Jurassic to Early Cretaceous. A phase of an earlier Penninic opening, is reflected as a significant change in lithology and composition of faunal assemblage in the uppermost Tithonian (at Nu 10.0 m).

There is no evidence for redeposition of ammonites, which are considered autochthonous and parautochthonous pelagic elements from the open sea. Four crinoid taxa are recorded in

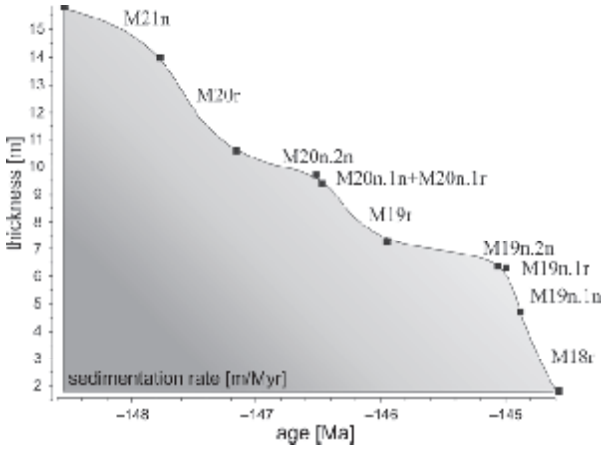

Fig. 7. Estimated average sedimentation rate diagram around the J/K boundary at Nutzhof based on magnetostratigraphic and biostratigraphic data.

the Tithonian Blassenstein Formation and comprise *Balanocrinus* sp., *Saccocoma tenella* (Goldfuss), *Crassicoma*? sp., and *Phyllocrinus belbekensis* Arendt. Only *S. tenella* is abundant. The other taxa, in particular the benthic isocrinids and phyllocrinids are rare. Preservation and ossicle size range of the latter groups indicate their allochthonous origin. The saccocomid remains are restricted to the Tithonian, the saccocomid-rich facies being overlain by calpionellid limestones.

The biostratigraphic study based on the distribution of calpionellids allowed an identification of the *Boneti* Subzone of the *Chitinoidella* Zone. The J/K boundary is recorded between the *Crassicollaria* and *Calpionella* Zone and is defined by the morphological change of *Calpionella alpina* tests. The base of the *Crassicollaria* Zone approximately coincides with the onset of *Tintinnopsella remanei* Borza and the base of the standard *Calpionella* Zone, with the monospecific calpionellid association being dominated by *Calpionella alpina* Lorenz. Two further Subzones (*Ferasini* and *Elliptica*) of the standard *Calpionella* Zone were recognized in radiolarian-calpionellid and calpionellid-radiolarian wackestones in the overlying uppermost part of the section.

The appearance of several important nannofossil genera allow the identification of the Lower, middle and Upper Tithonian, and a relatively accurate identification of the Tithonian-Berriasian boundary, and the definition of the Lower Berriasian nannofossil zones. Coccoliths of the family Watznaueriaceae and nannoliths of the genera *Conusphaera*, *Nannoconus* and *Polycostella* dominate the assemblages. The interval between the FAD of *Nannoconus wintereri* co-occurring with small nannoconids in sample Nu 9 (the uppermost Tithonian) and the FAD of *Nannoconus kamptneri minor* in sample Nu 5 (lowermost Berriasian) is interpreted as the Tithonian-Berriasian boundary interval. The nannoconid dominance in the lowermost Berriasian, known as the "*Nannoconus* world" sensu Tremolada et al. (2006) is now recorded in the Nutzhof section.

Paleomagnetic data across the J/K boundary strata allow the construction of a detailed magnetostratigraphic zonation. The interval between Nu 5 to 10.5 m provides a high-resolution profile with an almost continuous record of magnetic and paleomagnetic parameters, that records the critical intervals with boundaries of the magnetozones M19n–M20n. According to magnetozone M19n and Brodno Subzone, the J/K boundary is identified within the interval between Nu 6.5–7 m. Significant changes do not occur at the J/K boundary itself. The step of remanent magnetization and magnetic susceptibility, at level Nu 10.0, occurs in magnetozone M20n below the Kysuca Subzone. A similar jump of NRM and susceptibility lies in the M20n just above the Kysuca Subzone in the Bosso section. The average sedimentation rate in the Nutzhof section is ca. 3.7 m/Myr (Fig. 7), but with high dispersion (from 2–11 m/Myr) differing from the average sedimentation rates of 2.27 m/Myr recorded in Brodno and 2.88 m/Myr in Puerto Escaño. Relatively low rates (1 m/Myr) are recorded in the Bosso Valley, but higher rates (3–11 m/Myr) are reported by Grabowski & Pszczółkowski (2006) from the Tatra Mountains. No significant change can be noted at or within the J/K boundary interval. The integration of fossil and magnetostratigraphic data demonstrates a duration of approximately 7 million years (approximately 150–143 Ma) for the deposition of the Nutzhof section (Figs. 6 and 7).

The carbon isotope record documents a significant change in the C-cycle dynamic suggesting a sluggish 3-D dynamic of the marine system possibly associated with a decrease in primary productivity. Abrupt oscillations mainly recorded between the levels 10 and 6 m suggest a significantly unstable global carbon system during the Jurassic but a change towards balanced conditions in the Cretaceous interval.

Acknowledgments: We are indebted to Hans Egger (Geological Survey of Austria) who made us aware of the studied locality. The study was supported by the Austrian Science Fund (FWF; Project P20018-N10) and by the Grant Agency of the Czech Republic (Grant No. GACR 205-07-1365) and Research Plan of the IG AS CR No. CEZ AV0Z30130516. This is also a contribution to the 506 IGCP UNESCO Project, APVV-0280-07, APVV-0248-07, APVV- 0465-06, APVT 51-011305 and LPP 0120-09. MW thanks IGCP 555 and the Austrian Academy of Sciences for financial support. Thanks go to members of the Kilian Group (Lower Cretaceous Ammonite Working Group; president Stephane Reboulet, Lyon) for fruitful discussions on the ammonoid fauna. Technical support for photography was provided by Alice Schumacher (Vienna). Franz Topka (Vienna) assisted with the preparation of ammonoid specimens and Anton Englert (Vienna) prepared the thin sections. Paleomagnetic analyses were performed by Daniela Venhodová, Jana Drahotová, and Jiří Petráček. The software for the evaluation of paleomagnetic measurements was prepared by Otakar Man (Institute of Geology ASCR v.v.i.). We thank Luc Bulot (Marseille) and Jacek Grabowski (Warsaw) for their comments which helped to improve the quality of the manuscript.

References

Andreini G., Caracuel J.E. & Parisi G. 2007: Calpionellid biostratigraphy of the Upper Tithonian–Upper Valanginian inter-

val in Western Sicily (Italy). *Swiss J. Geosci*. 100, 179–198.
Bernouli D. 1972: North Atlantic and Mediterranean Mesozoic facies: A comparison. *Init. Repts. DSDP* 11, 631–643.
Bornemann A., Aschwer U. & Mutterlose J. 2003: The impact of calcareous nannofossils on the pelagic carbonate accumulation across the Jurassic-Cretaceous boundary interval. *Palaeogeogr. Palaeoclimatol. Palaeoecol*. 199, 187–228.
Bralower T.J., Monechi S. & Thierstein H.R. 1989: Calcareous nannofossil zonation of the Jurassic-Cretaceous boundary interval and correlation with the geomagnetic polarity timescale. *Mar. Micropaleont*. 14, 153–235.
Cžjžek J. 1852: Aptychenschiefer in Niederösterreich. *Jb. K.-Kön. Geol. Reichsanst.* 3, 3, 1–7.
Decker K. 1990: Plate tectonics and pelagic facies: Late Jurassic to Early Cretaceous deep-sea sediments of the Ybbsitz ophiolite unit (Estern Alps, Austria). *Sed. Geol*. 67, 85–99.
Decker K. & Rögl F. 1990: Early Cretaceous agglutinated foraminifera from limestone-marly rhythmites of the Gresten Klippen Belt (Eastern Alps Austria). *Abh. Geol. B.–A*. 41, 41–59.
Dercourt J., Ricou L.E. & Vrielynck B. (Eds.) 1993: Atlas Tethys palaeoenvironment maps, 14 maps, 1 pl. *Gauthier-Villars*, Paris, 1–307.
Dercourt J., Gaetani M., Vrielynck B., Barrier E., Biju Duval B., Brunet M.F., Cadet J.P., Crasquin S. & Sandulescu M. (Eds.) 2000: Atlas Peri-Tethys, Palaeogeographical maps, 24 maps and explanatory notes: I-XX. *CCGM/CGMW*, Paris, 1–269.
Erba E. 1989: Calcareous nannofossil zonation of the Jurassic-Cretaceous boundary interval and correlation with the geomagnetic polarity timescale. *Mar. Micropaleont*. 14, 153–235.
Faupl P. 2003: Historische Geologie: eine Einführung. *Facultas*, Wien, 1–271.
Faupl P. & Wagreich M. 2000: Late Jurassic to Eocene Palaeogeography and Geodynamic Evolution of the Eastern Alps. *Mitt. Österr. Geol. Gesell*. 92, 79–94.
Fisher R.A. 1953: Dispersion on a sphere. *Proc. R. Soc. London A*. 217, 295–305.
Flügel H.W. 1967: Die Lithogenese der Steinmühl-Kalke des Arracher Steinbruches (Jura, Österreich). *Sedimentology* 9, 23–53.
Gardin S. & Manivit H. 1993: Upper Tithonian and Berriasian calcareous nannofossils from the Vocontian Trough (SE France): Biostratigraphy and sequence stratigraphy. *Bull. Centres Rech. Explor.-Prod. Elf-Aquitaine* 17, 1, 277–289.
Gottschling P. 1965: Zur Geologie der Hauptklippenzone und der Laaber Teildecke im Bereich von Glashütte bis Bernreith (Niederösterreich). *Mitt. Geol. Gesell. Wien* 58, 23–86.
Grabowski J. & Pszczółkowski A. 2006: Magneto- and biostratigraphy of the Tithonian-Berriasian pelagic sediments in the Tatra Mountains (central Western Carpathians, Poland): sedimentary and rock magnetic changes at the Jurassic/Cretaceous boundary. *Cret. Research* 27, 398–417.
Grabowski J., Michalík J., Pszczółkowski A. & Lintnerová O. 2010: Magneto-, and isotope stratigraphy around the Jurassic/Cretaceous boundary in the Vysoká Unit (Malé Karpaty Mts, Slovakia): correlations and tectonic implications. *Geol. Carpathica* 61, 4, 309–326.
Gradstein F.M., Ogg J.G. & Smith A.G. (Eds.) 2004: A geologic time scale 2004. *Cambridge University Press*, Cambridge, U.K., 1–589.
Grün B. & Blau J. 1997: New aspects of calpionellid biochronology: proposal for a revised calpionellid zonal and subzonal division. *Rev. Paléobiol.* 16, 197–214.
Hardenbol J., Thierry J., Farley M.B., Jacquin T., de Graciansky P.C. & Vail P.R. 1998: Mesozoic and Cenozoic sequence stratigraphy of European basins. *SEPM, Spec. Publ.*, Tulsa 60, 1998.
Hennig S., Weissert H. & Bulot L. 1999: C-isotope stratigraphy, a calibration tool between ammonite- and magnetostratigraphy: the Valanginian-Hauterivian transition. *Geol. Carpathica* 50, 91–96.
Hess H., Ausich W.I., Brett C.E. & Simms M.J. 1999: Fossil crinoids. *Cambridge University Press*, Cambridge, MA, xv+275.
Hirano H. 1993: Phyletic evolution of desmoceratine ammonoids through the Cenomanian-Turonian oceanic anoxic event. In: House M.R. (Ed.): The Ammonoidea: environment, ecology, and evolutionary change. *Clarendon Press*, Oxford, UK, 267–283.
Holzer H.-L. 1968: Stratigraphie und Lithologie der Jura-Kreide-Folge im nördlichsten Pechgraben-Steinbruch. *Mitt. Naturwiss. Vereins Steiermark* 98, 47–57.
Holzer H.-L. & Poltnig W. 1980: Erster Nachweis einer Radialplatten-Fossillagerstätte der Schwebcrinoide *Saccocoma* im oberostalpinen Malm (Ostkarawanken, Kärnten). *Carinthia II* 170, 201–216.
Houša V., Krs M., Krsová M., Man O., Pruner P. & Venhodová D. 1999: High-resolution magnetostratigraphy and micropaleontology across the J/K boundary strata at Brodno near Žilina, western Slovakia: summary results. *Cret. Research* 20, 699–717.
Houša V., Krs M., Man O., Pruner P., Venhodová D., Cecca F., Nardi G. & Piscitello M. 2004: Combined magnetostratigraphic, paleomagnetic and calpionellid investigations across Jurassic/Cretaceous boundary strata in the Bosso Valley, Umbria, central Italy. *Cret. Research* 25, 771–785.
Keupp H. & Matyszkiewicz J. 1997: Zur Faziesrelevanz von *Saccocoma*-Resten (Schwebcrinoiden) in Oberjura-Kalken des nördlichen Tethys-Schelfs. *Geol. Blätter für Nordost-Bayern und angrenzende Gebiete* 47, 53–70.
Kirschvink J.L. 1980: The least-squares line and plane and the analysis of palaeomagnetic data. *Geophys. J. Roy. Astr. Soc*. 62, 699–718.
Kristan-Tollmann E. 1962: Stratigraphisch wertvolle Mikrofossilien aus dem Oberjura und Neokom der Nördlichen Kalkalpen. *Erdoel-Z*. 78, 637–549.
Kroh A. & Lukeneder A. 2009: Crinoids from the Late Jurassic–Early Cretaceous of the Nutzhof section (Lower Austria, Pieniny Klippenbelt). *Ann. Naturhist. Mus. Wien, Serie A* 110, 383–399.
Kühn O. 1962: Autriche. *Lexique Stratigr. Int.*, Europe 8, 1–646.
Küpper H. 1962: Beobachtungen in der Hauptklippenzone bei Stollberg, N.Ö. *Verh. Geol. B.–A*. 2, 263–268.
Lackschewitz K., Grützmacher U., Suhr J. & Kiel R.H. 1989: Synsedimentäre Kippschollentektonik: Becken- und Schwellenfazies oberjurassischer Karbonate der Chiemgauer Alpen. *Geol. Paläont. Mitt. Innsbruck* 16, 163–165.
Lierl H.J. 1992: Tenside — ihre Verwendung für die Präperation geologisch-paläontologischer Objekte. *Der Präperator* 38, 12–17.
Lukeneder A. 2009: New biostratigraphic ammonite data from the Jurassic/Cretaceous boundary at Nutzhof (Gresten Klippenbelt, Lower Austria). *Ann. Naturhist. Mus. Wien, Serie A* 110, 313–330.
Mandic O. & Lukeneder A. 2008: Dating the Penninic Ocean subduction: new data from planktonic foraminifera. *Cret. Research* 29, 901–912.
Masse J.P. et al. (12 co-authors) 2000: Early Aptian. In: Dercourt J., Gaetani M. et al. (Eds.). Atlas Peri-Tethys, Palaeogeographical Maps 13, (CCGM/CGMW) Paris.
McArthur J.M. & Howarth R.J. 2004: Strontium isotope stratigraphy. In: Gradstein F.M., Agterberg F.P. & Smith A.G. (Eds.): A geologic time scale 2004. *Cambridge University Press*, 96–105.
McArthur J.M., Howarth R.J. & Bailey T.R. 2001: Strontium isotope stratigraphy: LOWESS Version 3: best fit to the marine Sr-isotope curve for 0–509 Ma and accompanying look-up table for deriving numerical age. *J. Geol*. 109, 155–170.
McArthur J.M., Janssen N.M.M., Reboulet S., Leng M.J., Thirlwall

M.F. & van de Schootbrugge B. 2007: Early Cretaceous ice-cap volume, palaeo-temperatures (Mg, ^{18}O), and isotope stratigraphy (^{13}C, $^{87}Sr/^{86}Sr$) from Tethyan belemnites. *Palaeogeogr. Palaeoclimatol. Palaeoecol.* 248, 391–430.

Michalík J., Reháková D. & Halásová E. 1990: Stratigraphy of the Jurassic/Cretaceous boundary beds in the Hlboč Valley (Vysoká Unit of the Krížna Nappe, Malé Karpaty Mts). *Knihovnička ZPN* 9a, 183–204 (in Slovak, with English summary).

Michalík J., Reháková D. & Vašíček Z. 1995: Early Cretaceous sedimentary changes in west Carpathian area. *Geol. Carpathica* 46, 285–296.

Michalík J., Reháková D., Halásová E. & Lintnerová O. 2007: Integrated stratigraphy of the Jurassic/Cretaceous boundary at the Brodno section (the Kysuca Unit, Pieniny Klippen Belt, Western Carpathians). *Abstract book, International geological correlation programme 506 — Jurassic marine: non-marine correlation*, *Univ. Bristol*, 1–3.

Michalík J., Reháková D., Halásová E. & Lintnerová O. 2009: A possible West Carpathian regional stratotype of the Jurassic/Cretaceous boundary (the Brodno section near Žilina). *Geol. Carpathica* 60, 3, 213–232.

Nicosia U. & Parisi G. 1979: *Saccocoma tenella* (Goldfuss) — Distribuzione stratigrafica e geografica. *Boll. Soc. Paleont. Ital.* 18, 320–326.

Olóriz F., Caracuel J.E., Marques B. & Rodríguez-Tovar F.J. 1995: Asociaciones de Tintinnoides en facies Ammonitico Rosso de la Sierra Norte (Mallorca). *Rev. Esp. Paleont., No. Homenaje al Dr. G. Colom*, 77–93.

Özkan S. 1993: Calcareous nannofossils from the Late Jurassic–Early Cretaceous of Northwest Anatolia, Turkey. *Geol. J.* 28/3–4, 295–307.

Piller W. et al. 2004: Die Stratigraphische Tabelle von Österreich 2004 (sedimentäre Schichtfolgen). *Österr. Akad. Wissenschaft. Österr. Stratigr. Kommission*, Wien.

Pop G. 1994: Calpionellid evolutive events and their use in biostratigraphy. *Rom. J. Stratigraphy* 76, 7–24.

Pop G. 1997: Révision systématique des chitinoidelles tithoniennes des carpathes méridionales (Roumanie). *Compt. Rendus Acad. des Sci., Sér. IIa*, Paris 342, 931–938.

Pruner P., Schnabl P. & Lukeneder A. 2009: Preliminary results of magnetostratigraphic investigations across the Jurassic/Cretaceous boundary strata in the Nutzhof, Austria. *Ann. Naturhist. Mus. Wien*, *Ser. A* 110, 331–344.

Pszczółkowski A. & Myczyński R. 2004: Ammonite-supported microfossil and nannoconid stratigraphy of the Tithonian-Hauterivian limestones in selected sections of the Branisko Succession, Pieniny Klippen Belt (Poland). *Stud. Geol. Pol.* 123, 133–197.

Reháková D. 1995: New data on calpionellid distribution in the Upper Jurassic/Lower Cretaceous formations (Western Carpathians). *Miner. Slovaca* 27, 308–318 (in Slovak).

Reháková D. 1998: Calpionellid genus *Remaniella* Catalano 1956 in Lower Cretaceous pelagic deposits of Western Carpathians. *Miner. Slovaca* 30, 443–452.

Reháková D. 2000a: Calcareous dinoflagellate and calpinellid bioevents versus sea-level fluctuations recorded in the West-Carpathian (Late Jurassic/Early Cretaceous) pelagic environments. *Geol. Carpathica* 51, 4, 229–243.

Reháková D. 2000b: Evolution and distribution of the Late Jurassic and Early Cretaceous calcareous dinoflagellates recorded in the Western Carpathian pelagic carbonate facies. *Miner. Slovaca* 32, 79–88.

Reháková D. 2002: *Chitinoidella* Trejo, 1975 in Middle Tithonian carbonate pelagic sequences of the West Carpathian Tethyan area. *Geol. Carpathica* 55, 6, 369–379.

Reháková D. & Michalík J. 1997: Evolution and distribution of calpionellids — the most characteristic constituents of Lower Cretaceous Tethyan microplankton. *Cret. Research* 18, 493–504.

Reháková D., Michalík J. & Ožvoldová L. 1996: New microbiostratigraphical data from several Lower Cretaceous pelagic sequences of the Northern Calcareous Alps, Austria (Preliminary results). *Geol. Paläont. Mitt. Innsbruck* 4, 57–81.

Reháková D., Halásová E. & Lukeneder A. 2008: The Jurassic/Cretaceous boundary in the Austrian Klippen belt (Nutzhof, Lower Austria): Implications on micro- and nannofacies analysis. *Ber. Geol. B.–A.* 74, 95–97.

Reháková D., Halásová E. & Lukeneder A. 2009: The Jurassic-Cretaceous boundary in the Austrian Klippen Belt (Nutzhof, Lower Austria): Implications on Micro- and Nannofacies analysis. *Ann. Naturhist. Mus. Wien*, *Ser. A* 110, 345–381.

Remane J. 1986: Calpionellids and the Jurassic-Cretaceous boundary. *Acta Geol. Hung.* 29, 15–26.

Roth P.H., Medd A.W. & Watkins D.K. 1983: Jurassic calcareous nannofossil zonation, an overview with new evidence from Deep Sea Drilling Project Site 534A. In: Sheridan R.E., Gradstein F.M. et al. *Init. Repts. DSDP* 76, 573–579.

Řehánek J. 1992: Valuable species of cadosinids and stomiosphaerids for determination of the Jurassic-Cretaceous boundary (vertical distribution, biozonation). *Scripta* 22, 117–122.

Sauer R., Seifert P. & Wessely G. 1992: Guidebook to excursions in the Vienna Basin and the adjacent Alpine-Carpathian Thrustbelt in Austria. Part II. *Mitt. Österr. Geol. Gesell.* 85, 97–239.

Scotese C.R. 2001: Atlas of earth history. *Paleomap project*, Arlington, Texas, 1–52.

Spötl C. & Vennemann T. 2003: Continuous-flow isotope ratio mass spectrometric analysis of carbonate minerals. *Rapid Communications in Mass Spectrometry* 17, 1004–1006.

Stampfli G.M. & Borel G.D. 2002: A plate tectonic model for the Paleozoic and Mesozoic constrained by dynamic plate boundaries and restored synthetic oceanic isochrons. *Earth Planet. Sci. Lett.* 196, 17–33.

Stampfli G. & Mosar J. 1999: The making and becoming of Apulia. *Mem. Sci. Géol. Padova. Spec. Vol.*, *3rd Workshop on Alpine Geology* 51/1, 141–154.

Stampfli G.M., Borel G.D., Marchant R. & Mosar J. 2002: Western Alps geological constraints on western Tethyan reconstructions. In: Rosenbaum G. & Lister G.S. (Eds.): Reconstruction of the evolution of the Alpine-Himalayan Orogen. *J. Virtual Explorer* 8, 77–106.

Tavera J.M., Aguado R., Company M. & Olóriz F. 1994: Integrated biostratigraphy of the Durangites and Jacobi Zones (J/K boundary) at the Puerto Escaño section in Southern Spain (province of Cordoba). *Geobios* 17, 469–476.

Thierstein H. 1971: Tentantive Lower Cretaceous calcareous Nanoplankton Zonation. *Eclogae Geol. Helv.* 64, 3, 437–652.

Thierstein H. 1973: Lower Cretaceous calcareous nannoplankton biostratigraphy. *Abh. Geol. B.–A.* 29, 3–52.

Thierstein H. 1975: Calcareous nannoplankton biostratigraphy at the Jurassic-Cretaceous boundary. Colloque sur la Limite Jurassique-Crétacé. *Bur. Rech. Geol. Minieres, Mem.*, 84–94.

Tremolada F., Bornemann A., Bralower T., Koeberl C. & van de Schootbrugge B. 2006: Paleoceanographic changes across the Jurassic/Cretaceous Boundary: the calcareous phytoplankton response. *Earth Planet. Sci. Lett.* 241, 361–371.

van de Schootbrugge B., Föllmi K.B., Bulot L.G. & Burns S.J. 2000: Paleoceanographic changes during the Early Cretaceous (Valanginian–Hauterivian): Evidence from oxygen and carbon stable isotope. *Earth Planet. Sci. Lett.* 181, 15–31.

Vašíček Z., Reháková D., Michalík J., Peterčáková M. & Halásová E. 1992: Ammonites, aptychi, nanno- and microplankton from the Lower Cretaceous Pieniny Formation in the "Kysuca Gate" near Žilina (Western Carpathian Klippen Belt, Kysuca Unit).

Západ. Karpaty Paleont. 16, 43–57.

Weissert H. 1989: C-isotope stratigraphy, a monitor of paleoenvironmental changes: A case study from the Early Cretaceous. *Surv. Geophys.* 10, 1–16.

Weissert H., McKenzie J.A. & Channell J.E.T. 1985: Natural variations in the carbon cycle during the Early Cretaceous. In: The carbon cycle and atmospheric CO_2: Natural variations Archean to the present. *Geophysic. Monograph.* 32, 531–545.

Wessely G. 2008: Kalkalpine Schichtfolgen und Strukturen im Wienerwald. *J. Alp. Geol.* 49, 201–214.

Appendix

Crossplot of the $\delta^{18}O$ vs. $\delta^{13}C$ values at Nutzhof (both vs. V-PDB).

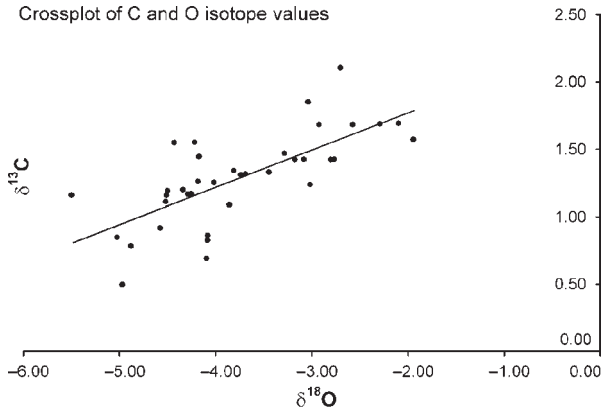

GEOLOGICA CARPATHICA, AUGUST 2010, 61, 4, 257–272 doi: 10.2478/v10096-010-0015-2

Stratigraphic correlation potential of magnetic susceptibility and gamma-ray spectrometric variations in calciturbiditic facies (Silurian-Devonian boundary, Prague Synclinorium, Czech Republic)

FRANTIŠEK VACEK[1], JINDŘICH HLADIL[2] and PETR SCHNABL[2]

[1]Charles University in Prague, Faculty of Science, Institute of Geology and Palaeontology, Albertov 6, 128 43 Prague 2, Czech Republic; fvacek@natur.cuni.cz
[2]Institute of Geology AS CR, v.v.i., Rozvojová 269, 165 00 Prague 6, Czech Republic; hladil@gli.cas.cz

(Manuscript received November 9, 2009; accepted in revised form March 11, 2010)

Abstract: Magnetic susceptibility (MS) and gamma-ray spectrometry (GRS) stratigraphy were used for correlation and characterization of eight Silurian-Devonian (S-D) sections in the Prague Synclinorium (Czech Republic). They represent two different facies developments: lower subtidal to upper slope deposits and slope-to-basin-floor distal calciturbidites. Sections from relatively shallow- and deep-water sections are easy to compare and correlate separately, although the detailed relationship between these two facies is still not entirely clear and correlations between the two settings are difficult. This may be due to sharp facies transitions and presence of stratigraphic gaps. The MS and GRS stratigraphic variations combined with sedimentologic data have been also used for reconstruction of the evolution of the sedimentary environment. The beds close above the S-D boundary show noticeably enhanced MS magnitudes but weak natural gamma-ray emissions. It may correspond to an increased amount of terrigenous magnetic material occurring with short-term shallowing (sedimentological evidence). In deep-water sections the uppermost Silurian is characterized by high MS and GRS values. It corresponds to a supply of recycled sediment to the lower wedge which occurred during the late Pridoli regression phase. The basal Devonian beds correspond to gradual deepening, but the overlying sequences reflect other shallowing episodes which are expressed in increasing MS and gamma ray activity of rocks. The MS and GRS fluctuations are interpreted as a result of local subsidence of the sea bottom along synsedimentary growth-faults and/or a biotic event rather than of eustatic sea-level changes.

Key words: Silurian-Devonian boundary, Prague Synclinorium, magnetic susceptibility stratigraphy, gamma-ray spectrometry, carbonate slope system.

Introduction

The Prague Synclinorium in central Bohemia (Czech Republic) provides many instructive sections exposing the Silurian-Devonian (Pridoli-Lochkovian) boundary strata, including the Global Boundary Stratotype Section and Point (GSSP) Klonk near Suchomasty and its auxiliary section at Budňanská skála (Budňany Rock) near Karlštejn. Two standard sections were approved by a decision of the International Commission on Stratigraphy at the 24th International Geological Congress in Montreal, 1972 (McLaren 1977). During more than thirty years of investigation these standard sections have been studied by various methods. Stratigraphic correlations here were traditionally based mainly on biostratigraphic data. In this stratigraphic succession graptolites and trilobites are practical for biozonation. However, the occurrences of index species depend on facies to various degrees. Microfossils, namely conodonts and Chitinozoa have high resolution potential, but detailed micropaleontological research was predominantly concentrated on the standard sections (Paris et al. 1981; Jeppsson 1988, 1989; Brocke et al. 2002, 2006; Carls et al. 2007). In many other sections precise biostratigraphic data are incomplete to mostly absent. In several recent papers different stratigraphic approaches were applied, including magnetic susceptibility (MS) stratigraphy (Crick et al. 2001) or chemostratigraphy (Hladíková et al. 1997; Herten 2000; Kranendonck 2000; Mann et al. 2001; Frýda et al. 2002; Buggisch & Mann 2004). Crick et al. (2001) introduced the MS stratigraphic profile for the GSSP at Klonk and a drilling core situated close to the surface section. They used the MS record for establishment of magnetosusceptibility event and cyclostratigraphic (MSEC) zones as an alternative stratigraphic tool. They also suggested possible interregional correlations with the area of the Anti-Atlas in Morocco using MSEC.

This study involves eight sections, which have been studied before for paleontology and sedimentology, but not for MS and GRS (gamma-ray spectrometry) stratigraphic variations. Both methods will be tested for the detailed stratigraphic correlations across varying facies and could also be used in combination with supplementary data for complex characteristics of the depositional environment and its evolution in several Silurian-Devonian (S-D) boundary sections in the Prague Synclinorium.

Geological setting

The Variscan folded Silurian and Devonian formations crop out in the central part of the Prague Synclinorium between Prague and vicinity of Beroun (Fig. 1). They consist of marine sediments (mostly shales and limestones; Chlupáč et al. 1998) and submarine volcanic rocks (basic volcanics and coeval basic/ultrabasic volcaniclastics; Fiala 1970; Patočka & Štorch 2004). Prague Synclinorium was interpreted as located on the northern margins of Gondwana during the S-D interval with affinities to Armorica (e.g. Krs & Pruner 1995; Krs et al. 2001), at a paleolatitude of about 17°S (Patočka et al. 2003).

The S-D boundary is situated close to the boundary between the Požáry (approximately corresponding to the Pridoli Series) and Lochkov Formations (~the Lochkovian Stage). Both formations are generally characterized by lateral transition from coarse-grained bioclastic limestones in the NW part of the synclinorium to fine-grained limestones and shales in the SE part (Chlupáč et al. 1998), defining a NW shallow zone and SE deeper zone. However, the boundaries of these two lithostratigraphic units are slightly diachronous over the region. Proximity of the S-D boundary is broadly characterized by blooms of pelagic crinoids with plate-type loboliths, typically *Scyphocrinites*, which often (but not always) occur in the beds of the latest Pridoli and early Lochkovian ages. They may form several meters thick beds of coarse-grained crinoidal limestones at the base of the Lochkov Formation, informally called the *Scyphocrinites* Horizon (*Scyphocrinites* H). It may be locally associated with cephalopod limestones and also with beds of flat-pebble conglomerates. It is better recognizable in the deeper zone because in the shallow-water environment it may be concealed by overall bioclastic deposition.

Several localities exposing the S-D boundary strata representing the two different facies were selected for study (see Fig. 1, Table 1). These facies were deposited on the margin of an open-sea carbonate shelf with adjacent carbonate slope environment (Vacek 2007). Generally a deepening trend can be traced from the NW to the SE of the basin.

Methods

Limestone "beds" are traditionally numbered 1, 2, 3, etc., designations such as 1/2, 2/3 are used for the shale "interbeds".

Magnetic susceptibility study

In the last ten years, the number of studies on stratigraphic MS variations in the Devonian marine carbonate or mixed sequences has increased significantly (Crick et al. 1997, 2000, 2001, 2002; Ellwood et al. 2000, 2001, 2006; da Silva & Boulvain 2006; Hladil et al. 2006; da Silva et al. 2009a,b, 2010; Koptíková et al. 2010).

The outcrop sections were sampled for the MS study at 0.05 m intervals. Small cubic or slice rock samples were collected (20–50 g). Only fresh samples were taken (i.e. avoiding the veins, visible pyrite or limonite aggregates, various spots related to late diagenetic alterations and weathering, epigenetic dolomitization and also shear-deformed parts of the rock). The thickness of the MS profiles ranges from 4 to 11 meters depending on geological conditions. The complete sample collection includes more than 1,000 samples. Measurements were carried out in the Laboratory of Paleomagnetism (Inst. Geol. AS CR, Prague) on Kappabridges KLY-2 and 3 (produced by Agico Ltd. Brno; for technical details we refer to www.agico.com). The values of magnetic susceptibility in this paper are expressed as mass-related magnetic susceptibility (10^{-9} $m^3 \cdot kg^{-1}$). These are further referred as MS values which are used for plotting the curves and assessment of their possible stratigraphic importance.

Magnetic susceptibility is the intrinsic property that determines the amount of magnetism, which a rock can have in a given magnetic field. It is related to bulk chemistry and magnetic mineralogy and particularly to the amounts of easily magnetizable minerals in a rock sample. The increased MS signal in limestones is induced by presence of various ferromagnetic (s.l.) minerals (magnetite, maghemite, hematite, monoclinic pyrrhotite), and also weakly magnetic but much more abundant paramagnetic minerals (clay minerals, pyroxene, amphibole, biotite, chlorite, pyrite, chalcopyrite, a.o.).

In contrast, diamagnetic minerals such as calcite, quartz, and others have very weak negative MS magnitudes and reduce mass susceptibility of a rock sample. However, the MS of detrital ferromagnetic and paramagnetic minerals is much greater than the MS of diamagnetic minerals. Therefore, a small amount of even weakly paramagnetic mineral can significantly outweigh the MS of volumetrically more abundant diamagnetic minerals (Ellwood et al. 2000).

The amount of magnetic particles mainly depends on terrigenous influx, which is mostly controlled by fluctuations in sea level. Generally, the maximum input of terrigenous detritus corresponds to intensive erosion during the lowstand of sea level. This is considered to be recognizable on both the regional and global scale because of synchronous variations in global erosion controlled by eustasy (Ellwood et al. 2000, 2001). The large-scale redistribution of sub-silt and silt-sized particles (< 63 μm) often comes about through eolian transport, and the deep parts of carbonate slopes can also be affected by distant riverine flux (Hladil 2002; Hladil et al. 2006).

Magnetite can also be produced by magnetotactic bacteria or algae. However, it is mostly formed in shallow-water conditions with restricted circulation, which is not the case of the studied sections. The other magnetically important mineral components related to deep-water carbonate or mixed carbonate-siliciclastic sediments are authigenic carbonates with iron in lattices or iron-oxide inclusions (siderite and rarely other minerals; e.g. Ellwood et al. 1988; Frederichs et al. 2003), and these are also tentatively related to bacterially-mediated precipitates. For more discussion on the primary and secondary magnetic minerals in carbonates we refer to da Silva et al. (2009a).

Rock magnetic methods

Several methods have been used for identification of possible carriers of the MS. They have been applied both on miner-

al concentrates obtained by dissolution in acids (10 samples; X-ray diffraction — XRD; temperature dependence of the MS; magnetic hysteresis) and the whole-rock samples (5 samples; isothermal remanent magnetization — IRM).

Mineral concentrates have been obtained by leaching in 10% hydrochloric and acetic acids, separately. However, some important magnetic minerals such as iron oxides may be dissolved in these acids, therefore we had to also use the IRM method applied to whole rock (see above).

The method of temperature dependent MS identifies magnetic minerals and mineralogical phase changes during heating. It was measured using KLY-4S Kappabridge (produced by Agico Ltd. Brno; Jelínek & Pokorný 1997) combined with a temperature control unit CS3 (Parma & Zapletal 1991) in the temperature range of 20–700 °C in an argon atmosphere. Paramagnetic minerals exhibit parabolic-shaped MS decay curves at relatively low temperatures (up to ~200 °C) because the MS of these minerals is inversely proportional to the temperature (Hrouda 1994). On the other hand, ferromagnetic minerals usually show increasing MS up to the point where it decays to the Curie temperature. For magnetite the Curie temperature is ~580 °C and for hematite it is ~680 °C.

The method of magnetic hysteresis is based on response of a magnetic material to magnetic field. Hysteretic behaviour is highly dependent on mineralogy and grain size (Tauxe et al. 1996). The sample is placed in an intensive magnetic field (+1 T) and magnetization is examined as the applied intensity drops to zero and then increases to the negative maximum (–1 T). Changes in magnetization during regaining of the original intensity (+1 T) are significant for interpretation of magnetic components. These measurements were performed on a vibrating sample magnetometer Model 3900 VSM (produced by Princeton Measurement Corporation).

IRM was measured on Pulse Magnetizer MMPM 10 (produced by Magnetic Measurements Ltd.) and magnetometer JR6a (produced by Agico Ltd. Brno) in order to identify coercivity spectra. The used field range was 10 to 2000 mT. Contribution of particular magnetic components ferromagnetic to the total remanent magnetization has been tested by the IRM component analysis (Kruiver et al. 2001). Various magnetic minerals can be identified by $B_{1/2}$ values, which is the magnetic field at which a half of Saturated Isothermal Remanent Magnetization (SIRM) is reached. For magnetite it is 20–63 mT, hematite 63–200 mT, and goethite >1 T (Grygar et al. 2003).

Gamma ray spectrometry study

The spectral gamma-ray approach is a significant parallel to MS-detected concentrations of background sediment impurity in limestone (Hladil et al. 2006). The MS-GRS combination has an overall potential to improve the quality of MS based stratigraphic correlation, with the background reasoning in magnetomineralogy.

The gamma-ray spectrometric (GRS) based correlations of outcrop logs have been frequently used in the last decade in the Devonian of the Czech Republic on the platform to basin formations of Moravia (Hladil et al. 2000, 2003a,b; Hladil 2002; Geršl & Hladil 2004; Bábek et al. 2007, a.o.) or Prague Synclinorium (Slavík et al. 2000; Koptíková et al. 2007, 2008, 2010).

For this study, a gamma-ray spectrometer Geofyzika-Satis-Geo GS-512 with NaI(Tl) scintillation detector 3″×3″ (7.62×7.62 cm) and 3″ photomultiplier was used (SatisGeo 2009). This instrument was used in the mode that the whole element concentrations of K (%), U (mg/kg=ppm) and Th (ppm) were automatically calculated. The instrument was calibrated at the regional reference centre of Bratkovice near Příbram (parameters frequently quoted, e.g. Lis et al. 1997). Using this technique and instrument, the gamma rays registered for this purpose correspond to isotopes ^{214}Bi and ^{208}Tl, uranium and thorium decay series isotopes in naturally occurring materials, respectively. The data on potassium is obtained using the spectra for ^{40}K isotope. The total natural gamma-ray variation has been inferred from selected energy windows, all above 720 keV. With this instrument, this additional parameter is set to display automatically a notional uranium equivalent (eU) that is routinely expressed in mg/kg (ppm) of U-equivalent contents, but for imagination or rough comparison only. In addition, the recalculation to API units or radioactive doses cannot be accomplished in general terms, for its relationships to techniques, conditions and details of probes or instruments (Geršl & Hladil 2004). These approximate data on the totals of natural gamma ray (NGR or GR) emission from measured sedimentary rocks often differs according to apparatuses and has, therefore, only relative and not absolute information value.

The thicknesses of the GRS logs are identical with the MS ones, except the lower part of the Praha-Podolí section, which could not be measured due to its intensive weathering.

The GRS measurement was performed with 0.25 m step at a time of 240 seconds, perpendicular to the rock face at the full contact. This regular spacing strategy was preferred over the irregular (rock-type selective) one. This choice was based on the preliminary-test findings that gamma-ray signal of different magnitudes and structure was obtained from the beds of comparable lithology (e.g. great variation within the class of coarse-grain calciturbidites, or the same for the very fine-grained shale interbeds). The size of this 0.25 m step was selected heuristically but with respect to the fact that approximately 95% signal at the front of the probe (with crystal) originates from a slightly deformed hemisphere of measured rocks that corresponds to a target of 0.25 m radius at an ideal planar surface (Løvborg et al. 1971). Hence, this empirically tested precondition for overlapping of measurements with these sections makes possible to keep the overlap below 15 % of the signal, even for irregular arrangements of beds and rock materials. The combined error from conditions, instrument and repeated measurements was established to be less than about ±7.5 % for the whole element U, Th, K automatically calculated results.

Detected concentrations of K, U, and Th are mostly related to amount of feldspars, micas, and clay minerals, among others. Uranium is also known to be remarkably trapped in organic matter (e.g. Durrance 1986). Higher concentrations of these elements should again reflect increased amount of non-carbonate impurities in limestones that are caused by detrital

influx from a supposed land surface in both the regional and interregional contexts.

Sedimentology and studied sections

The lithology, sedimentology, and biostratigraphy of the selected sections have been described in many previous papers (for more details we refer to Chlupáč et al. 1972; Hladil 1991, 1992; Čáp et al. 2003; Vacek 2007).

Shallow facies

The relatively shallow-water carbonate facies with predominance of bioclastic, mainly crinoidal packstones to grainstones is distributed in the NW flank of the synclinorium with several other finger-like projections in its western part (studied sections at Požáry Quarry near Praha-Řeporyje, Srbsko, and Opatřilka Quarry near Praha-Holyně; Fig. 1, Table 1). These deposits locally show reworking by storms, which indicates the conditions above the storm wave base. It corresponds to the lower subtidal to upper slope environment.

The shallow-water carbonate facies possess rich benthic fauna, including crinoids and trilobites, and brachiopods. The uppermost Silurian is characterized by abundant occurrence of the index trilobite *Tetinia minuta*. The first appearance of trilobite *Warburgella rugulosa rugosa* indicates the base of Devonian (Chlupáč et al. 1972).

Deep facies

Deep-water facies are distributed in the SE flank of the Prague Synclinorium (sections at Karlštejn, Klonk, Praha-Radotín and Praha-Podolí; Fig. 1, Table 1). These facies are characterized as dark bioclastic and peloidal wackestones/packstones to mudstones alternating with calcareous shales, locally with several meters thick *Scyphocrinites* H. They yield common pelagic fauna, including graptolites, cephalopods and ostracods. The S-D boundary interval is characterized by abundant occurrence of crinoids of *Scyphocrinites* sp. The uppermost Silurian corresponds to the graptolite *Monograptus transgrediens* Zone. The base of Devonian is marked by the first appearance of the index graptolite *Monograptus uniformis* (Chlupáč et al. 1972). Other fossil groups (conodonts,

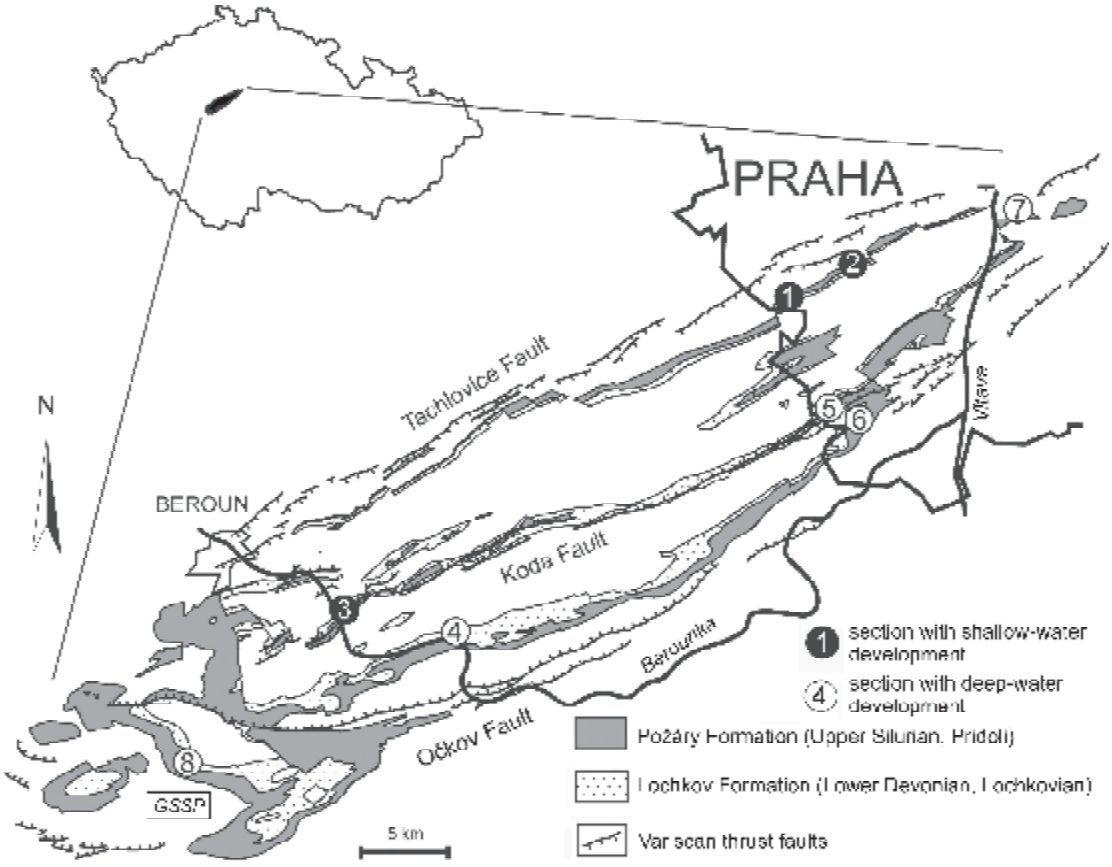

Fig. 1. Position of the studied localities in the Prague Synclinorium area: **1** — Požáry Quarry near Praha-Řeporyje; **2** — Opatřilka Quarry near Praha-Holyně; **3** — Srbsko; **4** — Karlštejn (Budňany Rock); **5** — Praha-Radotín (U topolů); **6** — Praha-Radotín (near Cement Plant); **7** — Praha-Podolí; **8** — Klonk near Suchomasty. **GSSP** — Global Boundary Stratotype Section and Point. The geological sketch map of the Prague Synclinorium benefits partly from the working materials provided by R. Melichar.

Table 1: List of studied sections with their geographical position, measured intervals and numbers of analysed MS samples and GRS measurements. * The GRS measurements were performed in the bed interval 10–12 only due to poor state of the lower part of the section.

No.	Section	Location	Sampling interval	MS	GRS	Environment
1	Požáry Quarry	50° 1' 42.3" N; 14° 19' 28.4" E	beds 155–163 (9 m)	177	36	Shallow
2	Opatřilka Quarry	50° 2' 8.1" N; 14° 21' 2.7" E	beds 1–8 (10 m)	200	41	Shallow
3	Srbsko	49° 56' 29.6" N; 14° 7' 57.2" E	beds 1–3 (6 m)	120	25	Shallow
4	Karlštejn	49° 56' 4.5" N; 14° 10' 51.4" E	beds 1–42 (11 m)	224	45	Deep
5	Praha-Radotín (U topolů)	49° 59' 51.2" N; 14° 20' 2.6" E	beds 1–31 (7 m)	141	28	Deep
6	Praha-Radotín (near Cement Plant)	49° 59' 33.9" N; 14° 20' 46.4" E	beds 9–14 (3.5 m)	70	15	Deep
7	Praha-Podolí	50° 3' 6.9" N; 14° 25' 7.6" E	beds 1–11 (3.5 m)	76	9*	Deep
8	Klonk near Suchomasty	49° 54' 1.3" N; 14° 3' 46.3" E	1–44 (12.75 m)	adopted from Crick et al. (2001)	52	Deep

Chitinozoa) can be used as auxiliary indicators (Paris et al. 1981; Brocke et al. 2002, 2006; Carls et al. 2007).

This facies is interpreted as rhythmical distal calciturbidites deposited on carbonate slope and its toe (often with the Bouma Tc and Td units). These turbidite beds alternate with layers of the "background" hemipelagic sediments (Te), which are preserved mostly in the form of highly compacted calcareous shales. The occurrences of channelized calciturbidite grainstones and rudstones with several layers of flat pebble conglomerates are interpreted as debris flow deposits or dense turbidite flows. The input of the coarse-grained detrital material of shallow-water origin was interpreted as the result of relative sea-level drop in the S-D boundary interval and possible subsidence along synsedimentary growth faults (Vacek 2007).

The MS and GRS stratigraphy of the studied sections

Main characteristics of the MS and GRS records of the shallow facies

Generally, the carbonate rocks in the studied sections have relatively low MS signal in the order of 10^{-9} $m^3 \cdot kg^{-1}$ (further referred as 10^{-9} SI Units). Shallow-water bioclastic packstones/grainstones exhibit relatively low differences of the average MS values between the Požáry and Lochkov Formations (see Table 2, Fig. 2). The MS curves mostly show only low to moderate oscillations (see Fig. 2). The critical S-D boundary interval in the shallow-water deposits (especially the Požáry Q and Opatřilka sections) is marked by enhanced MS values. In the Požáry Q this increase is observable directly above the boundary in the lowermost part of bed No. 159 (see Fig. 2A). In the Opatřilka section, the same pattern characterized by high oscillation is recognizable in bed No. 8 approximately 1 m above the first appearance of *W. rugulosa rugosa*, which determines the S-D boundary (Fig. 2B). However, this pattern is less distinctive in the Srbsko section (Fig. 2C).

This facies is characterized by relatively low concentrations and variations of potassium in the Požáry and Srbsko sections (0.3–0.5 %; Table 2). The concentrations of K show a considerably weak covariance with those of Th (R^2=0.37 and 0.47). On the contrary, at Opatřilka this covariance is very high (R^2=0.91). Correlation between K and U and Th and U is also generally weak, with the concentration of U changing quite independently of K and Th. Trends of the eU curves visually correspond mostly to variations of U, less to Th concentrations (Fig. 2A–C). It corresponds well to the fact that the Th/U ratio is generally very low, with an average of 0.17–0.39 (i.e. the GRS-based concentrations for U are much higher than

Table 2: Average magnitudes of the MS and GRS-based concentrations in the studied sections or their distinguished segments. **S** — Silurian; **D** — Devonian; **Po** — Požáry Fm; **Sc** — *Scyphocrinites* H; **Lo** — Lochkov Fm. The uppermost part of the Požáry Fm in the Podolí section was not GRS measured due to weathering. The "raw" MS data for the Klonk section were not available.

Sections/their segments	MSχ [10^{-9} $m^3 \cdot kg^{-1}$]	eU [ppm]	K [%]	U [ppm]	Th [ppm]
Požáry Q. *Po* (0.0–4.40 m)	9.8	7.5	0.5	5.3	1.5
Lo (4.45–8.7 m)	11.0	5.8	0.5	3.8	1.5
Srbsko *Po* (0.0–4.75 m)	7.3	4.5	0.3	3.6	0.9
Lo (4.8–6.0 m)	5.3	4.6	0.4	2.7	0.8
Opatřilka Q. *Po* (0.0–6.5 m)	9.0	14.9	1.0	10.3	2.1
Lo (6.55–9.9 m)	11.3	11.7	0.3	10.6	1.0
Klonk *Po* (0.0–5.25 m)	–	13.6	1.7	5.2	5.1
Lo (5.3–12.75 m)	–	8.8	1.2	3.1	3.2
Karlštejn *Po* (0.0–2.45 m)	30.2	22.4	1.7	13.6	5.6
Sc (2.5–7.45 m)	1.8	8.4	0.5	6.1	1.6
Lo (7.5–11.1 m)	10.2	7.2	0.8	3.6	2.3
U topolů *Po* (0.0–1.95 m)	28.9	14.8	1.9	6.0	4.6
Sc (2.0–3.35 m)	3.8	13.0	0.6	10.2	1.6
Lo (3.4–7.0 m)	5.6	9.3	0.9	5.4	2.2
Radotín *Sc* (0.0–1.15 m)	6.9	10.4	0.7	7.4	2.5
Lo (1.2–3.45 m)	5.9	6.5	0.6	3.8	1.9
Podolí *Po* (0.0–1.65 m)	29.5	–	–	–	–
Sc (1.7–3.75 m)	3.3	16.1	0.7	12.7	2.5

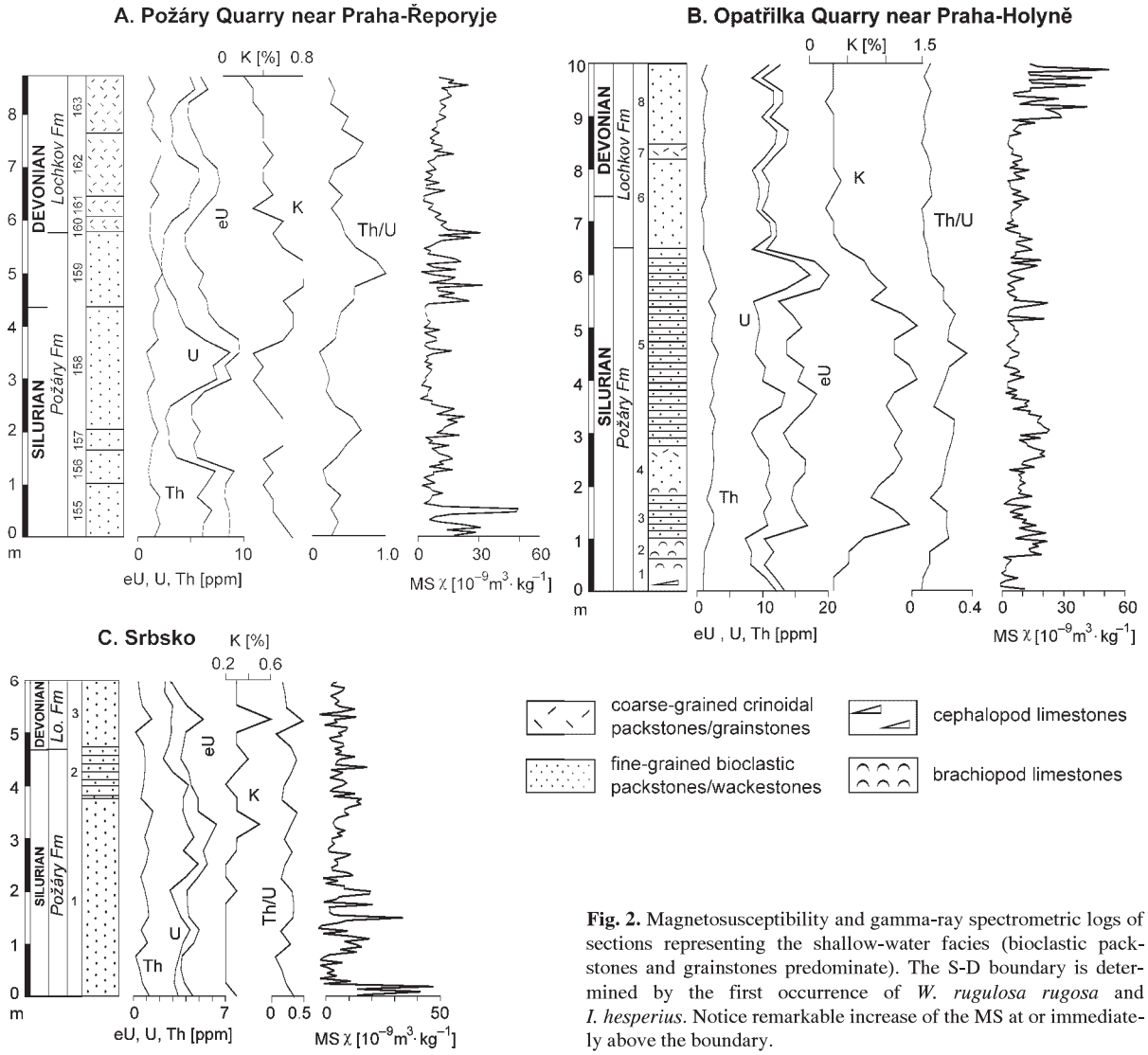

Fig. 2. Magnetosusceptibility and gamma-ray spectrometric logs of sections representing the shallow-water facies (bioclastic packstones and grainstones predominate). The S-D boundary is determined by the first occurrence of *W. rugulosa rugosa* and *I. hesperius*. Notice remarkable increase of the MS at or immediately above the boundary.

for Th) and shows only slight variations. The eU curves of all sections possess more or less conspicuous wave-like cyclic patterns.

Main characteristics of the MS and GRS records of the deep facies

Three different segments can be distinguished in the deep-water sections (mudstones/wackestones alternating with calcareous shales). The first one corresponds to the uppermost part of the Požáry Formation. It is characterized by high oscillations and the highest MS mean values in the studied sections (28.9–30.2 10^{-9} SI Units, maximum up to 95; Table 2). The overlying coarse-grained crinoidal limestones of the *Scyphocrinites* H (the lowermost part of the Lochkov Formation) have much lower average magnitudes (1.1–7.6 10^{-9} SI Units; see Fig. 3B–E). Amplitudes of the MS curves are also much lower. The upper segment corresponds to recovery of distal calciturbidite deposition higher in the sections. It is characterized by a slight increase in the MS (mean 5.6–10.2 10^{-9} SI Units), but not as high as in the uppermost part of the Požáry Formation.

The broader S-D interval is characterized by a remarkable decrease of the MS magnitudes associated with facies change (Fig. 3).

This facies shows much higher variations in the K content. The K concentrations are highest in the distal calciturbidite facies of the uppermost part of the Požáry Formation (average concentrations 1.7–1.9 %; Table 1). The K contents tend to decrease upwards and reach their minima within the *Scyphocrinites* H (average contents 0.5–0.7 %). The recovery of platy limestone/shale deposition is marked again by a slight increase in K concentrations (Fig. 3B–E). Generally, the amount of K shows excellent covariance with Th (R^2=0.87–0.98), while correlation between K and U and Th and U remains weak or has even slightly negative values (U topolů, Radotín,

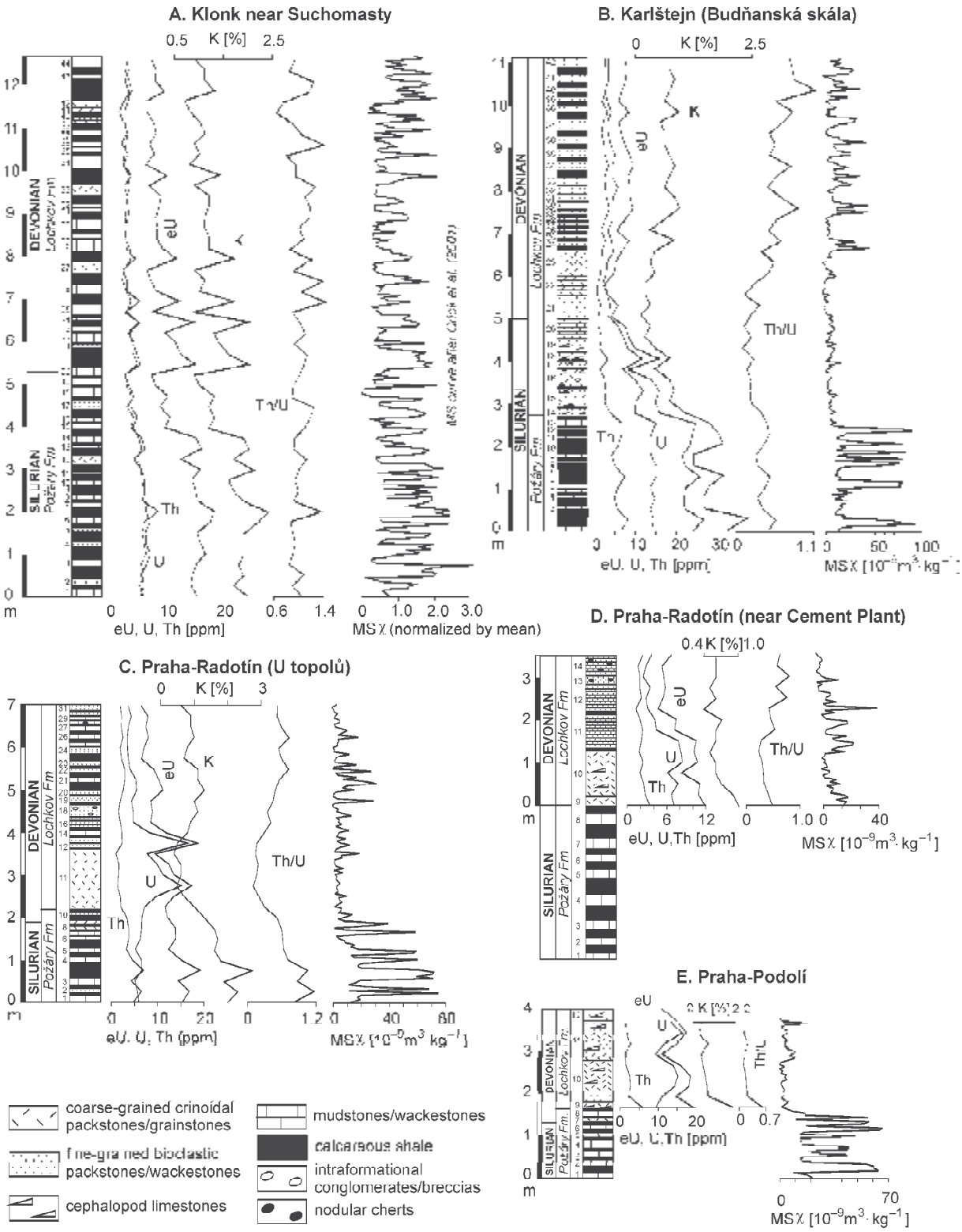

Fig. 3. Magnetosusceptibility and gamma-ray spectrometric record of sections representing the deep-water facies (slope distal calciturbidites predominate). The S-D boundary is determined by the first occurrence of *M. uniformis*. The lithological log of the GSSP at Klonk was modified after Chlupáč et al. (1972). The normalized MS curve was adopted from Crick et al. (2001).

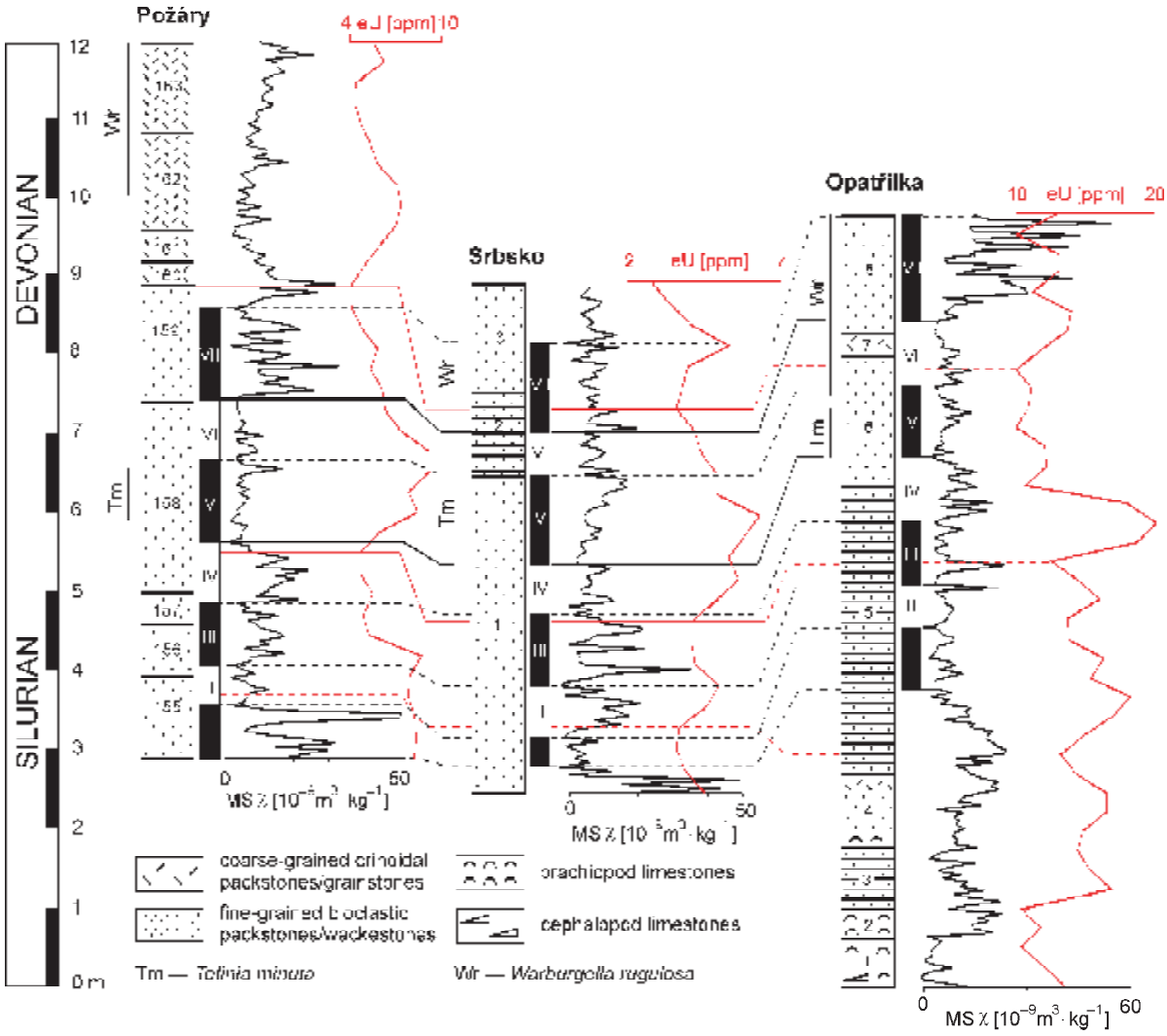

Fig. 4. The MS (**black lines**) and GRS (**red lines**) correlation of shallow-water sections. Correlative MS patterns are assigned by Roman numbers I–VII. Solid lines mark reliable, dashed lines mark less certain correlations. Taxon ranges after Chlupáč et al. (1972): solid lines indicate occurrence in this interval.

fossils in coarse-grained calciturbidites and mass flow conglomerates.

Magnetic susceptibility and mineral carriers

Several samples were collected from the studied sections for assessment of the magnetic composition of insoluble residue. These samples were taken in order to represent the main lithological types (macrofacies): crinoidal grainstones (Opatřilka Quarry, the upper part of bed No. 8; sample O8), coarse-grained crinoidal packstones of the *Scyphocrinites* H (Radotín — near the Cement Plant, the lower part of bed No. 10; sample R10), fine-grained mudstone to bioclastic wackestone (Karlštejn, bed No. 10; sample K10), laminated bioclastic wackestone (Karlštejn, bed No. 27), and calcareous shale (Karlštejn, bed No. 31/32). They were dissolved in 10% hydrochloric and acetic acids, separately. The amount of insoluble residue varies between 2 % (bioclastic packstones/grainstones) and 30 % (calcareous shales). The insoluble residues were analysed by X-ray diffraction (XRD), which identified common minerals including quartz (semi-quantitative content 60–80 %), albite (1–12 %), microcline (3–7 %), kaolinite (~1%), muscovite (5–10 %), chlorite-serpentine (1–12 %), and pyrite (1–20 %). However, some important magnetic minerals such as iron oxides may be leached during dissolution in acids. Therefore several rock magnetic methods applied to the whole-rock samples have been used for identification of them.

The results of rock magnetic analyses showed that most of the studied samples contain small amount of hematite, magnetite, and goethite. Our measured $B_{1/2}$ values for magnetite are in the range of 37–60 mT, hematite 63–200 mT, and goethite 1023–2884 mT. However, these minerals contribute only very little to the total MS (see Figs. 4 and 5). Both magnetite and

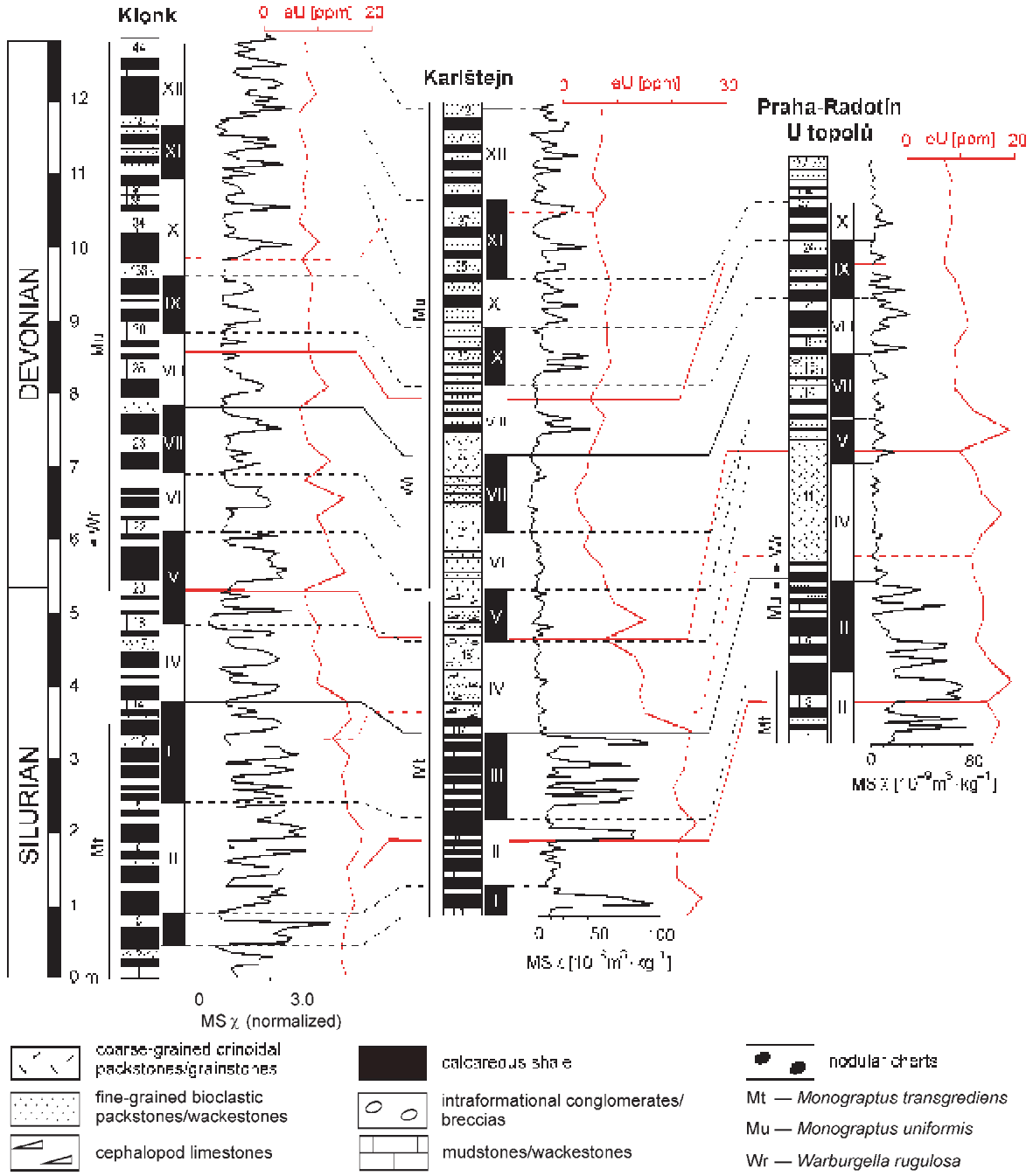

Fig. 5. The MS (**black lines**) and GRS (**red lines**) correlation of deep-water sections. Correlative MS patterns are assigned by Roman numbers I–XII. Solid lines mark reliable, dashed lines mark less certain correlation. Notice variable thickness or lack of distinguished MS patterns. It indicates unequal rate of preserved sediments due to variable supply or post-sedimentary erosion. Taxon ranges after Chlupáč et al. (1972) and Čáp et al. (2003): solid lines indicate occurrence in this interval, dots indicate occurrence in this bed only.

hematite can also be of diagenetic origin, while goethite is often a weathering product. If so its amount could not be related to depositional processes.

Possible effects of secondary magnetite and other ferromagnetic minerals have been tested by the IRM component analysis. Contribution of the above mentioned minerals has been measured on 37 samples with remarkably high or low MS. The percentage contribution of magnetite to the remanent magnetization has been compared with the bulk MS of the samples (Fig. 5). Their covariance is very low ($R^2 = -0.34$), showing that the MS does not depend on magnetite content, and thus the role of diagenetic magnetite may be excluded.

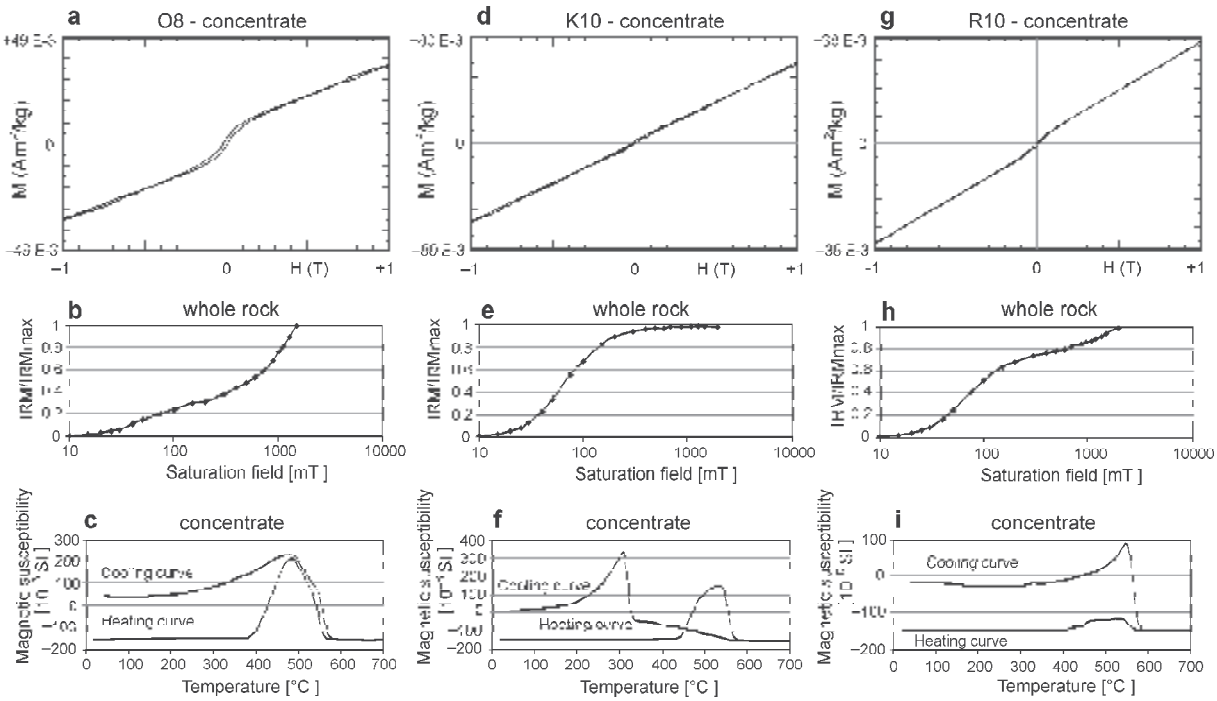

Fig. 6. Thermomagnetic and hysteresis behaviour of three mineral concentrates obtained by dissolution in acetic acid and isothermal remanent magnetization (IRM) curves measured on whole-rock samples. **Sample O8** (for description see the text): The hysteresis curve **a)** shows both paramagnetic and ferromagnetic behaviour. It is confirmed by the IRM acquisition curve **b)** with $B_{1/2}$ = 1071 mT typical for highly coercive goethite. The temperature variations of magnetic susceptibility **c)** indicate formation of magnetite between 400 and 500 °C. The Curie point of this magnetite is at 560 °C. **Sample K10**: The hysteresis curve **d)** indicates only paramagnetic behaviour. Nevertheless, the IRM acquisition **e)** proves that a small amount of low to medium coercivity mineral such as magnetite or hematite is present ($B_{1/2}$ = 72 mT). The temperature variations of susceptibility **f)** show formation of magnetite between the temperatures of 450 and 500 °C. The Curie point of this magnetite is at 570 °C. During progressive heating pyrrhotite is formed, its Curie is point at 320 °C. **Sample R10**: The hysteresis curve **g)** demonstrates paramagnetic behaviour and only subordinate indications of a ferromagnetic material. However, the IRM acquisition **h)** shows the presence of two different magnetic minerals: magnetite/hematite ($B_{1/2}$ = 70 mT) and goethite ($B_{1/2}$ = 2041 mT). The increase in magnetic susceptibility during heating above 400 °C **i)** is caused by newly-formed magnetite with the Curie point at 560 °C. Consequent heating creates pure magnetite with its Curie point at 580 °C.

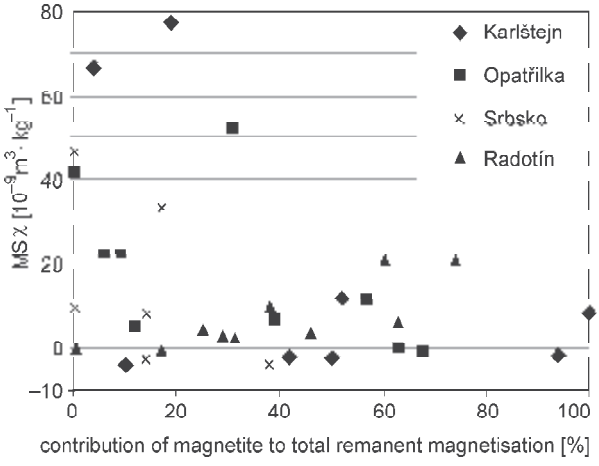

Fig. 7. Plot showing relationship between percentage magnetite contribution to the total remanent magnetization (IRM component analysis) and the MSχ. It is obviously weak (R^2 = −0.34) so that we can exclude possible effect of secondary diagenetic magnetite on the MS variations.

The major effects on rock magnetic susceptibility must be ascribed to varying amounts of paramagnetic detrital minerals (e.g. iron-bearing muscovite, chlorite) and only subordinately to oxides and sulphides (hematite/maghemite, pyrite/pyrrhotite). This fact justifies our following interpretations of the MS stratigraphic variations with respect to changing input of eroded detrital material related to sea-level fluctuations.

It is surprising that illite, which was often reported as an abundant component of the insoluble residues in the Požáry Formation on many places of the Prague Synclinorium (Suchý & Rozkošný 1996; Suchý et al. 1996) was not found. On the other hand, the indicated amounts of white mica are considerably higher than normally expected. It also belies the infrared-absorption and chemically based detections of up to several per cent of illite in the S-D sediments at Klonk (Hladil 1992) where the XRD evidence was also unclear. In this case, it was tentatively explained that due to the extensive damage to illite structures in ultrafine subcrystalline mixtures with quartz, organic matter, and carbonates. The absence of typical illite spectra in XRD diagrams can be explained by its low relative concentrations at ~ 1 % or less, but the possible presence

of both very high and very low crystalline forms related to illite remains unsolved.

The greatly increased amounts of albite and microcline are interesting in comparison with the proportions of plagioclases, pyroxenes and amphiboles, which were detected in these rocks together with small, basalt related volcaniclastic grains by direct observation and Energy Dispersive X-ray Spectroscopy (EDX; e.g. Hladil 1992), but which have no significant record in XRD. At least some of these albites and microclines can be considered authigenic, but the differentiation between the detrital and authigenic populations according to their crystal shapes and compositions (cf. Kastner 1971; Kastner & Siever 1979; Mišík 1994) does not yet provide unambiguous evidence in favour of this origin. Of course, quartz and also kaolinite (to lesser extent) are probably not only of purely detrital origin (Hladil 1992).

Interpretation of the MS and GRS records

The MS and GRS variations can be used not only for stratigraphic correlations of the studied sections but also for interpretation of sedimentary environments and their evolution (especially in combination with sedimentological data). It is based on methods and principles described in chapter Methods.

The lowermost Lochkovian (and approximately the basal part of the Lochkov Formation) in the shallow-water sections is characterized by an abrupt increase of the MS (Fig. 2). On the other hand, the eU curves mostly exhibit decreasing trend in the proximity of the S-D boundary (Fig. 2). It is mostly related to decline of U content. It does not need to respond to the decreasing content of clay, however. Very low covariance of K and U contents indicates different natures and sources of these two components. Potassium is related to clay minerals and K-feldspar, while U is also known to be significantly trapped in organic matter. A slight increase of K concentrations immediately above this pattern is indicative of higher amount of clay minerals.

Thus, both magnitudes indicate enhanced amount of non-carbonate impurities (magnetic components and clay) and may be interpreted as a result of sea-level fall, which caused increased erosion and terrigenous influx to marine environments (Ellwood et al. 2000). This is in accordance with sedimentological data, which also suggest a shallowing trend in the lowest parts of the Lochkov Formation (approximately the base of Lochkovian). It is expressed in partial sorting and reworking/rounding of bioclasts and washing out of fine-grained matrix in grainstone deposits in contrast to underlying strata (Vacek 2007).

In deep-water facies the high oscillation of the MS curve in the upper part of the Požáry Formation (generally the uppermost Pridoli) is related to alternation of limestone and shale interbeds (Figs. 3 and 8). It is noticeable that there are a number of analysed limestone beds, which have higher MS values than the background hemipelagic shale interbeds, which usually possess a higher amount of insoluble residue. It may be indicative of larger amount of detrital magnetic particles delivered to the basin with calciturbidites. The short-term facies change occurring in the slope environment as the *Scyphocrinites* H at the base of the Lochkov Formation (and close to the S-D boundary) is usually interpreted as a result of a relative sea-level fall, which caused increased erosion in shallow-water areas (e.g. Kříž et al. 1986; Chlupáč & Kukal 1988; Crick et al. 2001; Vacek 2007). Such facies changes indicating relative shallowing of sedimentary environments have been described from other regions of Europe (e.g. Carnic Alps — Schönlaub et al. 1994), and North America (e.g. central Nevada — Klapper & Murphy 1975; Matti & McKee 1977; Appalachian Basin — Denkler & Harris 1988). However, this event should be accompanied by increased magnitudes of the MS with enhanced supply with terrigenous detrital magnetic particles. It is interesting that the MS of these rocks is much lower than of the underlying limestone/shale sequence (Fig. 3). It might be explainable either by dispersion of fine-grained magnetic particles in the bulk of calcium carbonate (carbonate dilution effect) or by significant washing-out before re-deposition to slope and toe-of-slope environments (e.g. da Silva & Boulvain 2006). More properly, the observed effects of irregular washing of fine-grained matrix (often combined with current-driven orientation of cephalopod shells in these beds) suggest condensed deposition affected by bottom currents. Another explanation of deposition of *Scyphocrinites* H occurring in the described facies mosaics may be increased local subsidence at synsedimentary growth faults (namely "the precursor" Koda Fault, as presumed e.g. by Kříž 1992 or Vacek 2007) and a large amount of carbonate material with primary low concentrations of magnetic minerals derived from the upper part of the slope (as documented by the presence of carbonate lithoclasts derived from slope areas). Thus, this locally developed rapid carbonate sedimentation alternating with periods of sedimentary starvation is not expressed in enhanced MS values. Another explanation of the decline of the MS can be proposed as a restriction of terrigenous input during transgression. According to Schlager et al. (1994), the maximum thickness of calciturbidites corresponds to periods of increased carbonate production during sea-level rise (highstand shedding).

An evident decreasing eU tendency from the upper Požáry Formation to the lowermost Lochkov Formation (related to concurrently decreasing K, U, and Th concentrations) was documented in records from the deep-water sections (especially Klonk and Karlštejn; Fig. 3). In the latter, it culminates within the *Scyphocrinites* H. The overlying limestone/shale sequence of the Lochkov Formation is again characterized by a slight increase of detected GRS values (Fig. 3). Here, the main eU peaks partly correspond to background shale sediments with greater proportion of insoluble residue (namely clay minerals). However, there are also peaks situated within the seemingly massive bedding sets of proximal, often amalgamated calciturbidites (Karlštejn or Radotín-U topolů; Fig. 3B and C). At the U topolů section two distinctive U peaks (related to the GRS-based concentrations of 15.1 and 16.4 ppm) are situated within and slightly above the *Scyphocrinites* H (bed 11, section 2.75 and 3.75 m — Fig. 3C), which do not match enhanced K and Th values. Uranium is known to be highly mobile during diagenesis, so these enormous peaks may correspond to post-sedimentary concentration or indicate consider-

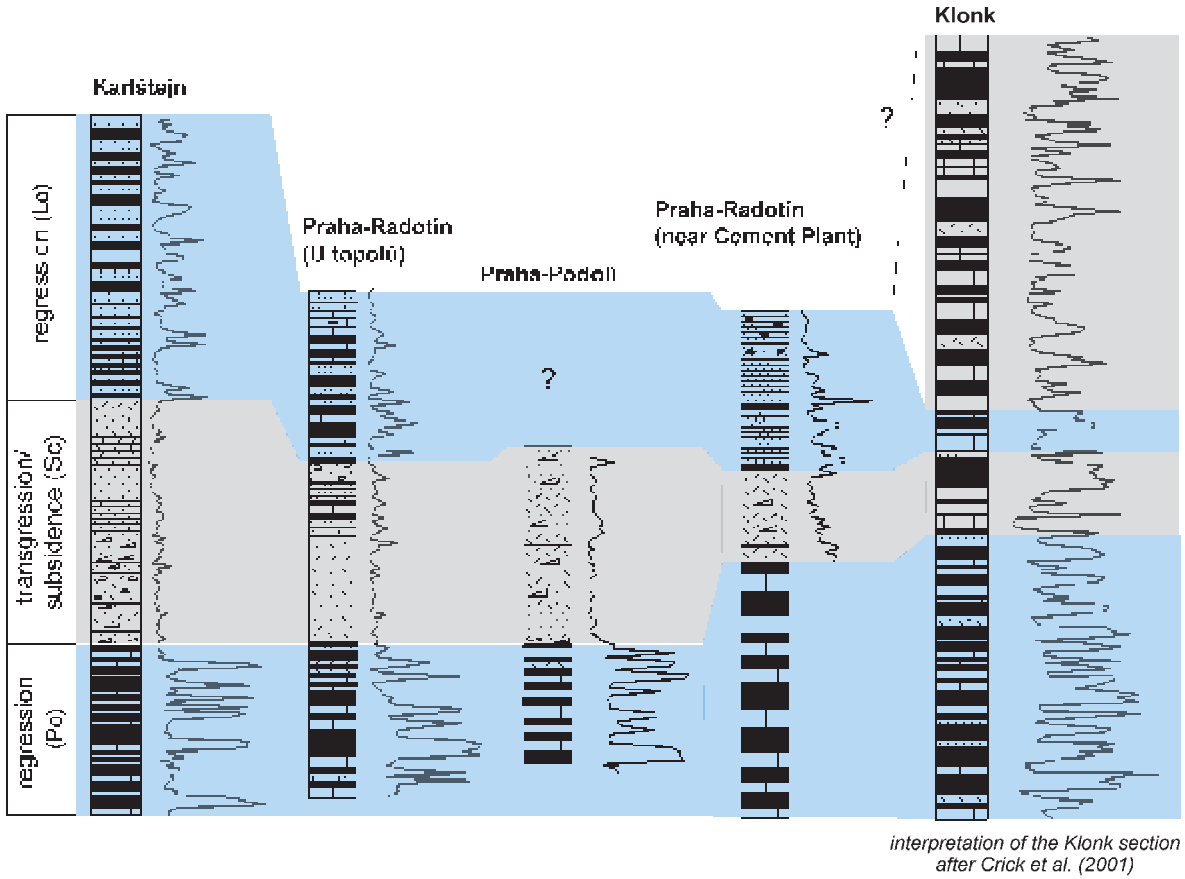

Fig. 8. Interpretation of the sea-level changes based on the MS records of the deep-water sections. Interpretation of the Klonk section was adopted from Crick et al. (2001), our results correspond in its lower part, but differs in the upper. **Po —** the upper part of the Požáry Fm, **Sc —** *Scyphocrinites* H., **Lo —** the lower part of the Lochkov Fm.

able dissolution (in some beds stylolites or extensive dissolutions can be observed). However, similar peaks can be traced at least in two other sections (Klonk section 5.5 m and Karlštejn section 4.0 m; Fig. 3A and B) and may therefore correspond to some widespread basinal events such as hiatuses or periods of sedimentary starvation, or delivery and concentration of exotic U-rich material.

At least three models must be considered for prograding of basinal carbonate deposits with reduced shale intercalations: 1) the increased input of eroded material from shallow-marine areas during the falling stage and lowstand system tracts; 2) the opposite situation of a period of enhanced carbonate production during the transgressive pulse, accompanied by highstand shedding effect (Schlager et al. 1994), and 3) other environmental effects influencing the shallow-water carbonate factories or pelagic carbonate productivity would be employed (e.g. increased abundance of pelagic crinoids, cephalopods).

Our interpretation based on evaluation of the GRS and MS records of the slope facies and comparison with published data is as follows: the uppermost part of the Požáry Formation has a regressive character, which is expressed in high MS and eU values (Figs. 3 and 8). Decreased carbonate productivity and low depositional rates have been accompanied by lithification of the sea-bottom. The lowermost part of the Lochkov Formation reflects a transgressive pulse, which resulted in decreased input of terrigenous material and pronounced decline of both magnitudes (Figs. 3 and 8). It was followed by slight MS and eU rise, which responded to gradual regression. However, it is possible that deepening during the S-D interval was caused by local sea-bottom subsidence and delivery of lithified deposits from underlying strata. The following regression might have corresponded to a eustatic sea-level fall well documented in shallow-marine areas. The deposition of the *Scyphocrinites* H also did not have to result only from increased supply of eroded material, which was formerly accumulated on appropriate shallower-water parts of the slope but rather was related to the mass development of floating echinoderms in general, as their distribution is widespread across the area and in many regions worldwide. Although it is certainly less conspicuous in the shallow-water deposits composed mostly of crinoidal limestones, thicker accumulations of *Scyphocrinites* debris are known, for example in the Daleje Valley (between the Požáry Q and Opatřilka sections).

This interpretation is partly in agreement with Crick et al. (2001), who presumed pronounced regression during the late Pridoli followed by a moderate transgressive/regressive pulse

in the critical S-D interval. According to results of the last mentioned study, the earliest Lochkovian has a clearly transgressive trend (focused on Klonk), and this is in contrast to our present results, which are based on several juxtaposed sections. The locally protracted high MS values with slowly decreasing GRS values in the combination with the presence of coarse-grained crinoidal beds up to the lower Lochkovian (magnetic intervals *VII–VIII*) are unexpected or even counter-intuitive with the first lower Lochkovian transgressive episode (compare Fig. 8 herein to figs. 3, 4 in Crick et al. 2001).

However, we are aware that there are also alternative interpretations based on the MS and GRS variations and other data (e.g. carbon and oxygen isotopes) described in numerous papers from the Silurian and Devonian of the Prague Synclinorium and other regions. Due to limited space we briefly refer for discussion to Hladíková et al. (1997), Slavík et al. (2000), Mann et al. (2001), Saltzman (2002), Buggisch & Mann (2004), Buggisch & Joachimski (2006), Bábek et al. (2007), and Malkowski et al. (2009).

Conclusions

The combined MS-and-GRS stratigraphic assessment and regional comparison of the carbonate facies around the S-D boundary in the Prague Synclinorium showed a significantly good correlative value between sections with similar facies development (i.e. lower subtidal to upper slope bioclastic grainstones/packstones and lower slope to toe-of-the-slope calciturbidites with predominance of bioclastic and peloidal wackestones/mudstones and calcareous shales). This comparison shows that the onset of the index species and the biostratigraphically determined S-D boundary may be diachronous and highly depend on facies. This fact makes the MS-and-GRS stratigraphy a powerful tool for precise correlation within the region. It also proved remarkable condensation and gaps in sedimentary record, especially in the lower slope conditions where distal calciturbidites predominate.

A major effect on the MS is ascribed to paramagnetic minerals, which have been delivered to the basin from land. Therefore, we can relate the changing amount of this terrigenous material detected by the MS and GRS to fluctuating erosion and sea-level changes.

The critical S-D interval is characterized in relatively shallow marine areas by increased values of MS, which are interpreted as related to a higher influx of terrigenous material during a regressive pulse. This interpretation is supported by contemporaneous increasing concentrations of GRS-detected potassium (clay) and is also supported by sedimentological evidence.

On the contrary, a broader S-D interval in the deep-water facies is characterized by visible facies change and decreasing of the MS values. Maxima of MS and GRS in the uppermost part of the Požáry Formation (generally upper Pridoli) are interpreted as a response to a regressive phase associated with a low depositional rate and sea-bottom lithification. The very lowermost part of the Lochkov Formation (generally the base of the Lochkovian) reflects a transgressive pulse leading to decreased input of terrigenous material and distinctive decline of both magnitudes. The overlying sequence characterized by slightly rising MS and eU corresponds to gradual regression. The deepening trend during the S-D interval was probably accompanied by local subsidence and influx of eroded lithoclastic material. The following regression may reflect a eustatic sea-level drop well supported by evidence from the shallowest marine areas. The facies change close to the S-D boundary and deposition of the *Scyphocrinites* H might predominantly result from a biotic event unrelated to sea-level changes and local subsidence, rather than from sea-level rise/drop.

Acknowledgments: We are grateful to A.C. da Silva, F. Hrouda and one anonymous reviewer for valuable comments and suggestions, which helped improve the original manuscript. Special thanks are due to colleagues who provided the complementary analyses used for the interpretation (V. Goliáš, XRD, Charles University, Prague; A. Langrová, EDX, WDS; P. Pruner, Academy of Sciences, Prague, rock magnetism), and those who discussed environmental constraints (J.E. Barrick, Texas Tech University, Lubbock, M.A. Murphy, University of California, Riverside and L. Slavík , Academy of Sciences, Prague) and the importance of the Klonk MS section and observed periodicities (B.B. Ellwood, Louisiana State University, Baton Rouge). The role of framework grants is appreciated (MSM 0021620855, AV0Z30130516, IAA300130702, IGCP 580).

References

Bábek O., Přikryl T. & Hladil J. 2007: Progressive drowning of carbonate platform in the Moravo-Silesian Basin (Czech Republic) before the Frasnian/Famenian event: facies, compositional variations and gamma-ray spectrometry. *Facies* 53, 293–316.

Brocke R., Wilde V., Fatka O. & Mann U. 2002: Chitinozoa and acritarchs at the Silurian/Devonian boundary: Examples from the Barrandian area. In: Brock G.A. & Talent J. (Eds.): 1st International Palaeontological Congress. *Abstracts,* Sydney, 192.

Brocke R., Fatka O. & Wilde V. 2006: Acritarchs and prasynophytes of the Silurian-Devonian GSSP (Klonk, Barrandian area, Czech Republic). *Bull. Geosci.* 81, 1, 27–41.

Buggisch W. & Joachimski M.M. 2006: Carbon isotope stratigraphy of the Devonian of Central and Southern Europe. *Palaeogeogr. Palaeoclimatol. Palaeoecol.* 240, 68–88.

Buggisch W. & Mann U. 2004: Carbon isotope stratigraphy of Lochkovian to Eifelian limestones from the Devonian of central and southern Europe. *Int. J. Earth Sci.* 93, 521–541.

Carls P., Slavík L. & Valenzuela-Ríos J.I. 2007: Revisions of conodont biostratigraphy across the Silurian-Devonian boundary. *Bull. Geosci.* 82, 2, 145–164.

Chlupáč I. & Kukal Z. 1988: Possible global events and the stratigraphy of the Barrandian Paleozoic (Cambrian–Devonian, Czechoslovakia). *Sbor. Geol. Věd, Geol.* 43, 83–146.

Chlupáč I., Jaeger H. & Zikmundová J. 1972: The Silurian-Devonian boundary in the Barrandian. *Bull. Canad. Petrol. Geol.* 20, 104–174.

Chlupáč I., Havlíček V., Kříž J., Kukal Z. & Štorch P. 1998: Palaeozoic of the Barrandian (Cambrian to Devonian). *Czech Geol. Surv.*, Prague, 1–183.

Crick R.E., Ellwood B.B., El Hassani A., Feist R. & Hladil J. 1997: Magnetosusceptibility event and cyclostratigraphy (MSEC) of the Eifelian-Givetian GSSP and associated boundary sequences

in north Africa and Europe. *Episodes* 20, 3, 167–175.

Crick R.E., Ellwood B.B., El Hassani A. & Feist R. 2000: Proposed magnetostratigraphy susceptibility magnetostratotype for Eifelian–Givetian GSSP (Anti-Atlas, Morocco). *Episodes* 23, 2, 93–101.

Crick R.E., Ellwood B.B., Hladil J., El Hassani A., Hrouda F. & Chlupáč I. 2001: Magnetostratigraphy susceptibility of the Přídolian–Lochkovian (Silurian–Devonian) GSSP (Klonk, Czech Republic) and a coeval sequence in Anti-Atlas Morocco. *Palaeogeogr. Palaeoclimatol. Palaeoecol.* 167, 73–100.

Crick R.E., Ellwood B.B., Feist R., El Hassani A., Schindler E., Dreesen R., Over D.J. & Girard C. 2002: Magnetostratigraphy susceptibility of the Frasnian/Famennian boundary. *Palaeogeogr. Palaeoclimatol. Palaeoecol.* 181, 67–90.

Čáp P., Vacek F. & Vorel T. 2003: Microfacies analysis of Silurian and Devonian type sections (Barrandian, Czech Republic). *Czech Geol. Surv., Spec. Pap.* 15, 1–40.

da Silva A.C. & Boulvain F. 2006: Upper Devonian carbonate platform correlations and sea level variations recorded in magnetic susceptibility. *Palaeogeogr. Palaeoclimatol. Palaeoecol.* 240, 373–388.

da Silva A.C., Mabille C. & Boulvain F. 2009a: Influence of sedimentary setting on the use of magnetic susceptibility: examples from Devonian of Belgium. *Sedimentology* 56, 1292–1306.

da Silva A.C., Potma K., Weissenberger J.A.W., Whalen M.T., Mabille C. & Boulvain F. 2009b: Magnetic susceptibility evolution and sedimentary environments on carbonate platform sediments and atolls, comparison of the Frasnian from Belgium and from Alberta. *Sed. Geol.* 214, 3–18.

da Silva A.C., Yans J. & Boulvain F. 2010: Early–Middle Frasnian (early Late Devonian) sedimentology and magnetic susceptibility of the Ardennes area (Belgium): identification of severe and rapid sea-level fluctuations. *Geologica Belgica* 13, 4, 319–332.

Denkler K.E. & Harris A.G. 1988: Conodont-based determination of the Silurian-Devonian boundary in the Valley and Ridge Province, Northern and Central Appalachians. *US Geol. Surv. Bull.* B 1837, B1–B13.

Durrance E.M. 1986: Radioactivity in geology: principles and applications. *Ellis Horwood*, Chichester, 1–441.

Ellwood B.B., Chrzanowski T.H., Hrouda F., Long G.J. & Buhl M.L. 1988: Siderite formation in anoxic deep-sea sediments: a synergetic bacterially controlled process with important implications in paleomagnetism. *Geology* 16, 980–982.

Ellwood B.B., Crick R.E., El Hassani A., Benoist S.L. & Young R.H. 2000: Magnetosusceptibility event and cyclostratigraphy method applied to marine rocks: Detrital input versus carbonate productivity. *Geology* 28, 12, 1135–1138.

Ellwood B.B., Crick R.E., Garcia-Alcade Fernandez J.L., Soto F.M., Truyóls-Massoni M., El Hassani A. & Kovas E.J. 2001: Global correlation using magnetic susceptibility data from Lower Devonian rocks. *Geology* 29, 7, 583–586.

Ellwood B.B., Garcia-Alcade Fernandez J.L., El Hassani A., Hladil J., Soto F., Truyóls-Massoni M., Wedigge K. & Koptíková L. 2006: Stratigraphy of the Middle Devonian boundary: Formal definition of the susceptibility magnetostratotype in Germany with comparisons to sections in the Czech Republic, Morocco and Spain. *Tectonophysics* 418, 31–49.

Fiala F. 1970: Silurian and Devonian diabases of the Barrandian. *Sbor. Geol. Věd, Geol.* 17, 7–97 (in Czech).

Frederichs T., Dobeneck T. Von, Bleil U. & Dekkers M.J. 2003: Towards the identification of siderite, rhodochrosite, and vivianite in sediments by their low-temperature magnetic properties. *Phys. Chem. Earth* 28, 669–679.

Frýda J., Hladil J. & Vokurka K. 2002: Seawater strontium isotope curve at the Silurian/Devonian boundary: a study of the global Silurian/Devonian boundary stratotype. *Geobios* 35, 21–28.

Geršl M. & Hladil J. 2004: Gamma-ray and magnetic susceptibility correlation across a Frasnian carbonate platform and the search for "punctata" equivalents in stromatoporoid-coral limestone facies of Moravia. *Geol. Quart.* 48, 3, 283–292.

Grygar T., Dědeček J., Kruiver P.P., Dekkers M.J., Bezdička P. & Schneeweiss O. 2003: Iron oxide mineralogy in late Miocene red beds from La Gloria, Spain: rock-magnetic, voltammetric and Vis spectroscopy analyses. *Catena* 53, 2, 115–132.

Herten U. 2000: Petrographische und geochemische Charakterisierung der Pelit-Lagen aus der Forschungsbohrung Klonk-1 (Suchomasty/Tschechische Republik). *Ber. Forschungszentrum Jülich* 3751, 1–78.

Hladil J. 1991: Evaluation of the sedimentary record in the Silurian/Devonian boundary stratotype at Klonk (Barrandian area, Czechoslovakia). *Newslett. Stratigr.* 25, 2, 115–125.

Hladil J. 1992: Are there turbidites in the Silurian/Devonian boundary stratotype (Klonk near Suchomasty, Barrandian, Czechoslovakia)? *Facies* 26, 35–54.

Hladil J. 2002: Geophysical records of dispersed weathering products on the Frasnian carbonate platform and early Famennian ramps in Moravia, Czech Republic: proxies for eustasy and palaeoclimate. *Palaeogeogr. Palaeoclimatol. Palaeoecol.* 181, 213–250.

Hladil J., Bosák P., Jansa L.F., Těžký A., Helesicová K., Hrubanová J., Pruner P., Krůta T., Špaček P. & Chadima M. 2000: Frasnian eustatic cycles viewed with gamma spectrometric and magneto-susceptibility stratigraphy tools (Moravia): Six major floodings on cratonized basement. *Subcommission on Devonian Stratigraphy, Newsletter* 17, 48–52.

Hladil J., Bosák P., Slavík L., Carew J.L., Mylroie J.E. & Geršl M. 2003a: A pragmatic test of early origin and fixation of gamma-ray spectrometric (U, Th) and magneto-susceptibility (Fe) patterns related to sedimentary cycle boundaries in pure platform limestones. *Carbonate Evaporite* 18, 2, 89–107.

Hladil J., Bosák P., Slavík L., Carew J.L., Mylroie J.E. & Geršl M. 2003b: Early diagenetic origin and persistence of gamma-ray and magnetosusceptibility patterns in platform carbonates: comparison of Devonian and Quaternary sections. *Phys. Chem. Earth* 28, 719–727.

Hladil J., Geršl M., Strnad L., Frána J., Langrová A. & Spišiak J. 2006: Stratigraphic variations of complex impurities in platform limestones and possible significance of atmospheric dust: a study with emphasis on gamma-ray spectrometry and magnetic susceptibility outcrop logging (Eifelian–Frasnian, Moravia, Czech Republic). *Int. J. Earth Sci.* 95, 4, 703–723.

Hladíková J., Hladil J. & Kříbek B. 1997: Carbon and oxygen isotope record across Pridoli to Givetian stage boundaries in the Barrandian basin (Czech Republic). *Palaeogeogr. Palaeoclimatol. Palaeoecol.* 132, 225–241.

Hrouda F. 1994: A technique for the measurement of thermal changes of magnetic susceptibility of weakly magnetic rocks by the CS-2 apparatus and the KLY-2 Kappabridge. *Geophys. J. Int.* 118, 604–612.

Jelínek V. & Pokorný J. 1997: Some new concepts in technology of transformer bridges for measuring susceptibility anisotropy of rocks. *Phys. Chem. Earth* 22, 179–181.

Jeppsson L. 1988: Conodont biostratigraphy of the Silurian boundary stratotype at Klonk, Czechoslovakia. *Geologica et Palaeont.* 22, 21–31.

Jeppsson L. 1989: Latest Silurian conodonts from Klonk, Czechoslovakia. *Geologica et Palaeont.* 23, 21–37.

Kastner M. 1971: Authigenic feldspars in carbonate rocks. *Amer. Mineralogist* 56, 1403–1442.

Kastner M. & Siever R. 1979: Low temperature feldspars in sedimentary rocks. *Amer. J. Sci.* 279, 453–479.

Klapper G. & Murphy M.A. 1975: Silurian–Lower Devonian Conodont Sequence in the Roberts Mountains Formation of Central Nevada. *Univ. California Publ., Geol. Sci.* 111, 1–62.

Koptíková L., Hladil J., Slavík L. & Frána J. 2007: The precise position and structure of the Basal Choteč Event: Lithological, MS-and-GRS and geochemical characterisation of the Emsian-Eifelian carbonate stratal successions in the Prague Syncline (Teplá-Barrandian Unit, Central Europe). In: Over D.J. & Morrow J. (Eds.): Subcommission on Devonian Stratigraphy and IGCP 499 Devonian Land Sea Interaction, Eureka NV 9-17 Sep 2007, Program and Abstracts. *Genesea*, NY, US, 55–57.

Koptíková L., Hladil J., Slavík L., Frána J. & Vacek F. 2008: Evidence of a significant change between Lochkovian and Pragian: detailed lithological, geophysical, geochemical and mineralogical aspects (Požáry 3 section in Prague Synform). In: El-Mehdawi A.D. & Koenigshof P. (Eds.): Abstracts of the Field Workshop IGCP 499 Devonian Land-Sea Interaction. *Libyan Petroleum Institute*, Tripoli, 10–14.

Koptíková L., Bábek O., Hladil J., Kalvoda J. & Slavík J. 2010: Stratigraphic significance and resolution of spectral reflectance logs in Lower Devonian carbonates of the Barrandian area, Czech Republic; a correlation with magnetic susceptibility and gamma-ray logs. *Sed. Geol.* doi: 10.1016/j.sedgeo.2010.01.004

Kranendonck O. 2000: Petrographische und geochemische Charakterisierung der Karbonatbänke aus der Forschungsbohrung Klonk-1 (Suchomasty/Tschechische Republik). *Ber. Forschungszentrum Jülich* 3750, 1–113.

Krs M. & Pruner P. 1995: Palaeomagnetism and palaeogeography of the Variscan formations of the Bohemian Massif, comparison with other European regions. *J. Czech Geol. Soc.* 40, 1–2, 3–46.

Krs M., Pruner P. & Man O. 2001: Tectonic and paleogeographic interpretation of the paleomagnetism of Variscan and pre-Variscan formations of the Bohemian Massif, with special reference to the Barrandian terrane. *Tectonophysics* 332, 93–114.

Kruiver P.P., Dekkers M.J. & Heslop D. 2001: Quantification of magnetic coercivity components by the analysis of acquisition curves of isothermal remanent magnetisation. *Earth Planet. Sci. Lett.* 189, 269–276.

Kříž J. 1992: Silurian field excursions. Prague Basin (Barrandian), Bohemia. *Nat. Mus. Wales, Geol. Ser.* 13, 1–111.

Kříž J., Jaeger H., Paris F. & Schönlaub H.P. 1986: Přídolí — the fourth subdivision of the Silurian. *Jb. Geol. Bundesanst.* 129, 2, 291–360.

Lis J., Pasieczna A., Strzelecki R., Wolkowicz S. & Lewandowski P. 1997: Geochemical and radioactivity mapping in Poland. *J. Geochem. Explor.* 60, 39–53.

Løvborg L., Wollenberg H., Sørensen P. & Hansen J. 1971: Field determination of uranium and thorium by gamma-ray spectrometry exemplified by measurements in the Ilimaussaq alkaline intrusion, South Greenland. *Econ. Geol.* 66, 368–384.

Malkowski K., Racki G., Drygant D. & Szaniawski H. 2009: Carbon isotope stratigraphy across the Silurian-Devonian transition in Podolia, Ukraine: evidence for a global geochemical perturbation. *Geol. Mag.* 146, 5, 674–689.

Mann U., Herten U., Kranendonck O., Poelchau H.S., Stroetmann J., Vos H., Wilkes H., Suchý V., Brocke R., Wilde V., Muller A., Ebert J., Bozdogan N., Soylu C., El Hassani A. & Yalcin M.N. 2001: Dynamics of the Silurian/Devonian boundary sequence: sedimentary cycles vs. organic matter variation. *Terra Nostra* 4, 44–48.

Matti J.C. & McKee E.H. 1977: Silurian and Lower Devonian paleogeography of the outer continental shelf of the Cordilleran Miogeocline, central Nevada. In: Stewart J.H., Stevens C.H. & Fritsche A.E. (Eds.): Paleozoic Paleogeography of the Western United States — Pacific Section. *SEPM*, Los Angeles, 181–215.

McLaren D.J. 1977: The Silurian-Devonian Committee. A final report. In: Martinsson A. (Ed.): The Silurian-Devonian boundary. *I.U.G.S. Ser. A* 5, 1–34.

Melichar R. 2004: Tectonics of the Prague Synform: a hundred years of scientific discussion. *Krystalinikum* 30, 167–187.

Melichar R. & Hladil J. 1999: Resurrection of the Barrandian nappe structures, central Bohemia. *Geolines* 8, 48–50.

Mišík M. 1994: Authigenic feldspars in carbonate rocks of the Western Carpathians. *Geol. Carpathica* 45, 103–111.

Paris F., Laufeld S. & Chlupáč I. 1981: Chitinozoa of the Silurian-Devonian boundary statotypes in Bohemia. *Sver. Geol. Unders., Ser. C* 4, 51, 1–29.

Parma J. & Zapletal K. 1991: CS-1 apparatus for measuring the temperature dependence of low-field susceptibility of minerals and rocks (in cooperation with the KLY-2 Kappabridge). *Leaflet, Geofyzika*, Brno.

Patočka F. & Štorch P. 2004: Evolution of geochemistry and depositional settings of Early Palaeozoic siliciclastics of the Barrandian (Teplá-Barrandian Unit, Bohemian Massif, Czech Republic). *Int. J. Earth Sci.* 93, 728–741.

Patočka F., Pruner P. & Štorch P. 2003: Palaeomagnetism and geochemistry of Early Palaeozoic rocks of the Barrandian (Teplá-Barrandian Unit, Bohemian Massif): palaeotectonic implications. *Phys. Chem. Earth* 28, 735–749.

Röhlich P. 2007: Structure of the Prague Basin: The deformation diversity and its causes (the Czech Republic). *Bull. Geosci.* 82, 2, 175–182.

Saltzman M.R. 2002: Carbon isotope ($\delta^{13}C$) stratigraphy across the Silurian-Devonian transition in North America: evidence for a perturbation of the global carbon cycle. *Palaeogeogr. Palaeoclimatol. Palaeoecol.* 187, 83–100.

SatisGeo, Ltd. 2009: GS-512 Gamma Ray Spectrometer. Manufacturer's leaflet with technical data. http://www.satisgeo.com/gs5.htm

Schlager W., Reijmer J.J.G. & Droxler A. 1994: Highstand shedding of carbonate platforms. *J. Sed. Res.* B64, 3, 270–281.

Schönlaub H.P., Kreuzer L., Joachimski M.M. & Buggisch W. 1994: Paleozoic boundary sections of the Carnic Alps (Southern Austria). *Erlanger Geol. Abh.* 122, 77–103.

Slavík L., Hladil J., Blažek R. & Krůta M. 2000: Anatomy of the Pragian stratigraphic column: gamma spectrometric record throughout complete 170-m thick Pragian section in calciturbidite/hemipelagite facies (Prague, section "Under Barrandov Bridge"). *Subcommission on Devonian Stratigraphy, Newsletter* 17, 46–47.

Suchý V. & Rozkošný I. 1996: Diagenesis of clay minerals and organic matter in the Pridoli Formation (Upper Silurian), the Barrandian Basin, Czech Republic: first systematic survey. *Acta Univ. Carol., Geol.* 38, 401–409.

Suchý V., Rozkošný I., Žák K. & Franců J. 1996: Epigenetic dolomitization of the Přídolí formation (Upper Silurian), the Barrandian basin, Czech Republic: implications for burial history of Lower Paleozoic strata. *Geol. Rundsch.* 85, 264–277.

Tauxe L., Mullender T.A.T. & Pick T. 1996: Pot-bellies, wasp-waists and superparamagnetism in magnetic hysteresis. *J. Geophys. Res.* 101, 571–584.

Vacek F. 2007: Carbonate microfacies and depositional environments of the Silurian-Devonian boundary strata in the Barrandian area (Czech Republic). *Geol. Carpathica* 58, 6, 497–510.

Kletetschka G., Pruner P., **Schnabl P.**, Šifnerová K., Tasáryová Z., Manda Š.

Magnetic scanning and interpretation of paleomagnetic data from Prague Synform's volcanics

Stud. Geoph. et Geodet. – V recenzním řízení

MAGNETIC SCANNING AND INTERPRETATION OF PALEOMAGNETIC DATA FROM PRAGUE SYNFORM'S BASALTIC DIKES

G. Kletetschka[1,2], kletetschka@gmail.com

P. Pruner[1], Pruner@gli.cas.cz

P. Schnabl[1], schnabl@gli.cas.cz

K. Šifnerová[1], sifnerova@gli.cas.cz

Z. Tasáryová[2], zuzana.tasaryova@geology.cz

[1]Institute of Geology, Academy of Science of the Czech Republic, v.v.i.

[2]Charles University in Prague, Faculty of Science, Czech Republic

Abstract:

Magnetic images have been produced at the distance of 0.1 mm from the polished basaltic thin sections from Prague Synform in Barrandian area. When combined with the optical microscopy images, the three magnetic textures revealed their relationship to the optically imaged structures. First magnetic texture revealed that most of the magnetic signature is localized within the amygdales formed later after the dike intruded into the sedimentary sequence. Second texture showed that the basaltic dike contains large grain size distribution of magnetic carriers tainted with variable viscous magnetizations. Third texture suggested a presence of magnetic anisotropy of igneous origin. Such textural magnetic information along with the paleomagnetic characteristics of the basaltic dikes of Silurian age constrained the interpretation of the paleomagnetic characteristic, its origin and timing.

Key words: paleomagnetism, magnetic scanner, magnetic mineralogy, amygdales, magnetic anomalies, magnetic texture.

Introduction:

Magnetic anomalies were obtained remotely from the surface of Mars and their interpretation is often quite complicated (Connerney et al., 2005; Connerney et al., 2001; Kletetschka et al., 2004; Kletetschka et al., 2009a; Kletetschka et al., 2000a, b). With the

advance of technological automatic processes (Oda et al., 2011) we have developed a magnetic scanner helping in interpretation of the geologic thin sections or polished plugs of rocks that are associated with somewhat stronger magnetization. Such studies were focusing mainly on meteorites due to their strong remanent magnetic properties. Reports from the Prague Synform (Aifa et al., 2007) suggests a presence of rocks with substantial magnetic properties, allowing magnetic detection with the Hall probe that can be combined into a magnetic scan over its surface with resolution of about 0.2 mm (Kletetschka et al., 2009b). Such resolution is enough to get more specific information about the nature of the remanent magnetization and its origin.

Geology setting of the samples:

We have selected three basaltic samples from Silurian volcanic region that is located in the NE sector of the today's relict of the Prague Synform. Revival of basaltic volcanism since the Late Ordovician generated a specific geological structure, where olivine basalt magma ascended along several deep, ENE-WSW trending fissures, parallel to the longitudinal axis of the Prague Synform. Additional basaltic fissures went along WNW-ESE trending faults perpendicular to this axis (Kříž, 1991).

The volcano-sedimentary sequence (Telychian–Gorstian) is exposed in the Svatý Jan volcanic center in northern flank of Holyň-Hostim Syncline between Beroun-Tetín and Mezouň Villages. The syncline is composed of up to 400 m thick succession of pyroclastics, tuffs, tuffitic shales, shallow water limestones and both effusive and intrusive basalts (Kříž, 1992, 1998). Additionally, the central part of Svatý Jan volcanic center formed an emergent elevation above the sea level from early Wenlock to late Llandovery, which is indicated by a presence of sub-aerial volcanic products. Despite the significant thickness of volcano-sedimentary complex, the effusive basalts formed only minor part of the succession and are concentrated into a few stratigraphic intervals.

The first of the three sites is site C5, near Loděnice–Bubovice road cut (Černidla).This road cut (~210 m) is along the road between Loděnice and Bubovice villages revealing a section of volcano-sedimentary facies of the Motol Formation ranging from mid-Sheinwoodian to late Homerian (Wenlock). Exposed volcano-sedimentary succession (early Sheinwoodian–Gorstian) consists of tuffitic shales and yellow-brown tuffs, with thin beds and lenses of skeletal limestones and mudstones corresponding to shallow-marine deposition, which are interrupted with several thick basalt lava flows (Bouček, 1942; Kříž, 1992).

The second site, Si07, is from U Vitáčků Section near Lištice**.** U Vitáčků section is on the left side of Berounka river, 2 km east from the Beroun railway station and represents the volcano-sedimentary succession at the boundary of Motol and Kopanina Formation of

Wenlock/Ludlow age. There the top of volcanic complex of the Lištice river section (tuffs, hyaloclastites, tuffitic shales) is exposed, overlain by 4 m thick basalt with calcite amygdales. Sub-marine lava flow overlain by a succession of grey bioclastic limestones containing brachiopod and coral dominated fauna corresponding with former "*C. beaumonti* Horizon", i.e. Gorstian stage. Thus, the underlying volcani-clastic deposits and effusions are likely of the earliest Gorstian age resting on the limestone of latest Wenlock (Kozla facies). The uppermost part of this volcano-sedimentary succession is preserved within 100 m distance. Major exposed rocks consist of agglomerates and yellow-green coarse grained tuffs, which contain basaltic bombs and limestone xenoliths. The 4 m thick effusive lava flow forms the top of the volcanic sequence (Fišera, 1965a; Horný, 1965; Kodym et al., 1931; Kříž, 1992).

The third site, Si08, comes from the Lištice quarry**.** To this quarry leads the road from Lištice to Beroun, exposing the basaltic intrusion and calcareous shales of lowermost Motol Formation, Telychian (Llandovery), representing the lowermost part of the Svatý Jan volcano-sedimentary section near Lištice. Exposure of the eastern part of the quarry includes a development of 60 cm thick fine-grained datolite chert representing contact aureola between basaltic intrusion and calcareous shale, containing graptolites of *S. grandis* Subzone, Telychian, latest Llandovery [P. Štorch, personal communication, see also (Kodym et al., 1931)]. Another basaltic body in the area is reaching its thickness of 50 m. The maximum age of the basaltic intrusion correspond to the latest Llandovery (Fišera, 1965b; Strnad, 1961).

Material and method:

Sampling:

Several oriented cores had been obtained from each of the sites. Each site provided about 12 cores that were used for making a geology thin section, magnetic scanning, thermal demagnetization, alternating field demagnetization and magnetization, and measurement of magnetic susceptibility.

Magnetic scanning:

We used a magnetic scanner built by Youngwood Science and Engineering (YSE) that consists of a stationary hall probe and a 2D motorized stage whose motion is controlled by software (MagScan) also developed by YSE. The hall probe senses the magnetic component perpendicular to the scanning surface (e.g. geologic thin section) and returns its value along with the X-Y coordinates to the computer. The output is a 2D image that shows the values of magnetization detected over the surface of the sample. For all our images the scanned area is 17 mm x 17 mm (the maximum capability of the 2D stage) with a spatial step of 0.2 mm.

We scanned three thin sections that were cut from three basaltic cores of the Barrandian area. These sections were scanned in saturated state both with and without any magnetic shielding. We found no significant difference. Saturation magnetization was acquired along the long side of all three thin sections.

Remanent magnetization:

Paleomagnetic directions were obtained from the 2.5cm in diameter and 2 cm long cores that were drilled out from the volcanic units so that their orientation was preserved in special coordinates. After measurements of natural remanent magnetization (NRM), these samples were subject of progressive thermal and/or alternating magnetic field (AF) demagnetizations. Thermal demagnetization was achieved using the MAVACS (Magnetic Vacuum Control System (Příhoda et al., 1989) equipment with temperatures ranging between 80°C and 580°C and with step intervals between 30°C and 40°C. Demagnetization by AF (LDA-3 apparatus, Agico Brno) up to 100 mT was done with the steps of every 5-20 mT. NRM measurements were carried out using either the spinner magnetometers JR-5A and JR-6A (AGICO Brno). The magnetic susceptibility (*k*) of the specimens was determined using a KLY-4 Kappabridge (Jelinek, 1966, 1973). Results of measurements were analyzed using the software package Remasoft (Chadima and Hrouda, 2006). Multicomponent analysis separated the remanent magnetization components (Kirschvink, 1980; Man, 2003).

At each step of the thermal demagnetization, the bulk magnetic susceptibility value was checked. Thermal treatment often results in chemical changes involving the magnetic carriers and thus compromising the data. Chemical changes often result in increase or decrease of the amount of magnetic carriers in the sample and therefore magnetic susceptibility conveniently monitors any chemical changes in the sample.

Coercivity spectra:

After AF demagnetization the samples were progressively magnetized by pulse magnetizer (MMPM10, Magnetic measurements U.K.) until they reached the saturation and then stepwise demagnetized by AF using LDA-3, until its maximum obtainable AF field of 100 mT.

Microscopy:

Standard geological thin sections were obtained from the relevant samples C5 (Černidla), Si07 (Lištice roadcut), and Si08 (Lištice quarry). Because the magnetic scanning has

a special resolution of only 0.2 mm and we needed comparison at the similar scale we placed a standard thin sections on the light table and took a photograph that was subsequently combined with the magnetic scan images (Figure 1, 2, and 3). The detailed nature of the regions with magnetic anomalies detected by the scanner was imaged and photographed using polarized light optical microscope Spencer.

Results:

Magnetic image of the sample Si07 (Figure 1) from early Ludlow showed eye-like magnetic texture. The image was combined with the optical image (Figure 1A, 1B, 1C). The regions that showed significant magnetic signature of up to 22 μTesla at 0.1 mm above the surface, were looked at in more detail (red squares in Figure 1A, A-1, A-2, using standard polarized microscope. The images show that these rocks contain numerous vesicles with associated amygdales. The original vesicle walls (shown in red in Figure 1A-1) and sometimes the entire vesicle (Figure 1A-2) is commonly filled with iron oxides. The rest of the section show glassy matrix and devitrified plagioclases with no significant magnetic signal.

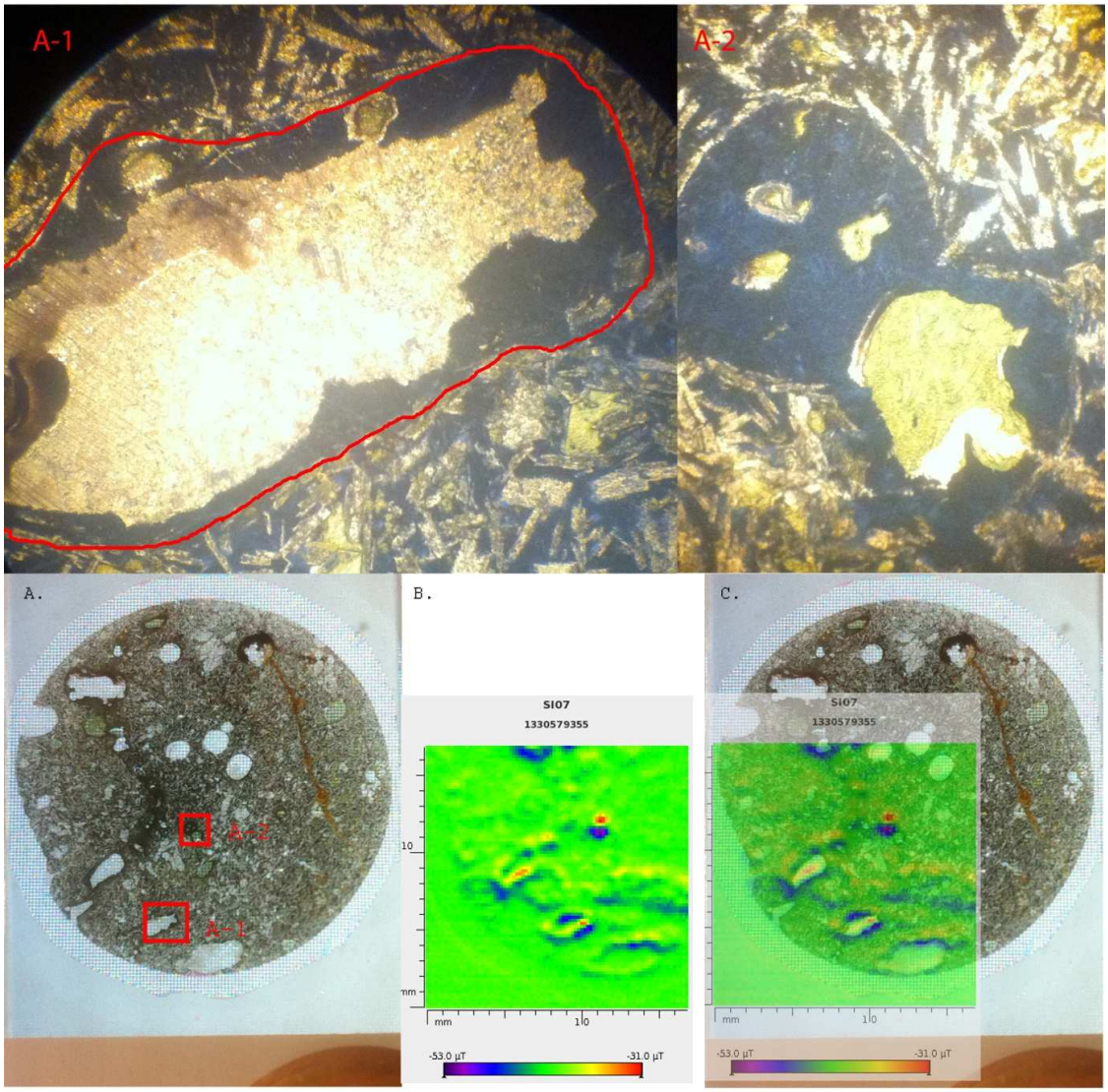

Figure 1: Combination of the optical transparent image with the magnetic scan. A. Optical image of the thin section Si07. Red rectangles are insets A-1 and A-2 B. Magnetic scan of the thin section Si07. C. Overlap of the magnetic image with the optical image.

Basaltic section C5 (Figure 2) from the Wenlock (Černidla) showed somewhat anisotropic magnetic texture with several of magnetic anomalies trending diagonally at 45 degree from bottom left to top right across the image (Figure 2B). This section contained a fracture that followed the anisotropic character. The detail of the regions near the fracture and within the matrix associated with magnetic anomalies was marked by red rectangle in Figure 2A and shown by two insets (A-1, and A-2) where one shows the detail near the fracture and one the pyroxene grain with associated magnetic anomaly up to 61 µTesla 0.1 mm over the surface. The magnetic and transmitted images were combined into one in Figure 2C.

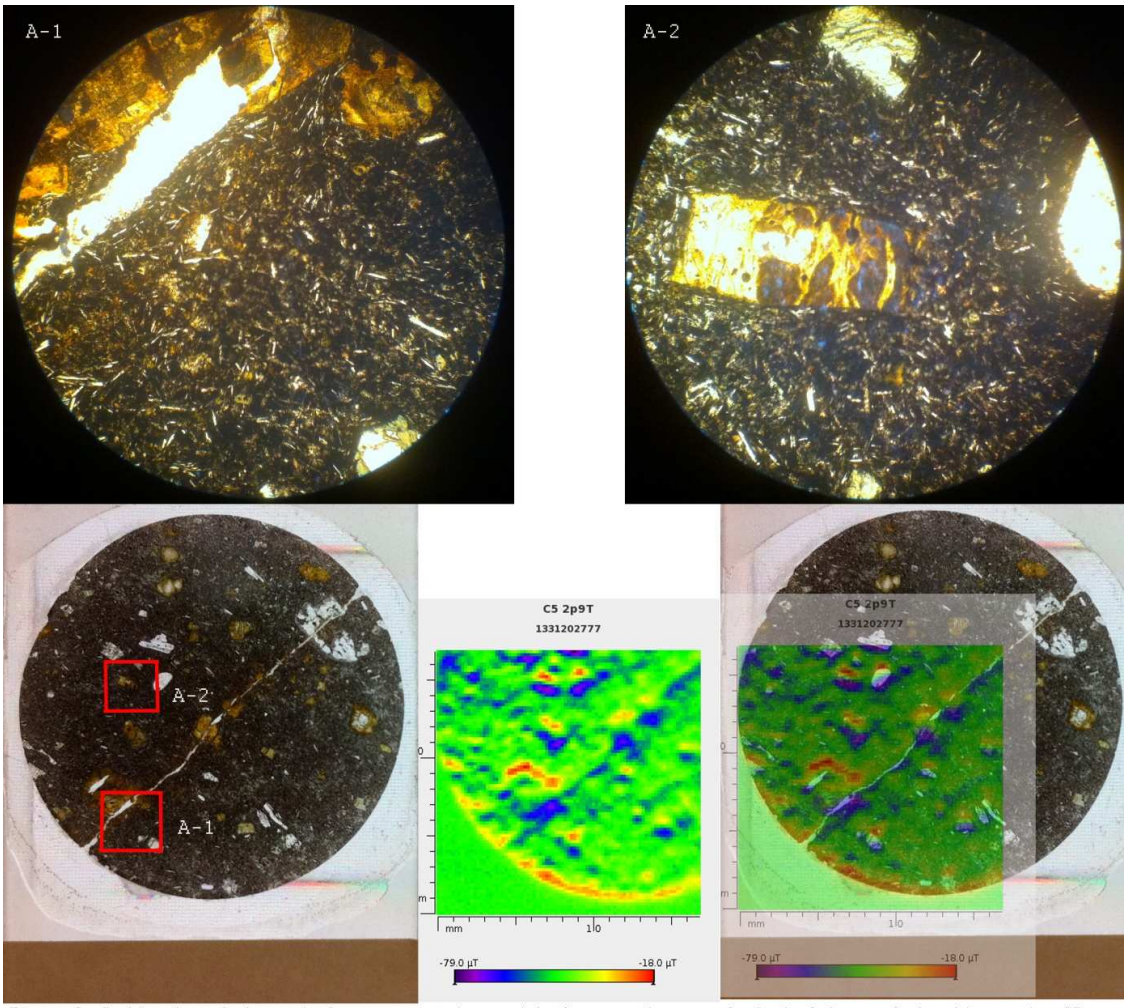

Figure 2: Combination of the optical transparent image with the magnetic scan. A. Optical image of the thin section C5. Two red rectangles are locations of the two insets, A-1, and A-2. B. Magnetic scan of the thin section C5. C. Overlap of the magnetic image with the optical image.

The latest Llandovery basaltic sample Si08 revealed an image with discrete magnetic anomalies separated from each other (Figure 3B). These magnetic anomalies were almost two orders of magnitude stronger than previous sections and reached 1160 µT at 0.1 mm over the surface (compared with 22 µT and 60 µT for Si07 and C5, respectively). Optical images revealed a presence of discrete magnetic oxides up to 1 mm in size, contributing to the large magnetic signature. These oxides have sharp edges indicating that the magnetic mineral was growing in size during the solidification of the basalt.

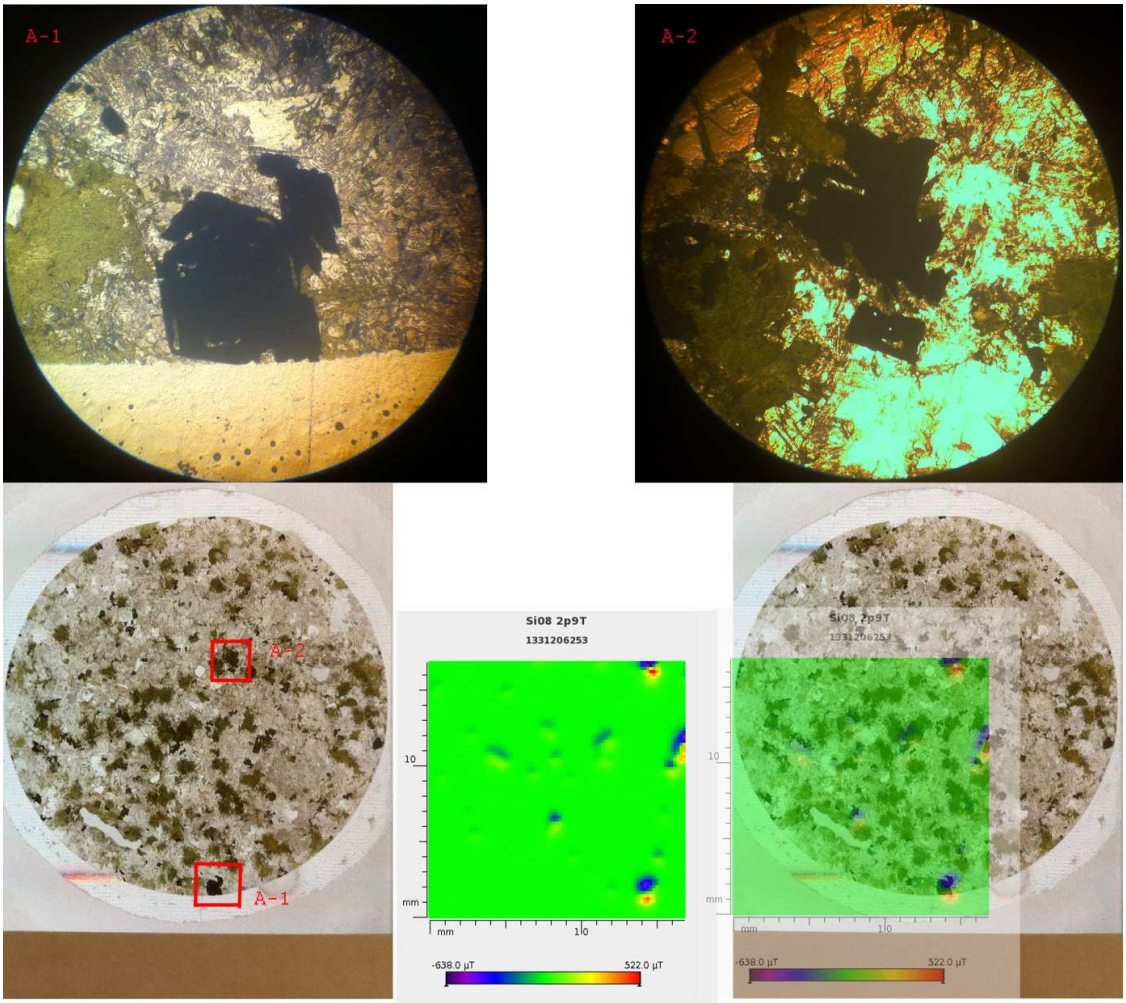

Figure 3: Combination of the optical transparent image with the magnetic scan. A. Optical image of the thin section Si08. Red rectangles show the locations of the insets A-1 and A-2. B. Magnetic scan of the thin section Si08. C. Overlap of the magnetic image with the magnetic anomalies transparent to identify parts of the thin sections with magnetic grains.

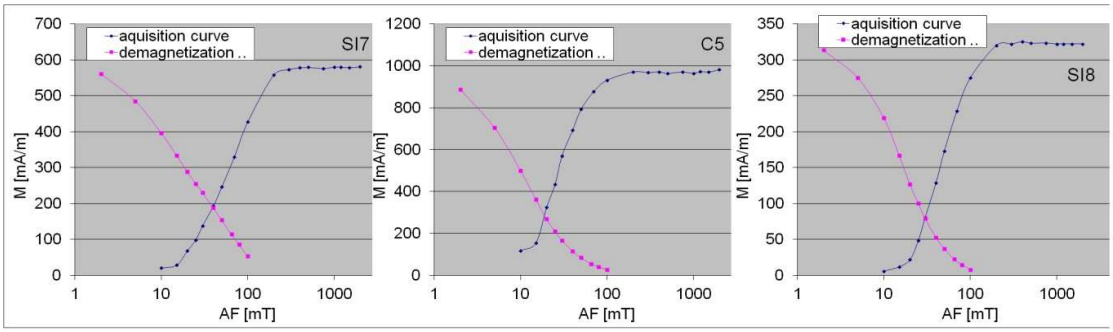

Figure 4: Acquisition of saturation remanence and its demagnetization for samples Si07, C5, and Si08.

The magnetic acquisition and demagnetization of these basalts (Figure 4) showed that saturated state of the basaltic sample C5 was the most magnetic reaching 980 mA/m, followed by Si07 with 580 mA/m and Si08 with 320 mA/m. Thus sample Si08 has the lowest overall magnetization when measured using rotational magnetometer, however when scanned with the magscan it shows the largest magnetic anomalies.

Sample C5 had 9 mT and 30 mT values for medium demagnetizing and magnetizing field, respectively. This is a minimum set of required field to demagnetize or magnetize when

compared with 15 mT and 70 mT medium fields for Si07 and 15 mT and 50 mT medium fields for Si08. Thus magnetically, sample Si07 is the hardest and sample C5 the softest.

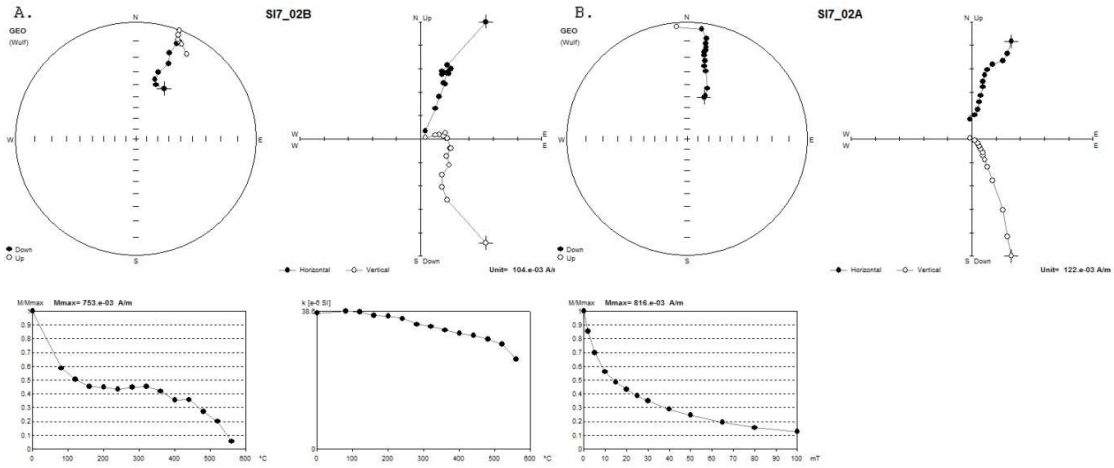

Figure 5: Demagnetization of the natural remanent magnetization (NRM) of sample Si07. A. Stereonet projection, Zijderveld projection, magnetization magnitude and magnetic susceptibility plots of thermal demagnetization; B. Stereonet projection, Zijderveld projection, magnetization magnitude of demagnetization by alternating field.

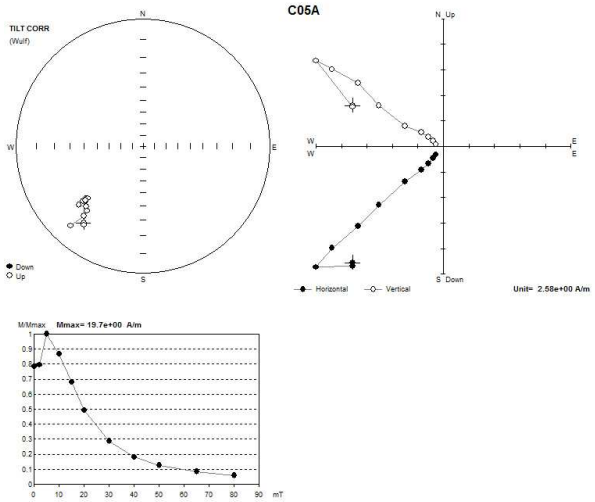

Figure 6: Demagnetization of the natural remanent magnetization (NRM) of sample C5. Stereonet projection, Zijderveld projection magnetization magnitude of demagnetization by alternating field.

When treating the original magnetic remanence of these basalts (Figures 5, 6, 7), we have sample C5 with the largest remanence (15.8 A/m) followed by Si07 (0.76 A/m) and Si08 (0.12 A/m). Magnetically the sample C5 had the largest (most stable remanence) medium demagnetizing field (MDF) just over 20 mT followed by almost exactly 15 mT for MDF of Si07 and magnetically weakest MDF of 10 mT was for sample Si08. Both C5 and Si07 show fairly stable paleodirections. Paleodirections for Si08 (Figure 7), however, are somewhat chaotic showing a viscous overprint.

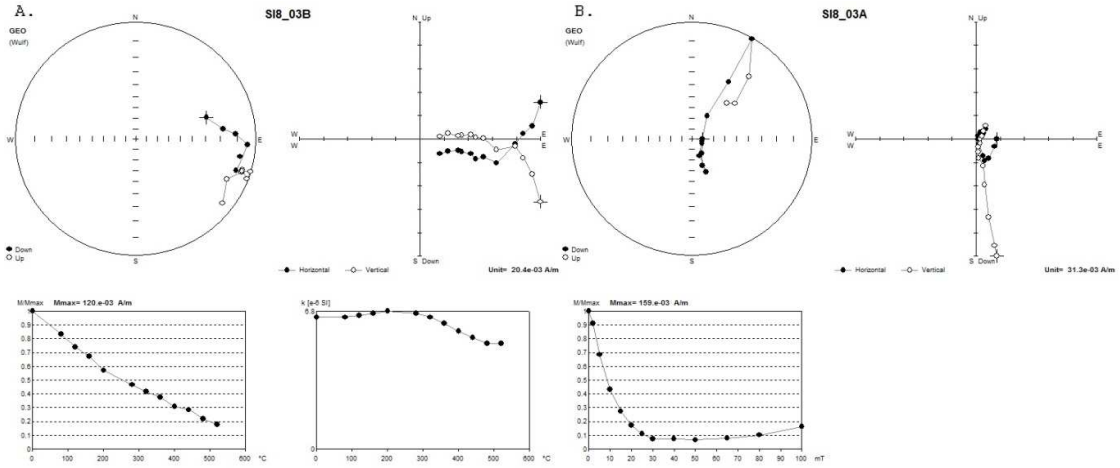

Figure 7: Demagnetization of the natural remanent magnetization (NRM) of sample Si08. A. Stereonet projection, Zijderveld projection, magnetization magnitude and magnetic susceptibility plots of themral demagnetization; B. Stereonet projection, Zijderveld projection, magnetization magnitude of demagnetization by alternating field.

Thermally most stable is the sample Si07 holding medium thermal stability (MTS), 50% of its remanence, up to 300°C followed by MTS of 260°C for sample Si08. In both cases the sample starts to have slight chemical changes as revealed by the susceptibility plots (Figure 5A, 7A, lower right section). Sample Si07 shows at least three components during the thermal demagnetization while S08 at least two directional components. We did not perform the thermal demagnetization for sample C5.

Discussion:

Without magnetic maps produced by magnetic scanner the demagnetization of the remanence is quite complicated and there are several pole directions and it is difficult to figure out what is the primary and what is the secondary component of magnetization. Even harder is to assign a specific time to individual components. However magnetic maps (Figure 1, 2, 3) helped to localize the magnetic carriers.

For example most of the magnetic signature associated with the basalt Si07 is carried by amygdales, the secondary (diagenetic) mineralization filling the vesicles of the buried lava flow (Figure 1 A, A-1, A-2). Most of the time formation of amygdales is associated with hydrothermal fluids that flow through the pores of the lava flow, dissolving the Si and Fe ions when fluids are of reduced nature and precipitating them as oxides when mixing with air inside the vesicles. The timing of this event is tied with the Permocarboniferous paleodirection (Krs et al., 2001) that seems to be fairly stable as shown both in AF and thermal demagnetization plots (Figure 5).

The basalt characterized by sample Si08 (Figure 3) revealed a unique characteristic of separated dipoles buried in the thin section as discrete magnetic grains whose magnitude is astounding, almost 2 orders of magnitude stronger compared with the other basaltic sections.

We don’t see any magnetic scaling like this in the remanence characteristics. In fact the remanence of this sample is the weakest of all (0.12 A/m for Si08 compared to 0.76 A/m for Si07 and 15.8 A/m for C5). Magnetic remanence of this basalt is somewhat chaotic and reflects the potential to acquire viscous magnetic signature by the large discrete grains in this basalt flow. Therefore, nearby lightning, sub-continental rotation, or any other magnetic disturbance would likely change the magnetic direction of individual grains according to values of individual grain magnetic coercivity. This is reflected in demagnetization plots. Thermal demagnetization at low temperatures looses smaller magnetic carriers with lower blocking temperature while AF demagnetization at low fields looses larger grains with lower magnetic coercivity. Therefore the final paleodirections differ when using either demagnetization technique. This difference, in fact, points to a unique lava flow because it is possible to separate the magnetic anomalies based on the magnetic scanning according to their size. Changes in the individual dipole direction may reveal the timing values acting on individual grains due to geomagnetic and environmental changes. Therefore, if the Prague Synform has been moving in respect to geomagnetic field, the grain size distribution of the carriers as detected in Figure 3 would randomize the paleo directions of individual grains in such a way that it would randomize the overall magnetic signature. This is consistent with our observation that the sample Si08 has the weakest natural remanent magnetization.

From the stability point of view and paleodirection characteristics, basalt C5 appears to be most reliable. C5 does not contain amygdales or discrete soft magnetic grains. Based on the Figure 2, it suggests certain anisotropy of magnetic anomalies detected over the surface, even if we neglect the anomaly that copies the fracture in the thin section. This is likely a signature of the solidification of this specific lava flow and this give certain credibility that the magnetic signature is genuine from the time of lava flow cooling. Sample C5 shows only slight signs of either viscous or diagenetic overprint (Figure 6) that was possible to clean using 5 mT AF field.

Conclusions:

Magnetic eye-like texture revealed during the scanning points to dominant magnetic carriers associated primarily with the amygdales formed inside the lava flow’s vesicles of sample Si07. Paleodirections are stable (D=20°, I=-4°) and points to the Permocarboniferous episode during which the amygdales formed.

Magnetic texture of the sample Si08 revealed strongly isolated dipolar signature, therefore the sample with large distribution of grain sizes of magnetic carriers. This phenomena, when occurring within the rock sample Si08, results in chaotic paleodirections due to variable

viscosity of contrasting grain sizes of magnetic minerals. The result is overall demagnetization of the original remanence and strong viscous overprint.

Magnetic scanning of sample C5 revealed homogeneous magnetic signature with signs of anisotropy, possibly pointing to the settling of the lava flow. This sample indicates the most reliable paleomagnetic characteristic and shows only little signs of either diagenetic and/or viscous overprint of the fairly stable Silurian paleomagnetic direction (D=227°,I=-26° or D=217°,I=-9° before the tilt correction) for the Prague Synform.

Magnetic scanner proved to be a vital tool when interpreting the paleomagnetic information from the basaltic lava flows.

Acknowledgement:

This research is supported by the Grant Agency CR under grant - P210/10/2351. We acknowledge help from Štěpán Manda, Stanislav Šlechta, Daniela Venhodová, Jiri Petráček, Jana Drahotová, Jaroslava Jabůrková, Petr Štorch, Vojtěch Janoušek, Jiří Frýda and Jakub Trubač.

References

Aifa, T., Pruner, P., Chadima, M., and Storch, P., 2007, Structural evolution of the Prague synform (Czech Republic) during Silurian times: An AMS, rock magnetism, and paleomagnetic study of the Svaty Jan pod Skalou dikes. Consequences for the nappes emplacement: Geological Society of America, v. 423, p. 249-265.

Bouček, B., 1942, O novém odkryvu siluru u Loděnic: Zpravodaj Geologického Ústavu Ćechy Morava, v. 17, p. 165-172.

Chadima, M., and Hrouda, F., 2006, Remasoft 3.0 - a user friendly paleomagnetic data browser and analyser: Travaux Geophysiques, v. XXVII, p. 20-21.

Connerney, J.E.P., Acuna, M.H., Ness, N.F., Kletetschka, G., Mitchell, D.L., Lin, R.P., and Reme, H., 2005, Tectonic implications of Mars crustal magnetism: Proceedings of the National Academy of Sciences of the United States of America, v. 102, p. 14970-14975.

Connerney, J.E.P., Acuna, M.H., Wasilewski, P.J., Kletetschka, G., Ness, N.F., Reme, H., Lin, R.P., and Mitchell, D.L., 2001, The global magnetic field of Mars and

implications for crustal evolution: Geophysical Research Letters, v. 28, p. 4015-4018.

Fišera, F., 1965a, Defilé na levém břehu Berounky mezi Lišticemia samotou "U Vitáčka". Paleovulkanity Českého masivu: Praha, Universita Karlova, p. 71-76.

Fišera, F., 1965b, Lom u silnice jižně od Lištic., Paleovulkanity Českého masivu: Praha, Universita Karlova, p. 67-70.

Horný, R., 1965, Tektonická stavba a vývoj siluru mezi Berounem a Tachlovicemi.: Časopis pro mineralogii a geologii, v. X, p. 147-155.

Jelinek, V., 1966, A HIGH SENSITIVITY SPINNER MAGNETOMETER: Studia Geophysica Et Geodaetica, v. 10, p. 58-&.

Jelinek, V., 1973, PRECISION AC BRIDGE SET FOR MEASURING MAGNETIC SUSCEPTIBILITY OF ROCKS AND ITS ANISOTROPY: Studia Geophysica Et Geodaetica, v. 17, p. 36-48.

Kirschvink, J.L., 1980, THE LEAST-SQUARES LINE AND PLANE AND THE ANALYSIS OF PALEOMAGNETIC DATA: Geophysical Journal of the Royal Astronomical Society, v. 62, p. 699-718.

Kletetschka, G., Connerney, J.E.P., Ness, N.F., and Acuna, M.H., 2004, Pressure effects on martian crustal magnetization near large impact basins: Meteoritics & Planetary Science, v. 39, p. 1839-1848.

Kletetschka, G., Lillis, R.J., Ness, N.F., Acuna, M.H., Connerney, J.E.P., and Wasilewski, P.J., 2009a, Magnetic zones of Mars: Deformation-controlled origin of magnetic anomalies: Meteoritics & Planetary Science, v. 44, p. 131-140.

Kletetschka, G., Lunsford, A., Petrochilos, L., and Fuller, M., 2009b, Hall Probe scanner for analysis of magnetization of polished sections, International Associateion of Geomagnetism and Aeronomy: Sopron, Hungary, IAGA, p. 115-WED-O1115-0592.

Kletetschka, G., Wasilewski, P.J., and Taylor, P.T., 2000a, Hematite vs. magnetite as the signature for planetary magnetic anomalies?: Physics of the Earth and Planetary Interiors, v. 119, p. 259-267.

Kletetschka, G., Wasilewski, P.J., and Taylor, P.T., 2000b, Mineralogy of the sources for magnetic anomalies on Mars: Meteoritics & Planetary Science, v. 35, p. 895-899.

Kodym, O., Bouček, B., and Šulc, J., 1931, Guide to the geological excursion to the neighbourhood of Beroun, Koněprusy a Budňany, 1-83 p.

Kříž, J., 1991, The Silurian of the Prague Basin-tectonic, eustatic and volcanic controls on facies and faunal development., *in* Bassett, M.G., Lane, O.D., and Edwards, D., eds., The Murchinson Symposium" proceeding of an international conference on the Silurian System. Special Paper Palaeont., Volume 44: London, p. 179-203.

Kříž, J., 1992, Silurian Field Excursion, Prague Basin (Barrandian), Bohemia, National Museum of Wales.

Kříž, J., 1998, Silurian, *in* Chlupáč, I., Havlíček, V., Kříž, J., Kukal, Z., and Štorch, P., eds., Paleozoic of Barrandian (Cambrian to Devonian), ČSG, p. 79-100.

Krs, M., Pruner, P., and Man, O., 2001, Tectonic and paleogeographic interpretation of the paleomagnetism of Variscan and pre-Variscan formations of the Bohemian Massif, with special reference to the Barrandian terrane: Tectonophysics, v. 332, p. 93-114.

Man, O., 2003, Analysis of multi-component natural remanent magnetization based on the thermal demagnetisation spectrum: Studia Geophysica Et Geodaetica, v. 47, p. 359-370.

Oda, H., Usui, A., Miyagi, I., Joshima, M., Weiss, B.P., Shantz, C., Fong, L.E., McBride, K.K., Harder, R., and Baudenbacher, F.J., 2011, Ultrafine-scale magnetostratigraphy of marine ferromanganese crust: Geology, v. 39, p. 227-230.

Příhoda, K., Krs, M., Pešina, B., and Bláha, J., 1989, MAVACS-A new system of creating a nonmagnetic environment for paleomagnetic studies.: Cuadernos de Geologica Ibérica, v. 12, p. 223-250.

Strnad, J., 1961, Datolitové rohovce-surovina boru: Časopis pro mineralogii a geologii, v. IV, p. 157-160.